CONCEPTUAL DESIGN OF AN ANNULAR-FUELED SUPERHEAT BOILING WATER REACTOR

by

YU-CHIH KO

B.S., Engineering and System Science (2002), National Tsing Hua University, Taiwan
M.S., Engineering and System Science (2004), National Tsing Hua University, Taiwan
M.S., Nuclear Science and Engineering (2008), Massachusetts Institute of Technology

Submitted to the Department of Nuclear Science and Engineering
in partial fulfillment of the requirements for the degree of

DOCTOR OF PHILOSOPHY IN NUCLEAR SCIENCE AND ENGINEERING

at the

MASSACHUSETTS INSTITUTE OF TECHNOLOGY

September 2010 [February 2011]

Signature of Author: _____
Department of Nuclear Science and Engineering
September 29, 2010

Certified by: _____
Mujid S. Kazimi, Thesis Supervisor
TEPCO Professor of Nuclear Engineering

Certified by: _____
Jacopo Buongiorno, Thesis Reader
Associate Professor of Nuclear Science and Engineering

Accepted by: _____
Mujid S. Kazimi
TEPCO Professor of Nuclear Engineering
Chairman, Department Committee on Graduate Students

CONCEPTUAL DESIGN OF AN ANNULAR-FUELED SUPERHEAT BOILING WATER REACTOR

by

YU-CHIH KO

Submitted to the Department of Nuclear Science and Engineering
on September 29, 2010 in partial fulfillment of the
requirements for the degree of

DOCTOR OF PHILOSOPHY IN NUCLEAR SCIENCE AND ENGINEERING

ABSTRACT

The conceptual design of an annular-fueled superheat boiling water reactor (ASBWR) is outlined. The proposed design, ASBWR, combines the boiler and superheater regions into one fuel assembly. This ensures good neutron moderation throughout the reactor core. A single fuel design is used in the core. Each annular fuel element, or fuel tube, is cooled externally by boiling water and internally by steam. Fuel pellets are made of low enrichment UO_2, somewhat higher than the traditional BWR fuel enrichment. T91 and Inconel 718 are selected as candidates for the cladding material in view of their excellent physical properties and corrosion resistance. The fuel-cladding gap is filled with pressurized helium gas, like the existing lighter water reactor fuels. The ASBWR fuel assembly contains sixty annular fuel elements and one square water rod (occupying a space of four fuel elements) in an 8 by 8 square array. Annular separators and steam dryers are utilized and located above the core in the reactor vessel. Reactor internal pumps are used to adjust the core flow rate. Cruciform control rods are used to control the reactivity of the core, but more of them may be needed than a traditional BWR in view of the harder spectrum.

The major design constraints have been identified and evaluated in this work. The ASBWR is found promising to achieve a power density of 50 kW/L and meet all the main safety requirements. This includes a limit on the minimum critical heat flux ratio, maximum fuel and cladding operating temperatures, and appropriate stability margin against density wave oscillations.

At the expected superheated steam of 520 °C, the plant efficiency is above 40%, which is substantially greater than the efficiency of 33 to 35% that today's generation of LWRs can achieve. In addition to generating electricity, the ASBWR may also be useful for liquid fuel production or other applications that require high temperature superheated steam.

The uncertainties about this design include the performance of cladding materials under irradiation, the attainment of desirable heat transfer ratio between the external and

internal coolant channels throughout the fuel cycle, and the response to the traditional transients prescribed as design basis events.

Thesis Supervisor: Mujid S. Kazimi
Title: TEPCO Professor of Nuclear Engineering

Thesis Reader: Jacopo Buongiorno
Title: Associate Professor of Nuclear Science and Engineering

ACKNOWLEDGEMENTS

I would like to express my deepest appreciation to Professor Mujid S. Kazimi for his supervision and encouragement during the past four years of my life. Working with Prof. Kazimi has been not only an honor, but also a very enriching experience for me, both personally and professionally. I particularly like his sense of humor, which has made all the regular group meetings so enjoyable. I am also grateful to my thesis reader, Prof. Buongiorno. This work has been modified based on his valuable comments and recommendations.

I want to thank the following people for their help on specific issues of my work: Dr. Karahan for the fuel performance and neutronic calculations, Dr. Pilat for the literature review and LWR operating experience, Dr. Hejzlar for his guidance in the initial design phase of this work and Prof. Schulenberg for providing me the rare documentation of the German nuclear superheater.

Special thanks go to Prof. Min Lee, Dr. Lin-wen Hu and Dr. J. Bernard. Without their support, I would not have entered MIT, finished my master thesis with the LEU project and passed the doctoral qualifying exam.

A big "Thank You" to all of my Taiwanese friends at MIT and my friends at the NSE department: Hung-An, Shiu-Pei, Hsiang-Chieh, Chien-Jen, Sidney and Scott, Sam and Joyce, Cheng-wei, Wu-hsi, Chih-Chao, Podo, Hsin-Fu, Chih-yu, Jacqueline (Pipi), Duck, Peggy, Tsung-Han, Haru, Mike and Marina, Bo and Daphne, Vivek, David and Michelle, Ji-yong, Rui Hu, and Liang. I may have forgotten how to solve a two-group, two-region diffusion equation, but I will always remember our friendship and those wonderful memories that you have brought to me.

Furthermore, I would like to thank my family for their endless love and support. My dad and mom have been waiting for so long to see I finally finish my education. The tickets to the commencement will be one of the best gifts that I have ever presented to them. My sister should be happy enough to change her Facebook title to "Doctor's sister."

Lastly, I want to thank my dear wife, Yen-Chia Lin, for her selflessness and sacrifices in the course of our MIT journey. With a doctorate, I expect myself to be able to provide her a pleasant shopping experience wherever we will be living in the future.

TABLE OF CONTENTS

ABSTRACT 3
ACKNOWLEDGEMENTS 5
TABLE OF CONTENTS 7
LIST OF FIGURES 11
LIST OF TABLES 15
ACRONYMS AND NOMENCLATURE 17

Chapter 1 Introduction 21
1.1 Motivation 21
1.2 Background 23
1.2.1 The Early Program in the United States 23
1.2.2 Research Activities in Other Countries 24
1.3 Objectives 26
1.4 Thesis Organization 26

Chapter 2 Literature Review of Superheat and Nuclear Reactors 29
2.1 Categorization of the Superheat Nuclear Power Plants 29
2.2 Comparison between Conventional and Nuclear Superheaters 30
2.3 General Approaches on the Design of an Integral Nuclear Superheater 33
2.3.1 Key questions for the design 33
2.3.2 Introduction of Direct and Indirect Heating Approaches 35
2.3.3 Indirect Superheating Approach 38
2.3.4 Direct Superheating Approach 40
2.3.5 Summary of the Design Approaches 47
2.4 Summary of the Historical Superheat Nuclear Reactors 51
2.5 Summary of the Conceptual Designs of Nuclear Superheaters 55

Chapter 3 The Annular-fueled Superheat Boiling Water Reactor 65
3.1 Design Considerations 65
3.2 General Description of the Proposed Design 67
3.3 Detailed Description of the Proposed Design 70
3.3.1 Reactor Vessel and Major Components 70
3.3.2 Flow Configuration 71
3.3.3 Fuel Assembly 74
3.3.4 Materials for the In-core and Out-of-core Structures 91
3.3.5 Key Advantages of the Proposed Design 95
3.3.6 Main Challenges of the Proposed Design 98
3.4 Comparison between the HDR and the Proposed Design 100
3.4.1 Comparison of Fuel Element 101
3.4.2 Comparison of Fuel Assembly 101
3.4.3 Overall Comparison between the HDR and ASBWR 103
3.5 Comparison between a Conventional BWR and the ASBWR 105

Chapter 4 Neutronic Analysis 111
4.1 Introduction 111
4.2 Computational Tools 111
4.2.1 CASMO-4 111
4.2.2 MCNP-4C 111
4.3 Benchmarking: Comparison between MCNP and CASMO 112
4.4 Two-Dimensional Neutronics 114
4.4.1 Water Rod Design of the ASBWR Assembly 114
4.4.2 Burnup Calculation for the Poison-free Assembly 116
4.4.3 Distribution of Enrichment and Poison Rods in the ASBWR Assembly 118
4.4.4 Assembly Power Peaking Factors 129
4.4.5 Void and Fuel Temperature Reactivity Coefficients 130
4.4.6 Considerations for the Control Rod Design 131
4.5 Estimation of Fuel Cycle Length 133
4.6 Impact of Enrichment on the Cost of Electricity 134

Chapter 5 Steady State Thermal-hydraulic Analysis 137
5.1 Computational Tools 137
5.1.1 The MIT ASBWR Single Channel Analysis Code 137
5.1.2 VIPRE-01 137
5.2 Thermal-hydraulic Constraints for the ASBWR 138
5.3 Single Channel Analysis 140
5.3.1 Assumptions 140
5.3.2 Heat Loss in the Unheated Region 141
5.3.3 Axial Temperature Profiles 142
5.3.4 Radial Temperature Profiles 151
5.3.5 Impact of Power Density on Steam, Clad and Fuel Temperatures 156
5.3.6 Steam Velocity and Pressure Drop 158
5.3.7 Water Power Split Fraction 161
5.4 Assembly Subchannel Analysis 162
5.4.1 Assumptions 162
5.4.2 Heat Generation and Flow Rates 164
5.4.3 MCHFR Calculation 166
5.4.4 Core Pressure Drop 169
5.5 Startup Analysis for the ASBWR 171
5.6 Proposed Startup and Shutdown Procedures for the ASBWR 174

Chapter 6 Preliminary Thermal Expansion and Stress Analyses 189
6.1 Assumptions and Cladding Properties 189
6.2 Stresses Caused by Pressure 190
6.3 Calculation of Thermal Stresses 193
6.4 Calculation of Strains and Thermal Expansion 195

Chapter 7 Stability Analysis 199

7.1 Introduction 199
7.2 Computational Tool 199
7.3 Modeling of the Annular Fuel for the Stability Analysis Code 200
7.4 Single Channel Thermal-hydraulic Stability Analysis 200
7.4.1 Assumptions 200
7.4.2 Results 202
7.5 In-Phase Stability Analysis 202
7.5.1 Assumptions 202
7.5.2 Results 205
7.6 Sensitivity Studies 205

Chapter 8 Summary and Recommendations for Future Work 207
8.1 Summary 207
8.2 Conclusions 215
8.3 Future Work 216

References 219

Appendix A Review of Historical Superheat Nuclear Reactors 227
A.1 Nuclear Power Plants with Fossil Fuel-fired Superheaters 227
A.1.1 The Elk River Reactor 227
A.1.2 Indian Point Nuclear Power Plant Unit 1 232
A.1.3 The Carolinas–Virginia Tube Reactor (CVTR) 235
A.2 Nuclear Power Plants with Non-integral Nuclear Superheaters 240
A.2.1 The Vallecitos Experimental Superheat Reactor (VESR) 240
A.3 Nuclear Power Plants with Integral Nuclear Superheaters 244
A.3.1 The Atomic Power Station 1 (APS-1) 244
A.3.2 The BORAX-V Reactor 245
A.3.3 The Pathfinder Reactor 251
A.3.4 The Boiling Nuclear Superheater (BONUS) 260
A.3.5 The Beloyarsk Nuclear Power Station 270
A.3.6 The Marviken Boiling Heavy-water Superheat Reactor (R4) 273
A.3.7 The German Superheat Nuclear Reactor (HDR) 274

Appendix B The MIT ASBWR Single Channel Analysis Code 283
B.1 Objectives of the MIT ASBWR Single Channel Analysis Code 283
B.2 Code Structure and Assumptions 283
B.3 Models for the Temperature Calculation 291
B.3.1 Coolant Conditions 291
B.3.2 Cladding Surface Temperature 292
B.3.3 Cladding Temperature Drop 293
B.3.4 Fuel-Cladding Gap Temperature Drop 293
B.3.5 Fuel Pellet Temperature Distribution 294
B.4 Benchmark Studies 295
B.4.1 The Modified FRAPCON-ANNULAR Code 295
B.4.2 Assumptions 296

B.4.3 Results 297
B.5 Source Code 300

Appendix C Subroutine for Generating VIPRE Input Files 325

Appendix D Derivation of the Lumped Annular Fuel Dynamics Model 337
D.1 Derivation of the Lumped Fuel Dynamic Equations 338
D.2 Coupling of Fuel Dynamics to Coolant Thermal-hydraulics Model 345

Appendix E Input Files 347
E.1 VIPRE-01 Input for the ASBWR Assembly Analysis 347
E.2 MCNP Input for the Benchmark Study 353
E.3 CASMO Input for the Benchmark Study 356
E.4 CASMO Input for the ASBWR Assembly Analysis 357
E.5 Single Channel Stability Analysis Input 358
E.6 In-Phase Channel Stability Analysis Input 360

LIST OF FIGURES

Figure 1-1 A non-ideal Rankine cycle with superheat 22

Figure 2-1 Categorization of the superheat nuclear power plants 29
Figure 2-2 Key questions for the design of an integral nuclear superheater 36
Figure 2-3 Indirect and direct superheating approaches 37
Figure 2-4 The two-region concept 41
Figure 2-5 The multi-region concept 44
Figure 2-6 The single assembly concept 45
Figure 2-7 The single element concept 46
Figure 2-8 Comparison of the four direct boiling and superheating design concepts ... 49
Figure 2-9 The ANL 1956 conceptual design 56
Figure 2-10 The 2007 conceptual design of Ferrara and Hochreiter 57
Figure 2-11 Flow path in the three pass core design concept 59

Figure 3-1 Simplified flow configuration of the ASBWR 69
Figure 3-2 Steam temperature vs. plant efficiency for a superheat BWR 70
Figure 3-3 Reactor vessel and major components of the ASBWR 72
Figure 3-4 Flow configuration of the ASBWR 73
Figure 3-5 The ASBWR fuel assembly 75
Figure 3-6 Top, front and side views of the upper tie plate 76
Figure 3-7 Locations of the tie rods 76
Figure 3-8 Cross-sectional view of the ASBWR fuel assembly (A-A) 77
Figure 3-9 Cross-sectional view of the ASBWR fuel assembly (B-B) 78
Figure 3-10 Cross-sectional view of the ASBWR fuel assembly (C-C) 79
Figure 3-11 Cross-sectional view of the ASBWR fuel assembly (D-D) 80
Figure 3-12 The ASBWR annular fuel element 81
Figure 3-12 The ASBWR annular fuel element 81
Figure 3-13 The ASBWR annular tie rod 82
Figure 3-14 The ASBWR annular fuel element with annular spring seal 83
Figure 3-15 Spring system of the ASBWR fuel assembly 84
Figure 3-16 The upper and lower steam boxes 85
Figure 3-17 Three-dimensional view of the steam box 86
Figure 3-18 Flow paths in and around the steam box 88
Figure 3-19 Horizontal cross-sectional view of the ASBWR fuel assembly 89
Figure 3-20 Coolant flow paths in the ASBWR assembly 90
Figure 3-21 Comparison of steam flow path in the HDR and ASBWR fuel assembly 103
Figure 3-22 Comparison of a BWR fuel pin and the ASBWR annular fuel element .. 107
Figure 3-23 The reference BWR assembly module 108
Figure 3-24 The ASBWR assembly module 109

Figure 4-1 Initial design of the ASBWR assembly 116
Figure 4-2 Burnup calculation for poison free fuels with various enrichments 118
Figure 4-3 Enrichment and poison rod distribution of the reference BWR 119
Figure 4-4 Fresh fuel power peaking factors of the reference BWR 119

Figure 4-5 Infinite multiplication factor versus burnup of the reference BWR 120
Figure 4-6 Enrichment and poison rod distribution of the ASBWR (Design A) 120
Figure 4-7 Enrichment and poison rod distribution of the ASBWR (Design B) 121
Figure 4-8 Enrichment and poison rod distribution of the ASBWR (Design C) 121
Figure 4-9 Infinite multiplication factor versus burnup of the ASBWR (Design A)... 123
Figure 4-10 Infinite multiplication factor versus burnup of the ASBWR (Design B). 124
Figure 4-11 Infinite multiplication factor versus burnup of the ASBWR (Design C). 124
Figure 4-12 Enrichment and poison rod distribution of the ASBWR assembly using Inconel 718 cladding 128
Figure 4-13 Infinite multiplication factor versus burnup of the ASBWR assembly using Inconel 718 cladding 128
Figure 4-14 Fresh fuel PPFs of the ASBWR using T91 cladding 129
Figure 4-15 Fresh fuel PPFs of the ASBWR using Inconel 718 cladding 129
Figure 4-16 Comparison of the conventional and ABWR-II control rod designs 132
Figure 4-17 Breakdown of the nuclear electricity generation cost 134

Figure 5-1 Axial power profiles of the ASBWR and reference BWR 140
Figure 5-2 Axial coordinate of the ASBWR single channel model 141
Figure 5-3 Axial temperature profiles of the water side (Hot channel, T91 cladding) 144
Figure 5-4 Axial temperature profiles of the steam side 144
(Hot steam down-flow channel, T91 cladding) 144
Figure 5-5 Axial temperature profiles of the steam side 145
(Hot steam up-flow channel, T91 cladding) 145
Figure 5-6 Comparison of the steam outlet temperature (T91 cladding) 145
Figure 5-7 Comparison of the inner cladding temperature (T91 cladding) 146
Figure 5-8 Comparison of the maximum fuel temperature (T91 cladding) 146
Figure 5-9 Axial temperature profiles of the water side
(Hot channel, Inconel 718 cladding) 148
Figure 5-10 Axial temperature profiles of the steam side
(Hot steam down-flow channel, Inconel 718 cladding) 148
Figure 5-11 Axial temperature profiles of the steam side
(Hot steam up-flow channel, Inconel 718 cladding) 149
Figure 5-12 Comparison of the steam outlet temperature (Inconel 718 cladding) 149
Figure 5-13 Comparison of the inner cladding temperature (Inconel 718 cladding) .. 150
Figure 5-14 Comparison of the maximum fuel temperature (Inconel 718 cladding) .. 150
Figure 5-15 Radial coordinate of the ASBWR single channel model 152
Figure 5-16 Radial temperature profile of the hot steam down-flow channel
(z = -10 cm, T91 cladding) 152
Figure 5-17 Radial temperature profile of the hot steam down-flow channel
(z = 2.0 cm, T91 cladding) 153
Figure 5-18 Radial temperature profile of the hot steam down-flow channe
(z = 93.7 cm, T91 cladding) 153
Figure 5-19 Radial temperature profile of the hot steam down-flow channel
(z = 292 cm, T91 cladding) 154
Figure 5-20 Radial temperature profile of the hot steam down-flow channel
(z = -10 cm, Inconel 718 cladding) 154

Figure 5-21 Radial temperature profile of the hot steam down-flow channel (z = 2.0 cm, Inconel 718 cladding) 155
Figure 5-22 Radial temperature profile of the hot steam down-flow channel (z = 93.7 cm, Inconel 718 cladding) 155
Figure 5-23 Radial temperature profile of the hot steam down-flow channel (z = 292 cm, Inconel 718 cladding) 156
Figure 5-24 Sensitivity of power density for T91 cladding 157
Figure 5-25 Sensitivity of power density for Inconel 718 cladding 158
Figure 5-26 VIPRE model of the ASBWR assembly 164
Figure 5-27 Power to flow operating map of a typical BWR 173
Figure 5-28 Calculation results of the startup analysis 173
Figure 5-29 Startup of the ASBWR (step 1) 176
Figure 5-30 Startup of the ASBWR (step 2) 177
Figure 5-31 Startup of the ASBWR (step 3) 178
Figure 5-32 Startup of the ASBWR (step 4) 179
Figure 5-33 Startup of the ASBWR (step 5) 180
Figure 5-34 Startup of the ASBWR (step 6) 181
Figure 5-35 Startup of the ASBWR (step 7) 182
Figure 5-36 Startup of the ASBWR (step 8) 183
Figure 5-37 Startup of the ASBWR (step 9) 184
Figure 5-38 Startup of the ASBWR (step 10) 185
Figure 5-39 Startup of the ASBWR (step 11) 186
Figure 5-40 Startup of the ASBWR (step 12) 187

Figure 6-1 Illustration of the pressures acting on cladding 191
Figure 6-2 Balance of the axial forces 192
Figure 6-3 Peak thermal stresses on the steam side (inner) cladding 194
Figure 6-4 Peak thermal stresses on the water side (outer) cladding 194

Figure 7-1 Illustration of the single channel instability loop 201
Figure 7-2 Illustration of in-phase stability model 203

Figure A-1 Elk River reactor pressure vessel 230
Figure A-2 Schematic flow diagram of the Elk River reactor 231
Figure A-3 Schematic flow diagram of the Indian Point unit 1 234
Figure A-4 Schematic flow diagram of the Carolinas–Virginia tube reactor 237
Figure A-5 Vertical section of the CVTR core 238
Figure A-6 Horizontal section of the CVTR core 239
Figure A-7 Vertical cross section of the Vallecitos experimental superheat reactor 242
Figure A-8 Fuel bundle of the Vallecitos experimental superheat reactor 243
Figure A-9 Central and peripheral superheat operation of BORAX-V 248
Figure A-10 The BORAX-V superheater fuel assembly 249
Figure A-11 The BORAX-V superheater fuel subassembly 250
Figure A-12 The schematic diagram of the Pathfinder power plant 255
Figure A-13 Cross section of the Pathfinder reactor core 256
Figure A-14 The Pathfinder superheater fuel element 257

Figure A-15 Sectional view of the Pathfinder reactor vessel 258
Figure A-16 Simplified flow diagram of the Pathfinder reactor 259
Figure A-17 Horizontal cross section of the BONUS reactor core 264
Figure A-18 Perspective of the BONUS boiler fuel assembly 265
Figure A-19 Perspective of the BONUS superheater fuel assembly 266
Figure A-20 BONUS boiler and superheater fuel rods 267
Figure A-21 Perspective of the BONUS reactor pressure vessel 268
Figure A-22 Simplified schematic diagram of the BONUS power reactor 269
Figure A-23 Simplified flow diagram of the AMB-100 reactor 272
Figure A-24 The original HDR fuel assembly design 277
Figure A-25 The HDR reactor vessel (original design) 278
Figure A-26 Flow Configuration of the HDR (original design) 279
Figure A-27 The revised HDR fuel assembly design 280
Figure A-28 The revised HDR flow configuration 281

Figure B-1 Simplified MASCAC flow chart 285
Figure B-2 Single channel model of the ASBWR 287
Figure B-3 Simplified single channel model of the ASBWR used in MASCAC 288
Figure B-4 Illustration of the fuel active and unheated regions 289
Figure B-5 Thermal conductivity of T91 290
Figure B-6 Thermal conductivity of Inconel 718 290
Figure B-7 FRAPCON and MASCAC radial temperature profiles (T91) 298
Figure B-8 FRAPCON and MASCAC radial temperature profiles (Inconel 718) 299

Figure D-1 Illustration of the lumped annular fuel dynamics model 337

LIST OF TABLES

Table 2-1 Matrix of the direct and indirect heating approaches 37
Table 2-2 Comparison of the indirect and direct superheating approaches 48
Table 2-3 Characteristics of the direct boiling and superheating concepts 50
Table 2-4 List of nuclear reactors with superheat 52
Table 2-5 Design characteristics of the nuclear power plants with superheat 53
Table 2-6 U.S. patents of the non-integral nuclear superheater 60
Table 2-7 U.S. patents of the integral nuclear superheater 61
Table 2-8 Features of the U.S. patented integral nuclear superheater 62

Table 3-1 Materials for key components in supercritical fossil power plants 91
Table 3-2 Composition of Zircaloy, T91 and Inconel 718 94
Table 3-3 Physical and nuclear properties of Zircaloy, T91 and Inconel 718 95
Table 3-4 Design characteristics of the HDR and ASBWR 102
Table 3-5 Major differences between the HDR and ASBWR 105
Table 3-6 Characteristics of a conventional BWR and the ASBWR 106
Table 3-7 Dimensions of the reference BWR and ASBWR fuel assemblies 110

Table 4-1 Assumptions adopted in the benchmark study 112
Table 4-2 Results of the benchmark study 113
Table 4-3 Input parameters for the 2D neutronic calculation. 115
Table 4-4 Assumptions adopted in the 2D neutronic calculation 115
Table 4-5 Constraints of neutronic analysis 116
Table 4-6 Results of burnup calculation for poison free, uniform enriched fuels 117
Table 4-7 Input parameters of the simulation cases 122
Table 4-8 Comparison of fast-to-thermal neutron flux ratio (poison-free case) 125
Table 4-9 Comparison of fast-to-thermal neutron flux ratio (poison rod case) 125
Table 4-10 Calculation results of the core average multiplication factors at EOC 127
Table 4-11 Calculation results of the void and fuel temperature coefficients 130
Table 4-12 Design specifications of the ABWR-II and ASBWR 131
Table 4-13 Main design objectives of the ABWR-II 131
Table 4-14 Control rod design of the ASBWR 133
Table 4-15 Estimation of the ASBWR fuel cycle length 133
Table 4-16 Assumptions adopted in the preliminary study of cost of electricity 135
Table 4-17 Results of the preliminary economic study 135

Table 5-1 Major thermal-hydraulic constraints of the ASBWR 139
Table 5-2 Assumptions adopted in the single channel analysis 140
Table 5-3 Heat loss of steam in the unheated region 142
Table 5-4 Comparison between the temperatures in the average and hot channels (T91 cladding) 147
Table 5-5 The predicted exit steam velocity and total steam pressure drop 160
Table 5-6 Calculation results of water power split fraction 161
Table 5-7 Assumptions adopted in the VIPRE assembly subchannel analysis 162
Table 5-8 Pressure loss coefficients as assumed in the VIPRE analysis 163

Table 5-9 Hot channel heat generation and flow rates 165
Table 5-10 Comparison of the calculated exit quality, void fraction and MCHFR_in the hot channel 168
Table 5-11 Exit conditions of the reference BWR and the base case 168
Table 5-12 Calculation results of the core pressure drop 170
Table 5-13 Assumptions adopted in the startup analysis 172

Table 6-1 Assumptions adopted in the thermal expansion and stress analyses 189
Table 6-2 Young's modulus of the cladding materials 189
Table 6-3 Linear thermal expansion coefficients of the cladding materials 190
Table 6-4 Calculation results of the stresses caused by pressure_at the beginning of fuel life in core 192
Table 6-5 Results of strain calculation of the base case (T91 cladding) 196
Table 6-6 Calculation results of axial growth due to pressure and thermal expansion 197
Table 6-7 Impact of power density on the axial growth 197

Table 7-1 Assumptions adopted in the thermal expansion and stress analyses 201
Table 7-2 Results of the single channel stability analysis 202
Table 7-3 Assembly grouping for the in-phase stability analysis 204
Table 7-4 Neutronic parameters for the in-phase stability analysis 204
Table 7-5 Results of the in-phase stability analysis 204
Table 7-6 Results of the power split sensitivity study 206

Table 8-1 Comparison of the goals and ASBWR preliminary design conditions_for the base case power density of 50 kW/L 213
Table 8-2 Comparison of design specifications between BWR and ASBWR 214

Table A-1 Design features of the Elk River reactor 229
Table A-2 Design features of the Indian Point unit 1 233
Table A-3 Design features of the Carolinas–Virginia tube reactor 236
Table A-4 Design features of the Vallecitos experimental superheat reactor 241
Table A-5 Design features of BORAX-V 247
Table A-6 Design features of the Pathfinder reactor 254
Table A-7 Design features of the BONUS reactor 263
Table A-8 Design features of the HDR 276

Table B-1 Heat transfer correlations used in MASCAC 292
Table B-2 Difference between the modified FRAPCON-ANNULAR and MASCAC 296
Table B-3 Summary of benchmark study (with T91 cladding) 298
Table B-4 Summary of benchmark study (with Inconel 718 cladding) 299

ACRONYMS AND NOMENCLATURE

ABWR	Advanced Boiling Water Reactor
AC	Allis-Chalmers Manufacturing Co.
ACF	American Car and Foundry, Inc. (reactor activities abandoned by AC)
ADS	Accelerator Driven System
AEC	Atomic Energy Commission, a predecessor of the Department of Energy
AMB-100	The Beloyarsk Nuclear Power Station Unit 1
AMB-200	The Beloyarsk Nuclear Power Station Unit 2
ANL	Argonne National Laboratory
ANS	American Nuclear Society
APS-1	Atomic Power Station-1 (the Obninsk Nuclear Power Plant)
ASBWR	Annular-fueled Superheat Boiling Water Reactor
ATWS	Anticipated Transient Without Scram
B&W	The Babcock & Wilcox Company
B1	Single-batch discharge burnup
Bd	Discharge burnup
BNL	Brookhaven National Laboratory
BOC	Beginning Of Cycle
BONUS	BOiling NUclear Superheater
BORAX	Boiling water reactor experiments
BORAX-V	Boiling Reactor Experiment No. 5
BWR	Boiling Water Reactor
CANDU	The CANada Deuterium Uranium reactor
CE	Combustion Engineering, Inc.
CHF	Critical Heat Flux
CVTR	Carolinas - Virginia Tube Reactor
DOD	Department of Defense
DOE	Department of Energy
DR	Decay Ratio
DWO	Density Wave Oscillations
EOC	End Of Cycle
ERR	Elk River Reactor
ESADA	Empire State Atomic Development Associates
EVESR	ESADA Vallecitos Experimental Superheat Reactor

GA	General Atomics Technologies
GE	General Electric Company,
GNEC	General Nuclear Engineering Corp. (became a division of Combustion Engineering Inc., in 1964)
H/HM	Hydrogen to Heavy Metal ratio
HDR	Heissdampfreaktor (German: Superheat Steam Reactor)
HPLWR	High Performance Light Water Reactor
IAEA	International Atomic Energy Agency
IASCC	Irradiation-Assisted Stress Corrosion Cracking
INEEL	Idaho National Engineering and Environmental Laboratory
LANL	Los Alamos National Laboratory
LOCA	Loss Of Coolant Accident
LOFA	Loss Of Flow Accident
LWR	Light Water Reactor
MASCAC	MIT ASBWR Single Channel Analysis Code
MCHFR	Minimum Critical Heat Flux Ratio
MCNP	Monte Carlo N-Particle transport code
MCPR	Minimum Critical Power Ratio
MSIV	Main Steam Isolation Valve.
NPP	Nuclear Power Plant
NPS	Nuclear Power Station
NRC	Nuclear Regulatory Commission
NSPC	Northern States Power Company
OECD	Organisation for Economic Co-operation and Development
pcm	Per cent mille; one one-thousandth of a percent
PDRP	Power Demonstration Reactor Program
PNL	Pacific Northwest Laboratory,
PPF	Power Peaking Factors
PREPA	Puerto Rico Electric Power Authority
PRWRA	Puerto Rico Water Resources Authority
PWR	Pressurized Water Reactor
R4	The Marviken boiling heavy-water superheat reactor
RCPA	Rural Cooperative Power Association
Ref.	Reference
RIP	Reactor Internal Pump
RPV	Reactor Pressure Vessel

SAB	The Stability Analysis of BWR code
SCC	Stress Corrosion Cracking
SCFPP	Supercritical Fossil Power Plant
SCWR	Supercritical Water Reactor
SS	Stainless Steel
SWU	Separative Work Unit
T91	Modified 9Cr - 1Mo steel
TD	Theoretical Density
Temp.	Temperature
USSR	Union of Soviet Socialist Republics
VBWR	Vallecitos Boiling Water Reactor
VIPAC	Vibration-Packing
VIPRE	Versatile Internals and component Program for Reactors; EPRI,
WAK	Karlsruhe nuclear fuel reprocessing plant
West.	Westinghouse Electric Company
Zr	Zircaloy

Chapter 1
Introduction

This work is focused on development of a conceptual design of a medium-sized nuclear reactor which can generate superheated steam. More specifically, the proposed design is a light water cooled, light water moderated nuclear reactor which utilizes annular fuels to vaporize water and superheat steam in the reactor vessel. Motivation, background, and objectives of this work are introduced in this chapter.

1.1 Motivation

Superheat, as one of the steam cycle features, has been used in power plants for several decades. Superheating of steam, i.e., raising the steam above its saturation temperature at a given pressure, is desirable for several reasons [1]. First, superheating of steam improves turbine performance. The life time of a steam turbine is limited by water droplet formation. As the water condenses, water droplets hit the turbine blades at a very high speed causing pitting and erosion, gradually decreasing the life of turbine blades. Superheating of steam avoids excessive wetness at the low-pressure end of the turbine, thus improving the turbine lifetime. Figure 1-1 is a typical temperature-entropy diagram (T-s diagram) of the steam cycle. As shown in Figure 1-1, state 3 of a non-ideal Rankine cycle is just above the two-phase region, so after expansion (state 3 to 4) the steam will be very wet. By superheating, state 3 will move to 3' and hence produce a much dryer steam after expansion.

Secondly, superheating of steam gives a considerable increase in the thermodynamic efficiency of the whole cycle, by increasing the proportion of "usable" heat to the total heat supplied to the steam. Figure 1-1 shows the additional usable heat in a superheat cycle. Significant impact on economy is expected, since higher plant efficiency would substantially reduce the cost of generating electricity and make nuclear power plants more competitive with alternative power plants.

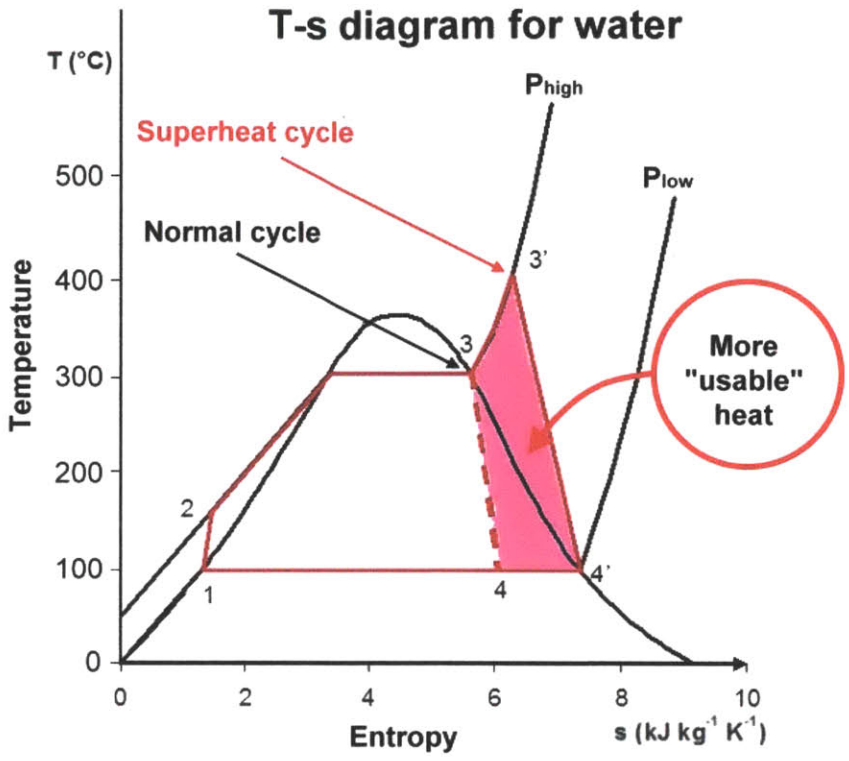

Figure 1-1 A non-ideal Rankine cycle with superheat

Furthermore, superheating steam to an elevated temperature level may diversify its application. In addition to generating electricity, superheated steam could potentially be used for liquid fuel production. A feasible application, for example, is to use the alkaline electrolysis process or the high-temperature electrolysis (HTE) to convert water into hydrogen [2][3]. If carbon dioxide (CO_2) is available, HTE can convert a steam-CO_2 mixture into syngas, which is a gas that contains varying amounts of carbon monoxide (CO) and hydrogen (H_2), by simultaneously electrolyzing steam and CO_2 [4]. With syngas as the input, liquid fuels would be produced by the classical Fischer-Tropsch (FT) process. The FT process can produce liquid fuels, such as JP-8, or a variety of liquid hydrocarbons.

Although the cost of electricity generation from today's commercial light water reactors is already in the realm of being competitive with that from fossil fuels, it is reasonable to

believe that the cost could be further reduced through nuclear superheat. In addition, superheat may benefit nuclear power plants in many other ways. If nuclear reactors can produce superheated steam at high pressures, the enhanced plant efficiency will be comparable with that of the most efficient fossil fuel-fired stations. The enhanced plant efficiency may also enable improvements in uranium utilization; reduction in waste production, and a potential saving in the capital cost.

The combination of a nuclear reactor, a steam producing boiler, and a superheater was an objective of power reactor designers from 1950s to 1970. However, a satisfactory means of producing steam and superheating it within a nuclear system to the temperatures desired for modern power plants has not been achieved. At the present state, there are still a number of problems that must be solved before economically competitive power with nuclear superheat may become a reality. Moreover, it is important to confirm that the advantages gained in higher thermal efficiency must not be lost through depreciating factors, such as lower allowable power density in the superheating region of the reactor or excessively higher superheater fuel fabrication costs.

In this work, an innovative conceptual design of an annular-fueled superheat boiling water reactor is proposed and explored. It is expected that the proposed design will be one of the most promising approaches to realize the nuclear superheat concept in terms of safety, technical feasibility and economic viability.

1.2 Background

1.2.1 The Early Program in the United States

In 1955, the United States Atomic Energy Commission (USAEC), which was the predecessor of the Nuclear Regulatory Commission (NRC) and the Department of Energy (DOE), initiated a Power Demonstration Reactor Program (PDRP) to invite private utility companies to own, build, and operate prototype power reactors [5]. The objective of this power demonstration program was to generate basic design and engineering

information that would allow the design concept to be scaled to larger, more commercial sizes [1].

Under the auspices of the PDRP, several superheat nuclear reactors were built and operated [6~8]. All these prototype reactors were small and had low power level since they were intended to provide a demonstration of the concept. Reactors which had been constructed in the PDRP were: (a) Boiling Water Experimental Reactor V (BORAX-V), by Argonne National Laboratory (ANL), in Idaho [9]; (b) Pathfinder reactor, by Allis-Chalmers Manufacturing Co. (A-C), in South Dakota [10]; (c) Boiling Nuclear Superheater (BONUS), by General Nuclear Engineering Corp. (GNEC), which was a subsidiary of Combustion Engineering (CE), in Puerto Rico [11-12]; and (d) Vallecitos experimental superheat reactor (VESR), by General Electric Co. (GE) and the Empire States Atomic Development Associates (ESADA), in California [13]. Detailed information about these prototype reactors is provided in Chapter 2 and Appendix A.

In addition to these construction projects, the USAEC had also awarded contracts to a number of companies within the United States for research leading to the development of superheat and steam-cooled reactor concepts [14~15].

1.2.2 Research Activities in Other Countries

Between 1950s ~ 1960s, nuclear superheat was one of the most prominent research topics in the area of nuclear technology. Not only in the United States, a considerable number of studies were also undertaken in other countries, such as the Union of Soviet Socialist Republics (USSR), Germany and Sweden [16]. In 1964, a special session was held for the subject of nuclear superheat at the Third International Conference on the Peaceful Uses of Atomic Energy in Geneva.

In Germany, the first studies on nuclear superheat were made in 1960. In 1961, the German Federal Ministry of Scientific Research initiated a three-year development program which included the selection of the reactor type, the necessary studies and experiments and the preparation of a detailed layout of a prototype reactor. As a product

of this three-year program, a natural circulation, annular-fueled superheat BWR was proposed and later built [17].

In Sweden, a boiling heavy water reactor with nuclear superheat was studied and proposed in 1962 [18]. This reactor, called the R4 Marviken heavy water reactor or the R4 reactor, was designed and built in 1964 by the AB Atomenergi, a government established atomic energy research organization in Sweden. The R4 reactor was cooled and moderated by heavy water. Separation of steam from the two-phase mixture was done by gravity in the reactor vessel. The target electric power output of the R4 reactor was 200 MW. However, the R4 reactor was never loaded with fuel. The project was aborted due to serious problems in 1970. The turbine hall was subsequently used for an oil-fired power station, and the pressure vessel and containment building were subsequently used for experiments into reactor behavior under accident conditions [19].

In 1958, the Soviet Union proposed a pressure-tube-type, graphite-moderated thermal reactor to produce superheated steam [20~22]. The Russian superheat reactor was designed to use low enrichment uranium fuel and had two groups of fuel assemblies. In the first group of fuel assemblies, thermal energy generated from the fuel was removed by boiling water in the pressure tubes and was transferred to the steam separator. The saturated steam, after leaving the separator, would then enter the second group of fuel assemblies, where it is superheated. The alternative design of the Russian superheat reactor was to use steam generator and separator for the saturated steam production. However, there is no indication that such a reactor was built.

More information about these foreign superheat reactors is provided in Chapter 2 and Appendix A.

1.3 Objectives

The following objectives are set for this work:

1. Develop a conceptual design of an advanced boiling water reactor with annular fuel elements, which enables the reactor to produce high temperature superheated steam with an improved thermal efficiency. The proposed design must have comparable or improved safety margins to that of the existing BWRs.

2. Point out the major challenges of the proposed design and provide possible solutions to solve the problems.

3. Provide a list of future tasks for further analysis and improvements for the proposed design.

1.4 Thesis Organization

Chapter 2 provides a comprehensive literature review of the superheat nuclear reactor concept, including categorization of superheat nuclear reactors, comparison between conventional and nuclear superheaters and summary of historical and conceptual superheat reactor designs. In addition, general approaches to a design of a superheat reactor are also provided in Chapter 2.

A detailed description of the proposed design is presented in Chapter 3. Also in Chapter 3, the proposed design is compared with the German superheat reactor and with a conventional boiling water reactor to display its distinguishing features and potential to improve the efficiency of light water reactors.

A series of analyses have been performed to evaluate the technical feasibility and

characteristics of the proposed design. Results of these analyses are given in various aspects in Chapter 4 to Chapter 7.

In Chapter 4, two-dimensional neutronic analyses and estimation of fuel cycle length are described. Steady state thermal-hydraulic analyses, including single channel analysis, assembly subchannel analysis, and start-up and shut-down procedures, are presented in Chapter 5. A preliminary study of thermal expansion and stresses for the fresh fuel is given in Chapter 6. Stability analysis for the proposed design is presented in Chapter 7.

Finally, a summary of conclusions and recommendations for future work is presented in Chapter 8.

Chapter 2

Literature Review of Superheat and Nuclear Reactors

2.1 Categorization of the Superheat Nuclear Power Plants

Figure 2-1 shows the general categorization of the superheat nuclear power plants (NPPs). Superheating can be incorporated in nuclear power plants by the addition of either a nuclear or fossil fuel-fired superheater. In Figure 2-1, a conventional superheater means it is fired by fossil fuels or other non-nuclear means. Nuclear superheaters can be further categorized into two types: (a) the separate or non-integral nuclear superheater and (b) the integral nuclear superheater [8]. The non-integral nuclear superheater is namely a steam-cooled reactor. It only adds superheat to steam and the steam coolant is supplied from other sources, such as a light water reactor (LWR) or fossil power plant. For the integral nuclear superheater, steam is generated and superheated by using the same core.

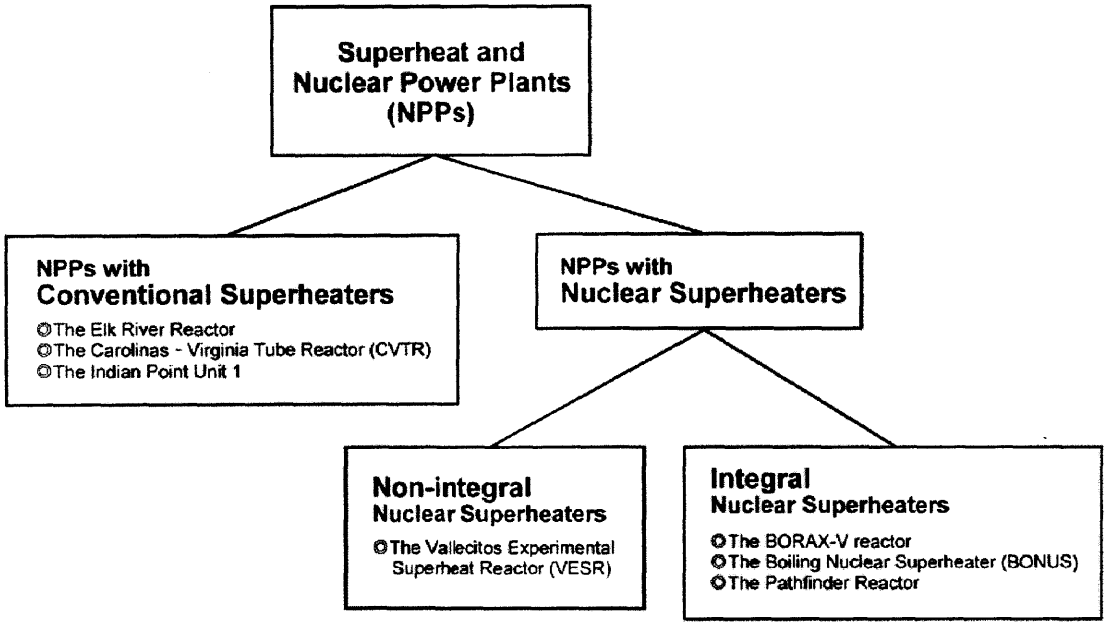

Figure 2-1 Categorization of the superheat nuclear power plants

Although the reactor design will be more complicated, it is believed that the integral nuclear superheater is more cost-effective than the separate one because it needs only one core and one reactor pressure vessel to produce superheated steam.

In addition to water, the integral nuclear superheater can also be cooled by other coolants, such as organic fluid, helium, carbon dioxide, molten salt or liquid metal, and use a heat exchanger to generate superheated steam. A comprehensive review of these superheat reactor concepts has been documented in the literature [45]. However, a gas-cooled or liquid-metal-cooled reactor is not within the scope of this work. In order to take advantage of the abundant experience from today's LWRs, as well as improve the LWR technology, this work is focused on the design of an integral nuclear superheater cooled by water and steam.

2.2 Comparison between Conventional and Nuclear Superheaters

During the 1960s, when the thermal efficiency and reliability of LWRs were still poor, a few nuclear power plants with secondary superheating by means of fossil fuels were constructed (i.e. Indian Point 1 in USA, Garigliano in Italy and Lingen in Germany) [23]. However, at that time the performance of the combined cycle was not good, due to low capacity factors and material failures [24, 25].

Nowadays, the technology of thermal power plants, both nuclear and conventional, is much more reliable (> 90% capacity factors for LWRs and 80% for coal plants). As a result, it is reasonable to reconsider the feasibility of combined advanced cycles that produce vapor by means of nuclear power — taking advantage of the lower heating costs — and superheat the secondary flow by means of fossil fuels, such as oil or gas.. Recently, economics of the combined nuclear-gas power cycle have been reevaluated [23, 26]. Results of these studies indicate that the combined nuclear-gas power cycle has possibilities to successfully compete in the near future electric market [23].

Although a combined nuclear-fossil fuel power cycle seems promising in terms of

economic viability, there are still some problems and issues that need to be taken into consideration. A detailed comparison between nuclear and fossil fuel-fired superheaters is provided below by listing the advantages and disadvantages of incorporating fossil fuel-fired superheaters into nuclear power plants [80].

Advantages of using fossil fuel-fired superheaters are:

1. Plenty of experience. Fossil fuels have been used for a very long time. Industry is familiar with this technology and it has satisfactory performance.

2. Less effort on plant design. Using fossil fuel-fired superheaters can save time and effort on the plant design since a steam-cooled nuclear reactor (a separate nuclear superheater) and a complex design of an integral nuclear superheater can be avoided.

3. No neutronic control and operating problems. Compared with nuclear power superheaters, fossil-fueled superheaters are relatively simple and would not have neutronic control and operating problems.

4. Less radioactive waste. The amount of radioactive waste would be reduced if the fossil fuel-fired superheaters are used.

5. Reduced burden on plant licensing. Using fossil fuel-fired superheaters may expedite the plant licensing process compared with using a separate or integral nuclear superheater.

Disadvantages of using fossil fuel-fired superheaters are:

1. Emission of carbon dioxide. Fossil fuel-fired superheaters will definitely emit CO_2 and lead to the aggravation of global warming.

2. Siting problem. Selecting an appropriate plant site will become very difficult if fossil fuel-fired superheaters are used. For nuclear power plants, a preferable plant site would be a sparsely populated area with stable weather and geological histories. However, when determining a site for fossil-fueled plants, it is always most desirable to have the site be as close as possible to the source of fuel. Conflicts may occur if we have to consider all the above issues.

3. Expanded personnel. The fossil fuel-fired superheater is a departure from nuclear power and would require two different lines of operators. Personnel cost may increase due to two different lines of technical support and maintenance.

4. Capacity loss in case of component failure. When a reactor is used for generating steam in conjunction with a fossil fired superheater, the superheater operating difficulties will impact the plant capacity factor. A failure of the superheater or any other components may require the entire plant to be shut down until the failure is repaired.

5. No contribution to nuclear technology. Today, our world is facing the not only the global warming problem but also an energy crisis. Nuclear energy has been recognized as one of the most promising means to solve these problems. Incorporating fossil fuel-fired superheaters into nuclear power plants apparently does not contribute much to nuclear technology.

In part because of the greenhouse effect, the primary objective of this work has been set to design a highly efficient reactor which could produce superheated steam by means of only nuclear energy. Therefore, fossil fuel-fired superheaters are not studied in this work. Furthermore, this work is particularly focused on the design of an integral nuclear superheater, since it has been regarded as more cost-effective and more challenging than the design of a steam-cooled reactor.

2.3 General Approaches on the Design of an Integral Nuclear Superheater

2.3.1 Key questions for the design

Designing a reactor with an integral nuclear superheater is a very challenging task. The layout of the core is usually much more complicated than that of a typical LWR core, which provides only boiling or heating of the primary coolant. In addition, many design margins of a LWR are reduced when the design is for an integral nuclear superheater. For example, the available space in the reactor vessel is further limited because more components related to superheating are expected to be integrated in the reactor vessel. Moreover, additional constraints will be applied to the design because of the elevated steam temperature and tougher operating conditions. Particularly, the fuel performance under superheating conditions is the most important issue to be addressed.

A successful design hinges on the designer's knowledge, experience and creativity. There are no guidelines or standard procedures for a design to start from; however, some general requirements do exist which must be met prior to further analysis. For the design of a nuclear reactor, the general considerations are safety, meeting the reactor physics, thermal-hydraulics, structural and material constraints, operation of the reactor and economic competitiveness. On the other hand, there are also some key questions for developing a reactor which has specific purposes or characteristics. In Figure 2-2, several key questions for the design of an integral nuclear superheater are listed. It should be noted that these questions are connected by multiple arrows because they are often asked iteratively in the course of the design.

A brief discussion of these key questions is provided below:

Production of the saturated steam

For an integral nuclear superheater, the steam coolant is self-supplied rather than from other sources. There are two common ways to produce saturated steam: boiling and

flashing. Boiling is widely adopted by the existing LWRs for generating saturated steam. The performance of steam production is reliable, either by means of direct boiling in the core (BWRs) or a steam generator (PWRs). Flashing or flash evaporation is well adopted by the geothermal power plants to produce saturated steam. The flash steam is formed when a heated liquid stream suddenly undergoes a reduction in pressure.

Flashing has not been used by LWRs due to the potential water-hammer hazards in the piping, low exergy efficiency in steam production [27-28] and other reasons. However, it might be worthwhile to reevaluate the feasibility of applying a flash evaporator to an integral nuclear superheater. An illustration of producing steam by flashing for an integral nuclear superheater can be found in the literature [29-30].

Separation

The means and location of the separation are important design features of an integral superheat reactor. There are many possibilities to perform separation. The steam can be separated from the two-phase mixture by a combination of chimney and gravity; or separator and forced circulation; or other innovative ways. The location of separation can be either in the vessel or outside of the vessel. Although the available space is quite limited, it is preferable to have the separation done in the vessel to avoid the need for additional loops and tank space, which increase the capital cost and provide a potential location for the loss of coolant accident (LOCA).

In the literature, some creative ways of performing separation have been proposed for an integral superheat reactor. For example, Ammon [31] integrated a chimney into the fuel assembly to achieve separation within the assemblies. Campbell [32] invented a device which allows steam to be separated from the two-phase mixture in fuel assemblies. Huet [33] invented a new type of fuel element which equips a helical apparatus to perform separation within each fuel rod.

On the other hand, separation may be not necessary for a specific design. Kluge [34] developed a conceptual superheat reactor, in which the water coolant is fully vaporized in

the fuel assemblies. Tower [35] suggested a pressure tube type integral nuclear superheater. The feedwater enters each pressure tube and is heated continuously during a plurality of passes till converting into superheated steam.

Heat source for boiling and superheating

The arrangement of heat for boiling (or increasing the water temperature if flashing is adopted for steam production) and superheating defines the main direction of the design. The fission energy generated in the core can be manipulated in many ways to boil the water coolant and superheat the formed steam. For example, an addition of a secondary system may be used for both boiling and superheating. Table 2-1 provides a matrix to distinguish the different arrangements of heat addition. Form the author's perspective, this might be a good initial question for a designer to start his/her work.

Selection of the fuel element type

After the heat sources have been arranged for boiling and superheating, one should contemplate which type of fuel element is more compatible with the design. The common options of the fuel element are (a) solid pin; (b) annular fuel which can be cooled internally and externally and (c) pressure tube. Other innovative fuel elements may also be applied.

2.3.2 Introduction of Direct and Indirect Heating Approaches

The current LWRs can be generally categorized into two types: (a) indirect boiling — if the feedwater does not boil in the core, such as PWRs; or (b) direct boiling — if boiling takes place in the core, such as BWRs. Similarly, the integral nuclear superheaters can also be categorized into two types: indirect superheating and direct superheating. As shown in Figure 2-3, the former approach uses means other than directly contacting the core to superheat steam while in the later approach steam is superheated directly in the core.

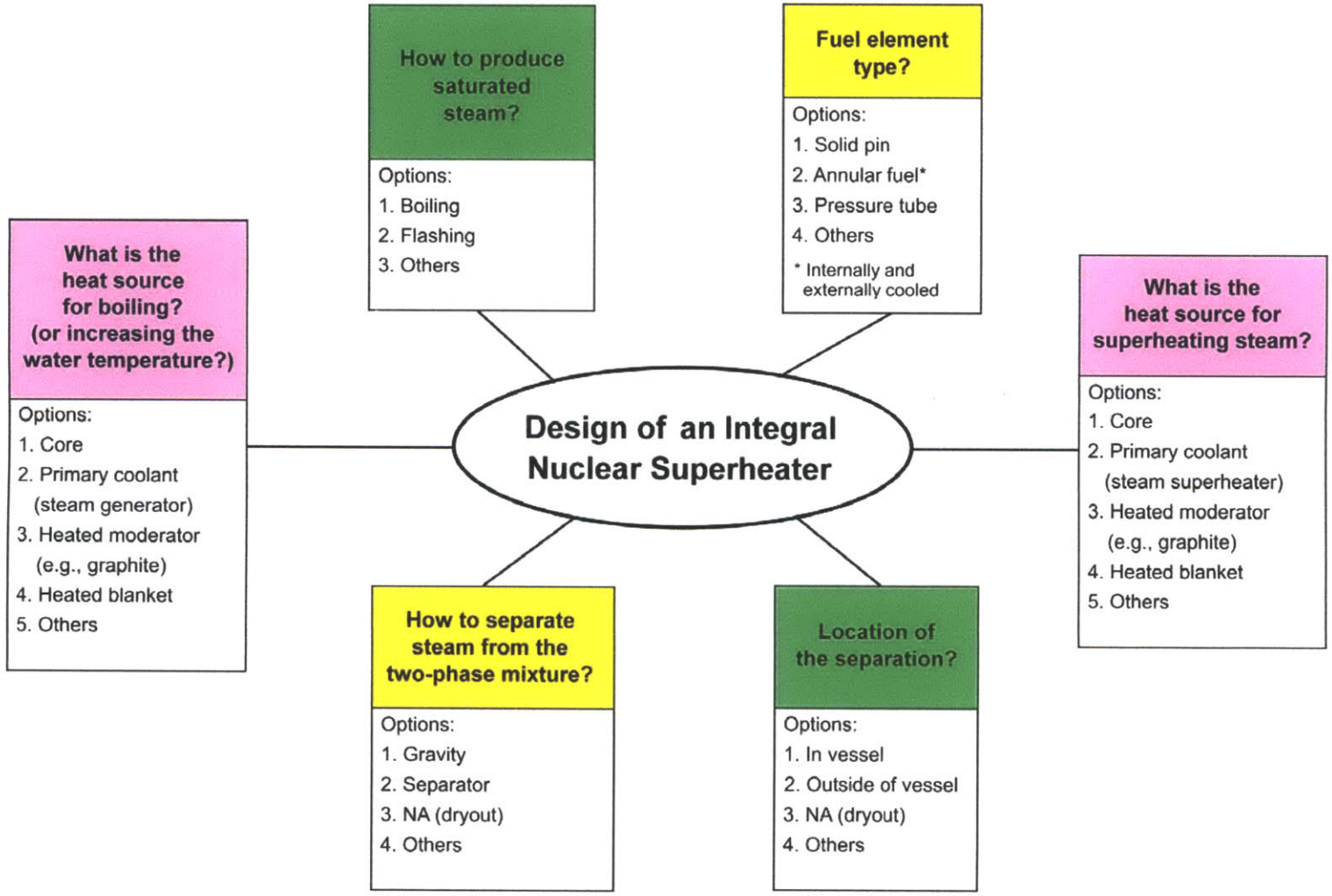

Figure 2-2 Key questions for the design of an integral nuclear superheater

Table 2-1 Matrix of the direct and indirect heating approaches

	Boiling does not occur in the reactor core*	**Boiling occurs in the reactor core**
Superheating of steam occurs in a heat exchanger	**Type I** "Indirect boiling" or "flashing" + "Indirect superheating"	**Type II** "Direct boiling" + "Indirect superheating"
Superheating of steam occurs in the reactor core	**Type III** "Indirect boiling" or "flashing" + "Direct superheating"	**Type IV** "Direct boiling" + "Direct superheating"

*Producing saturated steam by flashing is considered as Type I or Type III in this matrix

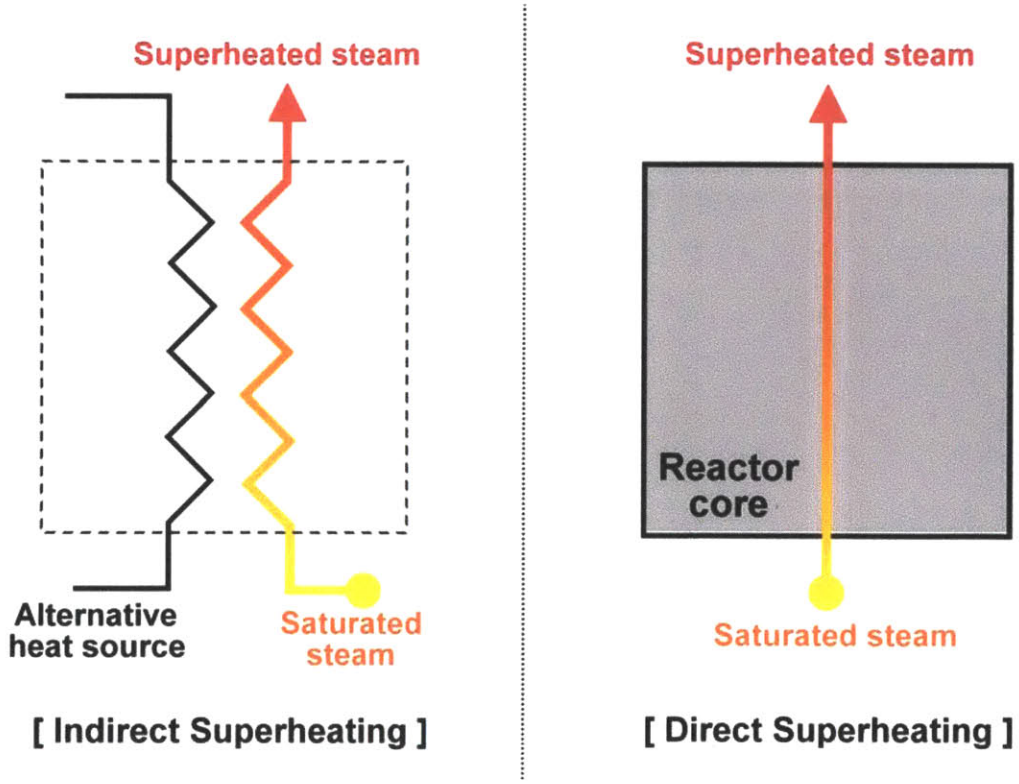

Figure 2-3 Indirect and direct superheating approaches

The design of an integral nuclear superheater is flexible in terms of the options for heating. As shown in Table 2-1, there are four combinations, of types, for designers to contemplate their work. In the literature, all these four types of integral nuclear superheaters have been proposed. The indirect and direct superheating approaches are discussed in detail in the following sections.

2.3.3 Indirect Superheating Approach

The primary advantage of the indirect superheating approach is to avoid the interaction between steam and the core, which may simplify the core arrangement and provide easiness for the neutronic design. If steam is superheated in the core, usually there is no sufficient moderation in the superheating region of the core and compensating means, such as water rods, have to be implemented. On the other hand, the indirect superheating approach requires the core to first heat up an intermediate heat transmission element, and then let the element transmit the energy to steam. The plant efficiency may be lowered due to these additional heat exchanges.

In the literature, many alternative methods have been proposed to indirectly superheat the steam coolant. Some of these ideas are not practical for now but may become possible in the future when advanced technologies are developed. Gas-cooled and liquid-metal-cooled reactors are not discussed below because they are not within the scope of this work.

The Type I Design

Metcalf [29] invented an integral nuclear superheater which employs a plurality of tubes or conduits formed of a highly neutron absorbent material, such as boron steel alloy, to superheat steam. The steam flows upwardly through the tubes and is superheated. As described in Metcalf's work, the tubes are supposed to be heated to a relatively high temperature by nuclear reaction, resulting from a continuation of neutron bombardment.

Wigner [30] proposed a superheat reactor which is graphite moderated and produces saturated steam by flashing. The saturated steam is then conveyed through a line into a steam inlet header. The header is connected to a plurality of steam tubes of any suitable material, such as stainless steel or beryllium having a relatively small neutron capture cross section. The steam is conveyed upwardly through the tubes, which pass through the neutron moderator. Thus, the steam passing through the tubes is superheated by heat developed within the graphite moderator as the result of the nuclear fission chain reaction.

Hackney [38] developed a reactor which uses a large heat exchange system to perform both boiling and superheating. A pressurized organic liquid is chosen as the primary coolant on account of its low vapor pressure, which allows the primary coolant to remain in liquid phase under high temperature conditions without considerably raising the pressure of the primary coolant. The secondary coolant (feedwater) flows into the annular region of the heat exchange system where it is allowed to boil. The two-phase mixture is separated by the cyclone steam separators. The separated steam then flows through the inner zone of the heat exchange system where it is superheated.

The Type II Design

Bryan [36] designed a reactor which utilizes a plurality of fertile material elements arranged in a closed blanket chamber which longitudinally embraces the core. Means are provided for generating steam from the heat released in the core and the steam is superheated by the heat released in the fertile material of the blanket. The fertile material and fuel elements are arranged to be interchangeably positioned and their position is programmed in respect to time of exposure in the reactor so that the percentage of heat absorbed in the blanket compared to the heat given up in the core is a substantially constant ratio over a long period of operation.

Ammon [37] invented a PWR type integral nuclear superheater. This reactor employs a

steam generator and a steam superheater. The high pressure primary coolant first flows through the steam superheater to heat the steam coolant and then flows through the steam generator to vaporize the feedwater.

2.3.4 Direct Superheating Approach

The direct superheating approach has been attempted many times in the past. All the integral nuclear superheaters constructed during the 1950s and the 1960s were based on the direct superheating approach. The main advantage of this approach is to directly use the fission energy to superheat steam. Since the fuel elements have the highest temperature within the reactor, the steam coolant can be superheated to a higher temperature level than the indirect superheating approach can offer. In other words, the superheated steam can have a higher temperature, thus higher plant efficiency, if the direct superheating approach is adopted.

However, the direct superheating approach also complicates the design because the steam coolant is a poor moderator. Alternative means have to be implemented to achieve a fairly thermal spectrum. In addition, control problems and a positive temperature reactivity coefficient may be incurred when the coolant and moderator are separated. If boiling and superheating both take place in the core (i.e., Type IV in Table 2-1), the design becomes more challenging. Insulation between the boiling and superheating regions, an uneven neutron spectrum across the core, and a reactivity insertion accident due to water flooding into the superheating region are the major concerns for a Type IV design.

The Type III Design

A representative of the Type III design (indirect boiling, direct superheating) is a pressure tube superheat reactor proposed by Russia in 1958 at the second United Nations international conference on the peaceful uses of atomic energy [20]. The Russian superheat reactor is moderated by graphite and cooled by light water (the primary coolant)

and steam. The reactor core is divided into two parts, one part for heating the primary coolant and the other part for superheating steam. The primary coolant is heated in the designated part of the core, and then flows through the steam generator where the secondary coolant, which is also light water, is allowed to boil. The saturated steam produced in the steam generator is separated from the two-phase mixture in the separator and then directed into the other part of the core for superheating. More details about the Russian superheat reactor are given in Appendix A.

The Type IV Design

For the Type IV design (direct boiling, direct superheating), usually the reactor core is divided into two or more regions for boiling and superheating, respectively. In the literature, there are four general concepts to configure the core: (a) two-region; (b) multi-region; (c) single assembly and (d) single element.

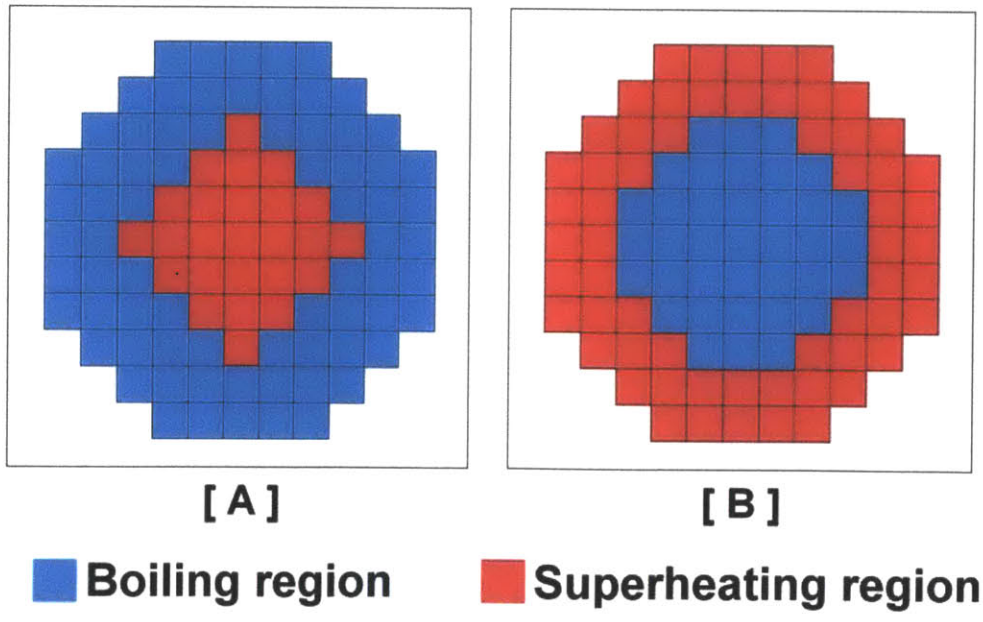

Figure 2-4 The two-region concept

(a) The Two-region Concept

Figure 2-4 is an illustration of the two-region concept, by which the reactor core is divided into one region for boiling and the other region for superheating. The conventional way is to adopt a central superheating region as "A" shown in Figure 2-4, or a peripheral superheating region as "B" in Figure 2-4. In the past, two integral nuclear superheaters were constructed based on this "two-region" concept. Pathfinder in South Dakota [10] employed the central superheater while the BONUS reactor in Puerto Rico [11-12] had the superheater on the periphery.

The major challenges of this concept are: (1) the reactor perhaps needs two different fuel assembly designs for the boiling and superheating regions; (2) the spectrum hardness varies between the boiling and superheating regions, which complicates control and operation of the reactor; (3) thermal insulation between the boiling and superheating regions is required; (4) the flow configuration including the means and location of separation needs to be considered thoroughly.

Furthermore, it is interesting to evaluate the impacts of the location of superheater on the neutron economy. Previous research results [39] indicate that a superheater on the periphery may have better neutron economy since the material, such as stainless steel, used for structural purposes in the superheater fuel assemblies has a high neutron absorption cross section, locating the superheater region at the radial periphery of the core, where the neutron flux is low, could minimize the amount of neutron absorbed by structural materials. On the other hand, previous studies also indicate that both the central and peripheral superheater arrangement may be not suitable for a medium or large reactor because of radial peaking issues [116]. However, it should be noted that these results are not universal and need to be further verified if the two-region concept is applied.

(b) The Multi-region Concept

In view of the uneven neutron spectrum across the two-region core, the multi-region concept has been proposed to address this issue. Figure 2-5 is an illustration of the multi-region concept, by which the reactor core is divided into multiple boiling and superheating regions. There are many possibilities for a multi-region design. The first example is to divide the core into three regions such as "A" and "B" shown in Figure 2-5. A conceptual design proposed by Linsenmeyer [40] in 1960 is a representative of this "three-region" or "sandwich" core concept. The second example is to divide the core into several regions like "C" in Figure 2-5. Valter [41] and Wadmark [42] developed their designs based on this concept. The third example is to have two types of fuel assembly for boiling and superheating, respectively, and then arrange these assemblies uniformly within the core. As a result, the core will look like a "checker board" as shown in "D" of Figure 2-5. Harrer et al. [43] developed a reactor which features this "checker board" core arrangement.

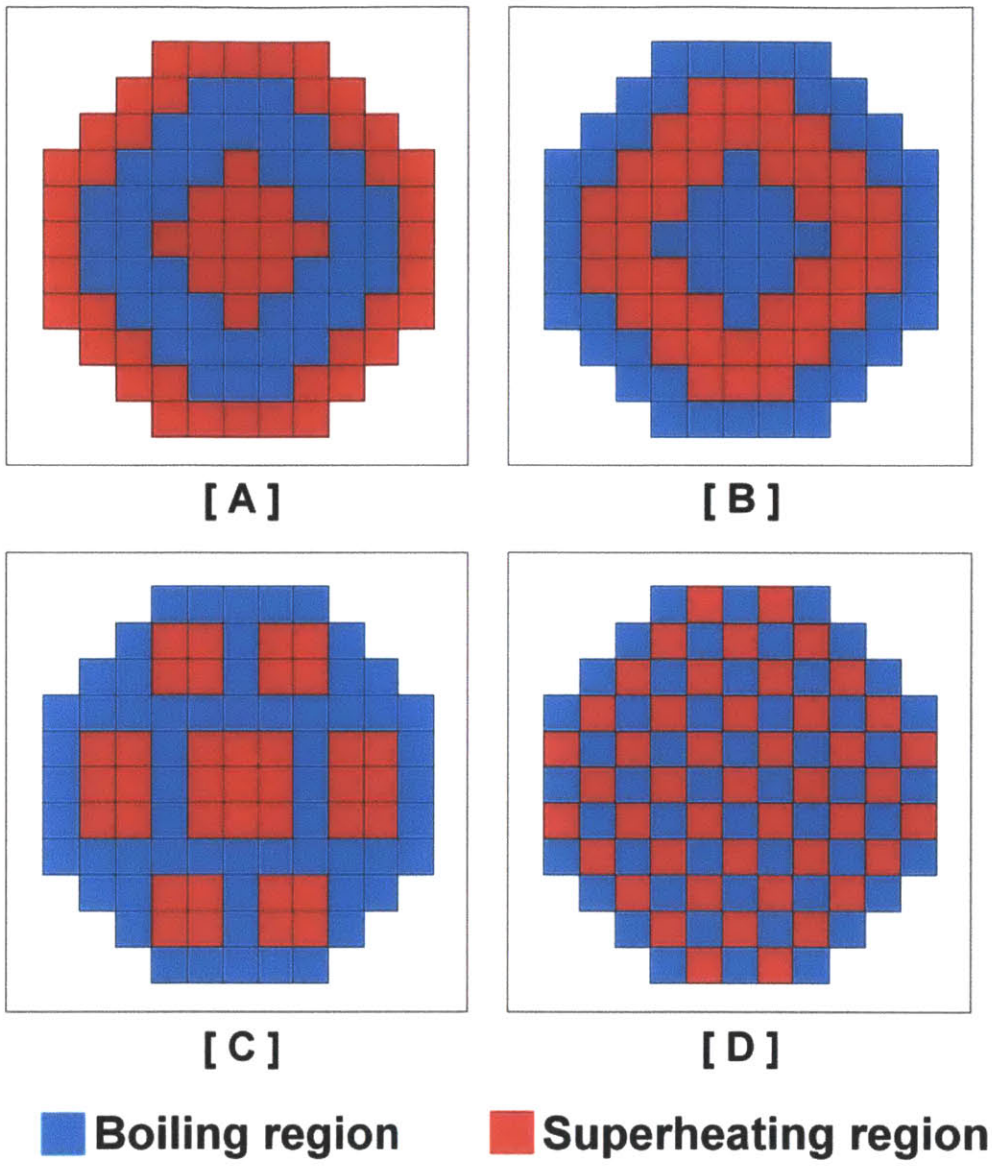

Figure 2-5 The multi-region concept

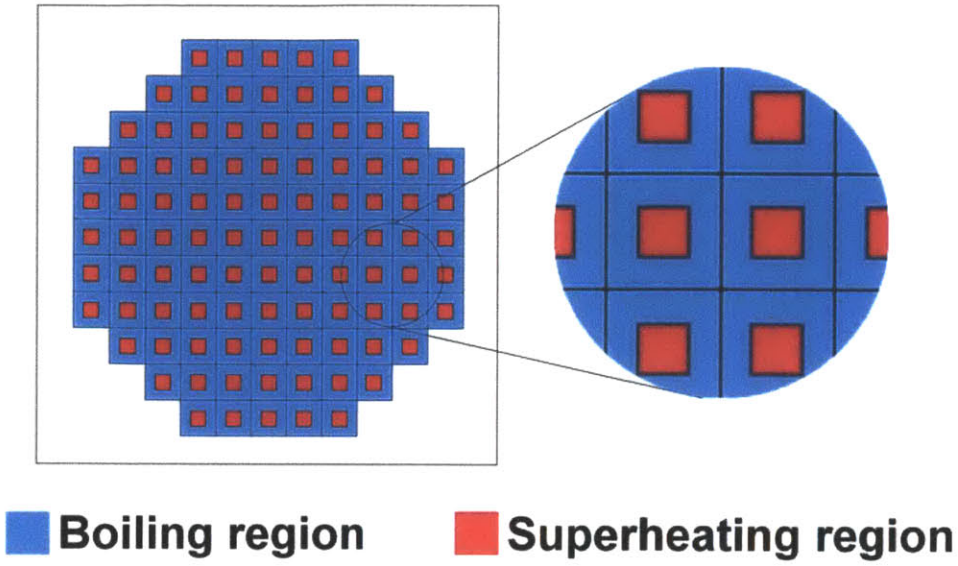

Figure 2-6 The single assembly concept

(c) The Single Assembly Concept

To achieve further uniformity of the boiling and superheating arrangement, the single assembly concept has been proposed. Figure 2-6 is an illustration of the single assembly concept. The essence of this concept is to use half of the assembly for boiling and the other half of the assembly for superheating. Therefore, each assembly is a boiler as well as a superheater. Based on this concept, Campbell [32] and Wheelock [44] conceptually developed their integral nuclear superheaters which could perform boiling and superheating within each assembly.

(d) The Single Element Concept

The multi-region and single assembly concepts may provide a more uniform spectrum than the two-region concept does, but the insulation problems are not solved and even exacerbated due to the scattered superheating regions. One of the solutions to address

this issue is using annular fuel elements, which could be internally and externally cooled, to avoid the need for insulation. This is called the single element concept, by which the annular fuel is cooled externally by water and internally by steam or vice versa. Therefore, in contrast to the single assembly concept, each fuel element is a boiler as well as a superheater. The main advantages of this concept are: (1) the boiling and superheating regions are properly separated by the annular fuel structure; (2) only one type of fuel element, assembly and control rod is needed; (3) in the event of losing steam coolant, the decay heat can be transferred by the external water coolant; (4) The surrounding water can provide sufficient moderation and a uniform thermal spectrum is expected.

On the other hand, there are also many challenges to be overcome in order to apply this concept, such as: (1) a desirable power split during the fuel cycle; (2) the uneven axial expansion between the inner and outer claddings; (3) start-up, shutdown, and operation of the reactor; and (4) guarantee of the long-term fuel performance.

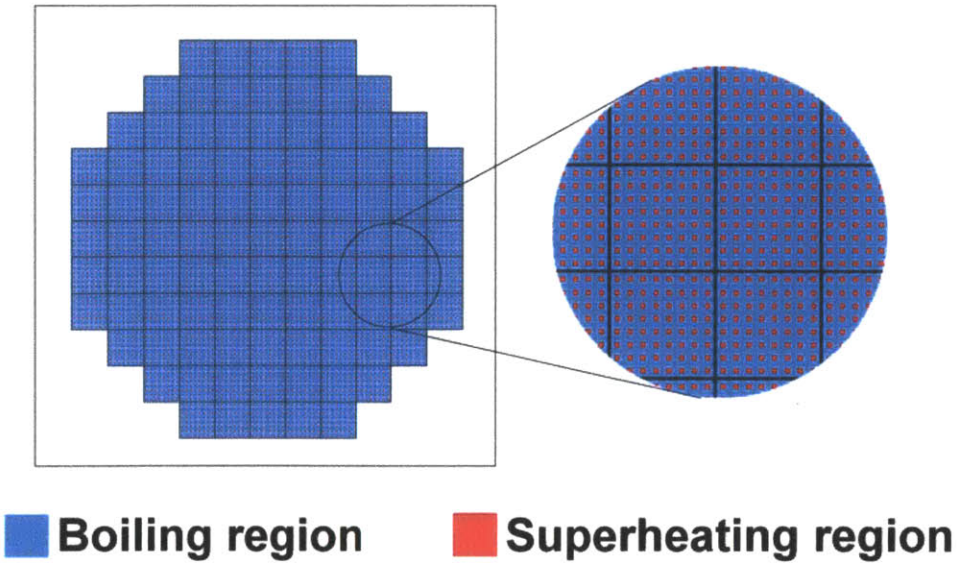

Figure 2-7 The single element concept

Researchers in Germany proposed and constructed a superheat reactor based on this concept during the late 1960s [17]. In the literature, there are several conceptual designs which employ annular fuel elements for superheating steam. Treshow [46] invented a horizontal superheat BWR with large annular fuel elements. Heckman [47] developed a reactor featuring a liquid control system and annular fuel elements, which are cooled internally by water and externally by steam. Huet [33] designed a novel fuel element, which is composed of three concentric tubes. Only the innermost and outermost tubes contain fissile material. The intermediate tube does not contain fissile material but equips a helical apparatus for separation. The feedwater flows within the outermost tube and boils, and then the steam-water mixture flows through the space between the intermediate and innermost tubes where the saturated steam is separated. Finally the saturated steam flows into the innermost tube and gets superheated.

2.3.5 Summary of the Design Approaches

The design of an integral nuclear superheater is flexible in terms of the options of heating. Based on how the boiling (or flashing) and superheating are performed, four types of heating approaches can be categorized as listed in Table 2-1. In general, the integral nuclear superheaters can be categorized into two types: indirect superheating and direct superheating. The former approach uses means other than directly contacting the core to superheat steam, while in the later approach steam is superheated directly in the core. Advantages and disadvantages of the indirect and direct superheating approaches are compared in Table 2-2.

The direct superheating approach, in particular the Type IV design (direct boiling and superheating), has received a lot of interest since the 1950s. All the integral nuclear superheaters constructed in the history are based on this direct boiling and superheating concept. Usually for the Type IV design, the reactor core is divided into two or more regions for boiling and superheating, respectively. In the literature, there are four general concepts to divide or arrange the core: (a) two-region; (b) multi-region; (c) single assembly and (d) single element.

Table 2-2 Comparison of the indirect and direct superheating approaches

Indirect Superheating	Direct Superheating
Definition: Steam is not superheated in the core.	Definition: Steam is superheated in the core.
Advantages: • There is no interaction between the core and steam coolant, which can avoid the problem of insufficient moderation in the superheating region of the core. • Only one type of fuel element, assembly design and control rod system is needed. • There are a variety of options for the reactor coolant, such as gas, molten salt and liquid metal.	**Advantages:** • Fission energy can be directly used to superheat steam. • Water and steam properties are well known and there is plenty of experience in LWR operation. • A heat exchanger and additional loops are not needed for superheating, which avoids the potential location for LOCA.
Disadvantages: • A heat exchanger is required to superheat steam, which may increase the capital cost and lower the plant efficiency. • Specific challenges may be incurred if the primary coolant is gas, molten salt or liquid metal.	**Disadvantages:** • Depending on the design, two types of fuel element, assembly design and control rod system may be needed for the boiling and superheating regions, respectively. • Flow configuration may be complicated if both boiling and superheating are taking place in the reactor vessel.

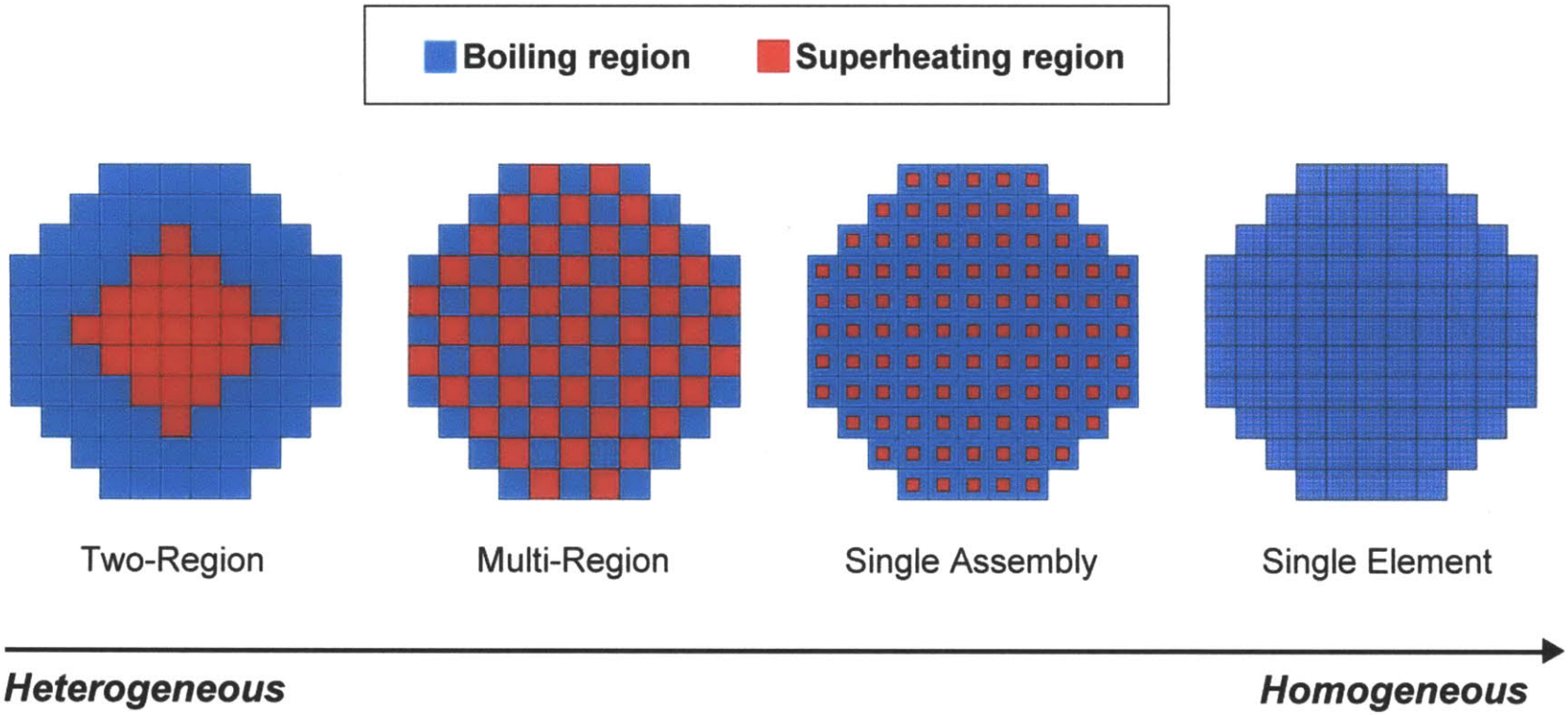

Figure 2-8 Comparison of the four direct boiling and superheating design concepts

One typical issue for the Type IV design is the difference in spectrum hardness between the boiling and superheating regions. The uneven neutron spectrum across the core will result in reactor control and operation difficulties. The conventional way to tackle this problem is to further divide the core and use water rods or other means to improve the moderation in the superheating region. However, this creates the burden of insulation and complicates the fuel design. The alternative solution is to use the annular fuel elements (the single element concept) for both boiling and superheating. Figure 2-8 illustrates the four Type IV design concepts. As shown in Figure 2-8, the two-region concept is quite heterogeneous and the single element concept is the most homogeneous one in terms of the distribution of the boiling and superheating regions. The more homogeneous the distribution is, the more uniform the neutron spectrum is expected. Characteristics of these four concepts are lasted in Table 2-3.

Table 2-3 Characteristics of the direct boiling and superheating concepts

	Characteristics
Two-region	• The core is divided into two regions for boiling and superheating, respectively. • Two types of fuel element, assembly and control rod designs are required. • Insulation between the boiling and superheating regions is needed.
Multi-region	• The core is divided into multiple regions for boiling and superheating, respectively. • Two types of fuel element, assembly and control rod designs are required. • Insulation between the boiling and superheating regions is needed.
Single assembly	• Each fuel assembly is a boiler as well as a superheater. • Two types of fuel element may be required. • Insulation between the boiling and superheating regions is needed.
Single element	• Each fuel element is a boiler as well as a superheater. • A desirable power split and long-term fuel performance need to be guaranteed. • The issue of uneven axial expansion between the inner and outer cladding has to be addressed.

2.4 Summary of the Historical Superheat Nuclear Reactors

In the past, several nuclear power plants with integral or non-integral superheaters have been built and operated. Most of these reactors were small and had low power level since they were intended to provide a demonstration of the concept. Unfortunately, due to mechanical failures, lack of research funding and other reasons, all these prototype superheat reactors had been shut down and decommissioned. Although these old superheat reactors did not have satisfactory performance, they provided valuable operating data and experience.

Table 2-4 lists the nuclear reactors with superheat constructed in the history. Three nuclear power plants with fossil-fired superheaters are listed, they are: the Elk River reactor, Indian Point unit 1 and the Carolinas–Virginia tube reactor (CVTR). One separate nuclear superheater, the ESADA Vallecitos experimental superheat reactor (EVESR), is introduced. In addition, eight integral nuclear superheaters are listed in Table 2-4: the Obninsk nuclear power plant (Atomic Power Station 1, APS-1), the boiling water experimental reactor V (BORAX-V), the Pathfinder reactor, the boiling nuclear superheater (BONUS), the Beloyarsk nuclear power station unit 1 (Beloyarsk-1 or AMB-100) and unit 2 (Beloyarsk-2 or AMB-200), the Marviken boiling heavy-water superheat reactor (the Marviken or R4 reactor) and the German superheat reactor (Heissdampfreaktor, HDR).

Table 2-5 summarizes the design characteristics of these reactors. Details of these historical superheat reactors are given in Appendix A.

Table 2-4 List of nuclear reactors with superheat

Reactor	Year	Location	Note**
A. Nuclear Power Plant with Fossil-fired Superheater			
Elk River	1962 ~ 1968 [48]	Elk River, MN, USA	BWR
Indian Point-1	1962 ~ 1974 [49]	Buchanan, NY, USA	PWR
CVTR	1963 ~ 1967 [50]	Parr, SC, USA	Pressure tube
B. Non-integral Nuclear Superheater			
EVESR	1963 ~ 1967 [51]	Pleasanton, CA, USA	Steam-cooled
C. Integral Nuclear Superheater			
APS-1	1954 ~ 2002 [81]	Obninsk, Russia	Type IV
BORAX-V	1962 ~ 1964 [52]	Idaho Falls, ID, USA	Type IV
Pathfinder	1964 ~ 1967 [10]	Sioux Falls, SD, USA	Type IV
BONUS	1964 ~ 1968 [12]	Rincón, Puerto Rico	Type IV
Beloyarsk-1	1964 ~ 1983 [53]	Beloyarsk, Russia	Type III
Beloyarsk-2	1967 ~ 1990 [79]	Beloyarsk, Russia	Type IV [84]
Marviken (R4)	Cancelled* [19]	Marviken, Sweden	Type IV
HDR	1969 ~ 1971 [56]	Karlsruhe, Germany	Type IV

* Construction started in 1962 but the project was cancelled in 1970

** Type III = indirect boiling, direct superheating;
Type IV = direct boiling and superheating (see Table 2-1)

Table 2-5 Design characteristics of the nuclear power plants with superheat (1/2) [13, 18, 21, 45, 50, 60]

Reactor	Designer	Moderator	Coolant	Thermal Power (MWt)*	Electric Power (MWe)	Efficiency (%)*	Steam Exit Temp.(°C)	Material*	
								Fuel	Clad
A. Nuclear Power Plant with Fossil-fired Superheater									
Elk River	AC	H_2O	H_2O	58.2 (N) 14.8 (F)	22.5	30.8	441	UO_2–ThO_2	SS
Indian Point I	B&W	H_2O	H_2O	585 (N) 215 (F)	255	32.0	538	UO_2–ThO_2	SS
CVTR	West.	D_2O	D_2O	65	19	29.2	385	UO_2	Zr-4
B. Non-integral Nuclear Superheater									
EVESR	GE	H_2O	Steam	17	---	---	493	UO_2	SS
C. Integral Nuclear Superheater (US design)									
BORAX-V	ANL	H_2O	H_2O & steam	35.7	3.5	(T)	454	UO_2 (B) UO_2–SS cermet (S)	304 SS (B) 304 SS (S)
BONUS	GNEC	H_2O	H_2O & steam	50	16.3	32.6	482	UO_2 (B) UO_2 (S)	Zr-2 (B) 316 SS (S)
Pathfinder	AC	H_2O	H_2O & steam	203	62	30.5	441	UO_2 (B) UO_2–SS cermet (S)	Zr-2 (B) 316L SS (S)

*(N) = Nuclear power plant; (F) = Fossil fuel power plant; (T) = Test reactor; (B) = Boiler; (S) = Superheater

Table 2-5 Design characteristics of the nuclear power plants with superheat (2/2) [45, 57, 58, 59, 60, 61, 78, 83]

Reactor	Designer	Moderator	Coolant	Thermal Power (MWt)*	Electric Power (MWe)	Efficiency (%)*	Steam Exit Temp.(°C)	Material*	
								Fuel	Clad
C. Integral Nuclear Superheater (non-US design)									
APS-1	USSR	Graphite	H_2O & steam	30	5	(T)	299	U-alloy	SS
Beloyarsk-1	USSR	Graphite	H_2O & steam	285	94	33	500	U-alloy	SS
Beloyarsk-2	USSR	Graphite	H_2O & steam	457	160	35	500	U-alloy	SS
Marviken	Sweden	Graphite	D_2O	593	200	33.7	475	UO_2 (B) UO_2 (S)	Zr-2 (B) Inconel (S)
HDR	Germany	H_2O	H_2O & steam	100	25	25.0	457	UO_2 (B) UO_2 (S)	SS (B) Inconel (S)

*(N) = Nuclear power plant; (F) = Fossil fuel power plant; (T) = Test reactor; (B) = Boiler; (S) = Superheater.

2.5 Summary of the Conceptual Designs of Nuclear Superheaters

Many conceptual designs of the superheat nuclear reactor have been proposed in the past. Most of them are light water cooled and moderated, boiling water reactor with integral or separate nuclear superheaters. Conceptual designs of nuclear superheaters that are published in journals, proceedings or filed as US patents are summarized in this section.

2.5.1 The 1956 conceptual design

In 1956, the Argonne National Laboratory (ANL) proposed a conceptual design for a superheat BWR and published the results in the journal "*Nuclear Science and Engineering*" [76]. The design employs tubular fuel elements to increase heat transfer area. Figure 2-9 shows the simplified flow configuration of the reactor which illustrates the steam and water distribution in the vessel.

The proposed reactor was designed to have an output of 10 MWt in the form of superheated steam at 600 psi and 700 °F. As shown in Figure 2-9, the fuel tubes were placed horizontally in a pressure vessel, similar to the celebrated Canadian deuterium-uranium reactor (CANDU).

The boiling water rises between the tubes, and the saturated steam, separating at the surface by gravity, passes through a pipe connection from the steam dome to a chamber adjoining the left tube sheet of the reactor core. The fuel tubes which are placed beyond a certain radius from the center line of the core are used for the primary pass of the steam. The saturated steam is first dried and superheated in this primary pass. The steam then flows through those tubes to a plenum chamber at the right. The final pass is through the centrally located tubes in which the heat generation is at maximum. The saturated steam (486 °F) would be superheated to 700 °F when passing through these fuel tubes. A central baffle cylinder in the steam chamber guides the superheated steam to the outlet pipe in the pressure vessel closure plug.

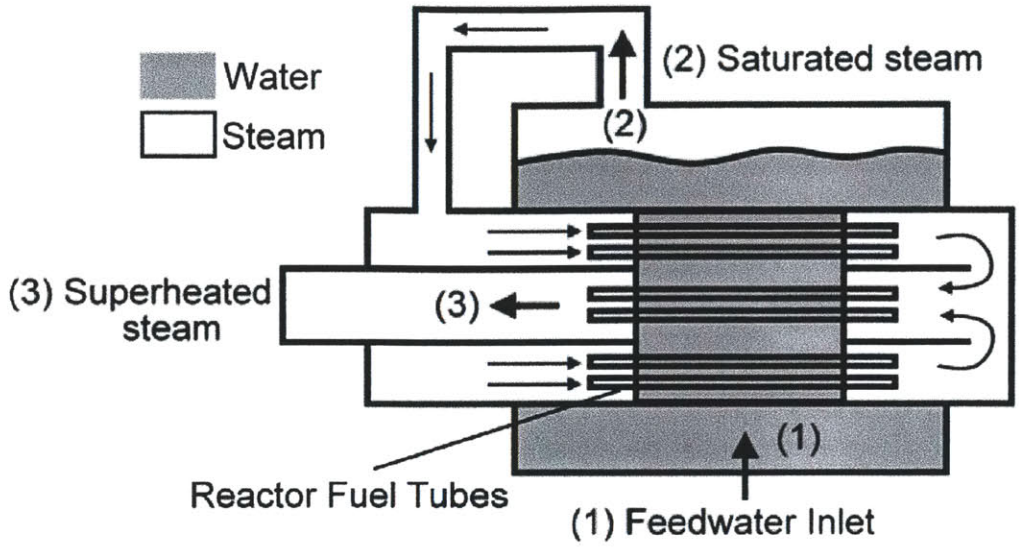

Figure 2-9 The ANL 1956 conceptual design [76]

2.5.2 The 2007 conceptual design

In 2007, a conceptual design of superheat BWR was proposed by Ferrara and Hochreiter [77]. The proposed reactor employs a central superheater in the core and has exit steam conditions at 850 °F and 1050 psia. Figure 2-10 shows the proposed flow paths of the design.

As shown in Figure 2-10, the design has a two-pass core. The boiler is located on the periphery and the superheater in located in the center of the core. A saturated two-phase mixture is generated in the boiler region and passes through the separators, which are at top of the boiler. Following that the saturated steam flows into the superheating region in core to be heated to 850 °F.

The boiler region would use the conventional BWR fuel assemblies with UO_2 fuel pellets and Zircaloy-2 cladding. The superheat core region uses UO_2 fuel and stainless steel or

Inconel as cladding material. Zirconium-hydride encased in the stainless steel cladding is proposed to be used to enhance the moderation in the superheating region. According to the authors [77], the objective of this design would be to keep enrichment at a maximum of 5% while achieving the necessary power output.

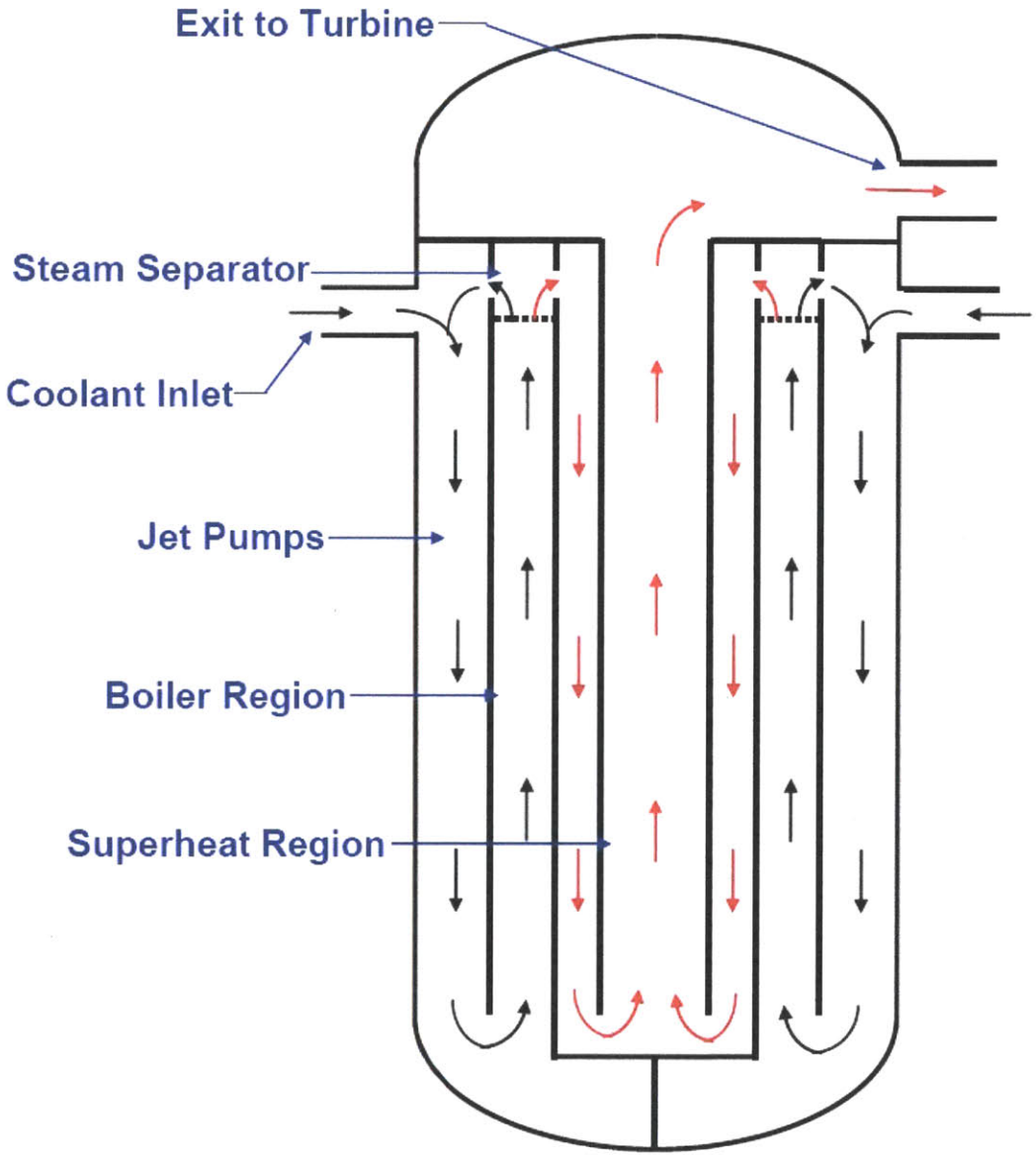

Figure 2-10 The 2007 conceptual design of Ferrara and Hochreiter [77]

2.5.3 The three pass core design proposal for a HPLWR

In 2008, Schulenberg et al. [93] proposed a three pass core design for the high performance light water reactor (HPLWR). The HPLWR is a reactor concept of the fourth generation which is cooled and moderated by water at supercritical pressures. Although it is proposed for a supercritical water reactor, this three pass core design is worthwhile to be described here for two reasons. First, it has similarity to Pathfinder, the BONUS reactor and Ferrara's work [77] that the reactor core is divided into multiple regions and the coolant is allowed to make a 180-degree turn to flow through the entire core. Second, its target coolant outlet temperature of 500 °C is within the same temperature level pursued by a typical superheat reactor. Therefore, research results and considerations of this three pass core design can certainly benefit and inspire a design for the integral nuclear superheater.

The three pass core design is based on the assembly design concept of Hofmeister et al [94]. The three-pass approach was chosen to alleviate the hot channel peaking, which is typically a major issue of a supercritical water reactor. The density ratio between core outlet steam and inlet feedwater is more than a factor of 8. This ratio exceeds even the density ratio across a core of a BWR. Therefore, the fuel assemblies are housed in assembly boxes to provide additional moderator water in the gaps between the assemblies like in a BWR. Inlet orifices are also installed to avoid flow instabilities. The moderator water flowing downwards through gaps between the assembly boxes and through the moderator boxes is mixed with downcomer water in the inner part of the lower mixing chamber to yield a mixed water coolant at the core inlet.

Figure 2-11 shows the proposed flow path in the three pass core design concept. The mixed water coolant is first heated up from 310 °C to 390 °C in the evaporator formed by a total 52 clusters with upward flow in the core center. Then, the water coolant enters the upper mixing chamber, where it makes a 180-degree turn and enters the first superheater. The first superheater is surrounding the evaporator and is formed by another 52 clusters. The water coolant is heated to 433 °C with a downward flow in the

first superheater. Finally, the water coolant again makes a 180-degree turn to enter the second superheater where it is superheated to 500 °C.

Austenitic stainless steel and Inconel have been proposed as cladding material for the HPLWR [93]. After a series of tests, a high temperature working limit of 620 °C has been assumed for the cladding material candidates. Preliminary calculation indicates that the peak cladding temperature of this design is 625 °C.

Due to the three passes that form a long flowing path through the core, the resultant pressure drop of the coolant is higher than the existing BWRs. Given a mass flow rate of 1160 kg/s and an electric power output of 1000 MWe, around 900 kW or 0.09% of the electric power, equivalent to 0.04% points of the net efficiency, is lost as a result of the excessive pressure drop. However, this can be easily offset by the expected plant efficiency of 40% at steam conditions of 500 °C.

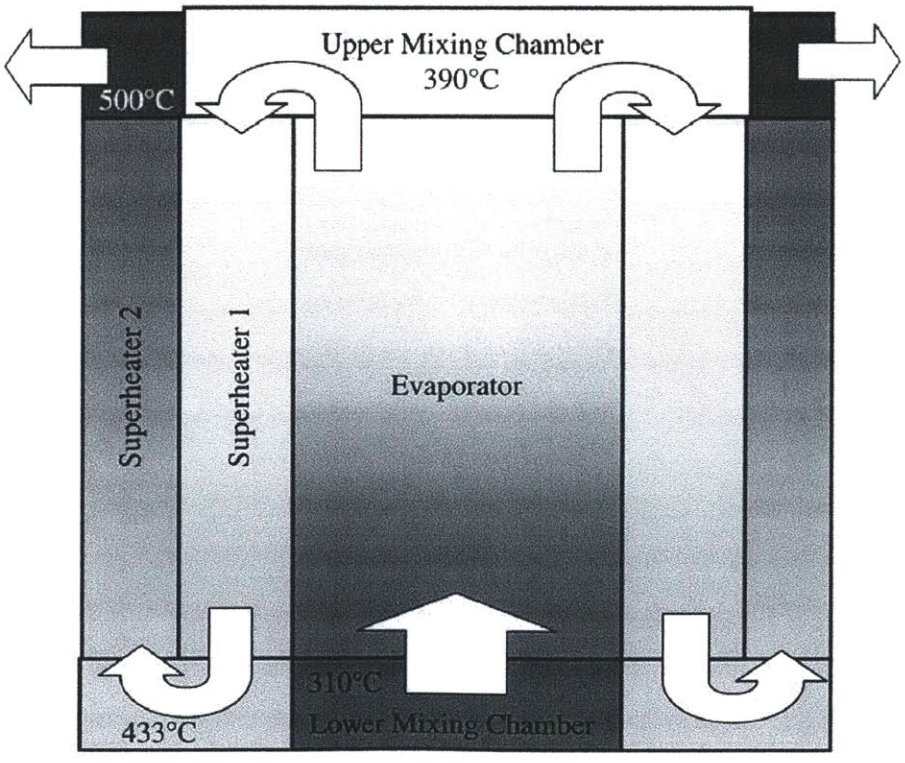

Figure 2-11 Flow path in the three pass core design concept [93]

2.5.4 The US patents of nuclear superheaters

In addition to the abovementioned three designs, there are more than 30 conceptual designs filed as U.S. patents. Table 2-6 lists the U.S. patents of the non-integral nuclear superheater. Table 2-7 lists the U.S. patents of the integral nuclear superheater. Gas-cooled and liquid-cooled reactors, although can be used to produce superheated steam, are not included in Table 2-6 and 2-7. These designs have innovative features to embody the concept of nuclear superheat. Table 2-8 summarizes the features of the patented integral nuclear superheaters. These innovative features, by taking advantage of today's technology, may become feasible and should be reconsidered in the future.

Table 2-6 U.S. patents of the non-integral nuclear superheater

U.S. Patent #	Filed Year	Title	Ref.
3,085,959	1959	Liquid Moderated Vapor Superheat Reactor	[71]
3,108,938	1959	Power Plant Using A Steam-Cooled Nuclear Reactor	[72]
3,188,277	1960	Superheater Reactor	[73]
3,212,986	1964	Three Tank Separate Superheat Reactor	[74]
3,575,002	1966	Combination Fossil Fuel and Superheated Steam Nuclear Power Plant	[75]
3,634,189	1968	Steam-Cooled Reactor	[70]

Table 2-7 U.S. patents of the integral nuclear superheater

U.S. Patent #	Filed Year	Title	Ref.
2,787,593	1946	Method and Means of Producing Steam in Neutronic Reactors	[29]
2,806,820	1947	Neutronic Reactor	[30]
2,938,845	1957	Superheating in A Boiling Water Reactor	[46]
2,982,712	1958	Boiler-Superheater Reactor	[47]
2,999,059	1958	Nuclear Reactor	[62]
3,034,977	1958	Nuclear Superheater for Boiling Water Reactor	[63]
3,049,487	1960	Direct-Cycle, Boiling-Water Nuclear Reactor	[43]
3,121,666	1962	Nuclear Reactor Fuel Assembly	[44]
3,132,999	1960	Boiling Water-Superheat Nuclear Reactor	[39]
3,150,052	1959	Steam Superheat Boiling Water Nuclear Reactor	[64]
3,153,617	1958	Method of Operating Boiling Coolant Reactor With Positive Reactivity Coefficient	[65]
3,156,626	1962	Nuclear Reactor Supplying Superheated Steam	[33]
3,185,630	1960	Boiling Coolant Reactor With integral Vapor Separation and Nuclear Superheat	[31]
3,206,372	1961	Boiling Water Nuclear Reactor Producing Superheated Steam	[34]
3,218,237	1959	Fuel Element for A Steam Superheat Boiling Water Nuclear Reactor	[66]
3,228,846	1966	Boiling Water Nuclear Reactor With Breeder Blanket Superheater	[36]
3,243,351	1962	Steam Producing Reactor and Fuel Therefor	[32]
3,245,881	1962	Integral Boiler Nuclear Reactor	[37]
3,253,998	1963	Boiling Liquid Nuclear Reactor	[38]
3,276,965	1963	Single Pass Superheat Reactor	[67]
3,284,310	1963	Boiling Water-Superheat Nuclear Reactor	[41]
3,311,540	1964	Integral Boiling and Superheating Nuclear Reactor and Pressure Tube Assembly Therefor	[35]
3,331,746	1965	Tubular Fuel Element for A Nuclear Reactor	[68]
3,454,467	1966	Integral Boiling Water-Superheat Nuclear Reactor	[42]
3,634,189	1968	Steam-Cooled Reactor	[70]
5,116,567	1990	Nuclear Reactor With Bi-Level Core	[69]

Table 2-8 Features of the U.S. patented integral nuclear superheater (1/3)

US patent #	Separation*	Fuel type	Features
2,787,593	Outside of RPV, Flashing	Solid	Steam is superheated by the heat developed within the insulated boron steel tubes as the result of neutron bombardment.
2,806,820	Outside of RPV, Flashing	Pressure tube	Annular fuels are enclosed by graphite. Water flows in the inner channel of the annular fuel. The heat source of superheater is from the heated graphite moderator.
2,938,845	In RPV, G	Annular	The horizontal superheat BWR. There are two paths for the steam flowing in the superheater fuel assemblies. Control plates are utilized.
2,982,712	In RPV, G	Annular	Water flows in the inner channel and steam follows upwardly in the outer channel of the annular fuels. The liquid control system (Hg-Cd) is used.
2,999,059	In RPV, G	Solid	A heavy water cooled and moderated superheat reactor. Fuel rods are the same but shorter in the boiler and longer in the superheater.
3,034,977	In RPV, S	Multi-layer annular	The famous Pathfinder reactor. It features a central superheater with three paths for steam in the superheating assemblies.
3,049,487	In RPV, G	Solid	An illustration of the "checker board" core concept. The superheater fuel assembly can be placed in any order in the core.
3,121,666	In RPV, G	Solid	An illustration of the "single assembly" concept. Each fuel assembly is a boiler as well as a superheater.
3,132,999	In RPV, G	Solid	An illustration of the "three-region" or "sandwich" core concept. This reactor can produce saturated or superheated steam by adjusting a dedicated "three-way valve".

*RPV = Reactor Pressure Vessel; G = Separation is done by gravity; S = Separation is done by separator

Table 2-8 Features of the U.S. patented integral nuclear superheater (2/3)

US patent #	Separation*	Fuel type	Features
3,150,052	In RPV, G	Solid	The reactor equips a central superheater similar to the Pathfinder reactor but steam is separated from the two-phase mixture by gravity.
3,153,617	Outside of RPV, S	Pressure tube	The reactor equips a peripheral superheater, similar to the BONUS reactor. It is light water cooled and heavy water moderated.
3,156,626	In-rod separator	Annular	A helical water-steam separator is integrated in each large fuel rod. Each fuel rod is a boiler as well as a superheater.
3,185,630	In-assembly separator	Annular	The reactor features a cyclone water-steam separator in each assembly. Each fuel rod is a boiler as well as a superheater.
3,206,372	NA (Dry-out)	Solid	The "one-direction" superheat BWR. Water flows upwards along the fuel rod till becoming saturated steam. The saturated steam keeps flowing upwards and gets superheated. Moderation is provided by water surrounding the heating path.
3,218,237	In RPV, G	Solid	Fuel assembly design for the steam superheat boiling water nuclear reactor (US patent # 3,150,052). Solid moderator (Zr-H) is used in the superheater assemblies.
3,228,846	In RPV, S	Solid	The heat source of superheater is from the breeding blanket, which is composed of fertile material elements. Fertile material may be natural uranium or thorium.
3,243,351	In-assembly separator	Solid and Annular	Water flows through the solid fuels and boils. Separation is done in the assembly. The saturated steam flows through the annular fuels and gets superheated.
3,245,881	In RPV, S	Solid	A superheat pressurized water reactor (PWR) equipped one steam generator and one steam superheater. The pressurizer is also integrated in the reactor vessel.
3,253,998	In RPV, S	Solid	A superheat reactor using a pressurized organic liquid as the primary coolant and a large steam generator/superheater.

*RPV = Reactor Pressure Vessel; G = Separation is done by gravity; S = Separation is done by separator

Table 2-8 Features of the U.S. patented integral nuclear superheater (3/3)

US patent #	Separation*	Fuel type	Features
3,276,965	In RPV, G	Solid	Single pass, once through design with very long fuel rods. Intentional highly asymmetric power distribution and would turn the fuel rods upside down for completely use of the fuel.
3,284,310	In RPV, S	Solid	Arcuately bent fuel plates are used to perform separation in the assembly. A heated reflector, which is composed of fissile elements, is used to preheat the steam coolant.
3,311,540	NA (Dry-out)	Pressure tube	Each pressure tube comprises a plurality of concentric annular fuel elements. The liquid coolant enters each pressure tube and is heated continuously during a plurality of passes. The liquid coolant is converted to superheated steam in the heating path.
3,331,746	Outside of RPV, G	Annular	Each fuel rod is a boiler as well as a superheater. Gas-filled insulation is used to optimize the axial heat transfer along the fuel element.
3,454,467	In RPV, G	Solid	The reactor contains a plurality of superheater tubes enclosed by water. Steam flows downward through the superheater elements where it is superheated.
3,634,189	In RPV, G	Solid	The core is cooled by steam and is divided into three parts. This design uses superheated steam exiting from the first two parts of the core as the primary coolant to vaporize feedwater (secondary coolant). Then the primary coolant flows through the third part of the core where it gets superheated to the point of use.
5,116,567	In RPV, G	Solid	This invention provides a special type of BWR with a two-stage core. A lower stage is a conventional BWR core which converts the subcooled water to saturated steam. An upper stage is cooled by the steam from the lower stage and converts it to superheated steam.

*RPV = Reactor Pressure Vessel; G = Separation is done by gravity; S = Separation is done by separator

Chapter 3

The Annular-fueled Superheat Boiling Water Reactor

3.1 Design Considerations

It is generally recognized that the addition of nuclear superheat is one of the attractive possibilities for improving the performance of light water reactors. The expected improvement results from the high temperature superheated steam and thus the higher plant efficiency. Additional complexity is to be expected in arranging the reactor core to serve both the boiling and superheating functions. However, the nuclear superheat must be accomplished without seriously compromising the simplicity of the system, or causing a marked lowering of power density or a deterioration of the neutron economy. In addition, the usual problems associated with LWRs and steam-cooled reactors and a number of particular challenges associated with coupling the boiling and superheating functions must be solved.

General considerations for the design of an integral nuclear superheater are discussed below.

1. Fuel element

The success of nuclear superheat is largely dependent on the development of a satisfactory fuel element. This fuel element must be capable of achieving high burnup under severe temperature and pressure conditions. Other desirable characteristics of the designed fuel element are having long-term integrity, good neutron economy and reduced fabrication costs.

2. Local Power Peaking

For an integral nuclear superheater which employs two different types of elements for boiling and superheating respectively, local distortion of the fluxes can take place which gives rise to local power peaking which may diminish the neutron economy.

3. Radioactivity

Since the superheated steam will be sent directly to the turbine, the amount of radioactive material carried over to the turbine and condenser should be within tolerable limits.

4. Materials

It is essential to use advanced materials for the in-core and out-of-core structures. The in-core structures, such as fuel cladding, are the most critical components in the pressure vessel, as they are exposed to the highest service temperature, to severe irradiation dose, and to the oxidizing superheated steam environment. The desirable characteristics of the in-core materials include good mechanical strength at high temperatures, resistance to radiation damage and corrosion, low neutron absorption cross section and good heat transfer properties. For the out-of-core structures, materials which are adopted by modern supercritical fossil power plants can also be applicable to the superheat nuclear reactor.

5. Control System

Control problems associated with the boiling water and steam-cooled reactors have to be taken into account. For an integral nuclear superheater, the impact of void fraction in the boiler and superheater regions should be analyzed to design an adequate control system. Design considerations include the material, size, number, and position of control elements. The control system should have good performance under both steady-state and transient conditions.

6. Reactor Stability

The usual concerns associated with the stability of a boiling water reactor are also present in a BWR with integral nuclear superheat. For an integral nuclear superheater, special attention should be paid to the void coefficient in the boiling region of the reactor if the boiling and superheating regions are designed to be coupled. .

7. Operational safety

The potential hazards associated with the flooding and unflooding of the superheating region should be avoided. Inner channel blockage by debris should also be avoided. Greater difficulties may be encountered in managing a proper power split between the boiler and superheater sections as power changes and fuel-burnup occur. In addition, startup and shutdown of an integral nuclear superheater are considered to be unique for a specific design. Adequate shut-down and emergency cooling for the superheater elements must be guaranteed under all circumstances.

3.2 General Description of the Proposed Design

There were several superheat reactor designs proposed in the course of this work. By preliminary calculations and discussion, it has been determined that integrating a BWR with annular fuel elements is the most promising concept. The selection criteria used to screen these various reactor concepts for their potential as superheaters are: first, the current technical feasibility to produce a specified steam temperature; second, the inherent characteristics of the concept favorable to long-term improvements in thermal efficiency; third, the potential of the concept to contribute to light water reactor technology; and finally, the economic promise of the concept.

The proposed reactor of this work is a direct boiling and superheating, single element type design according to the categorization described in Chapter 2. The core employs annular fuel elements which combine the boiler and superheater into one entity. Each annular fuel element, or fuel tube, is cooled internally by steam and externally by water. Fuel pellets are made of low enrichment UO_2. Stainless steel and nickel-base superalloy are selected as candidates for cladding material in consideration of their excellent physical properties and corrosion resistance. The fuel cladding gap is filled with helium gas and pressurized to around five atmospheres like the existing LWR fuels [95].

Figure 3-1 illustrates the main concept of the proposed design – the Annular-fueled

Superheat Boiling Water Reactor (ASBWR). As shown in Figure 3-1, the ASBWR consists of two independent cooling loops. The water coolant flows upward through the core (outer surface of the annular fuel elements) and boils, which is similar to the conventional BWRs. Annular separator and steam dryer are utilized and located in the reactor vessel above the core. Saturated steam is separated from the two-phase mixture and directed through the central void region of the annular separator and dryer to reenter the core for superheating. Before reentering the core, saturated steam can be preheated by the superheated steam plenum. The flow paths to and from the ASBWR assemblies are designed so that the steam coolant can flow first downward through the inner channels of half of the annular fuel elements in an assembly and then upward through the other half of the fuel elements before exiting the assembly.

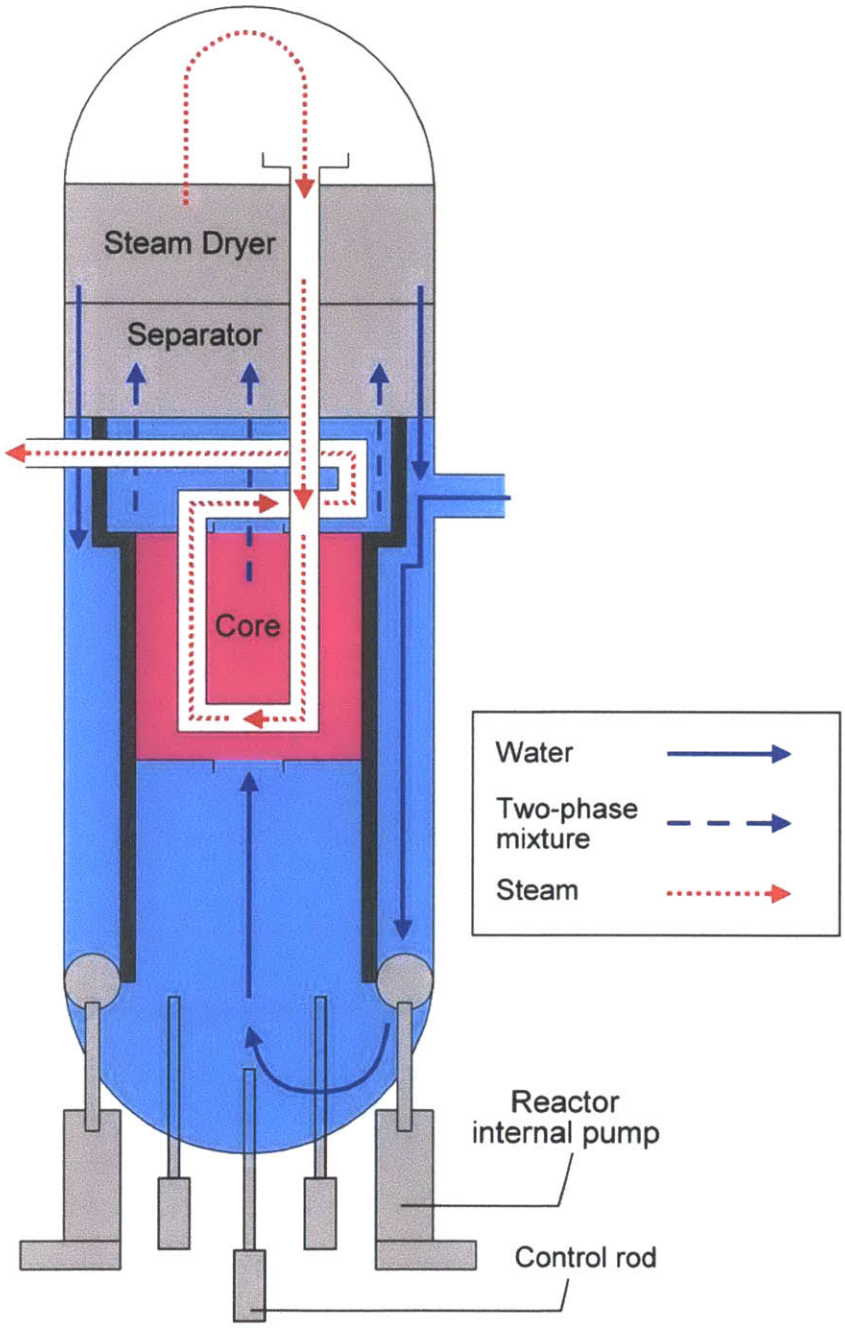

Figure 3-1 Simplified flow configuration of the ASBWR

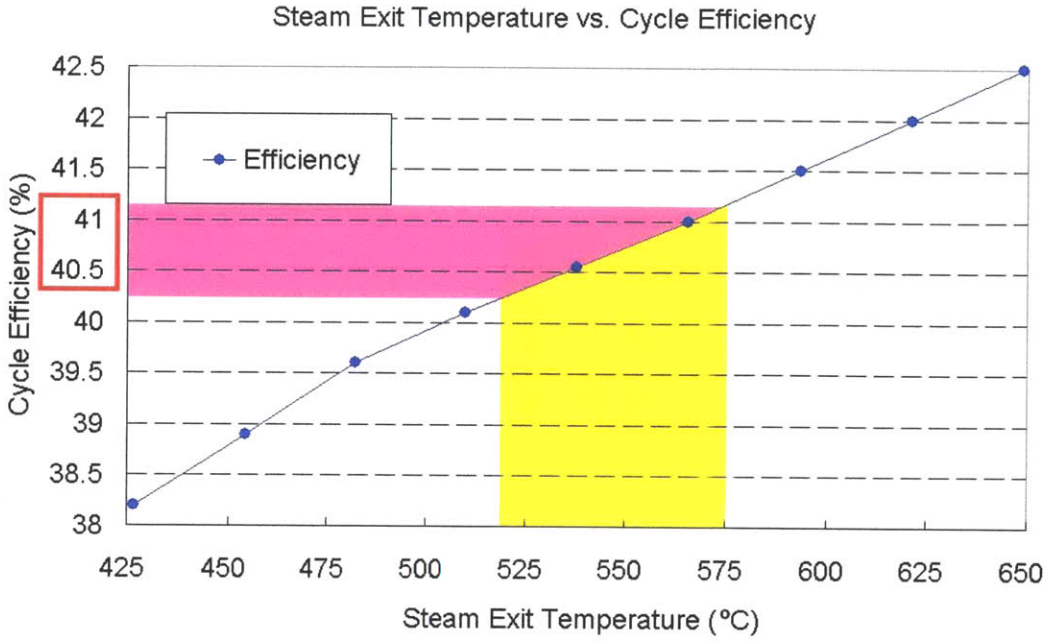

Figure 3-2 Steam temperature vs. plant efficiency for a superheat BWR [77]

The goal of this reactor is to generate superheated steam at a temperature of 520 °C or higher under similar pressure conditions to the existing BWRs. The impact of steam temperature on the plant efficiency has been studied for a BWR with nuclear superheat [77]. As shown in Figure 3-2, with an outlet steam temperature of 520 °C, the plant efficiency can be enhanced to above 40%, which is substantially greater than the plant efficiency of 33 to 35% that an advanced LWR can achieve nowadays.

3.3 Detailed Description of the Proposed Design

3.3.1 Reactor Vessel and Major Components

Figure 3-3 illustrates the pressure vessel and major components of the ASBWR. For simplicity, only two fuel assemblies are shown in Figure 3-3.

The major components in the ASBWR include fuel assemblies, control rods, reactor internal pumps, annular separator, annular steam dryer and steam coolant distributor. The fuel assemblies sit on the top fuel guide plate and are described in detail in the following section. Cruciform control rods are mounted at the bottom of the RPV, similar to current BWRs. The reactor internal pumps (RIPs), which have been adopted by the advanced BWRs, are installed in the vessel to provide sufficient driving force to circulate the water and steam coolant. The steam coolant distributor, connected with the annular separator, superheated steam outlet structure and fuel assemblies, is the key component that separates and defines the two-phase mixture, saturated steam and superheated steam plenums. It collects the saturated steam coolant and directs it to the fuel assemblies.

3.3.2 Flow Configuration

Figure 3-4 shows the flow configuration of the ASBWR. The feedwater flows into the downcomer region through nozzles and combines with saturated water exiting from the separators. The location of these nozzles is well above the top of the nuclear fuel assemblies. The combined water coolant then enters the reactor internal pumps (RIPs) that provide additional hydraulic head. Exiting the RIPs, the water coolant makes a 180-degree turn and flows up through the lower core plate into the fuel assemblies. In each fuel assembly, water is heated by the outer surface of the annular fuel elements and the steam-water or two-phase mixture is formed through the heating paths. The two-phase mixture, composed of about 12 to 15% saturated steam, continues to flow upward and enters the annular separator and dryer. The separated steam then makes a 180-degree turn and flows through the central void region of the annular separator and dryer to enter the steam coolant distributor, where it is preheated by the surrounding superheated steam plenum. The steam distributor is well connected to the fuel assemblies so that the preheated steam coolant can flow into the inner channels of the annular fuel elements. The preheated steam first flows downward through about half of the assembly fuel elements, making a 180-degree at the bottom, and then flows upward through the other half of the assembly. Within each assembly, the steam coolant is superheated by the inner surface of the annular fuel elements. Finally, the superheated

steam is collected in the superheated steam plenum and directed to the turbine.

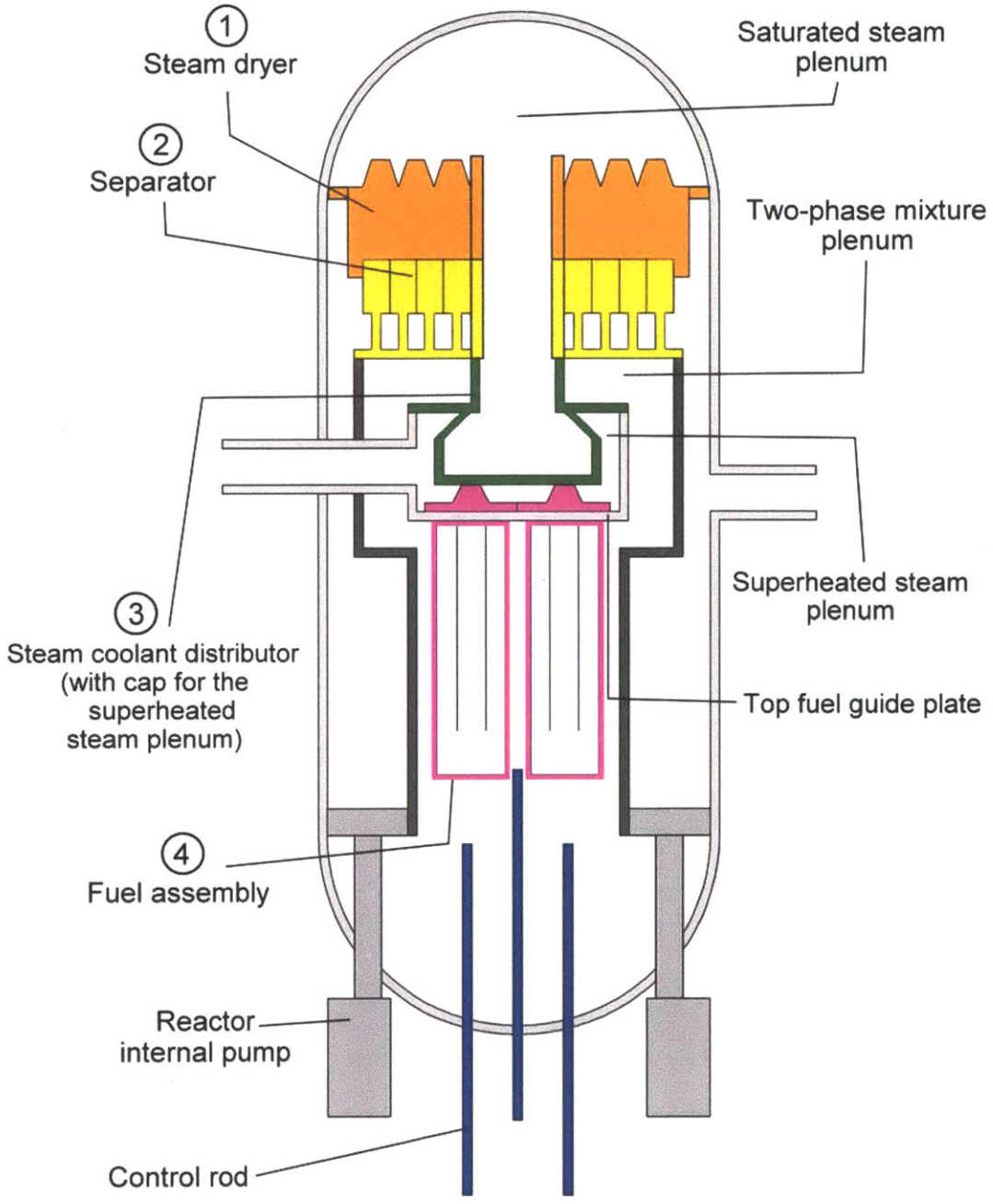

Figure 3-3 Reactor vessel and major components of the ASBWR

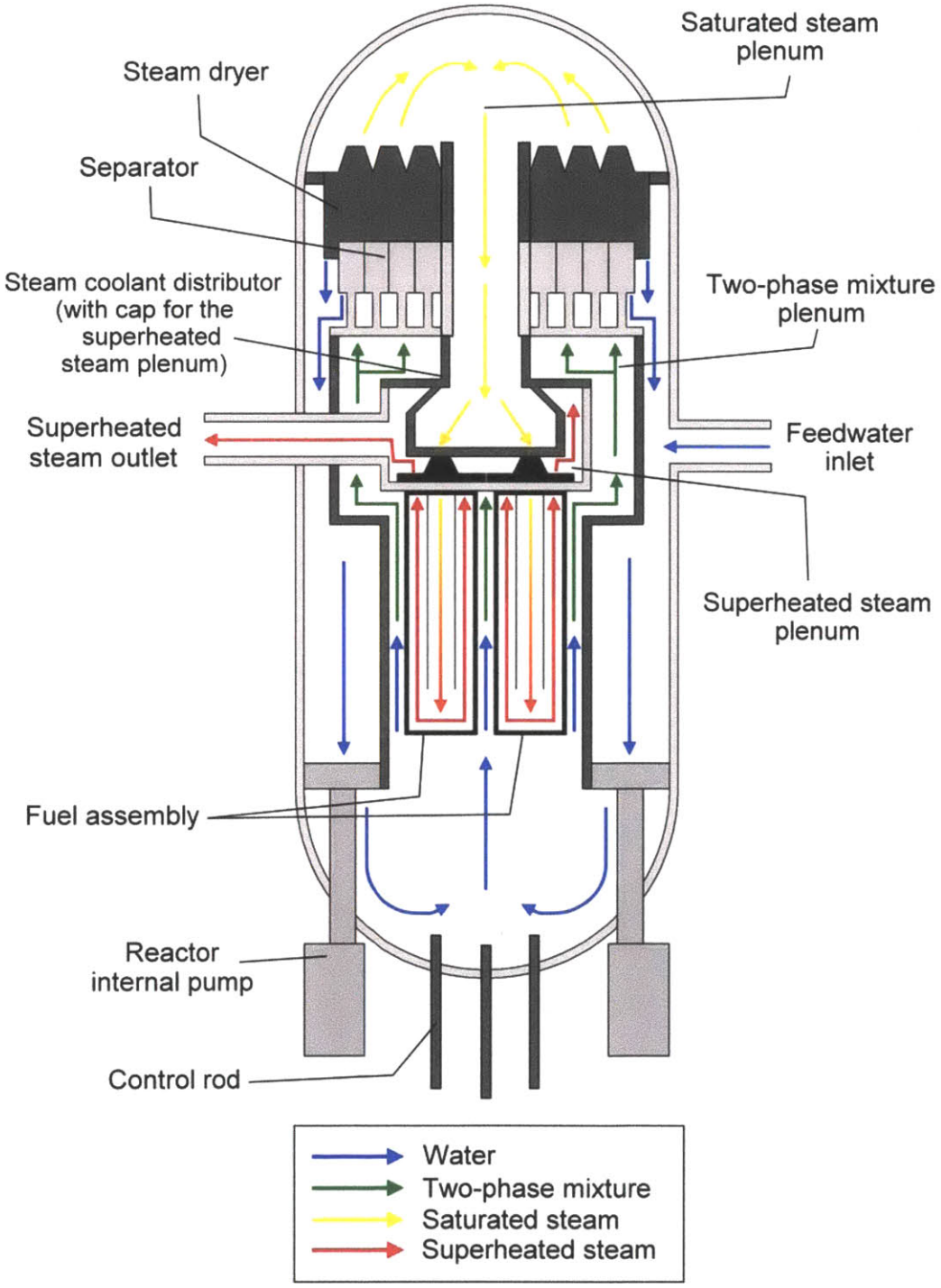

Figure 3-4 Flow configuration of the ASBWR

3.3.3 Fuel Assembly

General

Figure 3-5 shows the ASBWR fuel assembly. Each fuel assembly contains sixty annular fuel elements and one square water rod (occupies the space of four fuel elements) in an 8 by 8 square array. The sixty fuel elements include twenty-eight steam down-flow paths and thirty-two steam up-flow paths. The steam box is located near the bottom to collect the incoming steam coolant and direct the steam coolant to the peripheral fuel elements in an upward flow. Spacers are properly arranged along the axial length of the fuel assembly but are not shown in Figure 3-5. Cruciform control rods and box walls are made and placed in the location similar to a typical BWR fuel assembly design. The weight of the fuel assembly is primarily acting on the top fuel guide plate and secondarily supported by the bottom spring and the lower core plate.

Figure 3-6 shows the top, front and side views of the upper tie plate. The upper tie plate comprises the top nozzle for the steam coolant inlet, handle and 32 holes for the superheated steam outlet. Figure 3-7 shows the locations of the tie rods. There are eight tie rods and 52 regular fuel rods for an 8x8 fuel assembly. Figures 3-8 to 3-11 show four different vertical cross-sectional views of the fuel assembly.

Fuel element

Figure 3-12 shows a regular annular fuel element. Low-enriched annular UO_2 pellets are loaded into the cladding tube. Top and bottom end plugs are alternately welded to the fuel element. The fuel cladding gap is filled with helium gas and pressurized to around five atmospheres like the existing LWR fuels. Bellows are integrated into the fuel element in order to accommodate the expected difference in axial growth between the inner and outer claddings. The annular spring end, which is welded with the bellows, is used to compensate the overall axial growth of the fuel element due to thermal expansion and irradiation effects. In addition, the annular spring end also serves as a seal to prevent any leaks across the inner-outer channel boundary of the annular fuel element.

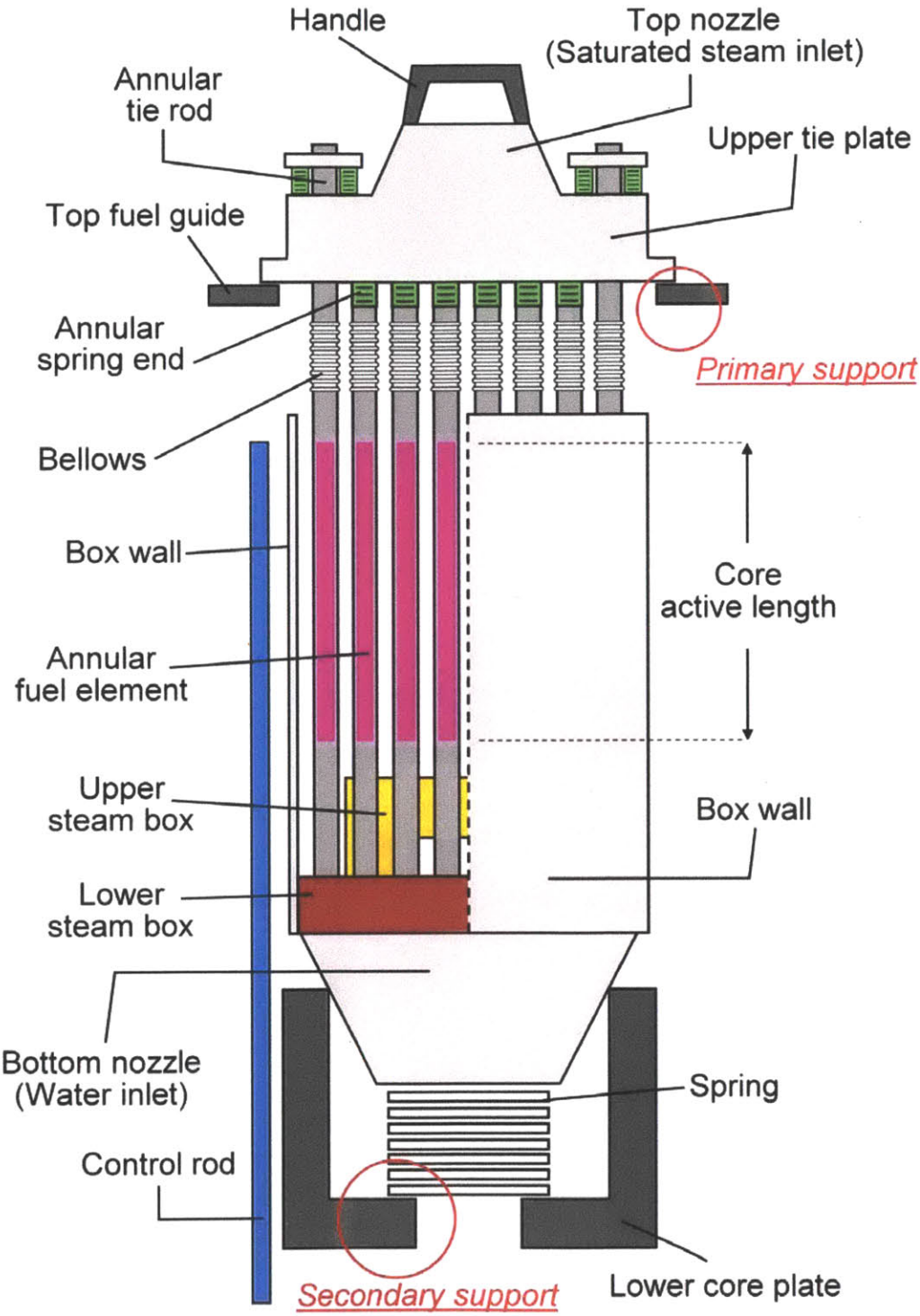

Figure 3-5 The ASBWR fuel assembly

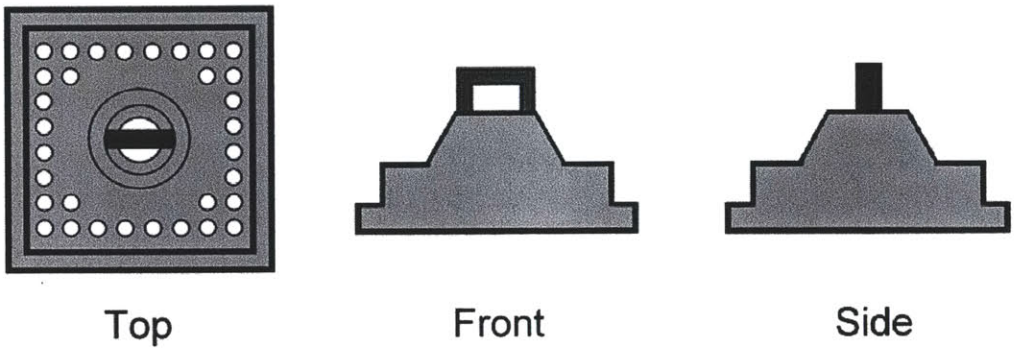

Figure 3-6 Top, front and side views of the upper tie plate

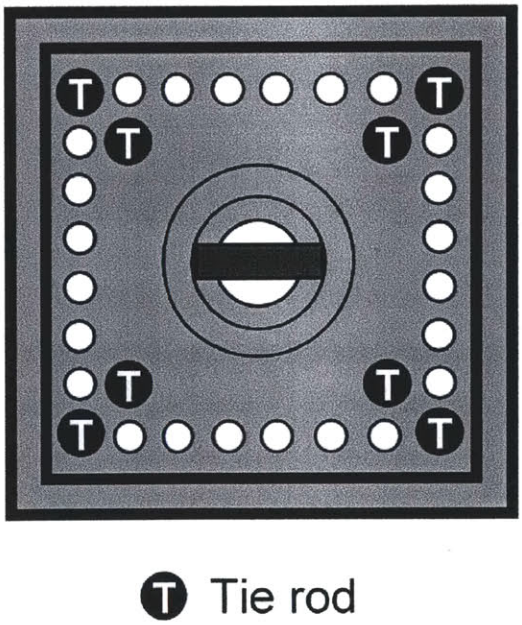

Figure 3-7 Locations of the tie rods

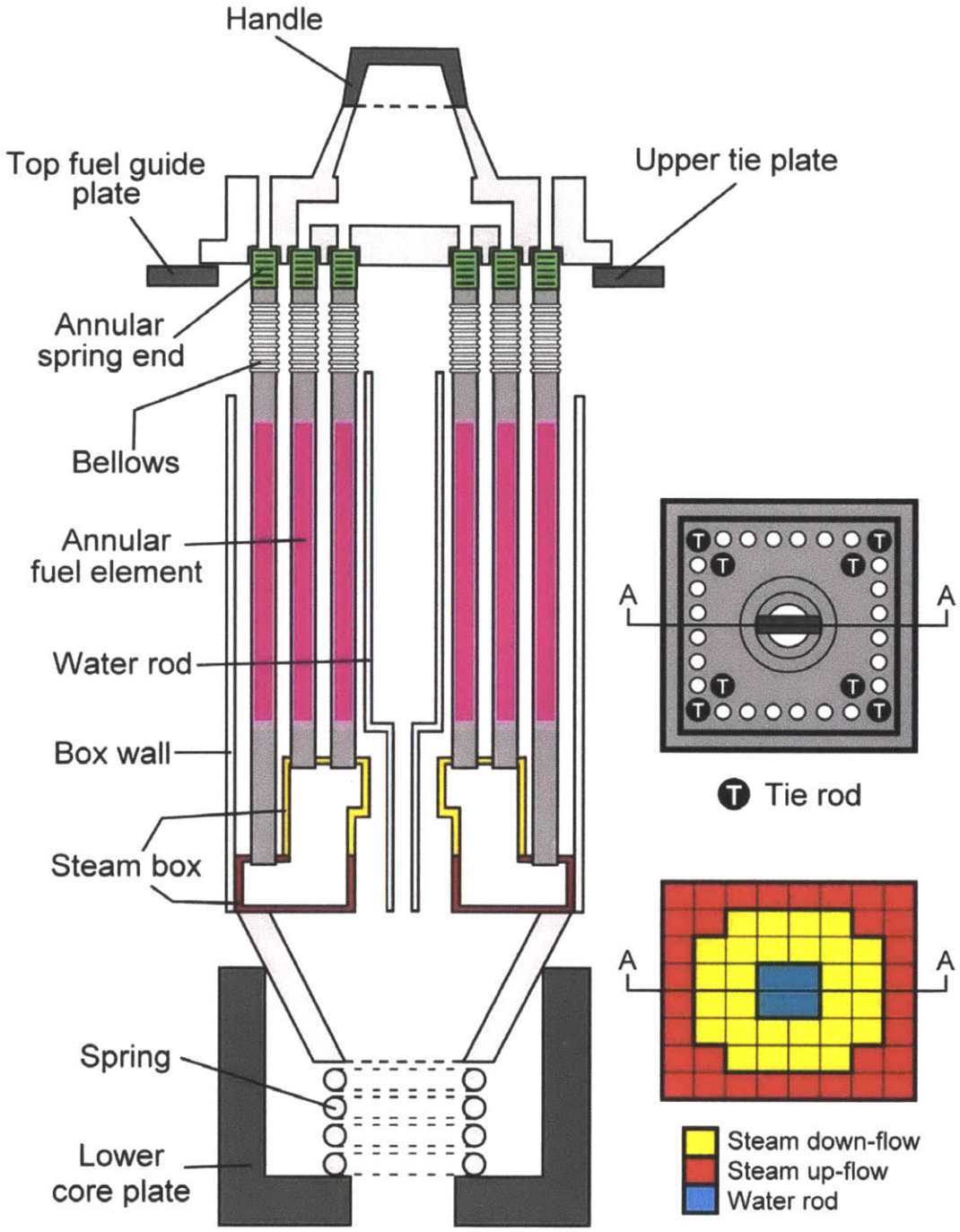

Figure 3-8 Cross-sectional view of the ASBWR fuel assembly (A-A)

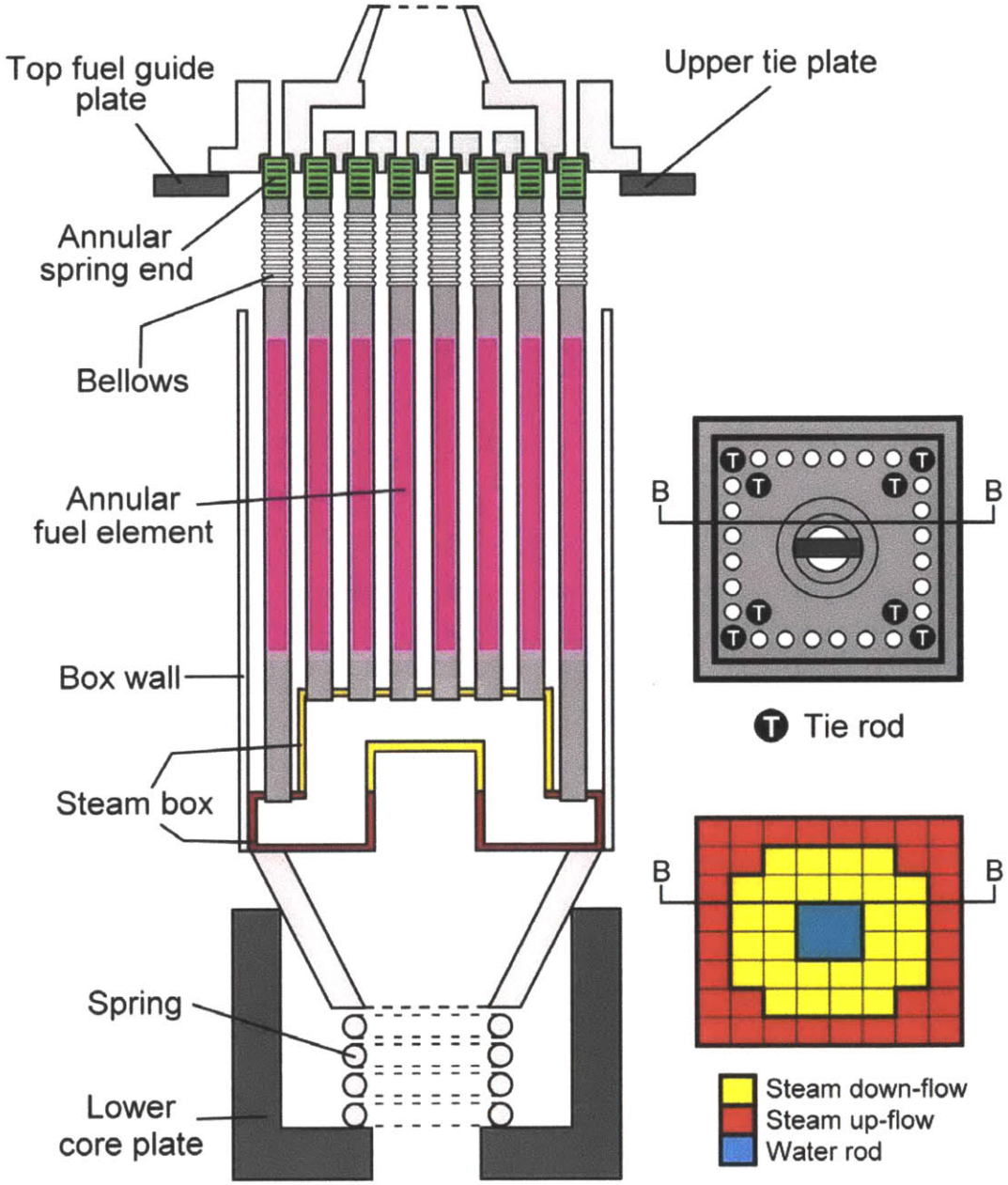

Figure 3-9 Cross-sectional view of the ASBWR fuel assembly (B-B)

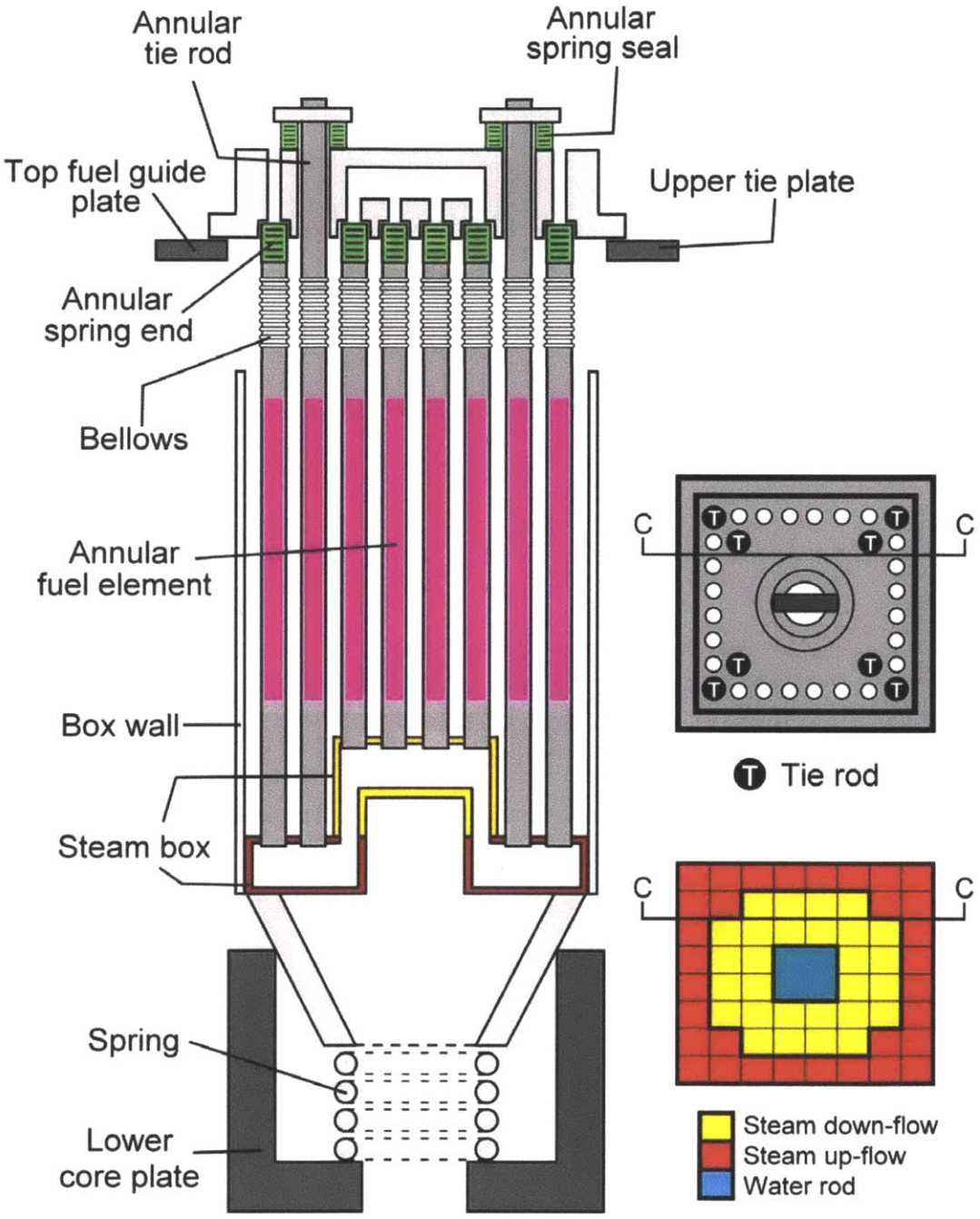

Figure 3-10 Cross-sectional view of the ASBWR fuel assembly (C-C)

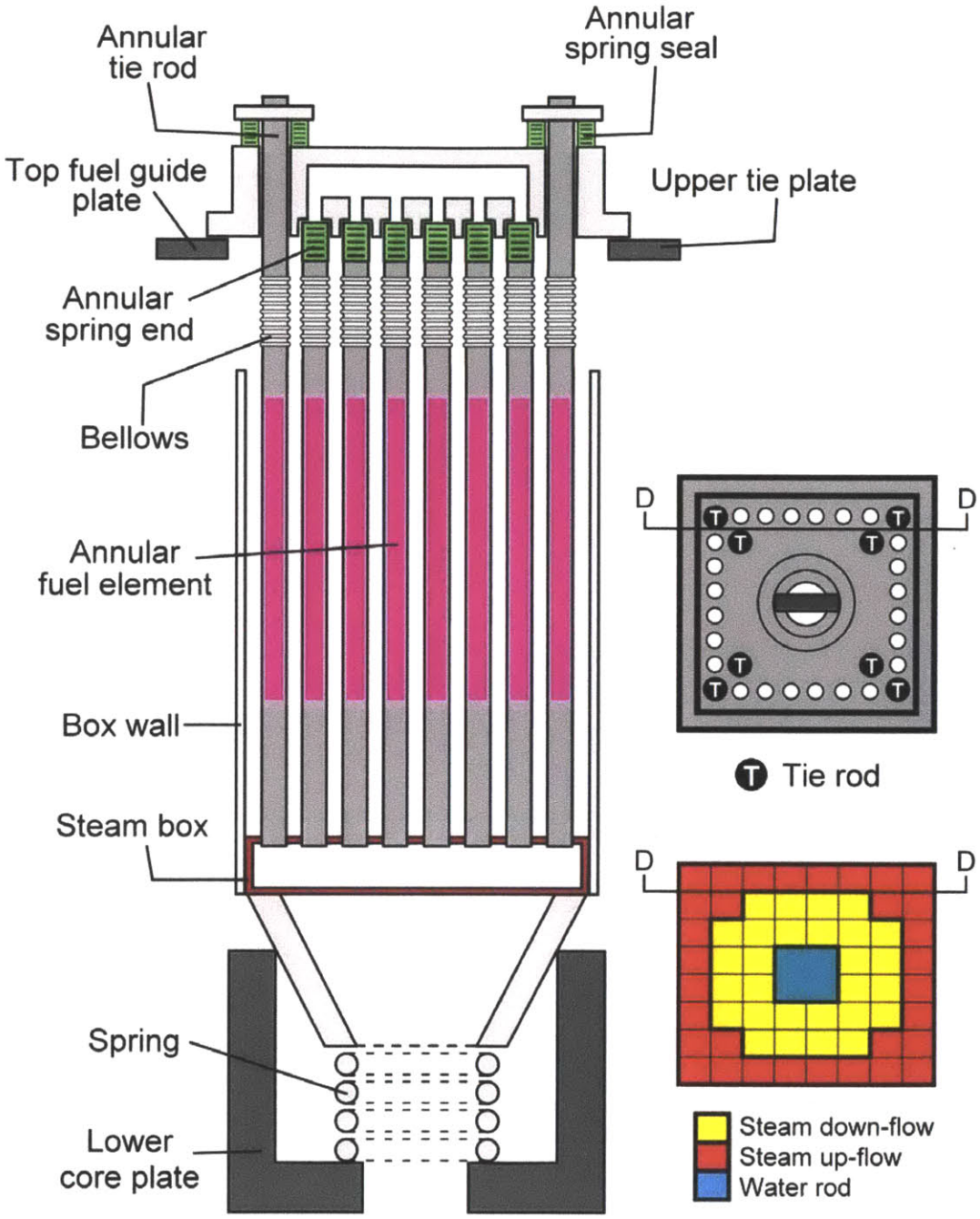

Figure 3-11 Cross-sectional view of the ASBWR fuel assembly (D-D)

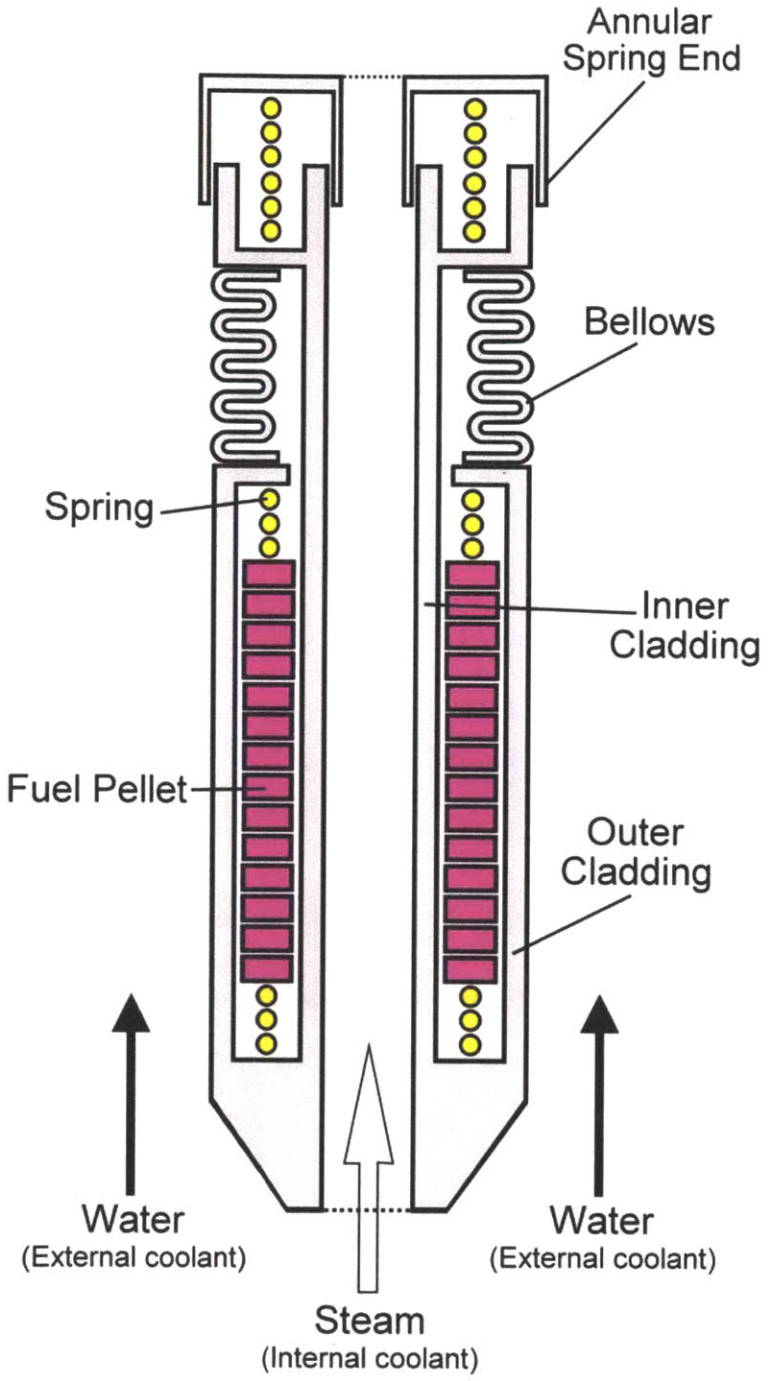

Figure 3-12 The ASBWR annular fuel element

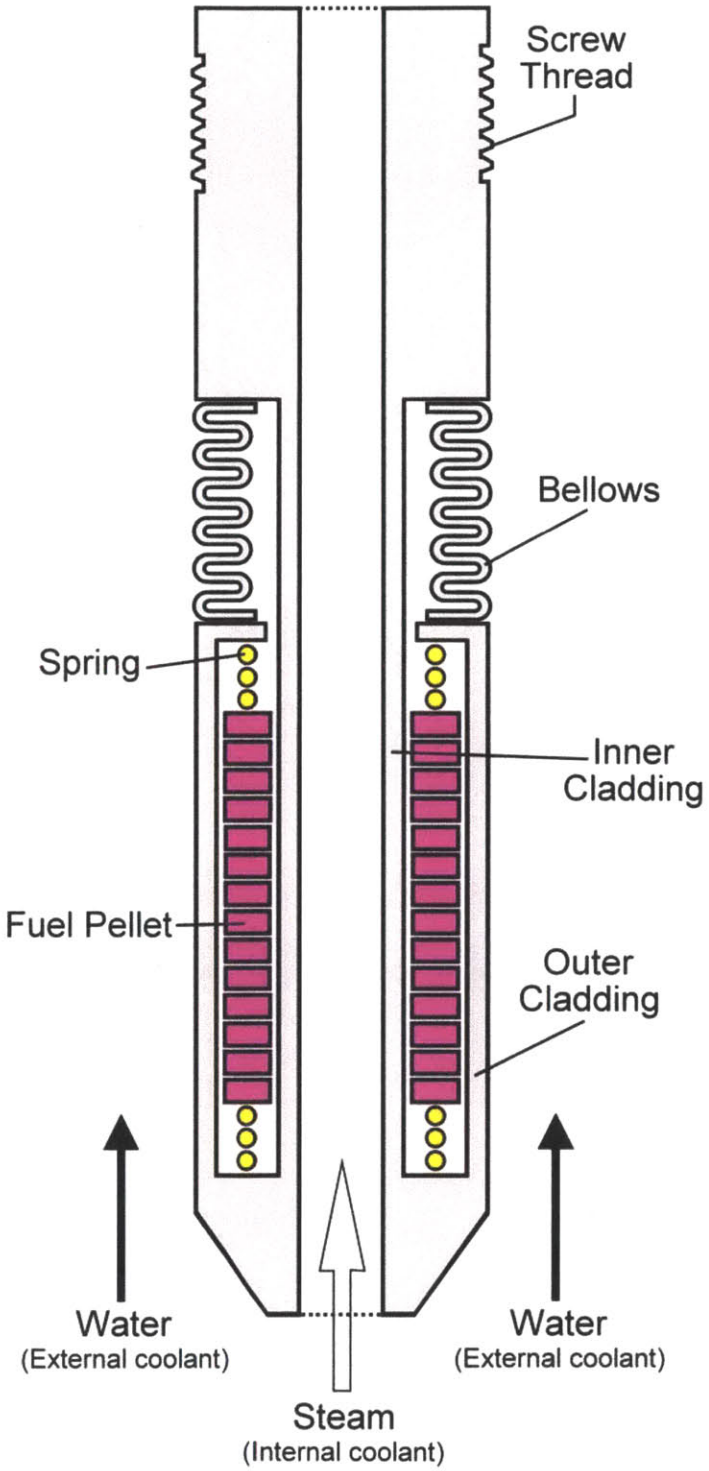

Figure 3-13 The ASBWR annular tie rod

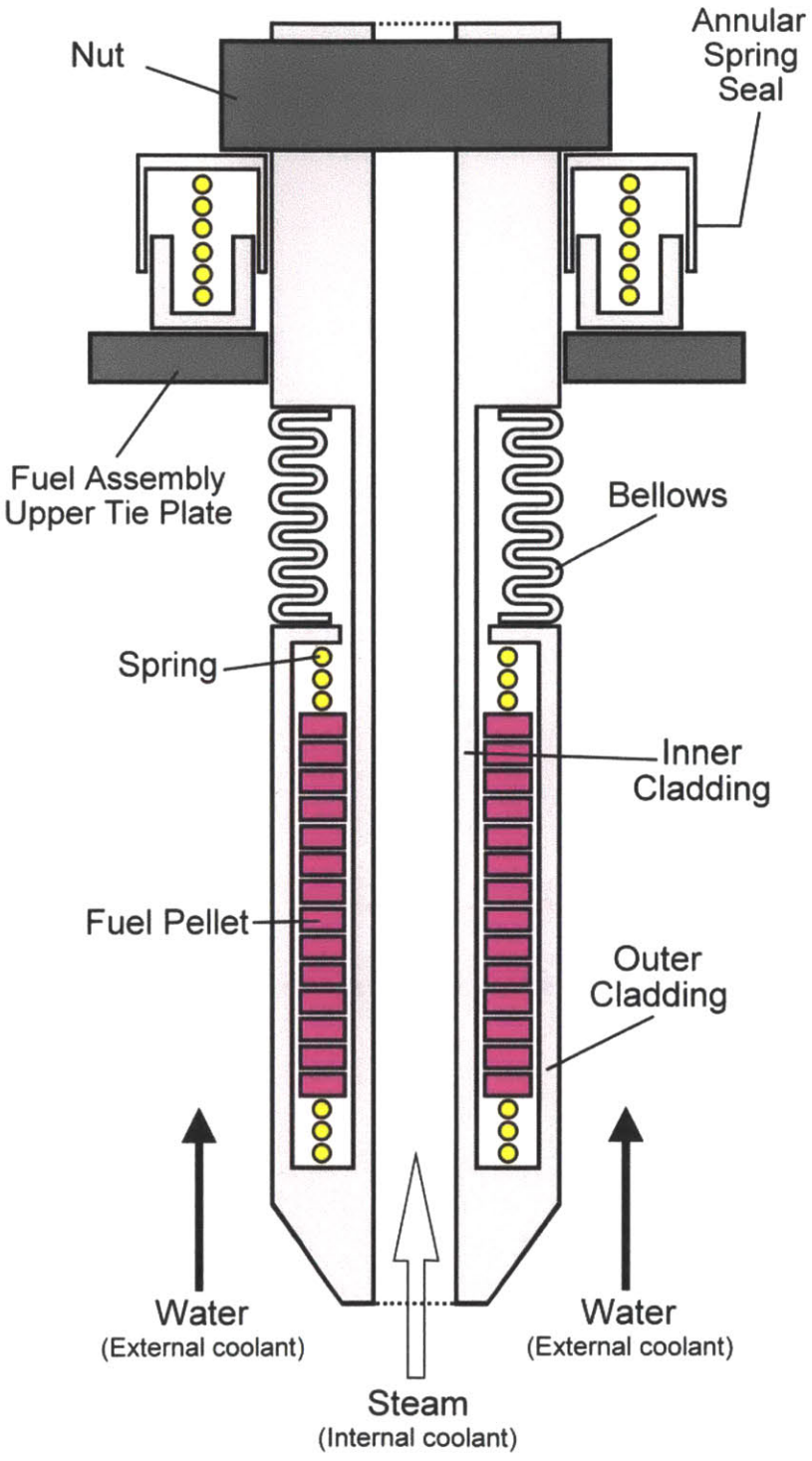

Figure 3-14 The ASBWR annular fuel element with annular spring seal

Figure 3-13 shows an annular tie rod with bellows. The tie rod has no annular spring end but screw threads near the upper end. The purpose of tie rod is connecting the upper tie plate to the bottom nozzle. Since the bottom nozzle and the steam box are welded together, the eight tie rods with nuts will carry the weight of the fuel assembly when inserting or withdrawing the assembly.

Figure 3-14 shows the annular tie rod with an annular spring seal and a nut. The annular spring seal, like the annular spring end but with a larger diameter, can compensate the overall axial growth of the tie rod and secure the inner-outer channel boundary of the annular fuel element.

The annular spring ends and annular spring seals comprise a spring system for the fuel assembly. Figure 3-15 illustrates the functions of this spring system.

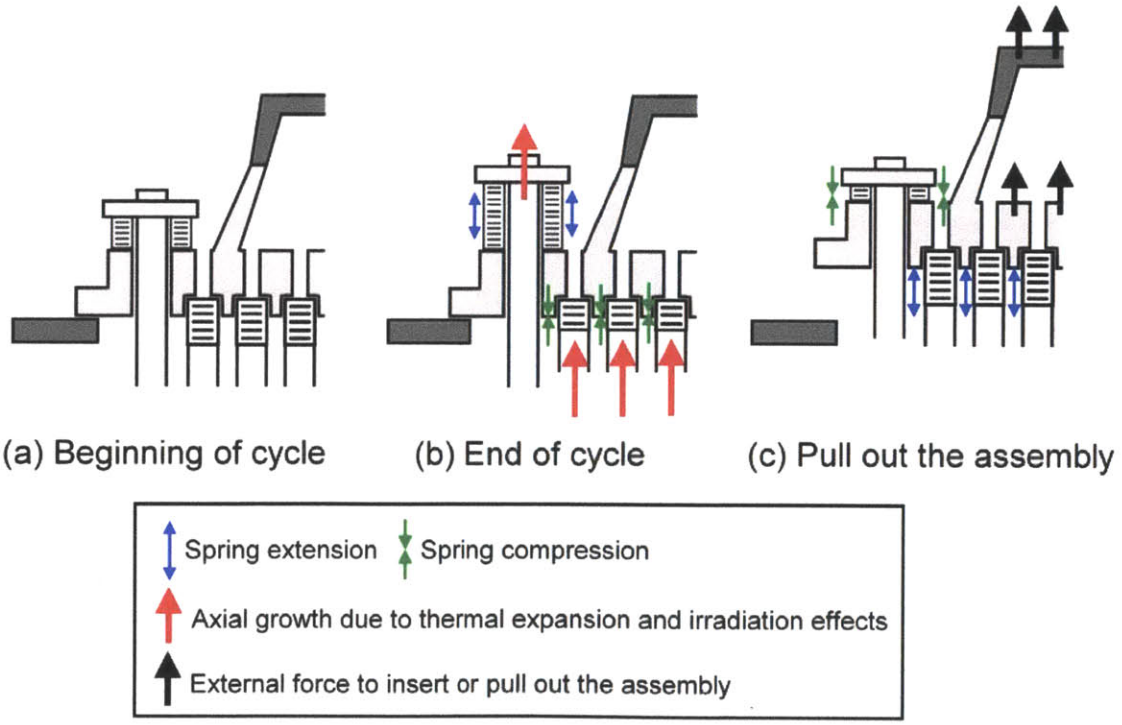

Figure 3-15 Spring system of the ASBWR fuel assembly

Steam box

The purposes of steam box are: (1) collecting the incoming steam coolant; (2) providing a mixing space for the steam coolant to reduce the local temperature peaking; and (3) directing the steam coolant back to the peripheral up-flow fuel elements. It consists of two parts: the upper steam box and the lower steam box. As shown in Figure 3-16, the upper steam box is welded to the twenty-eight steam down-flow fuel elements while the lower steam box is welded to the thirty-two steam up-flow fuel elements. The upper and lower steam boxes are connected by a steam box connection.

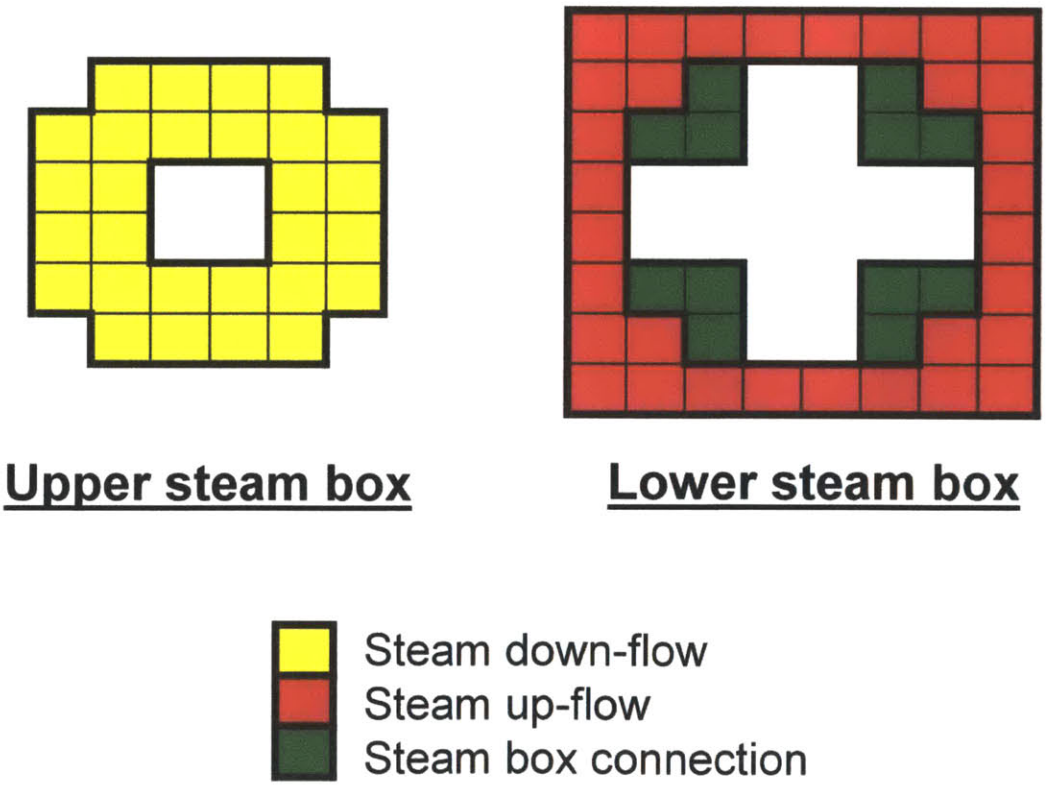

Figure 3-16 The upper and lower steam boxes

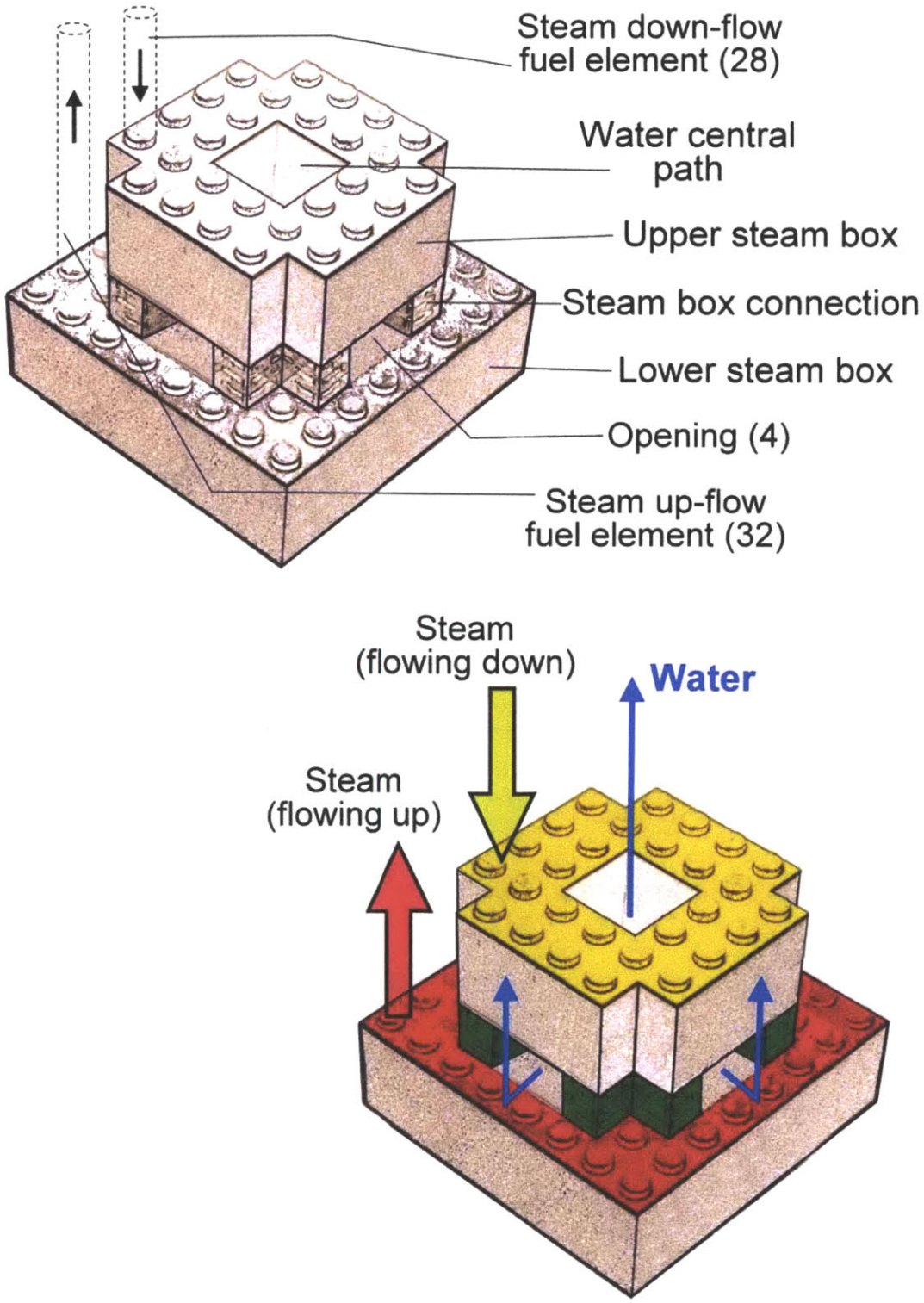

Figure 3-17 Three-dimensional view of the steam box

Figure 3-17 shows a three-dimensional view of the steam box. The water coolant enters the assembly from bottom can flow through the four openings and the central path to reach the outer surfaces of the fuel elements. Figure 3-18 shows the flow paths in and around the steam box. It can be seen that water flowing through the central path is directed separately to the square water rod and to the boiling region. To allow sufficient water flow via the central water path to the boiling region, the water rod is designed to have a narrow entrance and an inlet orifice which can be used to adjust the flow rate in the water rod. The fuel active region is about 35 ~ 40cm above the unheated region to allow the turbulence to be fully developed. As a result, the water coolant is expected to form a uniform flow distribution before entering the active region of the core.

Flow paths in the assembly

Figure 3-19 is the horizontal cross-sectional view of the fuel assembly. As shown in Figure 3-19, each fuel element is cooled internally by steam (up-flow or down-flow), and externally by boiling water. Neutron moderation in the reactor core is mainly provided by water in the boiling region, the square water rod, and water gaps. The steam coolant contributes negligible moderation due to its low density.

Figures 3-20 shows the flow paths of the water and steam coolants in the assembly. The preheated steam coolant flows downward into the top nozzle and then passes through the inner channels of the central annular fuel elements. After that, the steam coolant is collected in the steam box, where it is mixed and makes a 180-degree turn, and flows upward through the inner channels of the peripheral annular fuel elements until it exits the assembly. On the other hand, the water coolant flows upward into the bottom nozzle of the assembly, entering the water rod and passing through the outer channels of the annular fuel elements. A steam-water mixture is formed in the outer channels and then continues to flow upward until entering the separators.

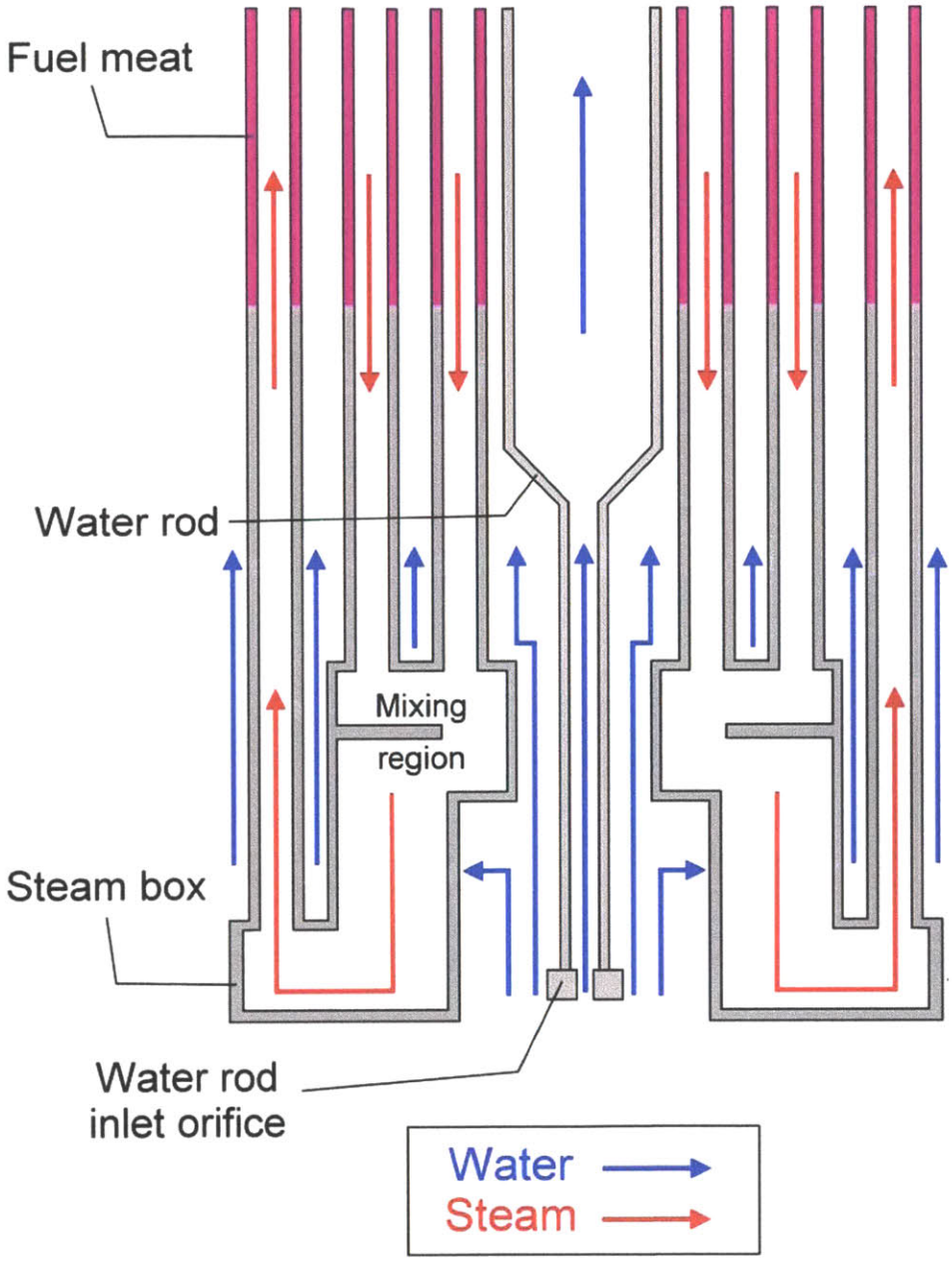

Figure 3-18 Flow paths in and around the steam box

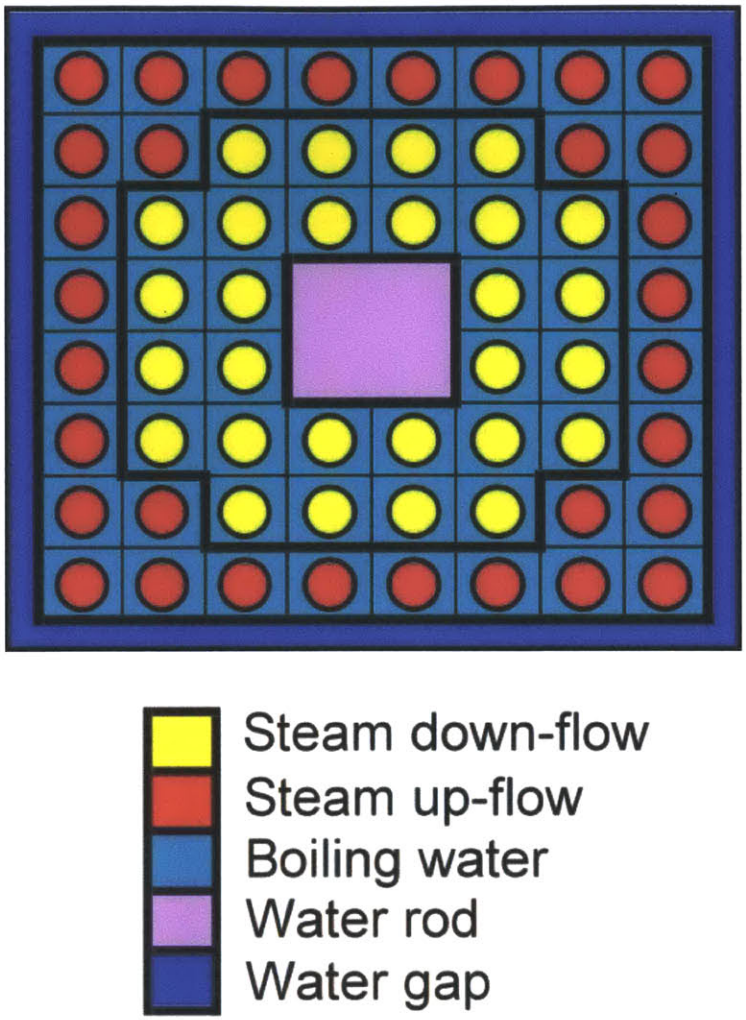

Figure 3-19 Horizontal cross-sectional view of the ASBWR fuel assembly

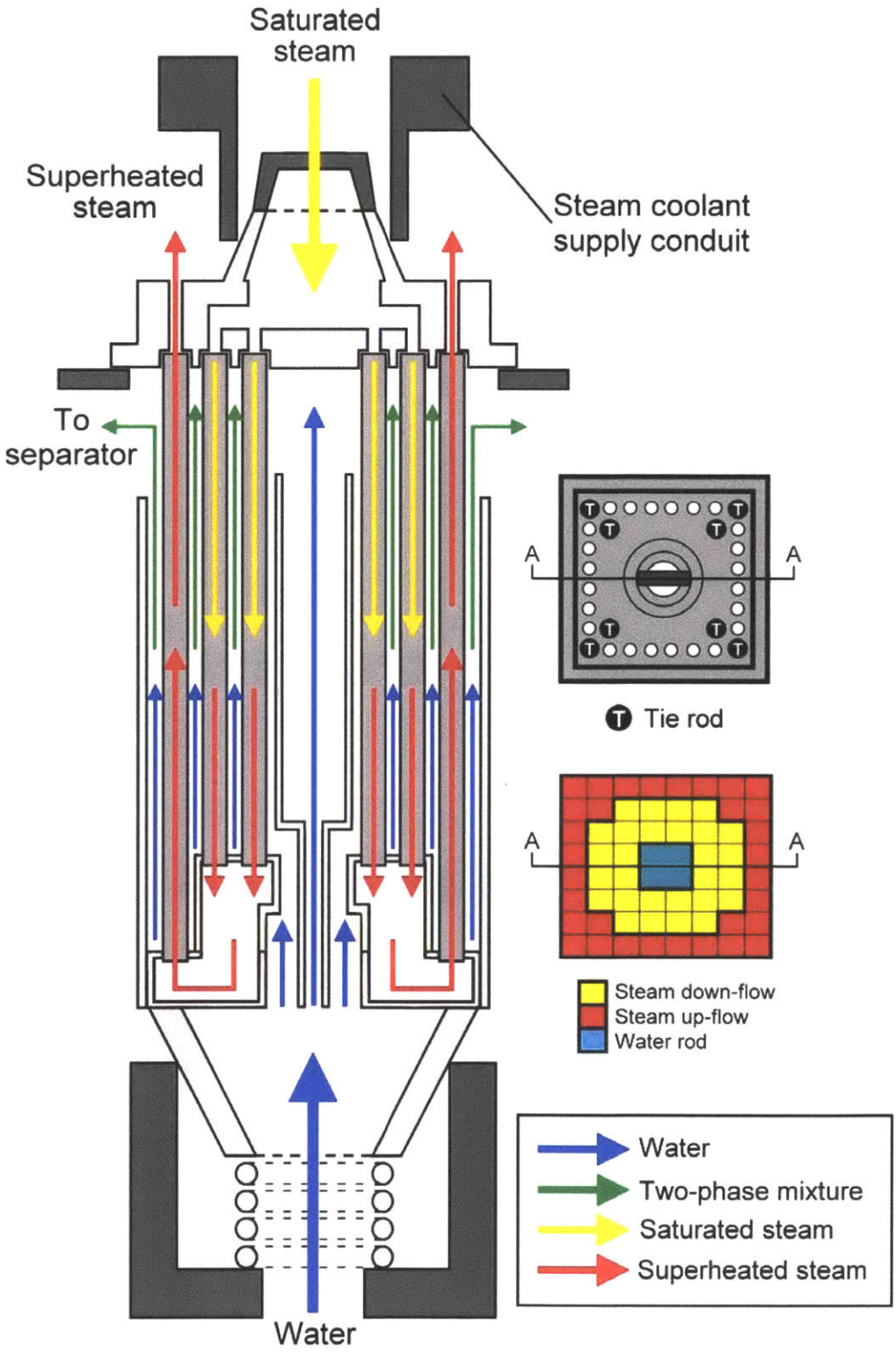

Figure 3-20 Coolant flow paths in the ASBWR assembly

3.3.4 Materials for the In-core and Out-of-core Structures

A preliminary study has been performed to investigate the operational conditions of the ASBWR and to evaluate the potential of existing structural materials for application in the ASBWR in-core and out-of-core components.

Out-of-core materials

The selection of appropriate structural materials for out-of-core components can be based on the data and experience developed for supercritical fossil power plants (SCFPP). Table 3-1 lists the materials of major components for a typical SCFPP [96]. These materials are mostly commercial ferritic/martensitic or austenitic stainless steels. The operational conditions of the ASBWR (520 °C, 71 bar) are moderate compared to the working temperature (540 ~ 600 °C) and pressure levels (250 ~ 275 bar) of a SCFPP; hence the materials used for a SCFPP should be applicable to out-of-core components of the ASBWR. However, further analyses and experiments are needed to evaluate the impact of radioactive cooling medium on the material behavior of these out-of-core components.

Table 3-1 Materials for key components in supercritical fossil power plants [96]

Component/material	Nominal composition (wt%)
Piping materials	
X20 CrMoV 12 1	0.2C–12Cr–1Mo–0.3V
T 91/P 91	0.1C–9Cr–1Mo–V–Nb
HCM12A	0.1C–11Cr–0.5Mo–1.8W–1Cu–V–Nb–N–B
1.4910	0.03C–17Cr–13Ni–3Mo–N–B
Super heaters	
TP347HFG	18Cr–10Ni–1Nb
Super 304H	18Cr–9Ni–0.4Nb–Cu–N
NF709	20Cr–25Ni–1.5Mo–0.25Nb–0.05Ti–N
Thick section boiler comp.	
NF616	0.1C–9Cr–0.5Mo–1.8W–V–Nb–N–B
HCM12A	0.1C–11Cr–0.5Mo–1.8W–1Cu–V–Nb–N–B
Turbine rotors	
COST E/F	0.12C–10Cr–1Mo/1.5Mo–1W/0W–V–Nb–N
COST B	0.17C–9.5Cr–1.5Mo–0.01B–V–Nb–N
HR1200	0.09C–11Cr–0.2Mo–2.7W–2.5Co–V–Nb–N–B

In-core materials

For in-core structures, the fossil materials experience is valuable but maybe not directly transferable to a nuclear power plant. It is not only because of the radiation damage and radiolysis effects, but also because fossil plants have a higher tolerance for oxidation and deposition of crud. For example, materials that work in fossil boiler tubes are allowed to develop very thick oxide layers for passivation. Sometimes these layers flake off and then become a source of erosion and possibly clogging. It may not cause any damage to a fossil boiler tube, which has a diameter of 2 cm, but will certainly cause serious problems in a nuclear fuel assembly, which has grid spacers and a rod-to-rod clearance of 4 mm.

A selection of available and promising materials for in-core components is based on their mechanical and nuclear properties, corrosion and creep fracture resistance, irradiation stability and manufacturing feasibility. Particularly for the fuel cladding material, radiation embitterment and irradiation-assisted stress corrosion cracking (IASCC) are the most important issues that have to be taken into account. Through a preliminary study, two materials are considered to have the potential to fulfill the requirements as in-core cladding and structural materials in the ASBWR.

The first candidate is the modified 9Cr–1Mo steel (T91). It is ferritic-martensitic steel currently used in fossil power plant superheaters. T91 has a lower thermal expansion coefficient compared to stainless steel and has excellent performance under 650 °C. The potential of T91 for nuclear applications has been recently studied. It is considered as one of the promising structural materials for the lead–bismuth-cooled accelerator driven system (ADS) [103]. In addition, the feasibility of using T91 as fuel cladding in supercritical water reactors is also under investigation [104].

The second candidate is Inconel 718. It is a precipitation-hardenable nickel-chromium alloy containing significant amounts of iron, niobium, and molybdenum along with lesser amounts of aluminum and titanium. Inconel 718 combines excellent corrosion resistance and tensile, fatigue, creep, and rupture strength with outstanding weldability, including resistance to postweld cracking. It has satisfactory performance when operated

between -423 to 1300 °F. Compared with stainless steel, Inconel 718 has improved ductile to brittle transition behavior under irradiation and thermal creep fracture resistance of the cladding during transients. In addition, Inconel 718 has been proposed as a cladding material for liquid metal and gas-cooled fast breeder reactors [105].

Table 3-2 summarizes the chemical composition of T91 and Inconel 718, compared with Zircaloy, the common LWR cladding material. Table 3-3 lists physical and nuclear properties of these three materials. It can be seen from Table 3-3 that T91 has better thermal conductivity but lower allowable maximum working temperature than Inconel 718. The linear thermal expansion coefficients of these two materials are about the same and larger than Zircaloy. In conjunction with a much higher operating temperature than BWRs, the ASBWR is expected to have appreciable axial expansion in fuel claddings. Moreover, both T91 and Inconel 718 have much higher thermal neutron absorption cross section than Zircaloy, which implies the ASBWR fuel would require a higher U-235 enrichment to reach similar burnup to the existing LWRs.

The development of in-core materials for advanced nuclear reactors is gradually approaching a mature stage of practical application. The suggested material candidates, T91 and Inconel 718, are among the options and should not restrict the design of the ASBWR. Their feasibility should be determined by the overall performance under appropriate irradiation and high temperature operating conditions. Further investigation and experimental data are essentially needed to confirm the qualification of T91 and Inconel 718 for the ASBWR in-core materials.

Table 3-2 Composition of Zircaloy, T91 and Inconel 718

Percent (%)	Zircaloy	T91	Inconel 718
Cr	0.1	8.26	17 ~ 21
Ni	0.055	0.13	50 ~ 55
Mn	--	0.38	0.35
V	--	0.2	--
Nb	--	0.08	4.75 ~ 5.5
Mo	--	0.95	2.8 ~ 3.3
Al	--	0.024	0.2 ~ 0.8
Cu	--	0.08	0.3
As	--	0.02	--
Sn	1.45	0.008	--
C	--	0.105	0.08
N	--	0.055	--
P	--	0.009	--
S	--	0.003	--
Si	--	0.43	0.35
Ti	--	--	0.65 ~ 1.15
Co	--	--	1.0
B	--	--	0.006
Hf	0.01	--	--
Fe	0.07 ~ 0.2	balance	balance
Zr	balance	--	--
Reference	[97]	[98]	[99]

Table 3-3 Physical and nuclear properties of Zircaloy, T91 and Inconel 718

Properties	Zircaloy	T91	Inconel 718
Density (g/cm^3)	6.55	7.79	8.19
Melting point/range (°C)	1850	1370 ~ 1415	1260 ~ 1336
Specific heat (J/kg-K)	317 (at 300°C)	560 / 750 (at 300 / 600°C)	435
Average linear thermal expansion coefficient (μm/m-K)	5.64	12.7	13.0
Thermal conductivity (W/m-K)	16.5 (at 300°C)	28.8 / 28.5 (at 300 / 600°C)	15.5 / 21.0 (at 300 / 600°C)
Microscopic thermal neutron absorption cross section, σ_a (barns)	0.21	2.64	4.07
Macroscopic thermal neutron absorption cross section, Σ_a (cm^{-1})	0.009	0.223	0.364
Maximum temperature limit for satisfactory performance (°C)	400	620 ~ 650	700 ~ 850
Reference	[97, 98, 99, 100, 101,102]		

*Excellent corrosion resistance and creep-rupture strength below this temperature are expected.

3.3.5 Key Advantages of the Proposed Design

The concept of the combined boiling-superheating fuel element involves a complicated fuel assembly design and raises several technological problems. However, this concept offers a series of advantages which seem to justify the efforts required to solve the problems involved. The key advantages of the proposed ASBWR are discussed below.

1. Internal and external cooling of the fuel element

The annular fuel can be cooled internally by steam and externally by water. In the event of reactor scram or loss of the steam coolant, the reactor core will not be excessively overheated since the residual thermal energy can be transferred to the boiling side. This is a superior feature to the traditional nuclear superheat designs which divided the reactor core into boiling and superheating regions, and therefore required a separate emergency cooling system for the superheating region.

2. Well-insulated interface between the boiling and superheating regions

Since the water and steam coolants are separated by the fuel, the heat loss from the superheating to the boiling side is prevented. No additional structure is needed for insulation.

3. Sufficient moderation for the superheating region

In the ASBWR, moderation is provided by water in the boiling region, water rod and water gaps for the entire core. There is no need for additional moderation for the superheating region. This is also one of the features that distinguish the ASBWR from the traditional nuclear superheat designs such as the Pathfinder and BONUS reactors.

4. Homogenized neutron spectrum

With the annular fuel elements, which serve both boiling and superheating functions, the distribution of the superheating regions in the core is extremely uniform. This leads to a homogenized neutron spectrum across the core and greatly simplifies the reactor control. The traditional designs had two different types of control rods for the boiling and superheating regions respectively because the neutron spectrum in the superheating region is harder than that in the boiling region. Therefore, control of these traditional superheat reactors was difficult and complicated, which further restricts the size of these reactors. In contrast, the ASBWR has no such restriction and can be designed as a small, medium or large reactor.

5. Use of only one type of fuel element and control rod

The ASBWR uses only one type of fuel element and control rod, which is convenient for manufacture, spare element storage and fuel reshuffling.

6. Low fuel peak temperature

Due to the internal and external cooling of the fuel element, the peak fuel temperature is very low. This alleviates the concerns about fuel melting in accidents and fission gas release from the damaged cladding.

7. Preheating of the steam coolant

The steam coolant can be preheated by the surrounding superheated steam plenum before reentering the core. This can help to prevent the reactivity insertion due to the residual liquid droplets in the saturated steam stream.

8. Well supported by currently available technologies

One of the most important advantages of the proposed design is that there are a lot of similarities between the ASBWR and a BWR. Therefore, the design and operation of the ASBWR can draw support from the available data of existing BWRs. The ASBWR can also benefit from the abundant experience in operating fossil-fueled superheaters since the temperature levels of steam are close. Furthermore, the annular fuel application has also been recently studied [106]. These all help to lower the technical barriers to achieve the ASBWR concept.

9. A more promising BWR evolution than the supercritical water reactor

The ASBWR design has some obvious similarities with the Supercritical Water Reactor (SCWR) concept. In particular, they are both direct-cycle systems that aim at a higher thermal efficiency, while maximizing the use of BWR and fossil-boiler technologies. However, the ASBWR does not suffer from the some of the potentially fatal flaws of the SCWR. For example, in an event of complete loss of feedwater flow, the ASBWR can

survive without damaging the fuel because the residual heat can be removed by a natural circulation path on the water side. In addition, due to its multiple coolant mixing chambers, the ASBWR is not subject to the severe hot channel temperature peaks that typically occur in the SCWR designs. In summary, the ASBWR appears to be a more promising BWR evolution than the SCWR.

3.3.6 Main Challenges of the Proposed Design

Having enumerated the advantages of the proposed design, it is necessary also to speak of the specific challenges or disadvantages involved.

1. Uneven thermal expansion between the inner and outer cladding

A main issue for this concept is the different axial thermal expansion between the inner cladding and outer cladding. The average temperature of the outer cladding is about 300 °C while the average and maximum temperature of the hottest inner cladding is about 580 °C and 630 °C, respectively. Possible solutions to this problem are: (i) preheating the outer cladding prior to being welded; (ii) the use of extendable tubes such as bellows to accommodate the uneven expansion; (iii) the use of different materials for the inner and outer claddings. In this work, efforts were concentrated on the first and second solution since the third one requires advanced welding techniques which are currently unavailable [107]. Even if the two materials can be welded perfectly, the third solution still needs further investigation to deal with the situations where only one side of the cladding is heated or cooled. Such situations include reactor start-up and emergency cooling etc. In addition, galvanic corrosion will be a concern when welding different alloys together.

2. Higher manufacturing cost of the fuel assembly

Higher manufacturing cost of the fuel assembly is expected because of the complicated assembly design. Welding and manufacturing of the annular fuel elements and steam box are the most difficult parts; however, the assembly is able to be fabricated by today's technology [108].

3. Required higher enrichment of UO_2

The enrichment of UO_2 is expected to be higher in order to achieve a similar burnup to BWRs. The neutron economy of ASBWR is not as good as BWRs because: first, the ASBWR core contains almost doubled cladding material compared to a typical LWR core due to the use of the annular fuel elements; and second, the cladding material, as shown in Table 3-3, has much higher thermal neutron absorption cross section than Zircaloy. However, this neutronic penalty can be offset by the greatly improved plant efficiency.

4. Uncertainty in achieving a desirable power split

For the annular fuel, the fuel performance depends a lot on the power split. Particularly for the ASBWR, the power split has direct impacts on the maximum cladding temperature and the superheated steam temperature. During the fuel cycle, the geometry of fuel pellets and inner/outer gap conductance would vary which causes uncertainty in predicting the power split. Achieving a desirable power split necessitates a detailed fuel modeling and fuel performance analysis.

5. Potential plugging of the annular fuel inner channel

The concern about potential plugging of inner channel with debris has been investigated for the PWR annular fuels [109]. The results indicate that the inner cladding would be subjected to damaging temperatures if full plugging of the inner channel occurs. The situation would be worse for the ASBWR since its inner cladding temperature is much higher than that of the PWR annular fuel. To prevent the full blockage of the inner channel by debris, it has been proposed to use inlet debris filters, which are installed in all current PWRs to minimize debris-induced fretting.

6. Flooding of the superheating regions

One of the anticipated problems associated with reactor safety is the reactivity insertion accident due to flooding of the superheating region. Neutronic analyses must be performed to evaluate the reactivity response during such events. Mechanical test of the fuel element and assembly structure must be conducted to prevent any possible way of

flooding during normal operation.

7. Carryover of radioactivity

The outlet superheated steam is expected to carry more radioactivity than BWRs since the duration of steam in the core is longer. This may represent a difficult operational or maintenance problem. In case of failure of the inner cladding, the release of fission products could be much greater than a similar release from a BWR fuel element because the steam coolant has no effective scrubbing action like water. To address this concern, high efficiency filters and activated charcoal traps are proposed to be installed near the steam outlet.

8. *Transients and Accidents*

Analysis of transients and accidents (e.g., loss of coolant accident (LOCA), loss of flow accident (LOFA), loss of feedwater flow, turbine trip, anticipated transient without scram (ATWS), and main steam line break) has to be performed thoroughly for the ASBWR. Although the ASBWR fuel element has a higher surface-to-volume ratio than LWRs, the inner surface of the annular fuel may still be overheated during transients and accidents. In addition, there is no natural circulation path for the steam-cooled inner channels. Further studies have to be performed to ensure there is sufficient long term cooling in the steam-cooled inner channels after a reactor scram.

3.4 Comparison between the HDR and the Proposed Design

The German superheat reactor, HDR, which also used annular fuel elements for boiling and superheating, is described in Appendix A. Obviously, there are some similarities between the HDR and the proposed ASBWR. A detailed comparison between these two reactors is provided in this section. Although the HDR failed after a few days of operation [58], the ASBWR is still considered promising because of its distinguishing features.

3.4.1 Comparison of Fuel Element

The design characteristics of the HDR and ASBWR are listed in Table 3-4. The fuel element of the HDR has similar dimension as the ASBWR. The main differences of these two fuel element designs are fuel type, cladding material and fuel active length. The HDR adopted powder fuel (Vibration-Packing, VIPAC), whereas the ASBWR uses sintered annular fuel pellets. For cladding, the HDR used two different materials for inner and outer claddings to deal with the uneven axial thermal expansion, whereas the ASBWR uses bellows and only one type of material for both claddings. The active length of the HDR fuel element is shorter than that of the ASBWR due to the difference in power level.

3.4.2 Comparison of Fuel Assembly

The HDR fuel assembly consisted of 24 fuel elements in a 5x5 square array, whereas the ASBWR assembly comprises 60 fuel elements and one square water rod in an 8x8 array. Figure 3-21 shows the simplified steam flow path in the HDR and ASBWR fuel assemblies. The original design of the HDR required the steam coolant to pass four times through the core to achieve the desirable temperature (500 °C), which means the steam coolant has to be collected twice before leaving the reactor vessel [17]. Thus, the HDR assembly was designed, as shown in Figure 3-21, such that the steam coolant can be easily collected for the next path. Although the prototype HDR, when built in 1965, simplified the design to reduce the steam paths from four to two times through the core, the assembly was still kept as it was conceptualized. However, this design caused difficulty in installing effective separators and dryers in the vessel, which led to the use of gravitational separation in the HDR. In contrast, the ASBWR adopts the opposite flow path which simplifies the overall flow configuration and allows the installation of separators and dryers in the vessel.

Table 3-4 Design characteristics of the HDR and ASBWR [17, 61]

	HDR	ASBWR
Thermal power (MWth)	100	1250
Electric power (MWe)	25	500 (goal)
Reactor pressure (bar)	90.0	71.4
Coolant inlet temperature (°C)	285	278
Coolant outlet temperature (°C)	457	520
Max cladding temp	630	<650
Flow pass through the core	One pass for water Two passes for steam	One pass for water Two passes for steam
Fuel assembly array	5×5	8×8
# of fuel elements per assembly	24	60
Assembly outer dimension (cm)	17.8	19.4
Water rod	No	Yes
Fuel element type	Annular, powder fuel (85% TD)	Annular, pellet fuel (sintered)
Enrichment (%)	5.0	5.0 ~ 7.5*
Fuel pin diameter (mm)	OD:26.5 ID:13.5	OD:19.6 ID:10.0
Fuel meat thickness (mm)	5.4	3.0
Cladding	Inconel 625 (inner) Tool steel (outer)	T91 or Inconel 718
Cladding thickness (mm)	0.5 (inner cladding) 0.6 (outer cladding)	0.8 (inner cladding) 0.8 (outer cladding)
Active fuel length (m)	1.8	3.0
Separation	In RPV (by gravity)	In RPV (by separator)
Reactor internal pump	No	Yes

*To be determined

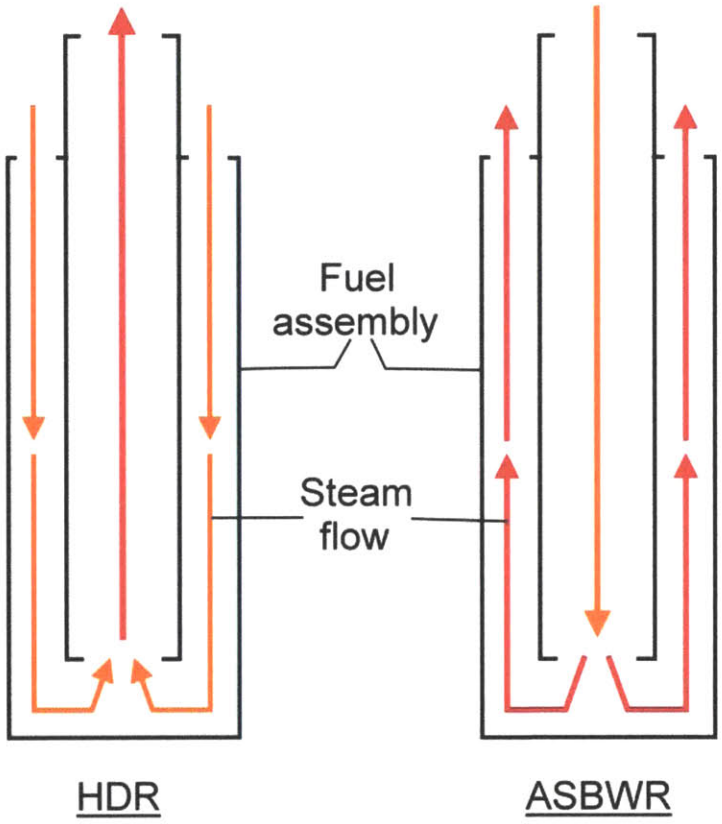

Figure 3-21 Comparison of steam flow path in the HDR and ASBWR fuel assembly

3.4.3 Overall Comparison between the HDR and ASBWR

The major differences between the HDR and ASBWR are listed in Table 3-5. Compared with the HDR, the ASBWR has the following distinguishing features.

1. Better fuel and assembly design

After only equivalent five full power days of operation, the HDR was shut down in 1971 due to deformation of the cladding tubes [92], which were mainly caused by failure of welding and undesirable interaction between cladding and the VIPAC fuel. This is not surprising because the performance of the VIPAC fuel for annular fuel application is still in a premature stage and welding of Inconel and steel is questionable even using today's

technology. To avoid this problem, the ASBWR fuel element uses sintered pellets, annular spring ends, bellows and only one type of material for both inner and outer cladding. In addition, the ASBWR fuel assembly includes a square water rod and is designed such that the flow configuration has been simplified. As a result, the ASBWR is expected to have better fuel performance than the HDR.

2. Better flow configuration

One of the challenges associated with the annular fuel superheater concept is to provide appropriate steam guidance and pressure head for steam to pass through multiple times in the core. The capacity of natural circulation and gravitational separation in the HDR was insufficient, thus the maximum achievable power level of a HDR-like design was limited to 100 MWe [17]. To ensure an adequate steam flow, the ASBWR employs forced circulation by means of reactor internal pumps and uses separators and dryers for steam-water separation. Therefore, there is no restriction on reactor size for the ASBWR and its flow configuration is considered better than that of the HDR.

3. Better technology

Perhaps the most important advantage is that the ASBWR is supported by up-to-date technologies. There is abundant experience in operating BWRs and fossil superheaters nowadays. Furthermore, understanding of material science, thermal-hydraulic principles, and reactor physics, manufacturing reliability, welding techniques, control of water chemistry, and computing power etc. have all been improved during the past fifty years. Consequently, it is believed that the ASBWR is very promising to realize the nuclear superheat concept.

Table 3-5 Major differences between the HDR and ASBWR

HDR	ASBWR
Fuel design • Powder fuel with 85% TD • Two different materials for inner and outer claddings • No water rod in the assembly	Fuel design • Sintered fuel pellet • Single material for both inner and outer claddings • Use of water rod in the assembly
Flow configuration • Natural circulation • Use of gravitational separation • No reactor internal pumps	Flow configuration • Forced circulation • Use of separators and steam dryers • Use of reactor internal pumps
Reactor size • Maximum power level of 100 MWe due to the capacity of natural circulation	Reactor size • No restriction on reactor size
Others • Limited experience in operating BWRs and fossil superheaters when the HDR was built. • 1960s' technology	Others • Plenty of experience in operating BWRs and fossil superheaters nowadays • 2010's technology

3.5 Comparison between a Conventional BWR and the ASBWR

Table 3-6 lists the main design parameters for a conventional BWR with GE11 fuel assemblies and the ASBWR. The BWR data are obtained from Reference [110]. For a better comparison, the ASBWR has been designed to have the same operating pressure and core inlet temperature as the reference BWR. The hot assembly peaking factor is also assumed to be the same as the reference BWR. Power density and fuel enrichment of the ASBWR will be determined by safety limits, such as the Minimum Critical Power Ratio (MCPR) and Minimum Critical Heat Flux Ratio (MCHFR), selection of cladding material, and other design constraints. Power split and local peaking factors are calculated by computational tools, which are discussed in detail in Chapter 4 and Chapter 5, respectively.

Table 3-6 Characteristics of a conventional BWR and the ASBWR [110]

	Conventional BWR	ASBWR
Operating pressure (bar)	71.4	71.4
Power (MWth)	3,323	1,250
Core diameter (m)	4.9	3.0 ~ 3.6*
Active core height (m)	3.7	3.0
Power density (kW/L)	50.5	40 ~ 60*
Specific power (kW/kg U)	24.6	20.8 ~ 31.2*
Fuel element geometry	Solid	Annular
Fuel average enrichment (w/o)	4.3	5.0 ~ 7.5*
Coolant type	Water	Steam (inner channel) Water (outer channel)
# of fuel assembly	764	160 ~ 250*
Fuel array	9 x 9	8 x 8
# of fuel rods	56,536	10,000 ~ 15,000*
Cladding material	Zircaloy-2	T91 or Inconel 718
Cladding thickness (mm)	0.71	0.8
Gap thickness (mm)	0.1	Steam side: 0.1 Water side: 0.1
Fuel rod diameter (mm)	11.18	19.6 (outer diameter) 10.0 (inner diameter)
Pitch (mm)	14.3	23
Pitch to diameter ratio	1.279	1.174
Core inlet temperature (°C)	278.3	278.3
Steam outlet temperature (°C)	287.2	520.0 (goal)
Core exit quality (%)	14.0	14.1
Hot assembly exit quality (%)	24.4	24.2
Hydrogen to heavy metal ratio	4.47	4.42
Hot assembly power (MWth)	6.3	7.6 ~ 11.4*
Hot assembly power peaking factor	1.45	1.45
Local power peaking	1.29	1.25
Hot assembly mass flow rate (kg/s)	15.2	13.7 ~ 20.5* (water side)
Hot assembly mass flux (kg/m^2-s)	1644	869 ~ 1303* (water side)
Efficiency (%)	33	40 (goal)

*To be determined

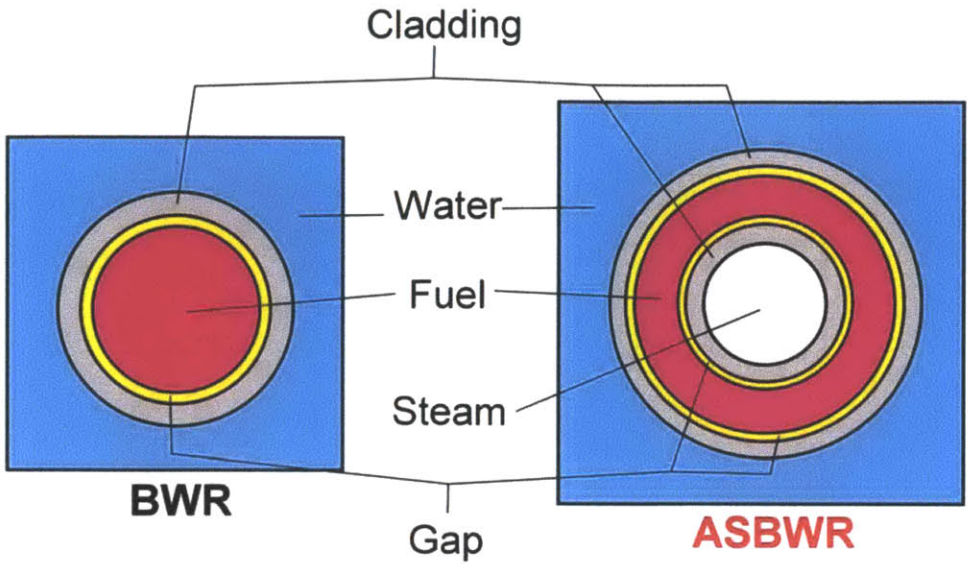

	BWR	ASBWR
Fuel rod diameter (mm)	11.2	Inner: 10.0 Outer:19.6
Cladding material	Zircaloy-2	T91 or Inconel 718
Cladding thickness (mm)	0.7	0.8
Gap thickness (mm)	0.1	0.1
Pitch to diameter ratio	1.28	1.17

Figure 3-22 Comparison of a BWR fuel pin and the ASBWR annular fuel element

Figure 3-22 illustrates the difference between a typical BWR fuel pin and the ASBWR annular fuel element. Figures 3-23 and 3-24 show the fuel assembly geometry of the reference BWR and the ASBWR. Dimensions of these two assemblies are listed in Table 3-7. It can be seen from Figures 3-23 and 3-24 that the ASBWR fuel assembly and control module consists of four fuel assemblies, one cruciform control rod and water gaps, which is similar to the BWR design.

In summary, the ASBWR has been intentionally designed to keep some of the BWR characteristics in order to benefit from the abundant experience of BWR operation. On the other hand, the ASBWR is distinguished from BWRs by the use of annular fuel

elements for superheating steam. In the following chapters, results of neutronic and thermal-hydraulic analyses are presented to display more features of the ASBWR design.

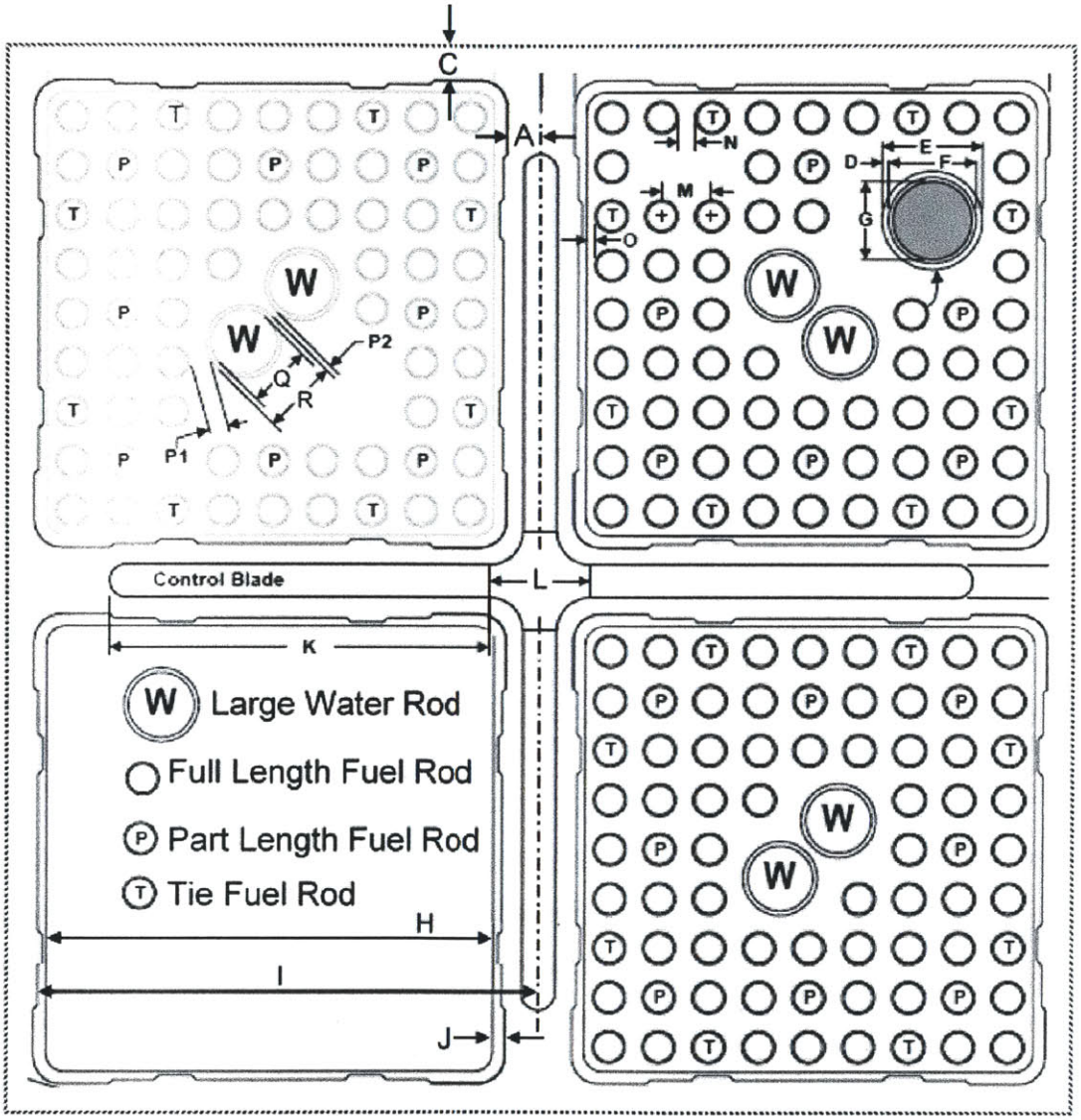

Figure 3-23 The reference BWR assembly module (dimensions given in Table 3-7)

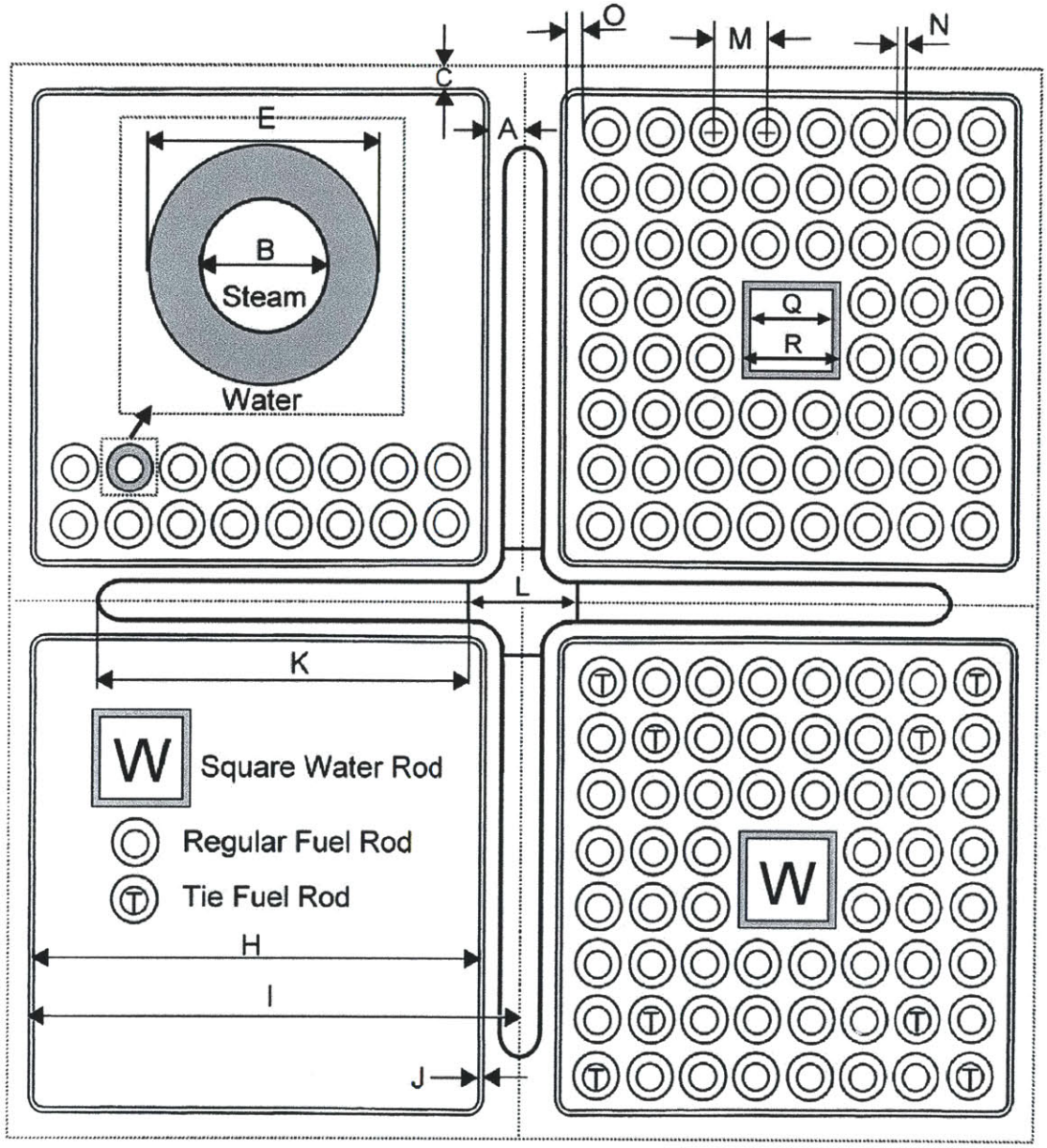

Figure 3-24 The ASBWR assembly module (dimensions given in Table 3-7)

Table 3-7 Dimensions of the reference BWR and ASBWR fuel assemblies

	Conventional BWR Assembly (GE11)	ASBWR Assembly
Geometry	9 x 9 square	8 x 8 square
A (mm)	7.4	7.5
C (mm)	7.4	7.5
E (mm)	11.18	19.6
B (mm)	---	10.0
M (mm)	14.3	23.0
O (mm)	3.53	4.0
N (mm)	3.09	3.4
H (mm)	132.5	188.6
I (mm)	145.0	201.2
J (mm)	2.54	2.54
K (mm)	115.0	*
L (mm)	40.13	40.13
Q (mm)	23.37	40
R (mm)	24.89	42
P1 (mm)	1.79	---
P2 (mm)	1.55	---
Pitch/Diameter	1.28	1.17
Active fuel rod height (mm)	3707.9	3000.0
Total fuel Rod height (mm)	4178.7	*
Fuel pins / Water rods per fuel assembly	74/2	60/1
Assembly outer dimension (mm)	137.58	193.68
Average rod linear power (kW/m)	15.85	32.2 (21.8 for water side 10.4 for steam side)

*To be determined

Chapter 4

Neutronic Analysis

4.1 Introduction

Two-dimensional (2D) neutronic analysis has been performed using CASMO-4 for the proposed ASBWR. The main purpose of the 2D neutronic analysis is to investigate the general physical characteristics of the ASBWR. Several tasks have been carried out in this preliminary neutronic study, including:

(1) single pin benchmark between CASMO-4 and MCNP-4C;
(2) water rod design for the ASBWR assembly;
(3) burnup calculation with various cladding materials;
(4) investigation on the desired distribution of enrichment and poison rods;
(5) calculation of void and fuel temperature reactivity coefficients;
(6) considerations for the control rod design
(7) estimation of the fuel cycle length
(8) evaluation of the impact of higher enrichment on the cost of electricity generation.

4.2 Computational Tools

4.2.1 CASMO-4

CASMO-4 [120], developed by Studsvik, is a multi-group two dimensional transport code written in FORTRAN 77. It is a deterministic lattice physics code used for burnup calculations of light water reactor assemblies or pin cells. The code can deal with geometries consisting of cylindrical fuel rods of varying compositions in a square or hexagonal lattice. CASMO-4 is capable of accommodating various rod types such as those containing gadolinium, burnable absorber rods, and cluster control rods etc.

4.2.2 MCNP-4C

MCNP [121] is a general purpose, generalized-geometry, continuous-energy, coupled neutron/photon/electron Monte Carlo N-Particle transport code developed by the Los

Alamos National Laboratory (LANL). It is used primarily for the simulation of nuclear reactions, such as fission, but has the capability to simulate particle interactions involving neutrons, photons, and electrons. The neutron energy regime is from 10-11 MeV to 20 MeV, and the photon and electron energy regimes are from 1 keV to 1000 MeV. MCNP is very different from the deterministic codes, such as CASMP-4. Deterministic codes solve the transport equation for the average particle behavior. By contrast, MCNP does not solve an explicit equation, but rather obtains answers by simulating individual particles and recording some aspects (tallies) of their average behavior. The models of MCNP are very realistic as the spatial and energy treatments are in principle exact. Therefore, given sufficient neutron histories and appropriate cross-section libraries, MCNP can determine the neutron flux distribution very accurately.

4.3 Benchmarking: Comparison between MCNP and CASMO

In order to investigate the feasibility of using CASMO to perform neutronic analysis for the proposed ASBWR, a benchmark study has been performed to compare the results of CASMO against that of MCNP. A single annular fuel pin has been modeled using both CASMO and MCNP. Input decks of this benchmark study are listed in Appendix E. Assumptions of this benchmark study are summarized in Table 4-1.

Table 4-1 Assumptions adopted in the benchmark study

(1)	T91 is used as cladding material
(2)	U-235 enrichment is 4.5 w/o
(3)	The active length of the annular fuel pin is 300 cm
(4)	Multiplication factor (k_∞) at three different axial locations (z) are calculated and compared: z = 30, 150 and 290 cm. These three locations represent the bottom, middle and top region of the fuel pin, respectively.
(5)	Water and steam densities and void fraction at these three locations are calculated by MASCAC*.

*MASCAC is introduced and described in Appendix B.

Table 4-2 Results of the benchmark study

Case 1: Cladding thickness = 0.5 mm						
z (cm)	Density (kg/m^3)		Void fraction (%)	Multiplication Factor (k_∞)		Difference* (%)
	Water	Steam		CASMO	MCNP	
30	739.7	23.84	0.0	1.34349	1.34284	0.05
150	417.3	21.33	46.3	1.24518	1.24005	0.41
290	246.3	19.18	70.2	1.14865	1.13225	1.45
Standard deviations of MCNP at z = 30, 150, 290 cm are 0.00036, 0.00027 and 0.00039, respectively.						
Case 2: Cladding thickness = 0.8 mm						
z (cm)	Density (kg/m^3)		Void fraction (%)	Multiplication Factor (k_∞)		Difference* (%)
	Water	Steam		CASMO	MCNP	
30	739.7	23.84	0.0	1.25653	1.25387	0.21
150	417.3	21.33	46.3	1.15125	1.14279	0.74
290	246.3	19.18	70.2	1.05809	1.03621	2.11
Standard deviations of MCNP at z = 30, 150, 290 cm are 0.00039, 0.00027 and 0.00041, respectively.						

*Difference = (CASMO k_∞ – MCNP k_∞) / MCNP k_∞

Results of the single pin benchmark study are summarized in Table 4-2. It is observed in Table 4-2 that CASMO always predicts higher k_∞ than MCNP does. In addition, the difference between CASMO and MCNP is increased if the local void fraction is higher. The principal cause of these differences is due to the fact that CASMO is optimized for solid pin geometry; hence it underestimates the amount of U-238 captures by applying self shielding within the solid pellet and not taking into account the additional captures which occur near the fuel surface in the inner annulus [122]. At locations where the void fraction is low, steam coolant provides insignificant moderation compared to water coolant in the boiling region. Therefore the amount of U-238 captures near the fuel surface in the inner annulus is also insignificant, which results in the slight difference

between CASMO and MCNP. On the other hand, at locations where void fraction is high, the density ratio is reduced between the water and the steam sides. Moderating power of the steam coolant is enhanced relatively. The difference between CASMO and MCNP is increased due to the underestimation of U-238 captures by CASMO.

The other observation from the comparison of Case 1 and Case 2 is that the difference between CASMO and MCNP is increased if there is more T91 cladding material. Similarly, this is due to the fact that CASMO is optimized for solid pin geometry; hence it underestimates the amount of inner cladding captures. This effect is more noticeable in the ASBWR than previous annular fuel BWR analyses [122] because T91 has much stronger thermal neutron absorption cross section than zircaloy.

Considering that the average void fraction of ASBWR is close to a typical BWR, which is about 40 ~ 45%, the difference between CASMO and MCNP is expected to be within an acceptable range of 1%. Therefore, CASMO is selected to be used for preliminary neutronic calculation for the ASBWR.

4.4 Two-Dimensional Neutronics

Two-dimensional neutronic calculations have been performed using CASMO for the ASBWR. Calculation results are compared with a conventional BWR which employs typical GE 11 fuel assemblies. Assembly dimensions of the reference BWR and ASBWR are described in Figures 3-23, 3-24 and Table 3-7. Table 4-3 and 4-4 list the input parameters and assumptions for the 2D neutronic calculation, respectively. Constraints of neutronic analysis are given in Table 4-5.

4.4.1 Water Rod Design of the ASBWR Assembly

Initially the ASBWR assembly was designed with no water rods, as shown in Figure 4-1, to increase power density. However, it was found afterwards that the burnup would be reduced due to insufficient moderation if there are no water rods in the assembly.

Table 4-3 Input parameters for the 2D neutronic calculation.

	Reference BWR	ASBWR
Active core height (m)	3.7	3.0
Fuel rod diameter (mm)	11.18	19.6 (outer diameter) 10.0 (inner diameter)
Gap thickness (mm)	0.1	Steam side: 0.1 Water side: 0.1
Coolant type	Water	Steam (inner channel) Water (outer channel)
Fuel array	9 x 9	8 x 8
Fuel average enrichment (w/o)	4.32	6.0 ~ 7.5*
Cladding material	Zircaloy-2	T91 or Inconel 718
Cladding thickness (mm)	0.71	0.8
Cladding microscopic thermal neutron absorption cross section, σ_a (barns)	0.21	T91: 2.64 Inconel 718: 4.07
Pitch (mm)	14.3	23
Hydrogen to heavy metal ratio	4.47	4.42
Specific power (kW/kgU)	24.6	26.0
Power density (kW/L)	50.5	50.0

*To be determined

Table 4-4 Assumptions adopted in the 2D neutronic calculation

(1) Average void fraction is assumed as 45%
(2) Steam coolant density is assumed as 21.3 kg/m^3 based on the results of MASCAC calculation
(3) Steam coolant temperature is assumed as 757 K based on the results of MASCAC calculation
(4) Power density is assumed as 50.0 kW/L for the ASBWR
(5) Compound of UO_2-Gd_2O_3 burnable poison rods are used
(6) Three-batch cycle is adopted

Table 4-5 Constraints of neutronic analysis

(1)	18 to 24-month cycle
(2)	1% reactivity shutdown margin
(3)	Average discharge burnup <60 MWd/kgU
(4)	Peak enrichment <20%wt. (only low-enriched uranium fuel is used)

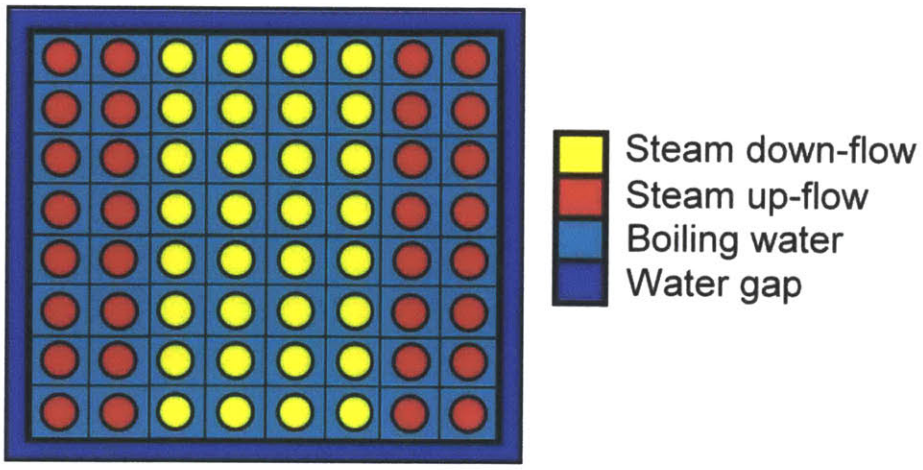

Figure 4-1 Initial design of the ASBWR assembly

In addition, the existence of water rods ameliorates the void coefficient. If there are no water rods in the assembly, the void coefficient is expected to be very negative, which may deteriorate the nuclear/thermal-hydraulic coupled stability of the system and create difficulty in achieving the desired shutdown margin. Therefore, the subsequent design, as shown in Figure 3-19, incorporates a square water rod into the assembly.

4.4.2 Burnup Calculation for the Poison-free Assembly

Burnup calculation for the assemblies consisting of poison-free, uniform enrichment fuels

has been performed using CASMO for the reference BWR and ASBWR. Table 4-6 summarizes the calculation results. Comparing Cases 1 and 2 in Table 4-6, it is found that the single-batch burnup (B_1) is increased by about 12% (from 19.39 to 21.76 MWd/kgU) when the square water rod is in the assembly. It is also observed in Table 4-6 that given the same enrichment, the ASBWR achieves much lower B_1 than the reference BWR does. Apparently the main reason for the decrease in burnup is due to the strong thermal neutron absorption cross section of T91 and Inconel 718, since the ASBWR could achieve a similar B_1 to the reference BWR if zircaloy is used as the cladding material.

Figure 4-6 shows the results of burnup calculation for the poison-free assemblies with various uniform enrichments. In order to achieve the same B_1 as the reference BWR, the enrichment of the ASBWR fuel has to be increased to above 6% when T91 is used as cladding. If using Inconel 718 as cladding, the neutron economy is worse and requires an enrichment of above 7% for a comparable B_1 to the reference BWR.

Table 4-6 Results of burnup calculation for poison free, uniform enriched fuels

Case	Reactor	Cladding material	Water rod	Single-batch burnup, B_1 (MWd/kgU)	Assembly design
1	BWR	Zircaloy-2	Yes	38.38	Figure 3-23
2	ASBWR	T91	No	19.39	Figure 4-1
3	ASBWR	Zircaloy-2	Yes	37.16	Figure 3-19
4	ASBWR	T91	Yes	21.76	
5	ASBWR	Inconel 718	Yes	14.98	
Note: All fuels are poison-free with a uniform enrichment of 4.32 w/o					

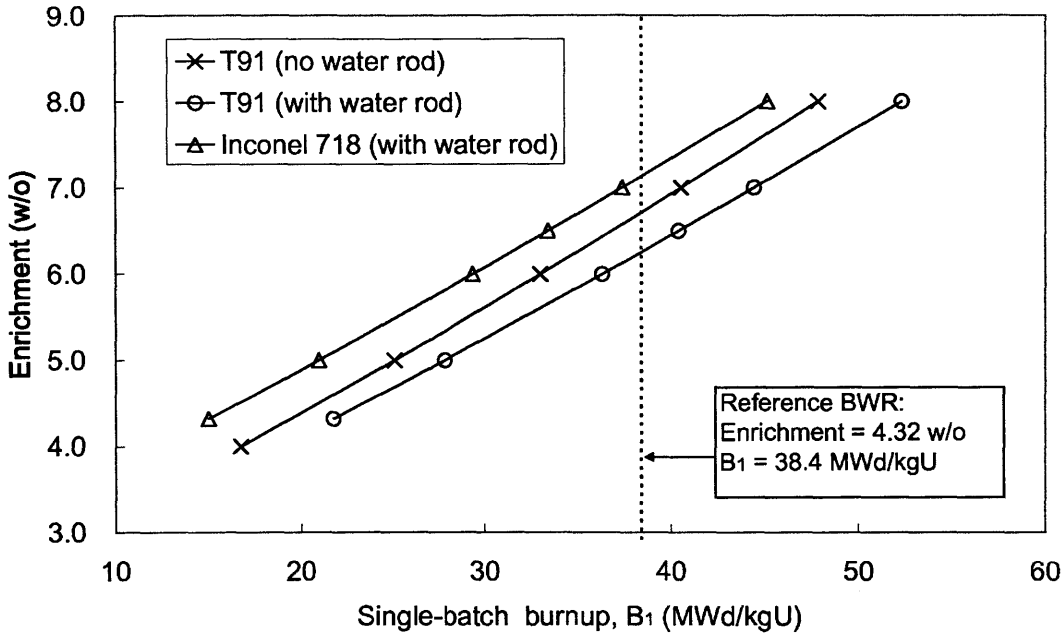

Figure 4-2 Burnup calculation for poison free fuels with various uniform enrichments

4.4.3 Distribution of Enrichment and Poison Rods in the ASBWR Assembly

The distribution of enrichment and poison rods is designed so that the ASBWR assembly could generate satisfactory local power peaking factors (PPF) and a comparable single-batch burnup to the reference BWR. Figures 4-3 and 4-4 show the enrichment design and fresh fuel PPFs of the reference BWR assembly, respectively. Infinite multiplication factor (k_∞) versus burnup of the reference BWR is plotted in Figure 4-5.

Three designs of the distribution of enrichment and poison rods have been proposed for the ASBWR assembly. Figures 4-6 to 4-8 illustrate the details of these designs. The numbers of poison rods in the three assembly designs are 8, 10 and 12, respectively. The weight percent of gadolinium has been varied to estimate the desirable amount of burnable poison in the assembly. Burnup calculations have been performed for a serious of cases. Table 4-7 lists the input parameters of these simulation cases.

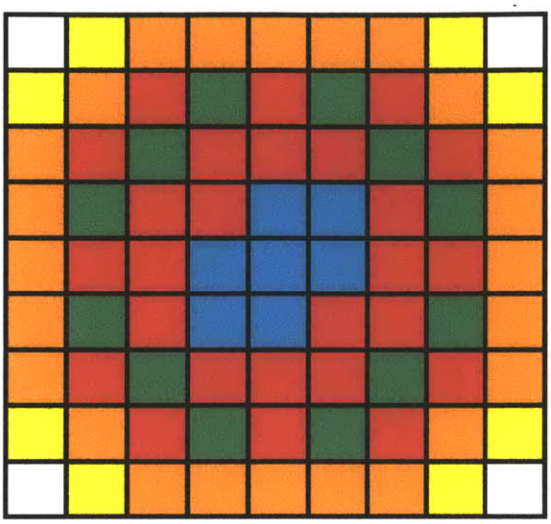

	U-235 (w/o)	Gd (w/o)	Note
	4.80	---	High enrichment
	4.30	---	
	3.45	---	
	2.60	---	Low enrichment
	4.45	5.0	Gd poison rod
	---	---	Water rod

Figure 4-3 Enrichment and poison rod distribution of the reference BWR

1.245	1.260	1.280	1.170	1.150	1.170	1.290	1.270	1.245
1.267	1.149	1.010	0.400	0.920	0.400	1.020	1.150	1.267
1.286	1.011	0.390	0.870	0.990	0.940	0.390	1.040	1.286
1.172	0.398	0.875	1.112			0.940	0.400	1.172
1.156	0.924	0.993				0.990	0.920	1.156
1.173	0.399	0.936			1.112	0.880	0.400	1.173
1.290*	1.019	0.394	0.936	0.992	0.874	0.390	1.020	1.290
1.269	1.152	1.019	0.399	0.923	0.398	1.009	1.147	1.269
1.246	1.268	1.288	1.171	1.154	1.170	1.283	1.264	1.241

***Highest peaking factor**

Figure 4-4 Fresh fuel power peaking factors of the reference BWR

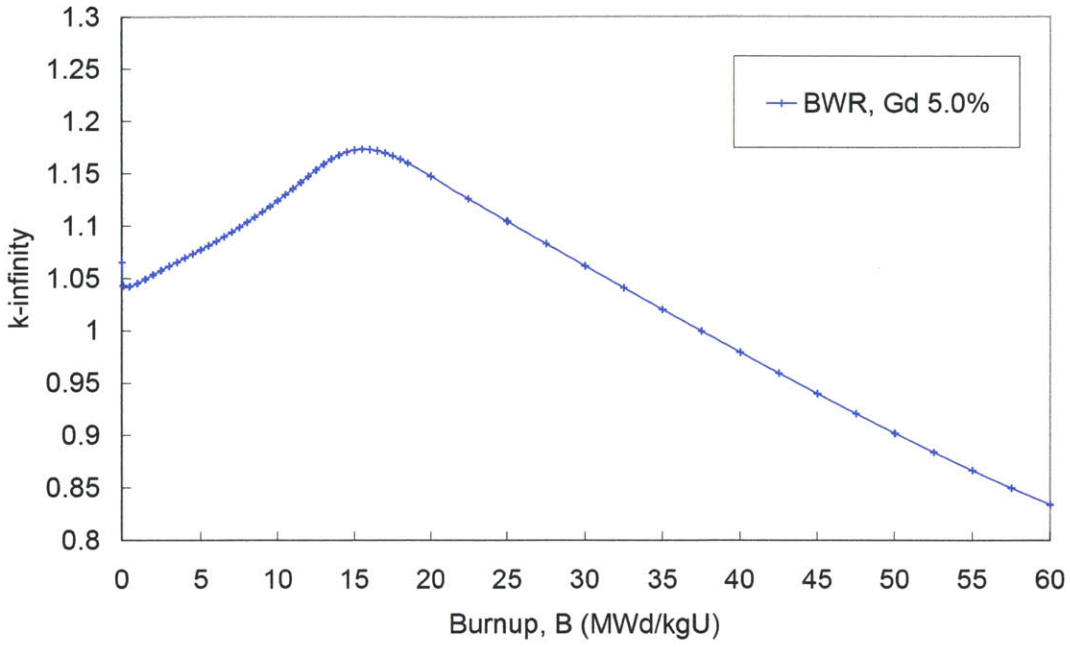

Figure 4-5 Infinite multiplication factor versus burnup of the reference BWR

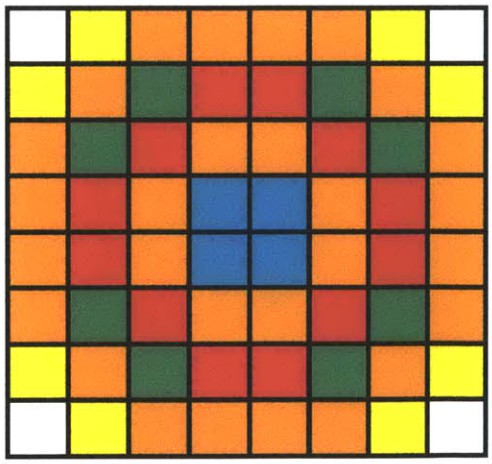

	U-235 (w/o)*	Gd (w/o)	Note
	7.00	---	High enrichment
	6.40	---	
	5.50	---	
	3.50	---	Low enrichment
	7.50	2.0 ~ 6.0	Gd poison rod
	---	---	Water rod

* For T91 cladding

Figure 4-6 Enrichment and poison rod distribution of the ASBWR (Design A)

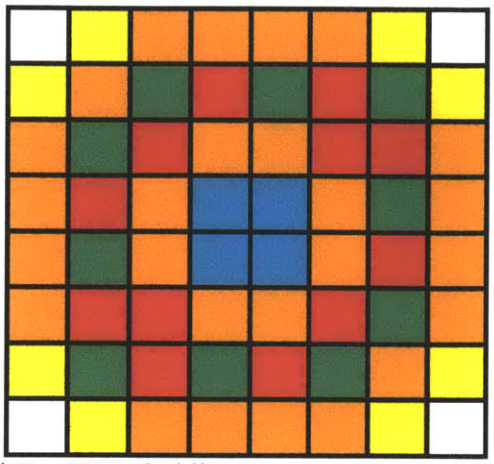

	U-235 (w/o)*	Gd (w/o)	Note
	7.00	---	High enrichment
	6.40	---	
	5.50	---	
	3.50	---	Low enrichment
	7.50	2.0 ~ 6.0	Gd poison rod
	---	---	Water rod

* For T91 cladding

Figure 4-7 Enrichment and poison rod distribution of the ASBWR (Design B)

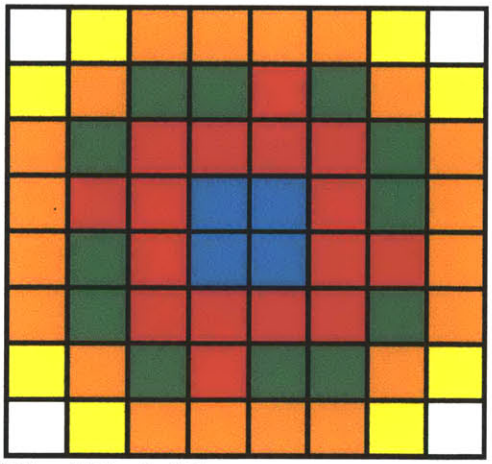

	U-235 (w/o)*	Gd (w/o)	Note
	7.00	---	High enrichment
	6.40	---	
	5.50	---	
	3.50	---	Low enrichment
	7.50	2 .0~ 6.0	Gd poison rod
	---	---	Water rod

* For T91 cladding

Figure 4-8 Enrichment and poison rod distribution of the ASBWR (Design C)

Table 4-7 Input parameters of the simulation cases

Case	Design*	Gd weight percent (w/o)	Number of poison rods	Cladding material	UO_2 average enrichment (w/o)
BWR					
Ref.	Fig. 4-3	5.0	12	Zircaloy-2	4.32
ASBWR					
TA2	A	2.0	8	T91	6.35
TA3	A	3.0	8	T91	6.35
TA4	A	4.0	8	T91	6.35
TA5	A	5.0	8	T91	6.35
TA6	A	6.0	8	T91	6.35
TB2	B	2.0	10	T91	6.39
TB3	B	3.0	10	T91	6.39
TB4	B	4.0	10	T91	6.39
TB5	B	5.0	10	T91	6.39
TB6	B	6.0	10	T91	6.39
TC2	C	2.0	12	T91	6.47
TC3	C	3.0	12	T91	6.47
TC4	C	4.0	12	T91	6.47
TC5	C	5.0	12	T91	6.47
TC6	C	6.0	12	T91	6.47
IA2	A'	2.0	8	Inconel 718	7.28
IA2-5	A'	2.5	8	Inconel 718	7.28
IA3	A'	3.0	8	Inconel 718	7.28
IA4	A'	4.0	8	Inconel 718	7.28
IA5	A'	5.0	8	Inconel 718	7.28

*Design A: see Figure 4-6;
Design A': see Figure 4-12;
Design B: see Figure 4-7;
Design C: see Figure 4-8.

The results of burnup calculation for the ASBWR using T91 as cladding are plotted in Figures 4-9 ~ 4-11. It can be found in Figures 4-9 ~ 4-11 that, regardless of the gadolinium weight percent, all the three designs give approximately the same single-batch burnup of 37.5 MWd/kgU as the reference BWR. The other important observation is that, compared with Figure 4-5, the ASBWR does not burn gadolinium as efficiently as the reference BWR does. In Figures 4-9 to 4-11, the peak of k_∞ is not noticeable and it seems to take more time to completely burn out the gadolinium. The main cause of this inefficient burning of gadolinium is due to the fact that the ASBWR neutron spectrum is somehow harder than the reference BWR. Since the hydrogen to heavy metal ratio (H/HM) is about the same for the two reactors as shown in Table 4-3, the principal reason for neutron spectrum hardening is due to the additional enrichment of U-235 and the stronger cladding absorber.

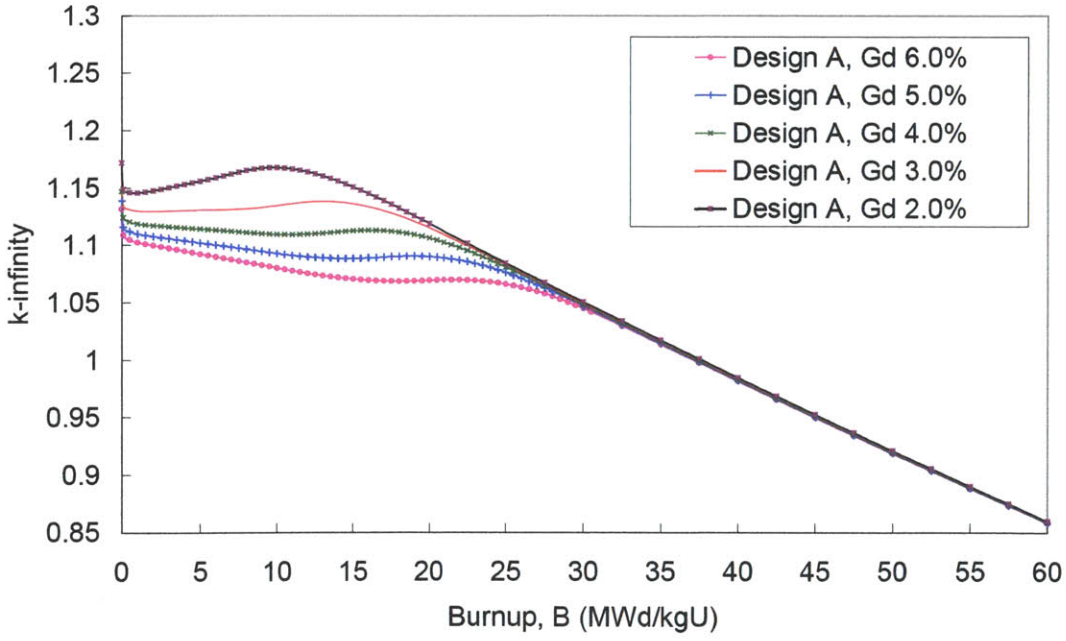

Figure 4-9 Infinite multiplication factor versus burnup of the ASBWR (Design A)

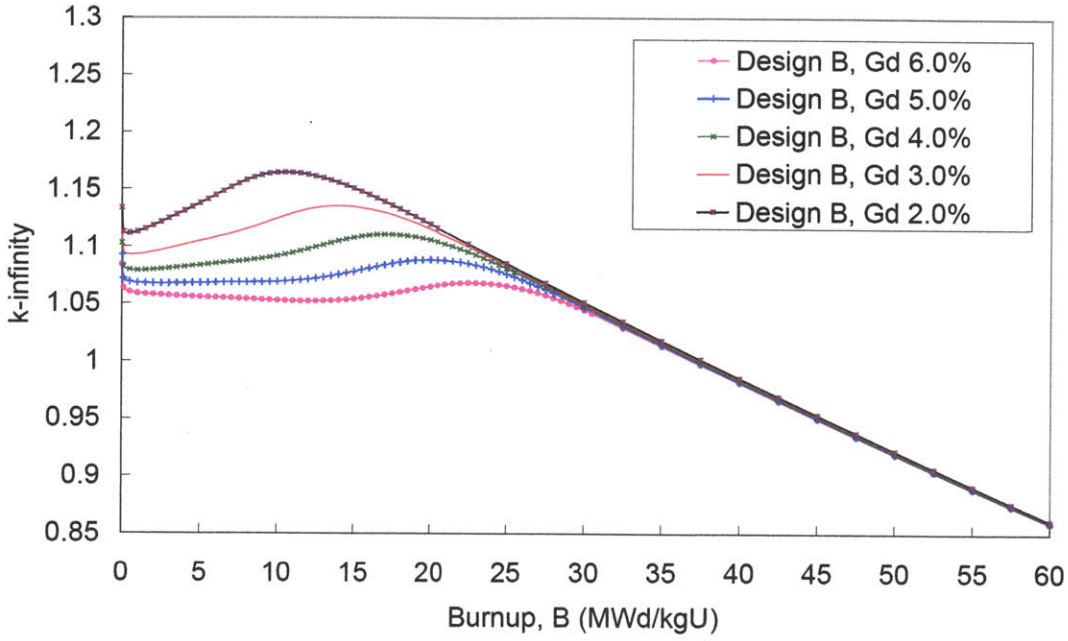

Figure 4-10 Infinite multiplication factor versus burnup of the ASBWR (Design B)

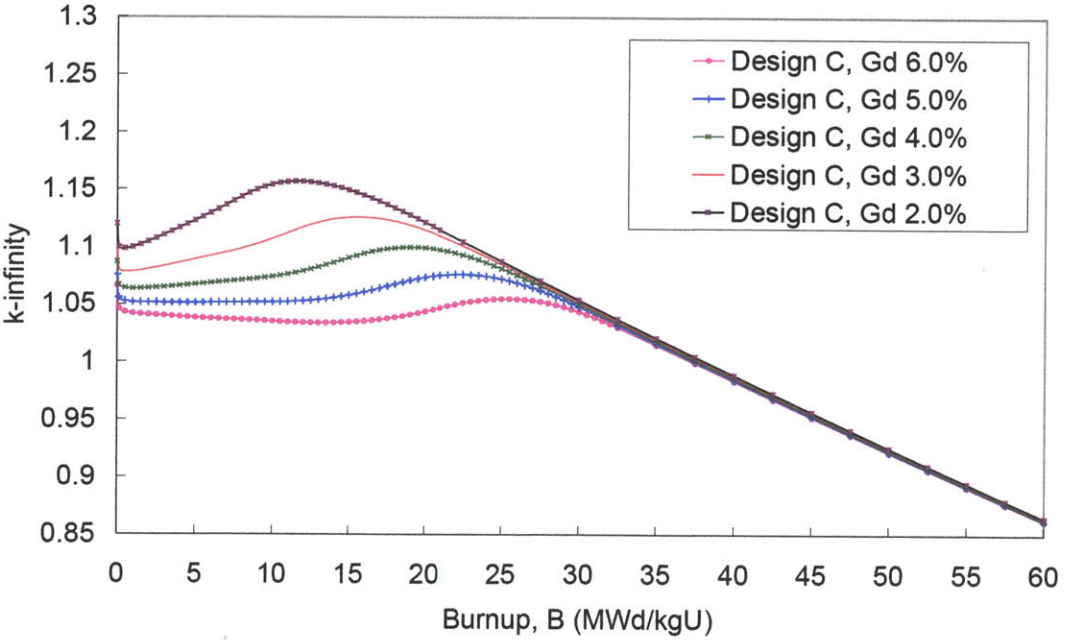

Figure 4-11 Infinite multiplication factor versus burnup of the ASBWR (Design C)

Table 4-8 Comparison of fast-to-thermal neutron flux ratio (poison-free case)

	BWR	ASBWR	ASBWR	ASBWR
Cladding	Zircaloy-2	Zircaloy-2	T91	Inconel 718
U-235 enrichment distribution	Uniform	Uniform	Uniform	Uniform
Average U-235 enrichment (w/o)	4.32	4.32	4.32	4.32
Assembly array	9 x 9	8 x 8	8 x 8	8 x 8
Number of Gd rods	0	0	0	0
Fast-to-thermal flux ratio (ϕ_F / ϕ_T)	5.104	5.229	5.434	5.547
Difference (%)*	---	+ 2.5	+ 6.5	+ 8.7
Note: Results are calculated for fresh fuel using CASMO.				

* Difference = [(ϕ_F / ϕ_T)$_{ASBWR}$ – (ϕ_F / ϕ_T)$_{BWR}$] / (ϕ_F / ϕ_T)$_{BWR}$

Table 4-9 Comparison of fast-to-thermal neutron flux ratio (poison rod case)

	BWR	ASBWR	ASBWR
Cladding	Zircaloy-2	T91	Inconel 718
U-235 enrichment distribution	Non-uniform (Figure 4-3)	Non-uniform (Figure 4-6)	Non-uniform (Figure 4-12)
Average U-235 enrichment (w/o)	4.32	6.35	7.28
Assembly array	9 x 9	8 x 8	8 x 8
Number of Gd rods	14	8	8
Gd weight percent (w/o)	5.0	5.0	5.0
B_1 (MWd/kgU)	37.5	37.5	37.5
Fast-to-thermal flux ratio (ϕ_F / ϕ_T)	5.492	7.009	7.668
Difference (%)*	---	+ 27.6	+ 39.6
Note: Results are calculated for fresh fuel using CASMO.			

* Difference = [(ϕ_F / ϕ_T)$_{ASBWR}$ – (ϕ_F / ϕ_T)$_{BWR}$] / (ϕ_F / ϕ_T)$_{BWR}$

Tables 4-8 and 4-9 list the comparison of fast-to-thermal neutron flux ratio (ϕ_F / ϕ_T) for the poison-free and poison rod cases, respectively. In Table 4-8, it can be seen that the doubled cladding material in the ASBWR results in a slightly higher fast-to-thermal neutron ratio than the reference BWR. Moreover, the difference in fast-to-thermal neutron flux ratio increases if the cladding material has a stronger thermal neutron cross section. For the practical design of the ASBWR assembly, results in Table 4-8 indicate that the difference increases further due to the addition of U-235 enrichment. In principle, a higher fast-to-thermal neutron flux ratio represents a harder neutron spectrum. Therefore, it can be concluded that the ASBWR tends to have a harder neutron spectrum than BWRs mainly because of the additional enrichment for attaining a comparable burnup.

In consideration of the fact that gadolinium-poisoned rods increase fabrication costs, heterogeneity and deteriorates fuel performance, Design A has been selected for the ASBWR assembly since it contains fewer poison rods compared with the other designs. The weight percent of gadolinium has been decided to ensure that the core average multiplication factor remains above 1.0 till the end of cycle (EOC). First, the discharge burnup is computed using the linear reactivity model [123]

$$B_d = (\frac{2n}{n+1}) B_1 \qquad (4\text{-}1)$$

where

n	=	number of batches
B_d	=	discharge burnup (MWd/kgU)
B_1	=	single-batch burnup (MWd/kgU).

Thus, the discharge burnup is 56.25 MWd/kgU given the assumed three-batch cycle and single-batch burnup of 37.5 MWd/kgU. The multiplication factors of the once-burned, twice-burned and thrice-burned assemblies (k_1, k_2 and k_3) could be estimated at burnup equal to 18.75, 37.5 and 56.25 MWd/kgU in Figure 4-9, respectively. Then the core

average multiplication factor can be obtained by averaging k_1, k_2 and k_3.

Table 4-10 summarizes the calculation results of the core average multiplication factors at EOC. As shown in Table 4-10, if T91 is used as cladding, gadolinium should not exceed 3.0 weight percent, otherwise criticality may not be sustained till the end of cycle.

Similar analyses have been performed for the Inconel 718 cladding. Figure 4-12 shows the distribution of enrichment and poison rods for the assembly using Inconel 718 cladding. Results of infinite multiplication factor versus burnup are plotted in Figure 4-13. As shown in Table 4-10, if using Inconel 718 as cladding, gadolinium should not exceed 2.5 weight percent in order to stay critical till the end of cycle.

For the following analysis, TA3 and IA2-5 are selected as the base cases because of their lower initial multiplication factors, which imply a lower peaking factor of the fresh assembly.

Table 4-10 Calculation results of the core average multiplication factors at EOC

Case	Gd weight percent (w/o)	k_1	k_2	k_3	$\frac{k_1+k_2+k_3}{3}$
TA2	2.0	1.12752	1.00096	0.88241	1.00363
TA3	3.0	1.12217	0.99994	0.88184	1.00132
TA4	4.0	1.10995	0.99903	0.88135	0.99677
TA5	5.0	1.09063	0.99820	0.88089	0.98990
TA6	6.0	1.06901	0.99743	0.88050	0.98231
IA2	2.0	1.11534	1.00085	0.89045	1.00221
IA2-5	2.5	1.11121	1.00026	0.89006	1.00051
IA3	3.0	1.10531	0.99974	0.88972	0.99826
IA4	4.0	1.08851	0.99872	0.88907	0.99210
IA5	5.0	1.06906	0.99766	0.88847	0.98506

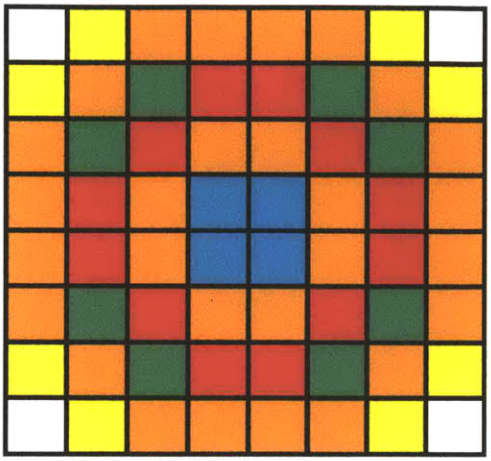

	U-235 (w/o)*	Gd (w/o)	Note
	8.00	---	High enrichment
	7.40	---	
	6.30	---	
	4.20	---	Low enrichment
	8.30	2.5	Gd poison rod
	---	---	Water rod

* For Inconel 718 cladding

Figure 4-12 Enrichment and poison rod distribution of the ASBWR assembly using Inconel 718 cladding

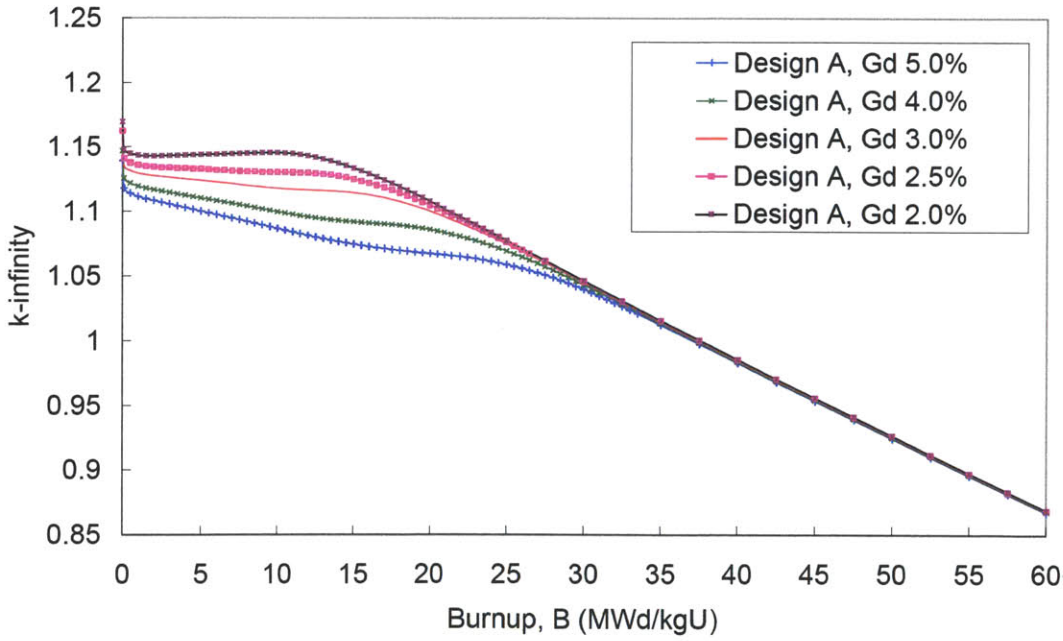

Figure 4-13 Infinite multiplication factor versus burnup of the ASBWR assembly using Inconel 718 cladding

4.4.4 Assembly Power Peaking Factors

Fresh fuel power peaking factors of the ASBWR using T91 and Inconel 718 claddings are shown in Figures 4-14 and 4-15, respectively. These PPFs are calculated by CASMO based on the simulation cases of TA3 and IA2-5 in Table 4-7.

1.182	1.245	1.182	1.148	1.148	1.182	1.244	1.183
1.245*	0.926	0.511	0.888	0.888	0.511	0.926	1.245
1.183	0.511	0.856	1.042	1.042	0.856	0.511	1.184
1.150	0.889	1.043			1.043	0.888	1.150
1.150	0.888	1.043			1.043	0.889	1.150
1.184	0.511	0.855	1.042	1.042	0.855	0.511	1.183
1.245	0.926	0.511	0.888	0.888	0.511	0.926	1.245
1.183	1.244	1.182	1.148	1.148	1.182	1.245	1.183

***Highest peaking factor**

Figure 4-14 Fresh fuel PPFs of the ASBWR using T91 cladding

1.232*	1.231	1.181	1.145	1.145	1.180	1.231	1.232
1.231	0.913	0.530	0.869	0.869	0.530	0.913	1.231
1.182	0.530	0.850	1.045	1.045	0.850	0.530	1.182
1.147	0.869	1.045			1.045	0.869	1.147
1.147	0.869	1.045			1.045	0.869	1.147
1.182	0.530	0.850	1.045	1.045	0.850	0.530	1.182
1.231	0.913	0.530	0.869	0.869	0.530	0.913	1.231
1.232	1.231	1.180	1.145	1.145	1.181	1.231	1.232

***Highest peaking factor**

Figure 4-15 Fresh fuel PPFs of the ASBWR using Inconel 718 cladding

4.4.5 Void and Fuel Temperature Reactivity Coefficients

Assembly-wise void and fuel temperature reactivity coefficients have been computed for both the reference BWR and ASBWR. In this calculation, control rods are assumed to be not present in the core. The main purpose of this calculation is to investigate the magnitude of void and fuel temperature coefficients relative to the reference BWR.

The void coefficient of a typical BWR characterizes the moderating power of the coolant. Since the ASBWR has approximately the same hydrogen to heavy metal ratio as the reference BWR, an increase in flow area leads to an increase of coolant worth and will result in more negative void coefficient. The increase in flow area can be observed by comparing the flow dimensions shown in Table 3-7.

The Calculated void and fuel temperature reactivity coefficients are summarized in Table 4-11. As shown in Table 4-11, the void coefficients of the ASBWR are higher (more negative) than that of the reference BWR. In addition, the fuel temperature coefficients of the ASBWR are also slightly higher (more negative) than that of the reference BWR. To calculate more accurate void and fuel temperature coefficients, a full core analysis is needed and the calculations should take into account the effects of control rods.

Table 4-11 Calculation results of the void and fuel temperature coefficients

	Cladding material	Void coefficient (pcm/ % void)	Fuel temperature coefficient (pcm / K)	Case description
BWR	Zircaloy-2	-58.3	-1.72	Ref., Table 4-7
ASBWR	T91	-67.1	-1.78	TA3, Table 4-7
ASBWR	Inconel 718	-73.5	-1.81	IA2-5, Table 4-7

4.4.6 Considerations for the Control Rod Design

Due to the harder spectrum and larger assembly dimensions, the ASBWR is expected to require either stronger control materials or a higher control rod number density to obtain a desirable shutdown margin.

Table 4-12 lists the design specifications of the ASBWR and the Advanced Boiling Water Reactor II (ASBWR-II) [110]. Table 4-13 lists the main design objectives of the ASBWR-II. To meet the design objectives, the ABWR-II uses a 1.5 times larger fuel bundle with a K-lattice control rod pattern. Figure 4-16 illustrates the K-lattice and the conventional N-lattice designs [124].

Table 4-12 Design specifications of the ABWR-II and ASBWR

	ABWR-II	ASBWR
Power density (kW/L)	58.1	50.0
Specific power (kW/kgU)	26.1	26.0
Active core height (m)	3.7	3.0
Assembly outer dimension (cm)*	21.4	19.4
Hydrogen to heavy metal ratio	3.58	4.42

*The assembly outer dimension is 13.8 cm for a conventional BWR.

Table 4-13 Main design objectives of the ABWR-II [110]

(1) Achieve 15% power density uprate while keeping the same safety margin as the current ABWR core design
(2) Achieve enough flexibility for future high burnup and longer cycle operation
(3) Reduce the number of fuel assemblies to simplify and shorten refueling outages

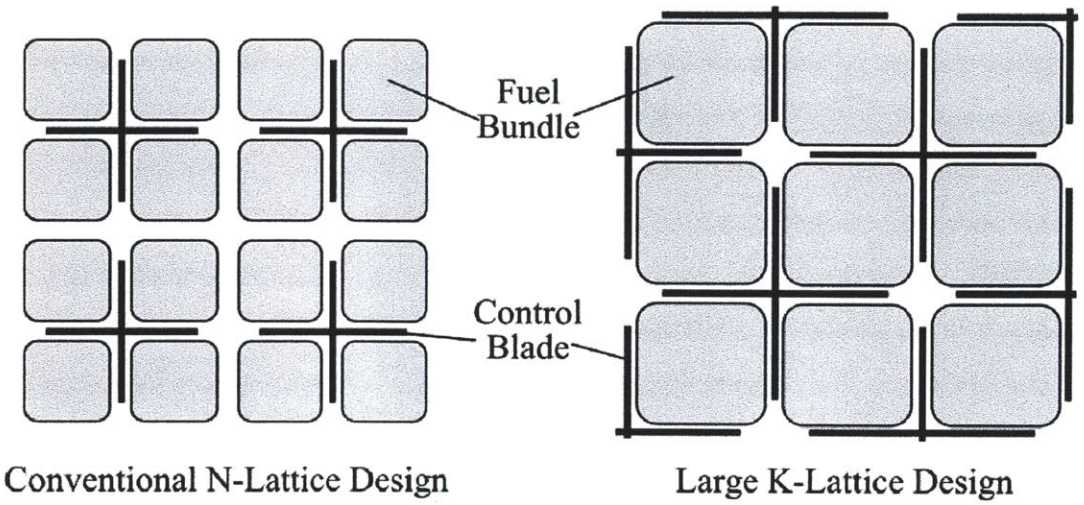

Figure 4-16 Comparison of the conventional and ABWR-II control rod designs [124]

As shown in Table 4-12, the ASBWR has a similar assembly dimension to the ABWR-II. In addition, the ABWR-II also has a harder neutron spectrum than conventional BWRs due to the increased heavy metal inventory [110]. Therefore, the large K-lattice control rod pattern may be applied to the ASBWR as well.

On the other hand, if the conventional N-lattice control rod pattern is used, the absorbing material inside the control rod should have stronger reactivity worth and/or the control blade width should be increased. The required control rod composition and dimensions of a fresh assembly at cold zero power have been investigated. Calculation results are summarized in Table 4-14. As shown in Table 4-14, the absorbing material selected for the ASBWR control rod is 80% enriched boron carbide. The required control blade width to satisfy the 1% shutdown margin are 16.25 and 17.1 cm for the assembly using T91 and Inconel 718 cladding, respectively. However, the reactor core contains not only fresh assemblies but also once-burned and twice-burned assemblies. The control rod design should be further studied using a full core model to determine which rod pattern, N-lattice or K-lattice, is more favorable for the ASBWR.

Table 4-14 Control rod design of the ASBWR

Control rod pattern	N-lattice design	
Absorbing material	80% enriched boron carbide (B_4C)	
Radius of the absorbing cylinder	0.3 cm	
Pitch between absorbing cylinders	0.72 cm	
Cladding material	T91	Inconel 718
Control rod length	16.25 cm	17.40 cm
Infinite multiplication factor	0.98989	0.98976

4.5 Estimation of Fuel Cycle Length

The fuel cycle length has been estimated for the ASBWR. Table 4-15 lists the results for two-batch and three-batch cores. For the base case, a power density of 50 kW/L and a three-batch core are assumed, which leads to an approximately 24-month cycle length.

Table 4-15 Estimation of the ASBWR fuel cycle length

Power density (kW/L)	Specific power (kW/kgU)	Number of batches	Discharge burnup (MWd/kgU)*	Cycle length (month)
40	20.8	2	50.0	39.5
45	23.4	2	50.0	35.2
50	26.0	2	50.0	31.6
55	28.6	2	50.0	28.8
60	31.2	2	50.0	26.4
65	33.8	2	50.0	24.3
70	36.3	2	50.0	22.6
40	20.8	3	56.25	29.7
45	23.4	3	56.25	26.4
50	**26.0**	**3**	**56.25**	**23.7**
55	28.6	3	56.25	21.6
60	31.2	3	56.25	19.8
65	33.8	3	56.25	18.3
70	36.3	3	56.25	16.9

* Discharge burnup is calculated by Eq. (4-1) with $B_1 = 37.5$ MWd/kgU.

4.6 Impact of Enrichment on the Cost of Electricity

A preliminary economic analysis has been performed to evaluate the impact of the ASBWR's higher enrichment on the cost of electricity. Assumptions of this preliminary economic analysis are listed in Table 4-16. The separative work unit (SWU) is calculated based on a 0.3% tails assay. Figure 4-17 shows a typical cost breakdown of nuclear electricity generation [133]. It can be seen that the cost of uranium purchase and enrichment is about 12% of the busbar cost. For a better comparison, the reactor size of the ASBWR is assumed to be the same (3000 MWt) as the reference BWR. Except for the uranium purchase and enrichment cost, the rest of the plant cost is assumed to be the same for the reference BWR and ASBWR.

Results of the analysis are summarized in Table 4-17. As shown in Table 4-17, the uranium purchase and enrichment cost of the ASBWR is increased by 24 ~ 45% due to the higher enrichment. The cost of electricity generation is reduced by 9 ~ 12% given the assumed plant efficiency. The reduction in the cost of electricity generation might be slightly overestimated since the ASBWR fuel fabrication cost is expected to be higher than the reference BWR. A thorough economic analysis of the cost of the fuel assembly fabrication is needed and is recommended for the future work.

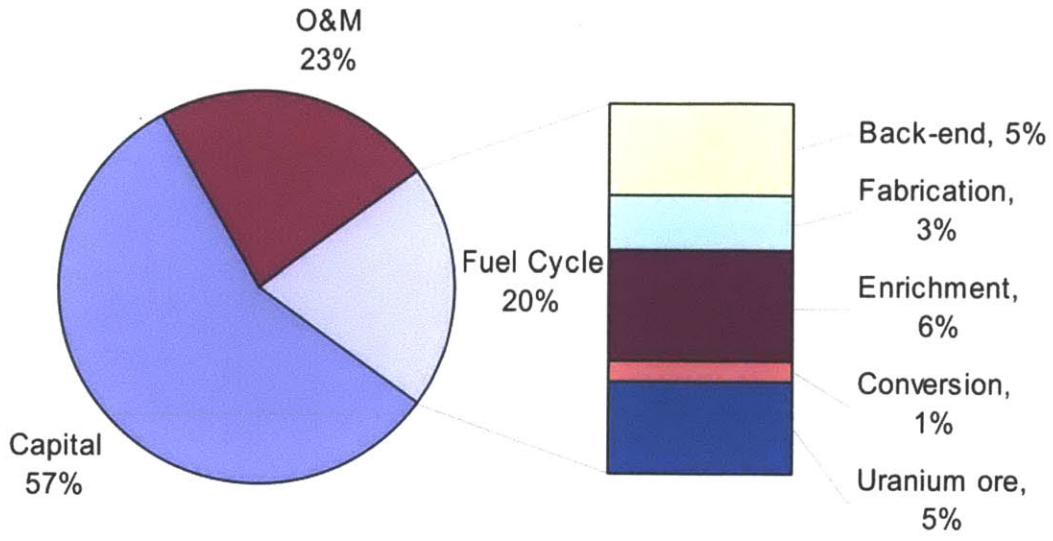

Figure 4-17 Breakdown of the nuclear electricity generation cost [133]

Table 4-16 Assumptions adopted in the preliminary study of cost of electricity

(1)	Natural UF_6 price is \$130 per kilogram uranium [132]
(2)	SWU price is \$153 per SWU [132]
(3)	Plant efficiency is 33% for the reference BWR and is 40% for the ASBWR
(4)	Power density is 50 kW/L for both the reference BWR and ASBWR
(5)	Thermal power output is 3000 MWt for both the reference BWR and ASBWR
(6)	Discharge burnup is 50 MWd/kgU for both the reference BWR and ASBWR
(7)	The fraction of uranium purchase and enrichment cost is 12% of the total cost of electricity generation [133]
(8)	Except for the uranium purchase and enrichment cost, the rest of the plant cost is assumed to be the same for the reference BWR and ASBWR
(9)	The fuel cycle length and capacity factor is assumed the same for the reference BWR and ASBWR

Table 4-17 Results of the preliminary economic study

	Reference BWR	ASBWR	
Thermal power (MWt)	3000	3000	
Plant efficiency (%)	33	40	
Electric power (MWe)	990	1200	
Power density (kW/L)	50	50	
Specific power (kW/kgU)	25	26	
Discharge burnup (MWd/kgU)	50	50	
Cladding material	Zircaloy-2	T91	Inconel 718
Average fuel enrichment (w/o)	4.32	6.35	7.28
Total amount of fuel (ton)	134	130	130
Separative work (SWU)	717,722	1,137,856	1,353,225
Cost of uranium purchase and enrichment (cents/kWe-hr)*	0.57	0.70 (+24%)	0.82 (+45%)
Cost of electricity generation (cents/kWe-hr)*	4.72	4.16 (-12%)	4.27 (-9%)

*Compared with the cost of the reference BWR

Chapter 5
Steady State Thermal-hydraulic Analysis

The main objective of the steady-state thermal-hydraulic analysis is to select the assembly thermal power and identify safety margins and thermal-hydraulic performance of the ASBWR. The MIT ASBWR Single Channel Analysis Code (MASCAC) and VIPRE-01 are used for the single channel analysis and assembly subchannel analysis, respectively.

5.1 Computational Tools

5.1.1 The MIT ASBWR Single Channel Analysis Code

Due to the unique design of the superheater annular fuel elements and flow configuration, it is difficult to find an existing commercial code which can be directly used for preliminary thermal-hydraulic analysis for the ASBWR. As a result, the MIT ASBWR Single Channel Analysis Code (MASCAC) has been developed in order to serve this purpose.

MASCAC is programmed in the MATLAB compiler. It is a steady-state, two-dimensional numerical solver, which uses a finite difference approach to calculate the temperature distribution in the fuel region. MASCAC has been benchmarked against the modified FRAPCON-ANNULAR code [113] and the results predicted by these two codes are in good agreement. Detailed descriptions of MASCAC and the benchmark study are given in Appendix B.

5.1.2 VIPRE-01

VIPRE-01 [125] is a subchannel analysis tool designed for general-purpose thermal-hydraulic analysis of the LWR cores under normal operating conditions, operational transients, and events of moderate severity. VIPRE-01 predicts the three

dimensional velocity, pressure, enthalpy and fuel temperature distributions for single and two phase flow in PWR and BWR cores. The code solves the finite difference mixture equations for mass, energy and momentum conservation for an interconnected array of channels, assuming incompressible thermally expandable flow. Although the formulation is based on the mixture equations, empirical models are incorporated for subcooled boiling and vapor/liquid slip in two-phase flow.

The main purpose of using VIPRE-01 in this study is to calculate the dryout margin (MCHFR) for the ASBWR and reference BWR fuel assemblies. Because VIPRE-01 is not developed for multiple automatic runs, a script file written in MATLAB is used to generate the VIPRE input files for the sensitivity study. The script file for generating VIPRE input files is included in Appendix C.

5.2 Thermal-hydraulic Constraints for the ASBWR

As described in Chapter 3, the ASBWR is a unique design which arranges the reactor core, by using annular fuel elements, to serve both boiling and superheating functions. Consequently, almost all the design constraints of BWR are applied to the ASBWR due to boiling of coolant in the vessel. In addition, some of the constraints related to high temperature gas cooled reactors may be also applied to the ASBWR.

Table 5-1 lists the major thermal-hydraulic constraints of the ASBWR. For the water side (boiling region), the major constraint is the Minimum Critical Heat Flux Ratio (MCHFR), which is set to prevent cladding failure due to dryout. In this study, the ASBWR is required to have the same or higher MCHFR than the reference BWR. For the steam side (superheating region), the major constraint is the maximum cladding temperature, which is set to prevent cladding failure due to thermal creep, loss of strength, excessive thermal expansion, and other high-temperature related concerns. For the T91 and Inconel 718, the maximum allowable working temperatures are 650 and 850 °C, respectively.

For the whole system, stability and total pressure drop are the two important issues. The constraint has been set that the ASBWR should have comparable or better performance in terms of the thermal-nuclear coupled stability than the reference BWR. The results of stability analysis of the ASBWR are compared with the results of the reference BWR and described in Chapter 6. Moreover, the ASBWR is expected to have a considerable pressure drop due to the superheated steam flowing with high velocities in the core. In this preliminary study, the ASBWR is designed to have a pressure drop low enough so that the required pumping power is equal to that of the reference BWR. This also limits the maximum steam velocity in the annular fuels and thus alleviates the concerns of erosion and vibration induced by the high velocity superheated steam.

Table 5-1 Major thermal-hydraulic constraints of the ASBWR

(1)	**Minimum Critical Heat Flux Ratio (MCHFR)** The ASBWR should have the same or higher MCHFR on the water side than that of the reference BWR. The MCHFR of the reference BWR is 1.23.
(2)	**Maximum cladding temperature** The maximum cladding temperature should be lower than the maximum allowable working temperature of the cladding material. For T91 and Inconel 718, the working temperatures are limited to 650 and 850 °C, respectively.
(3)	**Thermal-nuclear coupled stability** The ASBWR should have comparable or better performance in terms of the thermal-nuclear coupled stability than the reference BWR
(4)	**Pressure drop** The pressure drop should be low enough so that the required pumping power is equal to that of the reference BWR.

5.3 Single Channel Analysis

5.3.1 Assumptions

Table 5-2 lists the assumptions adopted in the single channel analysis. Operating conditions and fuel element dimensions are listed in Tables 3-6 and 3-7. Figure 5-1 shows the axial power profiles of the ASBWR and reference BWR.

Table 5-2 Assumptions adopted in the single channel analysis

(1)	Hot channel factor is assumed to be 1.45, which is the same as the reference BWR.
(2)	A typical BWR axial power profile is used for the ASBWR (Figure 5-1).
(3)	Power density is assumed to be 50 kW/L for the base case.
(4)	The length of the unheated region is assumed to be 20 cm (Figure 5-2).
(5)	Steam coolant is preheated to 290 °C (2.8 °C superheat) before reentering the core.
(6)	Steam inlet flow rate is adjusted by the orifices located on the steam coolant distributor (Figure 3-3). The steam flow rate in the hot channel is assumed to be 40% higher than the average steam flow rate.

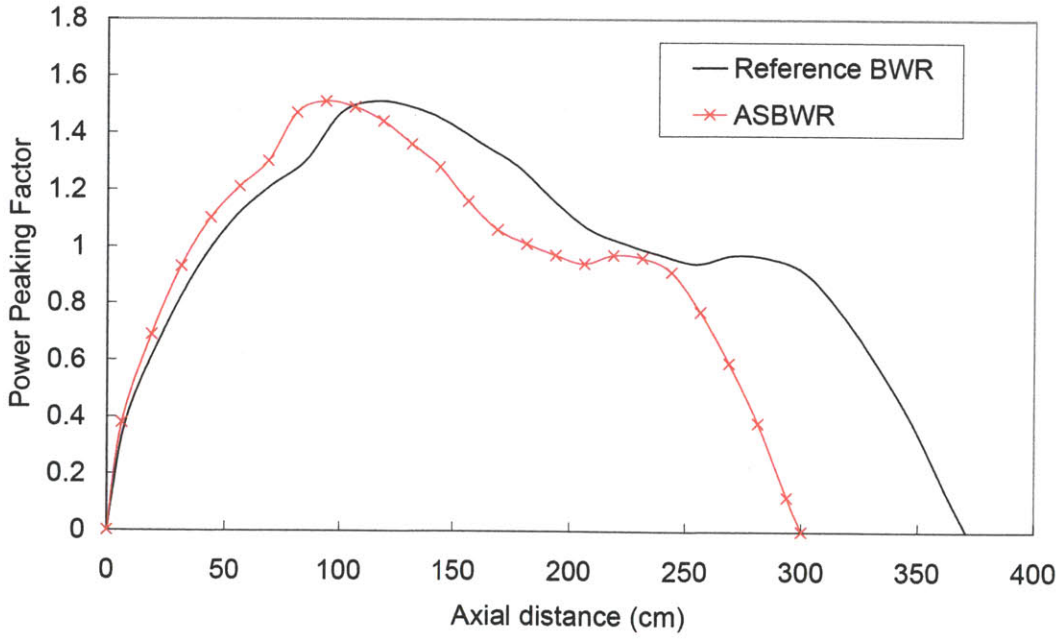

Figure 5-1 Axial power profiles of the ASBWR and reference BWR

5.3.2 Heat Loss in the Unheated Region

Figure 5-2 shows the axial coordinate of the ASBWR single channel model. Detailed description of this single channel model is given in Appendix B. As shown in Figure 5-2, the length of the unheated region is h_1 while the fuel active region is 300 cm long. Due to the high temperature difference between the superheated steam and the subcooled water, the superheated steam is expected to lose some heat in the unheated region. The amount of heat loss is depending on the length of the unheated region, h_1. Heat loss of steam in the unheated region has been calculated using MASCAC and the results are summarized in Table 5-3. Cladding material is T91 in this calculation.

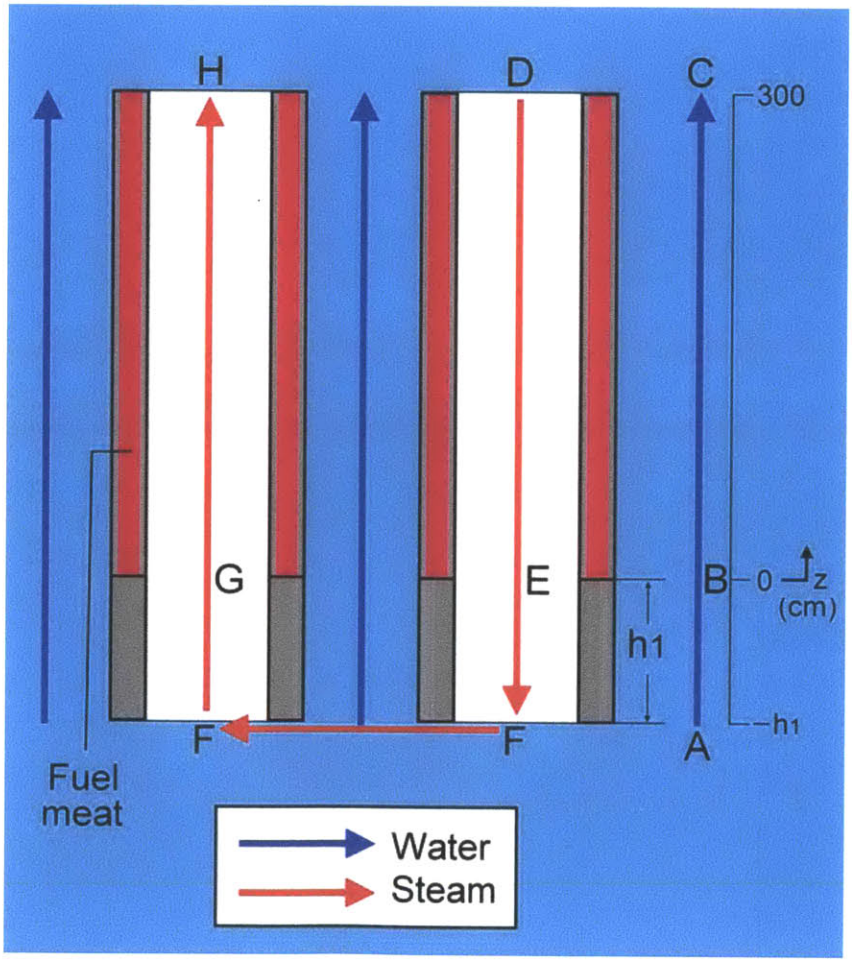

Figure 5-2 Axial coordinate of the ASBWR single channel model

Table 5-3 Heat loss of steam in the unheated region

Location*	A	B		E	G	
	Water temperature (°C)			Steam temperature (°C)		
h_l (cm)	T_A	T_B	$T_B - T_A$	T_E	T_G	$T_E - T_G$
15	278.3	279.3	0.97	404.9	390.2	14.7
20	278.3	279.6	1.29	404.9	385.8	19.1
25	278.3	280.0	1.65	404.9	381.5	23.4
30	278.3	280.3	2.01	404.9	377.4	27.5

*Locations refer to Figure 5-2

As shown in Table 5-3, the heat loss of steam could be 27.5 °C, which leads to an increase of 2 °C in water temperature, if the unheated region is 30 cm. Since the steam temperature is expected to be raised from 288 °C to about 520 °C, a loss of 27.5 °C is actually more than 10% of the absorbed energy. In general, the unheated region should not be too long otherwise the outlet steam temperature would be lower, and thus the plant efficiency is reduced. However, the length of the unheated region may be extended intentionally in order to obtain a desirable power split.

For this preliminary study, the unheated region is assumed to be 20 cm in the following analyses.

5.3.3 Axial Temperature Profiles

T91 cladding

Axial temperature profiles of the hot channel with T91 cladding are plotted in Figures 5-3 ~ 5-5. The axial coordinate is given in Figure 5-2. The unheated region is from -20 to 0 cm while the fuel active region is from 0 to 300 cm.

Figure 5-3 shows the water and outer cladding temperatures. In the unheated region,

since there is no heat supplied from a fuel to the cladding material, the temperature near the inner surface of the outer cladding is plotted. As shown in Figure 5-3, water temperature starts to increase in the unheated region and gradually reaches the saturated temperature. The heat source in the unheated region is the high temperature superheated steam. The outer cladding temperature drops at the bottom of the fuel active region (z = 0) because: 1) axial conduction is not taken into account in MASCAC and 2) in the unheated region, the outer cladding exchanges heat with the superheated steam via conduction while in the fuel active region the heat source and the outer cladding are separated by gaps. Thus, the outer cladding has a much lower temperature in the heated region.

Figure 5-4 shows the steam, inner cladding and peak fuel temperatures in the steam down-flow channel. Likewise, in the unheated region, the temperature near the inner surface of the inner cladding is plotted. As shown in Figure 5-4, steam is heated from point D to near the bottom of the fuel active region. Due to the low heat generation rate, at z = 3.6 cm the fuel temperature is below the steam temperature and the fuel is heated by steam from z = 3.6 to 0 cm. This particular "reverse heating" can be observed more clearly in the radial temperature profile, which is given in the next section. From z = 3.6 to -20 cm, it can be seen that the steam temperature is decreasing and superheat is slightly reduced.

Figure 5-5 shows the steam, inner cladding and peak fuel temperatures in the steam up-flow channel. The maximum cladding and fuel temperatures are found to be 616.2 and 921.1 °C, respectively. It is also observed that the steam is losing superheat not only in the unheated region but also near both ends of the fuel active region.

The steam outlet temperature, inner cladding and maximum fuel temperatures in the average and hot channels are plotted and compared in Figures 5-6 ~ 5-8. The steam outlet temperatures are 520.8 and 548.5 °C for the average and hot channels, respectively. Table 5-5 summarizes the results of the comparison.

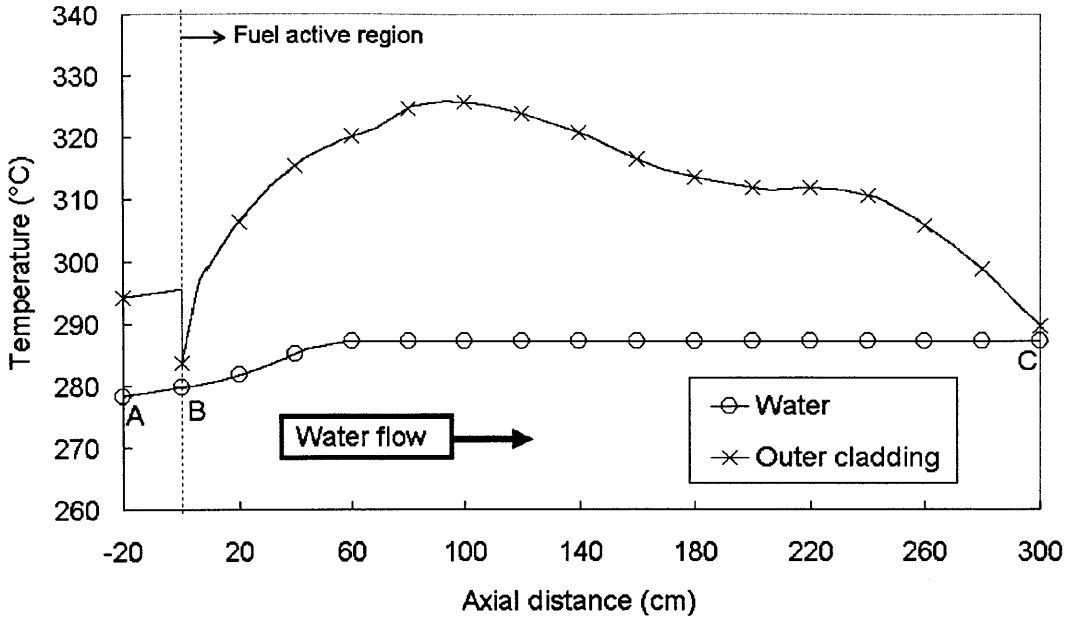

Figure 5-3 Axial temperature profiles of the water side (Hot channel, T91 cladding)

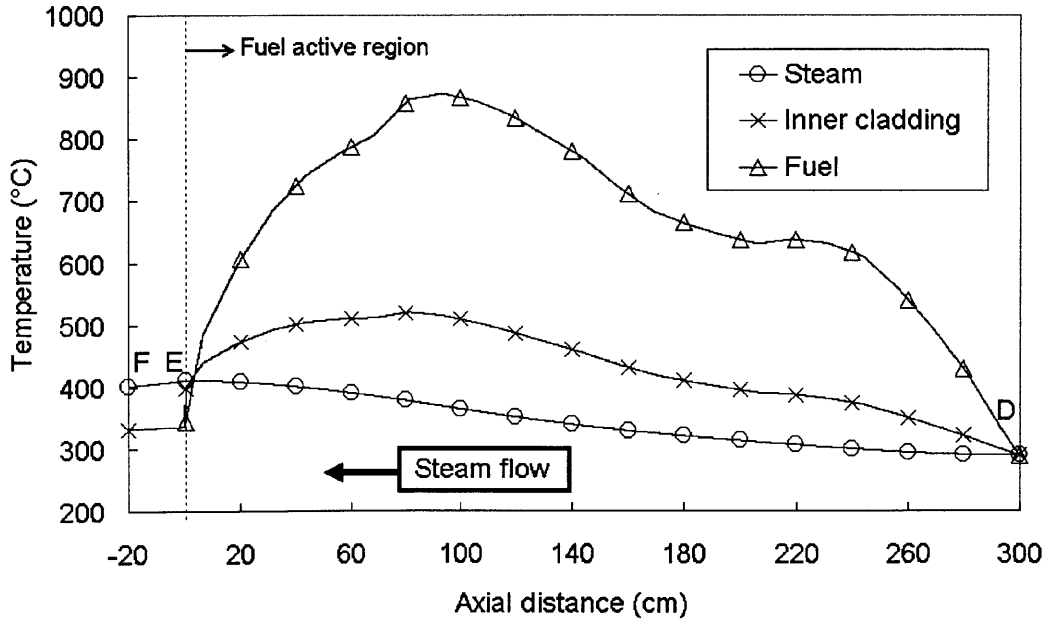

Figure 5-4 Axial temperature profiles of the steam side
(Hot steam down-flow channel, T91 cladding)

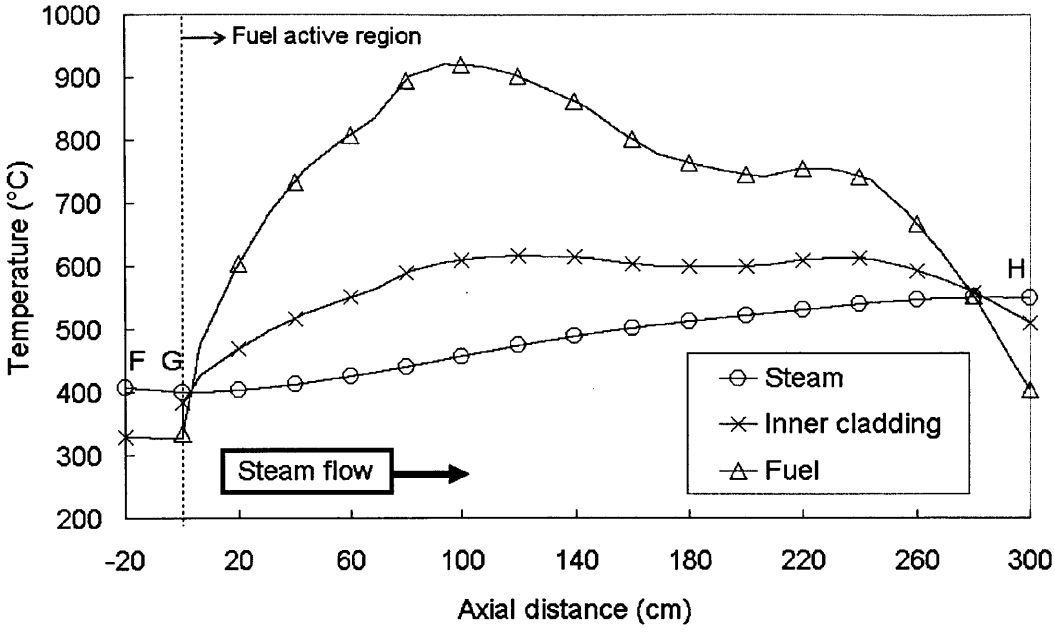

Figure 5-5 Axial temperature profiles of the steam side
(Hot steam up-flow channel, T91 cladding)

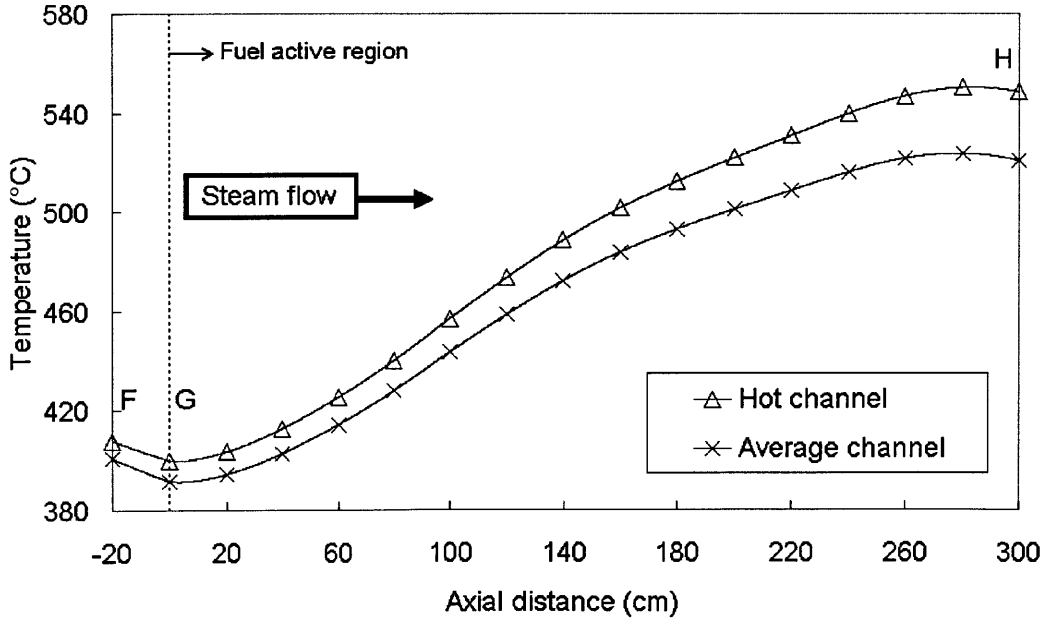

Figure 5-6 Comparison of the steam outlet temperature (T91 cladding)

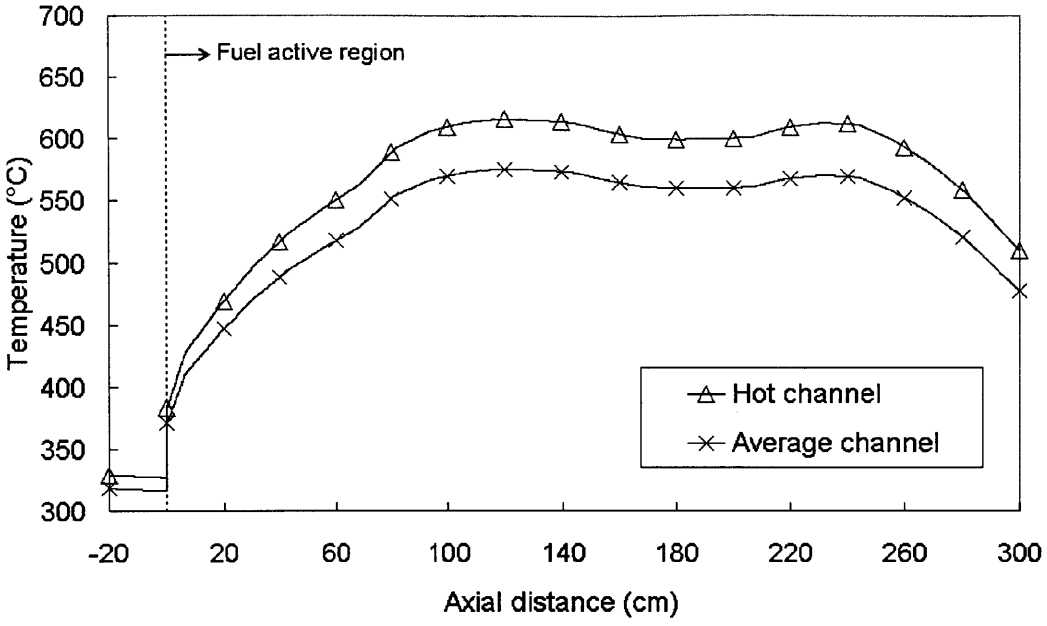

Figure 5-7 Comparison of the inner cladding temperature (T91 cladding)

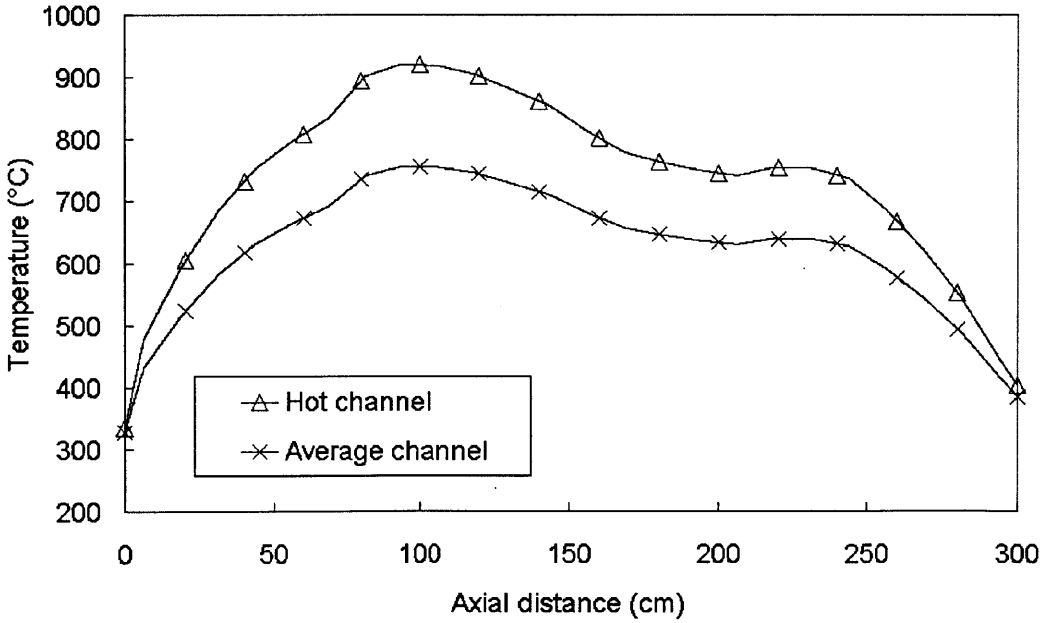

Figure 5-8 Comparison of the maximum fuel temperature (T91 cladding)

Table 5-4 Comparison between the temperatures in the average and hot channels (T91 cladding)

	T91 cladding		Inconel 718 cladding	
	Average channel	Hot channel	Average channel	Hot channel
Steam outlet temperature (°C)	520.8	548.5	524.6	551.9
Maximum cladding temperature (°C)	576.1	616.2	584.2	626.5
Maximum fuel temperature (°C)	756.3	921.1	767.8	936.7

Inconel 718 cladding

Axial temperature profiles of the hot channel with Inconel 718 cladding are plotted in Figures 5-9 ~ 5-11. Figure 5-9 shows the water and outer cladding temperatures. Compared with Figure 5-3, the Inconel 718 cladding has a higher temperature due to its relatively low thermal conductivity. The outer cladding temperature of Inconel 718 is about 350 °C, which is 25 °C higher than that of T91.

Figures 5-10 and 5-11 show the steam, inner cladding and peak fuel temperatures in the steam down-flow and up-flow channels, respectively. The "reverse heating" (i.e., steam is heating the fuel meat) is also observed near both ends of the fuel active region in Figure 5-11.

The steam outlet temperature, inner cladding and maximum fuel temperatures in the average and hot channels are plotted in Figures 5-12 ~ 5-14. The steam outlet temperatures are 524.6 and 551.9 °C for the average and hot channels, respectively. Table 5-4 summarizes the results of the comparison.

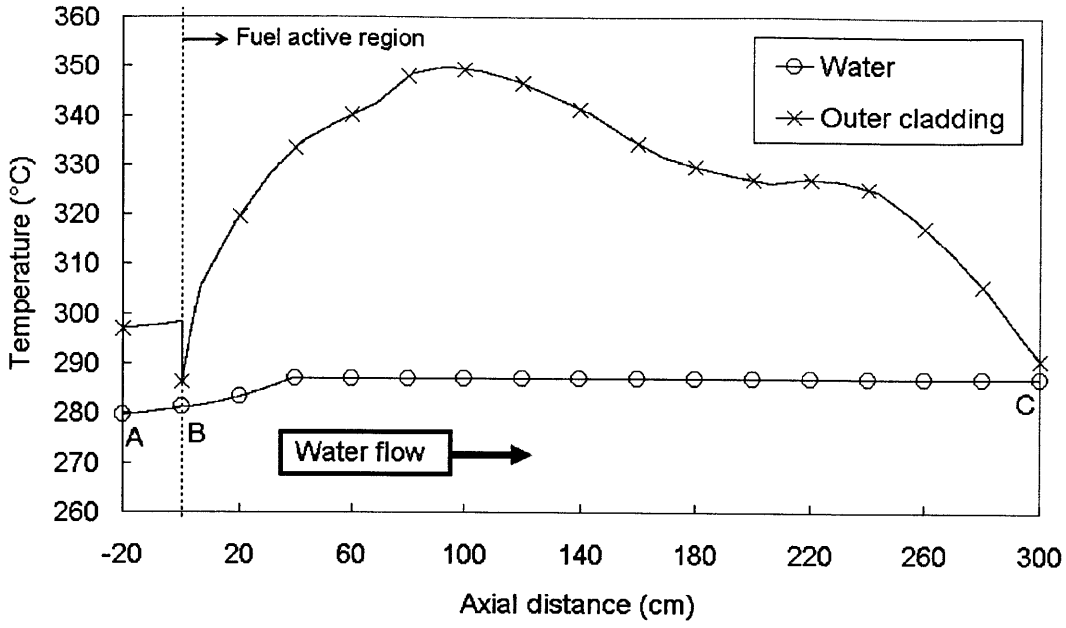

Figure 5-9 Axial temperature profiles of the water side
(Hot channel, Inconel 718 cladding)

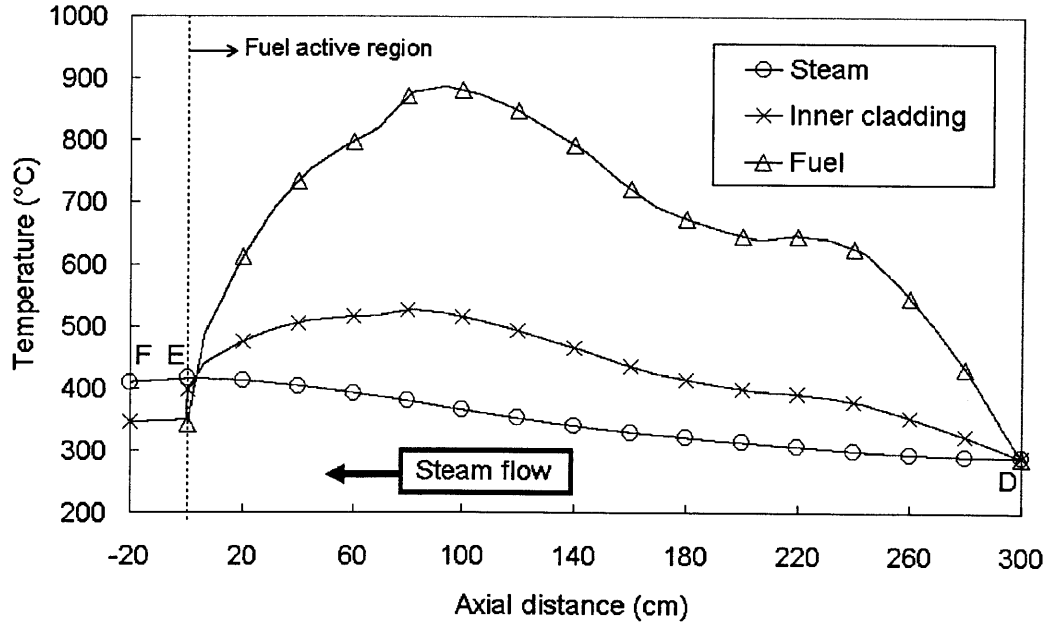

Figure 5-10 Axial temperature profiles of the steam side
(Hot steam down-flow channel, Inconel 718 cladding)

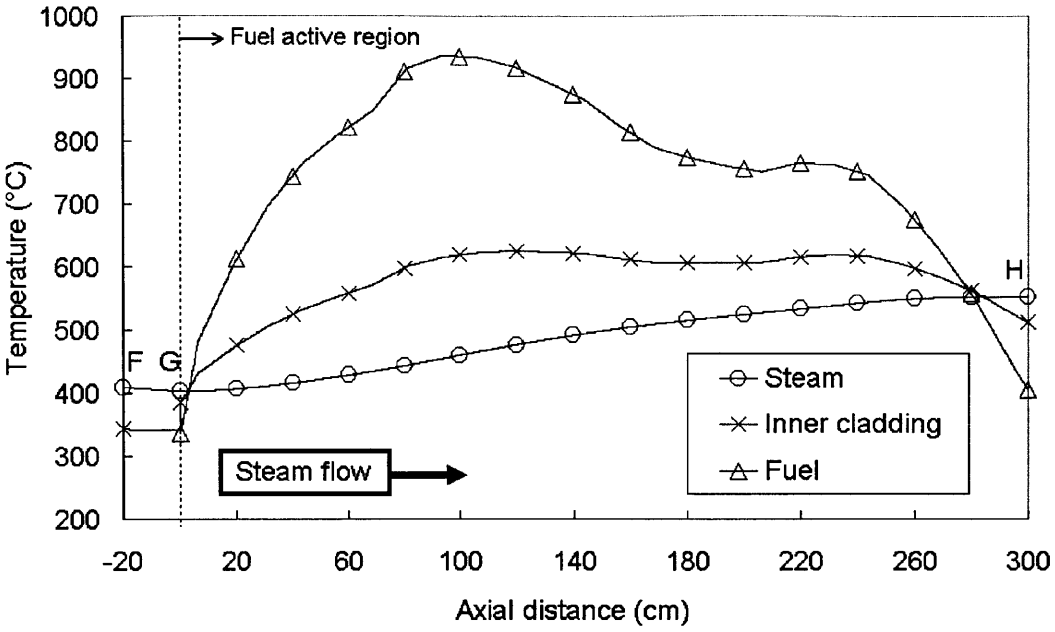

Figure 5-11 Axial temperature profiles of the steam side
(Hot steam up-flow channel, Inconel 718 cladding)

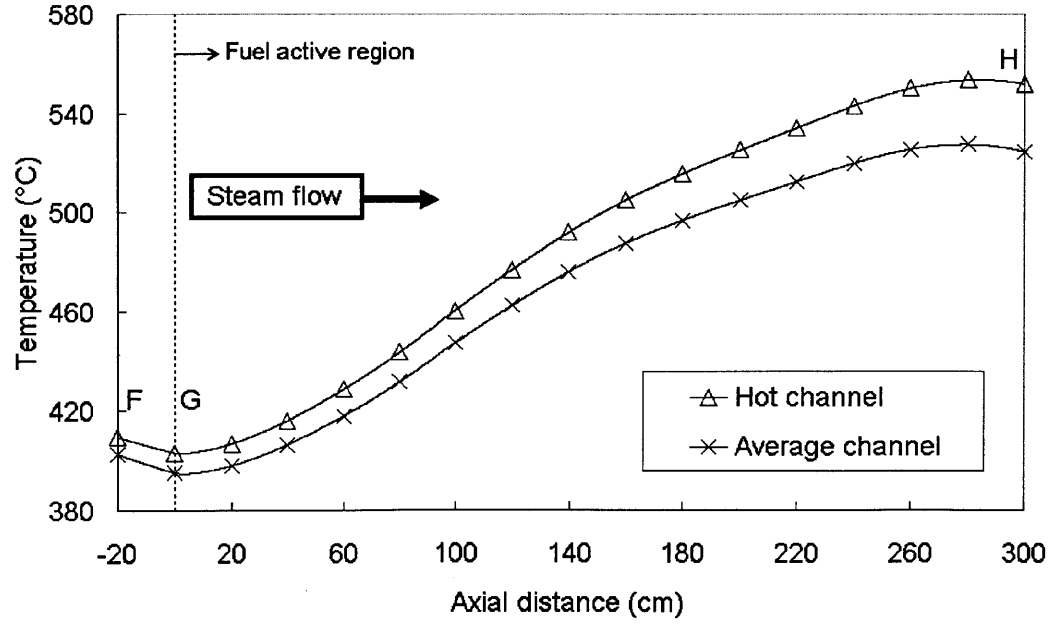

Figure 5-12 Comparison of the steam outlet temperature (Inconel 718 cladding)

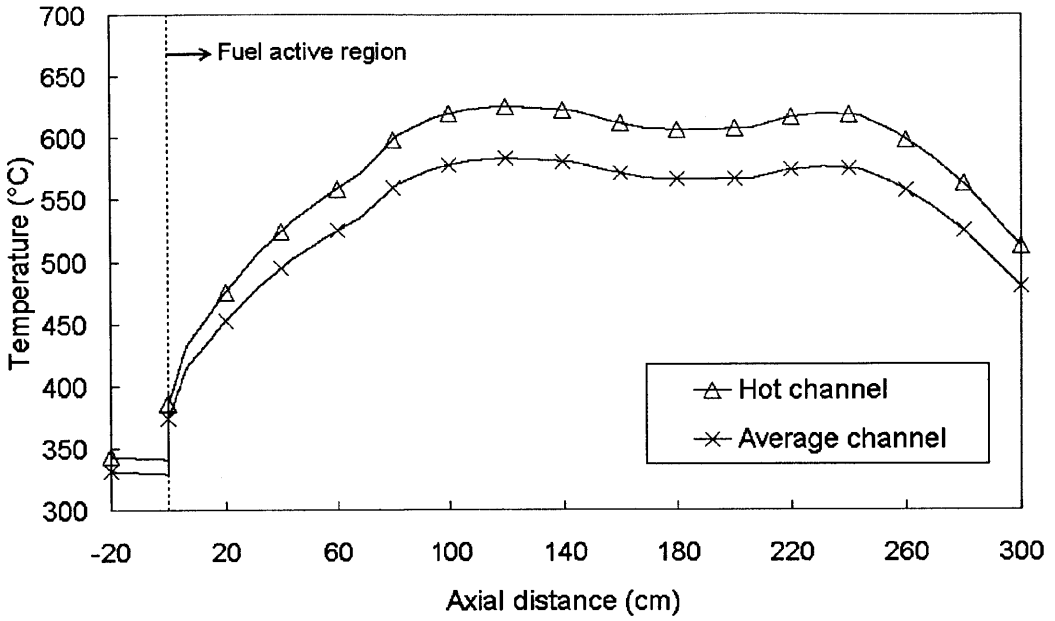

Figure 5-13 Comparison of the inner cladding temperature (Inconel 718 cladding)

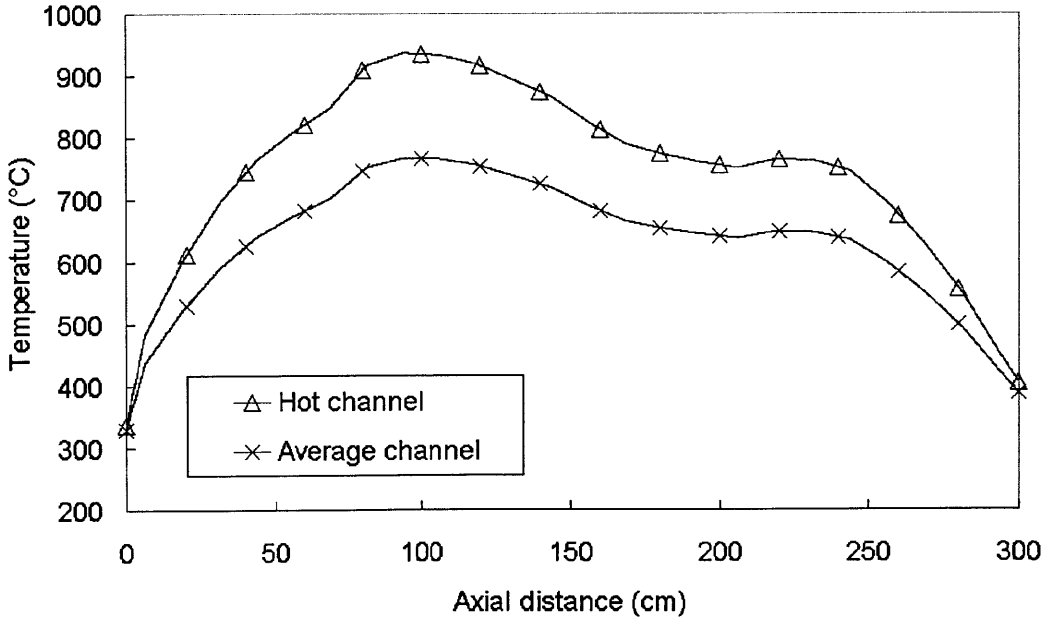

Figure 5-14 Comparison of the maximum fuel temperature (Inconel 718 cladding)

5.3.4 Radial Temperature Profiles

Figure 5-15 shows the radial coordinate of the ASBWR single channel model. Radial temperature profiles of the hot steam up-flow channel with the T91 cladding are plotted in Figures 5-16 ~ 5-19. Figure 5-16 shows the radial temperature profile at z = -10 cm (middle of the unheated region). In the unheated region, the high temperature steam is losing superheat and the subcooled water temperature is increasing. Figure 5-17 shows the radial temperature profile at z = 2.0 cm, which is near the bottom of the fuel active region. Due to the low heat generation rate in the fuel meat, fuel temperature is lower than steam temperature, and thus the steam is heating the claddings, gaps, fuel meat and water. This "reverse heating" occurs near both ends of the fuel active region in the steam up-flow channel. In the steam down-flow channel, "reverse heating" is observed only near the bottom end of the fuel active region because at the top end (steam coolant inlet), both the water and steam sides are at saturated temperature.

Figure 5-18 shows the radial temperature profile at z = 93.7 cm, where the maximum fuel temperature of 921.1°C is found near r = 7.0 mm. Figure 5-18 illustrates the typical radial temperature profile of the ASBWR fuel. Figure 5-19 shows the radial temperature profile at z = 292 cm, which is near the top end of the fuel active region. Again, "reverse heating" is observed due to the high steam temperature and the low heat generation rate in the fuel.

Radial temperature profiles of the hot steam up-flowing channel with Inconel 718 cladding are plotted in Figures 5-20 ~ 5-23. Similar trends can be found in these figures but the temperatures are slightly higher because of the somewhat lower thermal conductivity of Inconel 718.

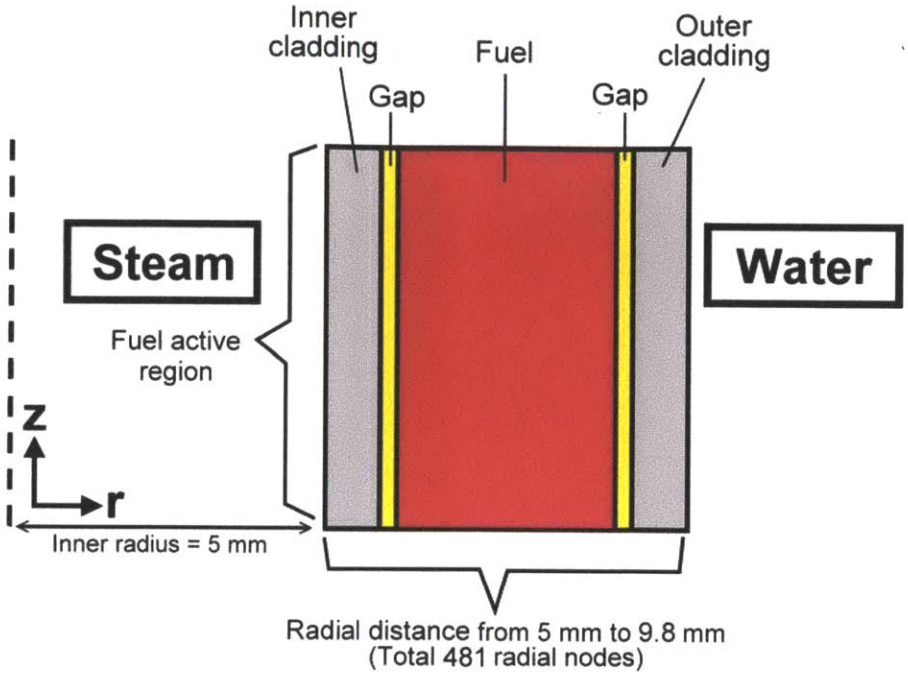

Figure 5-15 Radial coordinate of the ASBWR single channel model

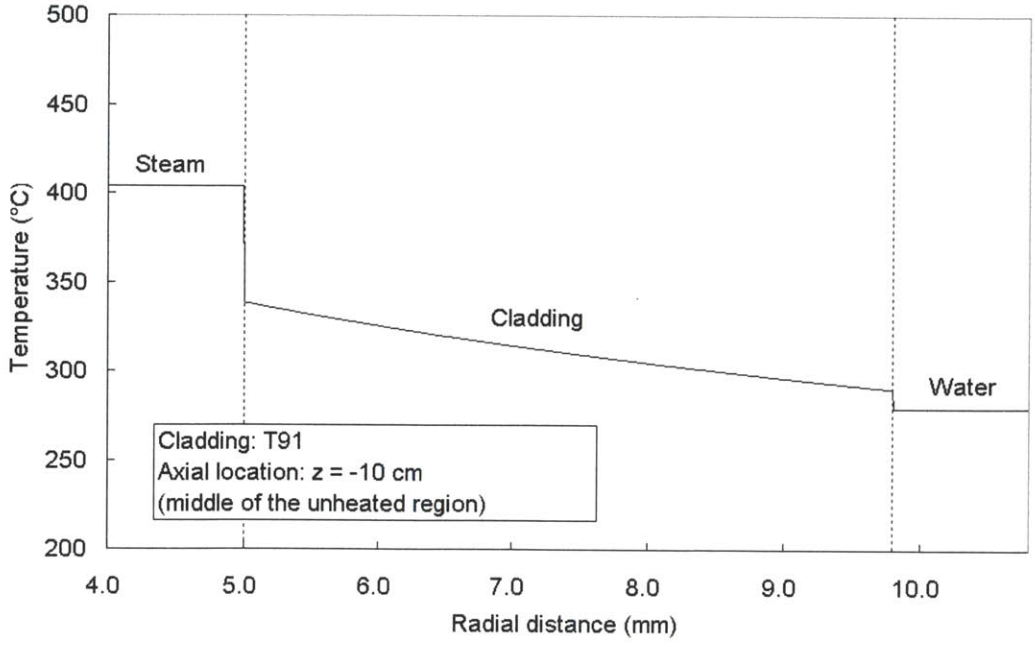

Figure 5-16 Radial temperature profile of the hot steam down-flow channel (z = -10 cm, T91 cladding)

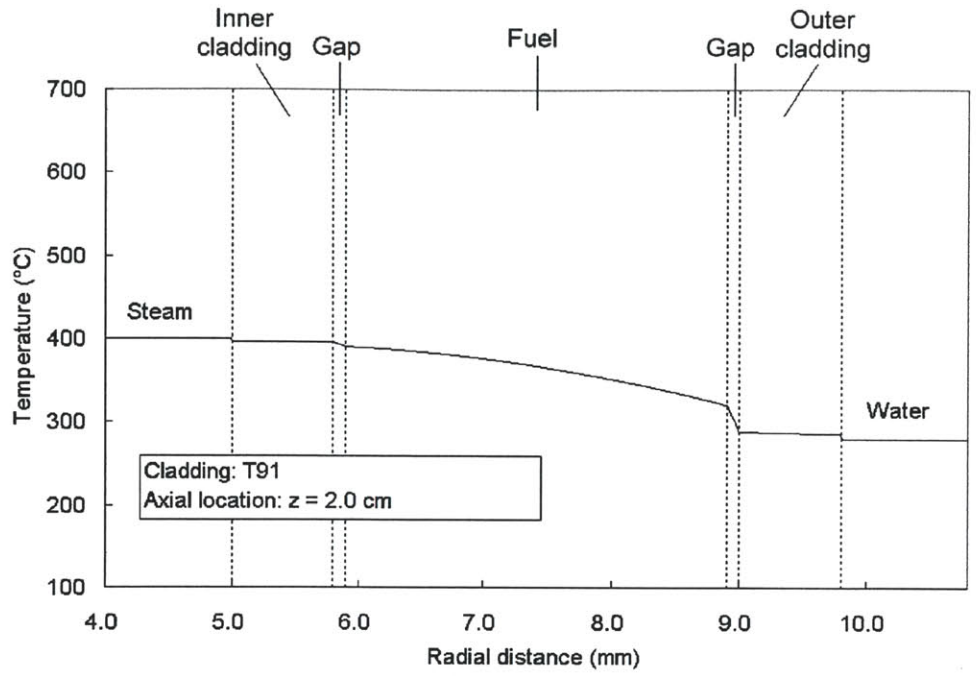

Figure 5-17 Radial temperature profile of the hot steam down-flow channel (z = 2.0 cm, T91 cladding)

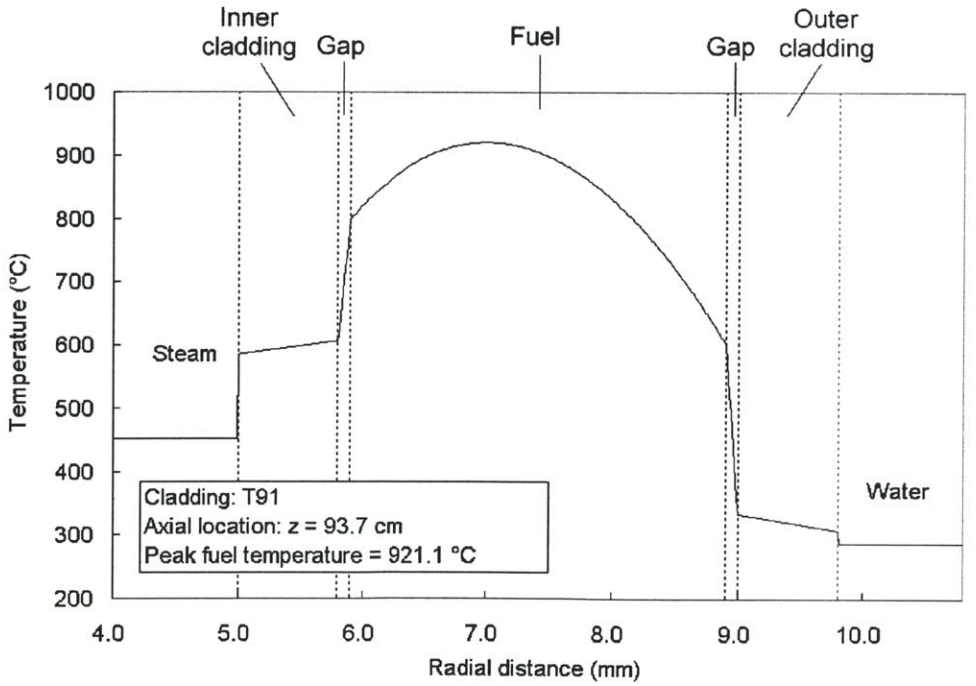

Figure 5-18 Radial temperature profile of the hot steam down-flow channel (z = 93.7 cm, T91 cladding)

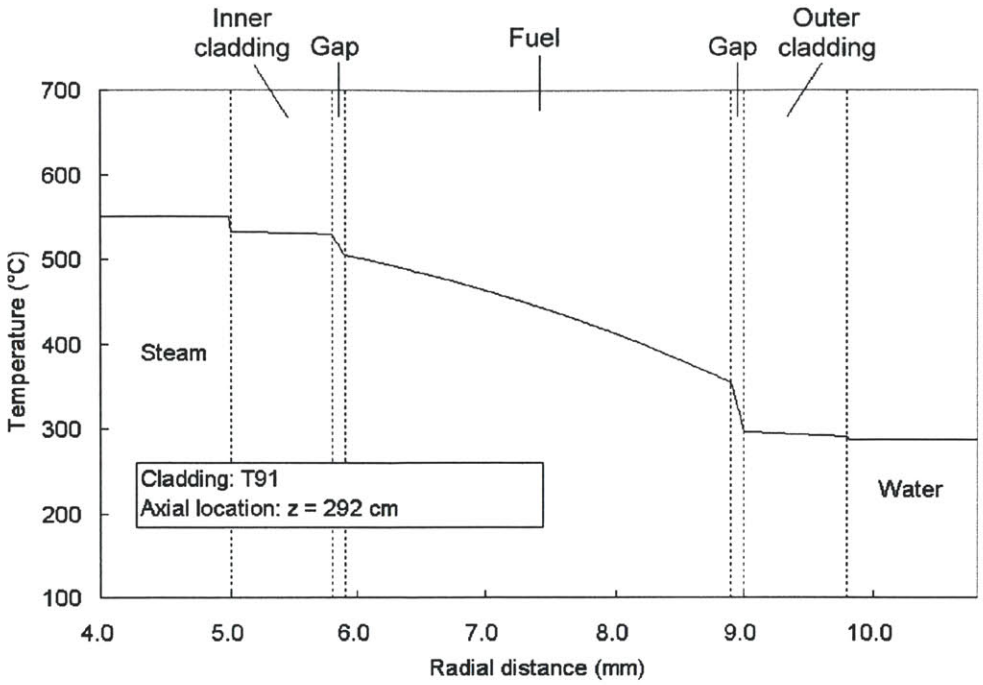

Figure 5-19 Radial temperature profile of the hot steam down-flow channel (z = 292 cm, T91 cladding)

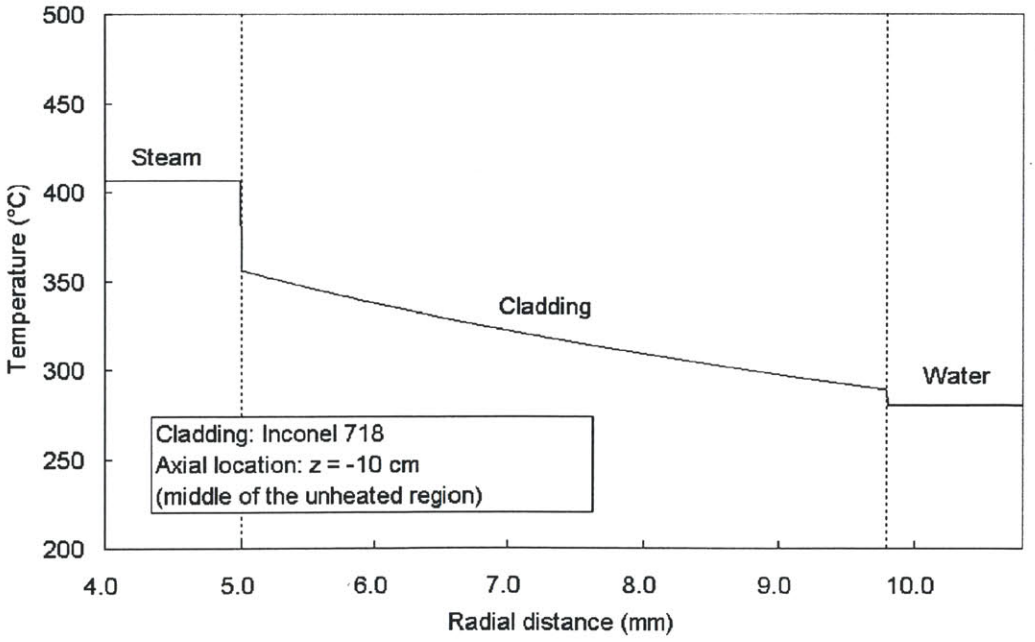

Figure 5-20 Radial temperature profile of the hot steam down-flow channel (z = -10 cm, Inconel 718 cladding)

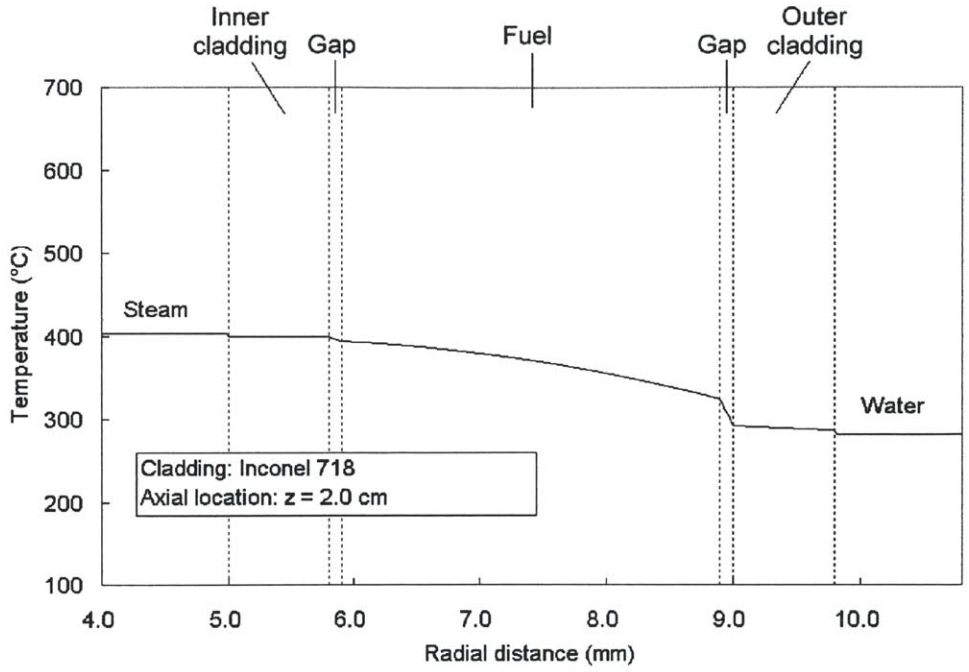

Figure 5-21 Radial temperature profile of the hot steam down-flow channel (z = 2.0 cm, Inconel 718 cladding)

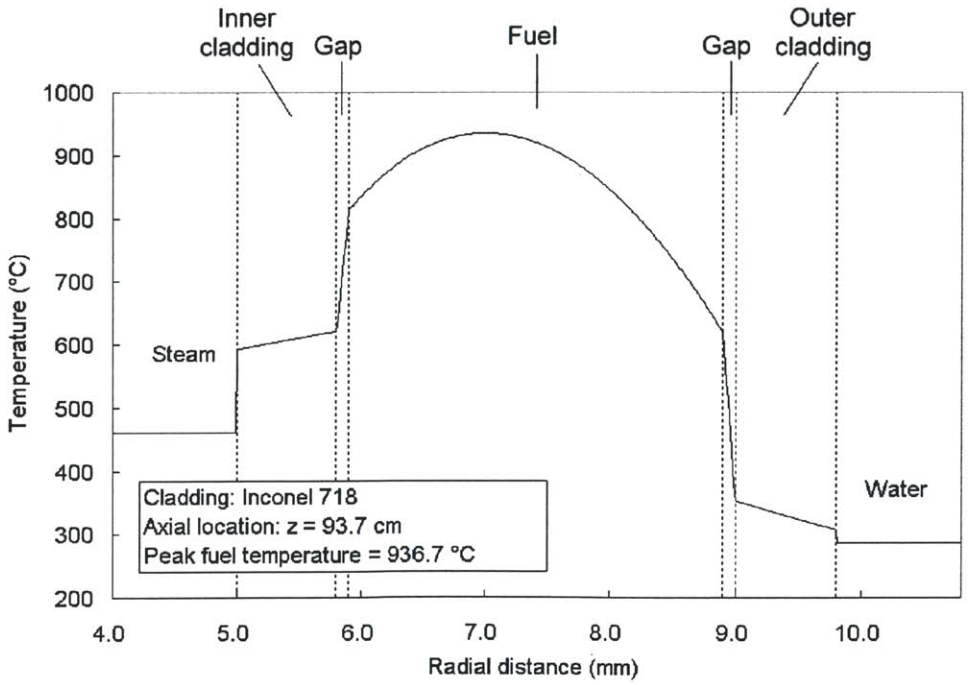

Figure 5-22 Radial temperature profile of the hot steam down-flow channel (z = 93.7 cm, Inconel 718 cladding)

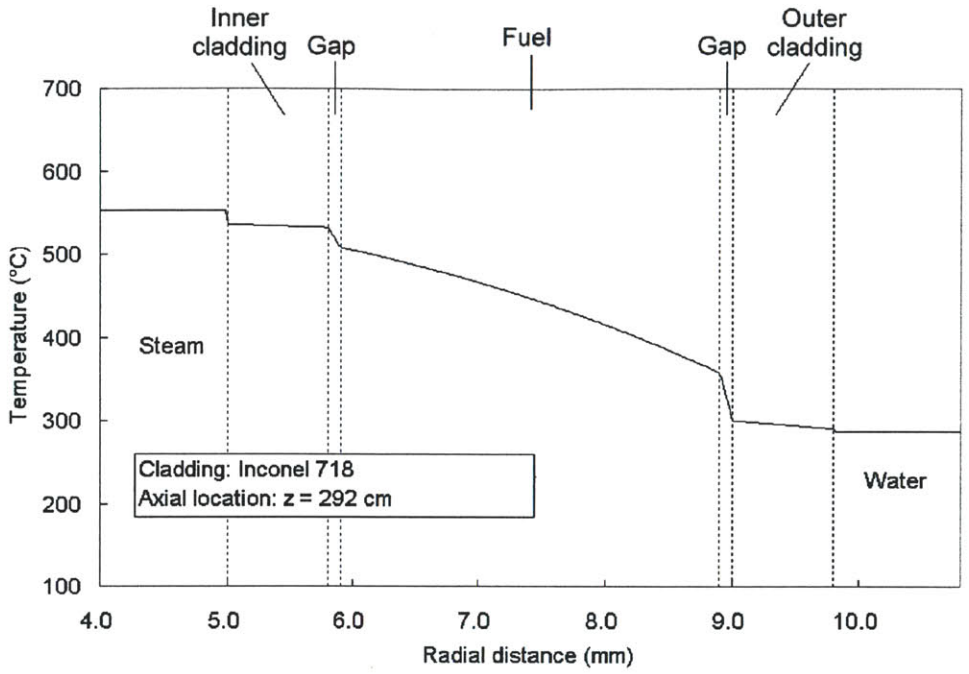

Figure 5-23 Radial temperature profile of the hot steam down-flow channel (z = 292 cm, Inconel 718 cladding)

5.3.5 Impact of Power Density on Steam, Cladding and Fuel Temperatures

Increasing the power density is an effective approach to improve the economic attractiveness of nuclear reactors. The capital cost of a typical BWR is of the order of 65% of the total power cost. If more energy can be extracted from an existing reactor or the physical size of a reactor can be reduced, the total cost of nuclear power generation may be reduced considerably.

A series of calculations has been performed to investigate the potential to increase the power density of the ASBWR design. In this sensitivity study, the power density and core flow rate are increased proportionally to maintain the same exit quality. The goal is to maximize the power density while meeting all the requirements listed in Table 5-1. For the single channel analysis, the main constraint is the maximum cladding temperature.

The results are summarized in Figures 5-24 and 5-25. Figure 5-24 shows the average steam outlet temperature and the maximum T91 cladding and fuel temperatures. It can be found that for T91 cladding, if the power density is below 50 kW/L, the steam outlet temperature would be below 520 °C and the design plant efficiency of 40% may not be obtained. On the other hand, the higher the power density, the higher the cladding temperature. As shown in Figure 5-23, a power density higher than 65 kW/L would result in a maximum cladding temperature beyond the 650 °C working limit of T91. Therefore, Inconel 718 should be considered as the preferable cladding material for such a high power density design.

Figure 5-25 shows the average steam outlet temperature and the maximum Inconel 718 cladding and fuel temperatures. As shown in Figure 5-25, the power density can be increased to 80 kW/L while the maximum cladding temperature is still much lower than the 850 °C working limit of Inconel 718. However, other constraints, especially for long term fuel performance, should also be taken into account to evaluate the feasibility of the cladding material under high power density operation.

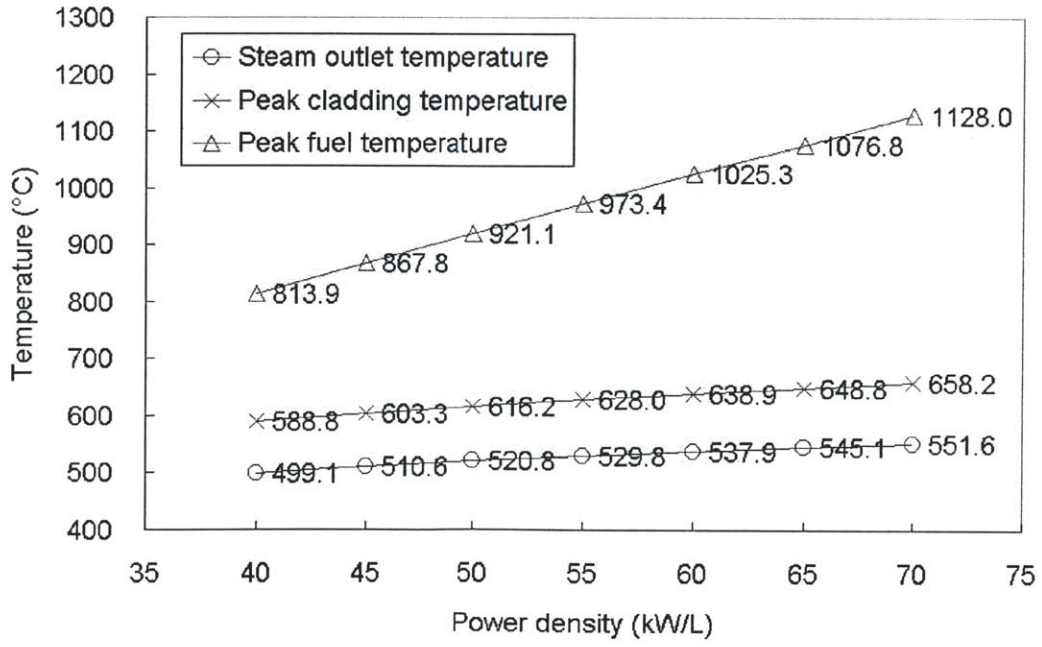

Figure 5-24 Sensitivity of power density for T91 cladding

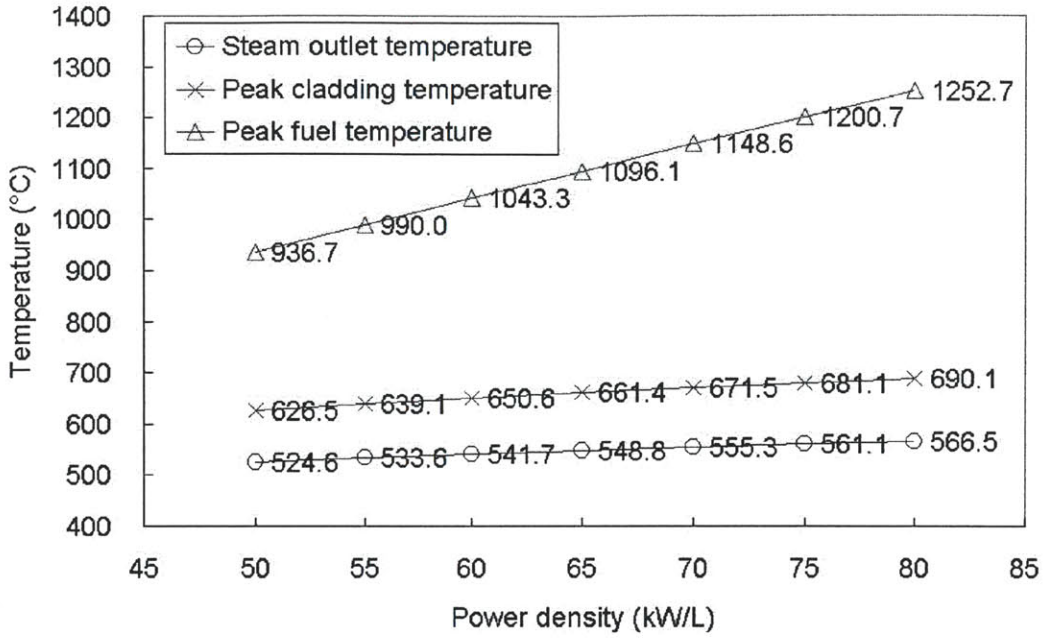

Figure 5-25 Sensitivity of power density for Inconel 718 cladding

5.3.6 Steam Velocity and Pressure Drop

Steam velocity and the steam core pressure drop have been calculated by MASCAC. The total steam core pressure drop is the sum of acceleration, friction, gravity and form pressure drops [117]:

$$\Delta p_{total} = \Delta p_{acc} + \Delta p_{fric} + \Delta p_{gravity} + \Delta p_{form} \tag{5-1}$$

$$\Delta p_{acc} = \rho_2 V_2^2 - \rho_1 V_1^2 \tag{5-2}$$

$$\Delta p_{fric} = \int_0^L \frac{f(l)}{2D_e} \rho(l) V^2(l) dl \tag{5-3}$$

$$\Delta p_{gravity} = \rho g h \tag{5-4}$$

$$\Delta p_{form} = \sum_i K_i (\frac{\rho V^2}{2}) \tag{5-5}$$

where

Δp_{total} = total pressure drop (kPa)

Δp_{acc} = pressure drop due to acceleration (kPa)

Δp_{fric} = pressure drop due to friction (kPa)

$\Delta p_{gravity}$ = pressure drop due to gravity (kPa)

Δp_{form} = pressure drop due to form loss (kPa)

ρ = density (kg/m^3)

V = velocity (m/s)

f = friction factor

$= 0.316\,\mathrm{Re}^{-0.25}$ *for* $\mathrm{Re} < 30{,}000$ *(Blasius)*

$= 0.184\,\mathrm{Re}^{-0.2}$ *for* $30{,}000 < \mathrm{Re} < 1\times10^6$ *(McAdams)*

$= 0.0056 + 0.5\,\mathrm{Re}^{-0.32}$ *for* $1\times10^6 < \mathrm{Re} < 3\times10^6$ [126]

Re = Reynolds number

$$= \frac{\rho V D_e}{\mu}$$

μ = viscosity (Pa-s)

D_e = hydraulic equivalent diameter (m)

g = gravity = 9.8 (m/s^2)

H = height (m)

K = form loss coefficient

= 0.4 *for pipe entrance from a plenum* [117]

= 0.4 *for 180° elbows and return bend* [131]

= 1.0 *for pipe exit to a plenum* [117]

Table 5-5 summarizes the calculation results. As shown in Table 5-5, steam velocity increases as the power density increases. Given a power density of 50 kW/L, the average exit steam velocity is about 50 m/s. These results are comparable to that of the BONUS reactor which had a power density of 33.6 kW/L and an average exit steam velocity of 37.2 m/s [8]. However, the ASBWR needs a further study on the erosion and

vibration issues since the steam is flowing with high velocities in the small inner channels of the annular fuel. Furthermore, it can be seen in Table 5-5 that an increase in power density leads to a considerable increase in the core pressure drop. For example, if the power density is increased by 50% (from 40 to 60 kW/L), the total pressure drop would be increased by more than 100% (from 315.3 to 692.5 kPa). The need of additional pumping power would also reduce the margin to increase the power density.

Table 5-5 The predicted exit steam velocity and total steam pressure drop

ASBWR with T91 cladding			
Power density (kW/L)	Average channel Exit steam velocity (m/s)	Hot channel Exit steam velocity (m/s)	Hot channel Total steam core pressure drop (kPa)
40	38.0	59.6	315.3
45	43.5	68.1	396.5
50	49.1	76.6	486.3
55	54.8	85.2	585.1
60	60.5	93.8	692.5
65	66.2	102.5	808.4
70	72.0	111.2	933.3
ASBWR with Inconel 718 cladding			
Power density (kW/L)	Average channel Exit steam velocity (m/s)	Hot channel Exit steam velocity (m/s)	Hot channel Total steam core pressure drop (kPa)
50	50.1	78.1	501.7
55	55.9	86.8	603.5
60	61.7	95.6	714.1
65	67.6	104.4	833.9
70	73.4	113.3	962.4
75	79.3	122.2	1099.9
80	85.3	131.1	1246.5

5.3.7 Water Power Split Fraction

Water power split fraction or power split ratio is defined as the amount of heat transferred by the water coolant divided by the total heat generation. It is one of the most important factors that affect the overall performance of the ASBWR. One of the design challenges for the ASBWR is to achieve a desirable power split during the whole fuel cycle.

Table 5-6 shows the calculated results of power split. Since the effectiveness of the steam side heat transfer is a function of Reynolds number, the higher the steam velocity, the higher the heat transfer coefficient in the steam-cooling region. An increase in power density leads to a higher steam velocity, and thus power split is reduced because more heat is absorbed by the steam coolant.

Table 5-6 Calculation results of water power split fraction

T91 cladding		
Power density (kW/L)	Average channel power split	Hot channel power split
40	0.759	0.720
45	0.748	0.712
50	0.739	0.704
55	0.731	0.697
60	0.723	0.690
65	0.715	0.683
70	0.708	0.675
Inconel 718 cladding		
Power density (kW/L)	Average channel power split	Hot channel power split
50	0.732	0.696
55	0.724	0.689
60	0.716	0.683
65	0.709	0.678
70	0.703	0.672
75	0.697	0.666
80	0.692	0.661

5.4 Assembly Subchannel Analysis

5.4.1 Assumptions

The water side of the ASBWR assembly has been modeled and analyzed using VIPRE. Figure 5-26 shows the VIPRE model of the ASBWR assembly. Table 5-7 lists the assumptions adopted in this assembly subchannel analysis. The core inlet temperature is assumed to be 2 °C higher than the reference BWR to take into account the addition of heat in the unheated region. Assembly local peaking factors are from the results of CASMO calculation. Power split of the hot assembly is assumed to be 0.72 and 0.70 for T91 and Inconel 718 claddings, respectively. This is a conservative assumption since the single channel analysis, as shown in Table 5-6, indicates that power split decreases as the power density increases. Locations of the spacers and pressure loss coefficients are listed in Table 5-8. Although the active length of the ASBWR core is shorter than that of the reference BWR, the number of spacers is kept the same in consideration of the anticipated additional vibration caused by the high velocity superheated steam.

Table 5-7 Assumptions adopted in the VIPRE assembly subchannel analysis

	Reference BWR	ASBWR
Hot assembly peaking factor	1.45	1.45
Local peaking factors	Figure 4-4	Figures 4-14 and 4-15
Axial power profile	Figure 5-1	Figure 5-1
Pressure loss coefficients	Table 5-8	Table 5-8
The core inlet temperature (°C)	278.3	280.3
Hot channel flow disparity*	0.9	0.9
Power split of the hot assembly	NA	0.72 (T91 cladding) 0.70 (Inconel 718 cladding)

*Water flow in the hot channel is assumed to be only 90% of that in the average channel

Table 5-8 Pressure loss coefficients as assumed in the VIPRE analysis

	Reference BWR	ASBWR
Active fuel height (cm)	370.8	300.0
Number of spacers	7	7
Location of spacers (cm)	49.5	40.1
	99.1	80.1
	148.6	120.2
	198.1	160.3
	247.7	200.4
	297.2	240.4
	346.7	280.5
Spacer loss coefficient	1.203	1.203
Inlet orifice loss coefficient	21.089	21.089
Lower tie plate loss coefficient	9.4609	9.4609
Upper tie plate loss coefficient	0.3751	0.3751

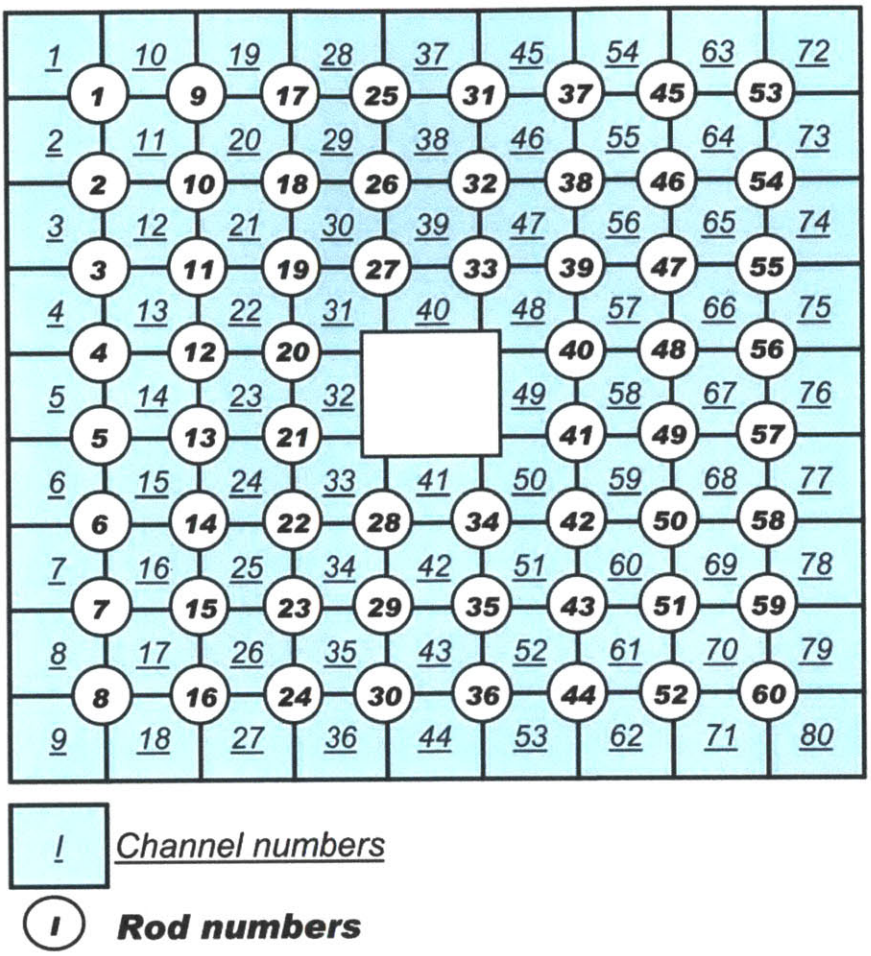

Figure 5-26 VIPRE model of the ASBWR assembly

5.4.2 Heat Generation and Flow Rates

Table 5-9 lists the input data of heat generation and flow rates in the subchannel analysis. All the data in Table 5-9 account for the water side. Comparing the base case (T91 cladding, 50 kW/L) with the reference BWR, it is found that the ASBWR has a higher rod linear power but the assembly power is only slightly higher than the reference BWR since the ASBWR assembly contains only 60 fuel rods. The ASBWR assembly flow rate is also higher but the mass flux is smaller than that of the reference BWR due to its larger hydraulic equivalent diameter (i.e., larger flow area).

Table 5-9 Hot channel heat generation and flow rates

Power density (kW/L)	Rod linear power (kW/m)	Assembly power (MW)	Assembly flow rate (kg/s)	Mass flux (kg/m^2-s)
Reference BWR				
50.5	23.0	6.30	15.24	1645
ASBWR with T91 cladding				
40	30.3	5.46	13.65	869
45	34.1	6.14	15.35	978
50	37.9	6.82	17.06	1087
55	41.7	7.50	18.77	1195
60	45.5	8.19	20.47	1304
65	49.3	8.87	22.18	1413
70	53.1	9.55	23.89	1521
ASBWR with Inconel 718 cladding				
50	36.9	6.64	17.06	1087
55	40.6	7.30	18.77	1195
60	44.2	7.96	20.47	1304
65	47.9	8.63	22.18	1413
70	51.6	9.29	23.89	1521
75	55.3	9.95	25.59	1630
80	59.0	10.62	27.30	1738

5.4.3 MCHFR Calculation

The MCHFR is calculated by VIPRE using the EPRI-Columbia correlation [110]:

$$q''_{CHF} = \frac{AF_A - x_{in}}{C(F_C + F_g) + [\frac{x - x_{in}}{q''_L}]} \tag{5-6}$$

where

A	=	$P_1 P_r^{P_2} G^{[P_5 + P_7 P_r]}$	
C	=	$P_3 P_r^{P_4} G^{[P_6 + P_8 P_r]}$	
q''_L	=	local heat flux (MBtu/hr-ft^2)	
x	=	local equilibrium quality	
x_{in}	=	inlet quality	
G	=	local mass velocity (Mlbm/hr- ft^2)	
P_r	=	critical pressure ratio; system pressure/critical pressure	
F_A	=	$G^{0.1}$ (Cold wall correction factor)	
F_C	=	1.183 $G^{0.1}$ (Cold wall correction factor)	
F_g	=	1.3 – 0.3 C_g	
C_g	=	Grid loss coefficient	
P_1	=	0.5328	(Optimized constant)
P_2	=	0.1212	(Optimized constant)
P_3	=	1.6151	(Optimized constant)
P_4	=	1.4066	(Optimized constant)
P_5	=	–0.3040	(Optimized constant)
P_6	=	0.4843	(Optimized constant)
P_7	=	–0.3285	(Optimized constant)
P_8	=	–2.0749	(Optimized constant)

The EPRI-Columbia correlation is selected because it has been benchmarked against BWR experimental data, and found to be the most accurate yet conservative one among several CHFR correlations [110].

Table 5-10 summarizes the calculation results of exit quality, void fraction and MCHFR. For T91 cladding, the power density should not be higher than 60 kW/L to ensure that the MCHFR is lower than the reference BWR. For Inconel 718 cladding, the power density should be lower than 65 kW/L to obtain a sufficient dryout margin on the water side.

Table 5-11 compares the results of the reference BWR and the ASBWR base case. It can be seen in Table 5-12 that the base case has a similar exit quality and void fraction to that of the reference BWR. In addition, the base case has a higher MCHFR than the reference BWR mainly due to its relatively low mass flux.

Table 5-10 Comparison of the calculated exit quality, void fraction and MCHFR in the hot channel

Power density (kW/L)	Exit quality	Exit void fraction	MCHFR
Reference BWR			
50.5	0.244	0.798	1.226
ASBWR with T91 cladding			
40	0.242	0.794	1.602
45	0.242	0.794	1.497
50	0.242	0.796	1.408
55	0.242	0.796	1.332
60	0.242	0.796	1.266
65	0.242	0.797	1.207
70	0.242	0.797	1.154
ASBWR with Inconel 718 cladding			
50	0.235	0.790	1.441
55	0.235	0.791	1.363
60	0.235	0.791	1.296
65	0.235	0.791	1.236
70	0.235	0.792	1.182
75	0.235	0.792	1.133
80	0.235	0.792	1.089

Table 5-11 Exit conditions of the reference BWR and the base case

	Reference BWR	**ASBWR base case**
Cladding material	Zircaloy-2	T91
Power density (kW/L)	50.5	50
Average channel exit quality	0.140	0.141
Average channel exit void fraction	0.689	0.690
Hot channel exit quality	0.244	0.242
Hot channel exit void fraction	0.798	0.796
MCHFR	1.226	1.408

5.4.4 Core Pressure Drop

Core pressure drop of the water and steam sides have been calculated by VIPRE and MASCAC, respectively. Calculation results are summarized in Table 5-12. It can be seen that the steam side core pressure drop is much higher than the water side due to 1) the flowing distance of steam is twice as that of water; 2) the compressibility, high velocity of steam and the decrease in steam density lead to a high acceleration pressure drop; and 3) the high steam velocity leads to a high friction and form loss pressure drop. In addition, when the ASBWR power density is higher than 50 kW/L, the pumping power would be larger than that of the reference BWR, which requires pumps with higher capacity to compensate the additional core pressure drop.

Table 5-12 Calculation results of the core pressure drop

Power density (kW/L)	Water side core pressure drop (kPa)	Steam side core pressure drop (kPa)	Total core pressure drop (kPa)	Feedwater inlet flow rate (kg/s)	Pumping power* (kW)
Reference BWR (Thermal power = 3,323 MW)					
50.5	162.2	NA	162.2	1811.8	388.0
ASBWR with T91 cladding (Thermal power = 1,250 MW)					
40	51.6	315.3	366.9	511.3	247.7
45	61.9	396.5	458.4	511.3	309.4
50	73.3	486.3	559.6	511.3	377.7
55	85.7	585.1	670.8	511.3	452.7
60	99.2	692.5	791.7	511.3	534.3
65	113.8	808.4	922.2	511.3	622.4
70	129.4	933.3	1062.7	511.3	717.2
ASBWR with Inconel 718 cladding (Thermal power = 1,250 MW)					
50	72.5	501.7	574.2	511.1	387.4
55	84.8	603.5	688.3	511.1	464.4
60	98.1	714.1	812.2	511.1	547.9
65	112.5	833.9	946.4	511.1	638.5
70	128.0	962.4	1090.4	511.1	735.6
75	144.5	1099.9	1244.4	511.1	839.5
80	162.0	1246.5	1408.5	511.1	950.2

*Pumping power needed to compensate the total core pressure drop

5.5 Startup Analysis for the ASBWR

The startup of an integral superheat reactor is unique in that the steam produced in the boiling region is needed for the cooling in the superheating region. Because of the high radiation dose during fuel loading, the superheater has to be initially flooded and then voided before the reactor is brought to full power operation. It is found in the literature that previous superheat reactors basically all applied this general approach. The startup processes of the Pathfinder and BONUS reactors are briefly described below.

Startup of the Pathfinder Reactor

The reactor was first brought up to approximately 5 MWt with the superheat assemblies flooded by withdrawing boiler region control rods. The reactor pressure was maintained high enough to provide sufficient subcooling to prevent the formation of steam in the superheater region. When the reactor water reached 450 °F the reactor was temporarily shutdown. The superheater assemblies were drained after allowing sufficient time for decay heat to drop to 0.4 MWt, the reactor was again brought up to criticality with boiler control rods only. After approximately one hour of operation at low power, the reactor reached the operating pressure and temperature. The reactor was then brought to the desired operating power [39].

Startup of the BONUS Reactor

The reactor was brought to criticality with the reactor water at 92°F and the superheater assemblies flooded. Heating up was very slow to raise the temperature to 350 °F, and then the superheater assemblies were drained. The reactor power was kept low until the operating pressure and temperature were reached. The reactor was then brought to the desired operating power with the exit superheated steam temperature around 900 °F [39].

For Pathfinder and BONUS, their superheater assemblies could be easily flooded and drained since they were separate from the boiler assemblies. For the ASBWR, however, draining the superheater is difficult due to the overall design of the assembly. Instead, it is proposed to void the superheater by vaporizing all the water in the inner channel of the annular fuel element. After the inner channel is dried out, fuel failure due to

overheating would not be a serious concern since cooling of the fuel elements is still provided by the surrounding water (i.e., the water side). Nevertheless, it is essential to investigate the maximum cladding temperature during the reactor startup since after the inner channel is dried out, inefficient heat transfer on the steam side is anticipated.

Startup analysis for the ASBWR has been performed using MASCAC. The assumptions of the analysis are listed in Table 5-13. To be conservative, the steam side is assumed to be insulated and thus all the heat generated by the fuel is transferred to the water side. Figure 5-27 shows the power to flow operating map of a typical BWR. For the startup of a BWR, the reactor is kept below 5% of the rated power before sufficient pressure is reached. The corresponding core flow is about 30 ~ 35% of the rated flow rate with the minimum recirculation pump speed. In this analysis, 30% rated core flow rate is assumed with various power levels to calculate the maximum cladding temperature.

Figure 5-28 shows the calculation results. It can be seen that given a 30% rated core flow and 5% rated power, the maximum cladding temperature is below 350 °C, which is much lower than the cladding working limit. The maximum cladding temperature is below 580 °C at the 25% rated power. The actual cladding temperature should be lower, since in reality the steam side is not insulated during the startup. Therefore, this dryout approach is considered feasible for the startup of the ASBWR.

Table 5-13 Assumptions adopted in the startup analysis

(1)	Hot channel factor is 1.45
(2)	Minimum recirculation pump speed is assumed
(3)	Power density is 50 kW/L for full power operation
(4)	Steam side is assumed to be insulated
(5)	Core inlet temperature is 278.3 °C
(6)	T91 is used as cladding
(7)	30% rated core flow is assumed

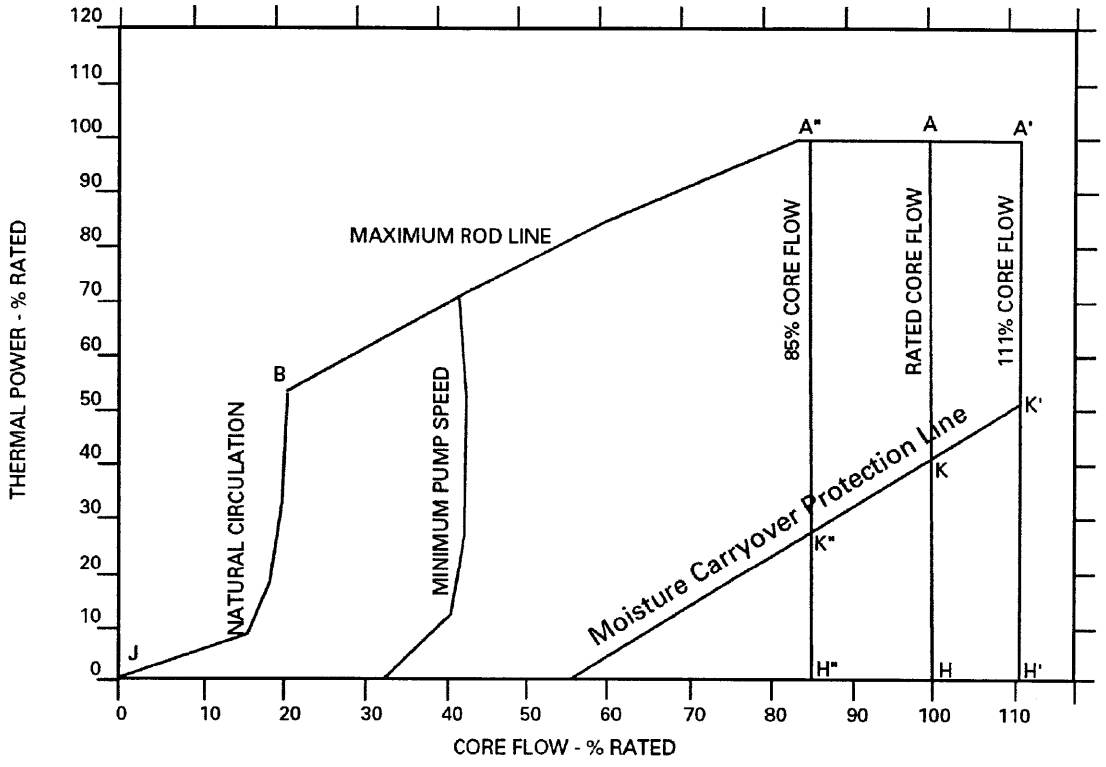

Figure 5-27 Power to flow operating map of a typical BWR [127]

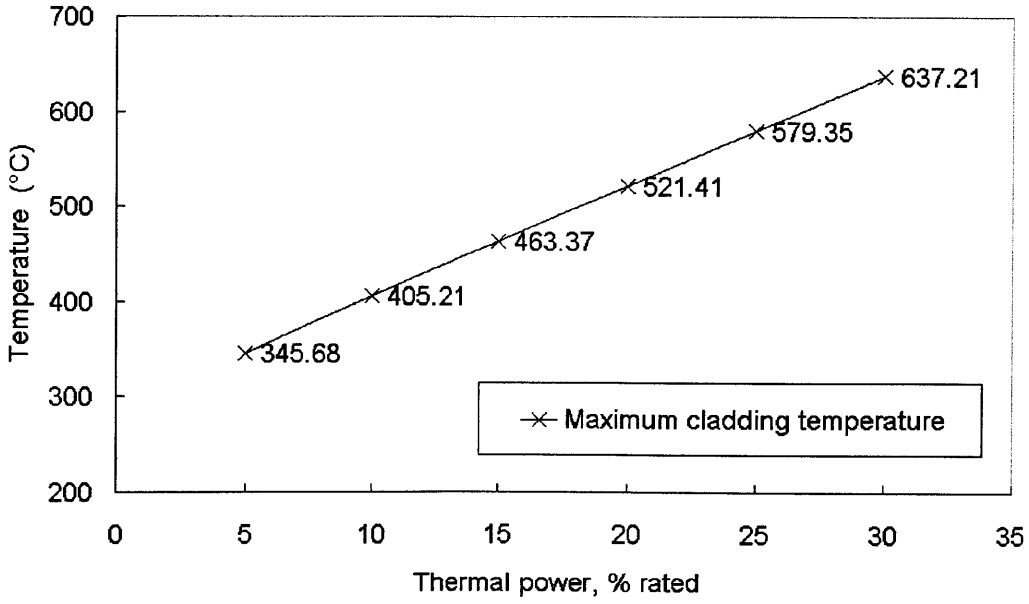

Figure 5-28 Calculation results of the startup analysis

5.6 Proposed Startup and Shutdown Procedures for the ASBWR

Tentative startup and shutdown procedures have been defined for the ASBWR. These procedures are described qualitatively to demonstrate a possible way to start up and shut down the ASBWR. Figures 5-29 ~ 5-40 demonstrate the main steps in the startup procedures. For simplicity, the reactor core is represented by a single assembly containing annular fuel elements in a 4 x 4 array.

5.6.1 Startup of the ASBWR

Figures 5-29 to 5-33

Fuel assemblies, steam coolant distributor, separator and steam dryer are installed in sequence.

Figure 5-34

The reactor vessel head is moved back. Some air stays in the reactor vessel.

Figure 5-35

The excessive water is directed to a storage tank.

Figure 5-36

The reactor is brought to criticality at low pressure. The reactor power is kept low and the amount of water in the inner channels of the annular fuels is slowly decreasing due to vaporization. The recirculation pumps are running at the minimum speed.

Figure 5-37

After a period of time, the inner channels of the annular fuels are voided. There is no air in the vessel at this step. The reactor is kept heated until the desired water level in the reactor vessel is reached. The recirculation pumps are running at the minimum speed.

Figure 5-38

Valves are closed again. The reactor is slowly pressurized and heated up by withdrawing the control rods. The recirculation pumps are running at the minimum speed.

Figure 5-39

When sufficient pressure level is established, bypass valves will open. Feedwater is allowed to enter the vessel. The main steam isolation valve (MSIV) is opened to allow warm-up and pressurization of the steam line to the steam turbines. The recirculation pump speed starts to increase to raise the core flow accordingly.

Figure 5-40

The heatup is continued and reactor pressure is raised to near the full operating pressure. A turbine generator startup is performed. Then the reactor can be brought to the desired operating power by adjusting the core flow rate and withdrawing the control rods.

5.6.2 Shutdown of the ASBWR

To shut down the ASBWR, the reactor power has to be lowered slowly by decreasing the core flow rate and inserting control rods. When the reactor is shutdown and reactor pressure is low enough, a considerable amount of feedwater can be injected into the vessel and flood the inner channels of the annular fuel elements. A sufficient shutdown margin must be guaranteed since the flooding of the annular fuel inner channels will cause positive reactivity insertion.

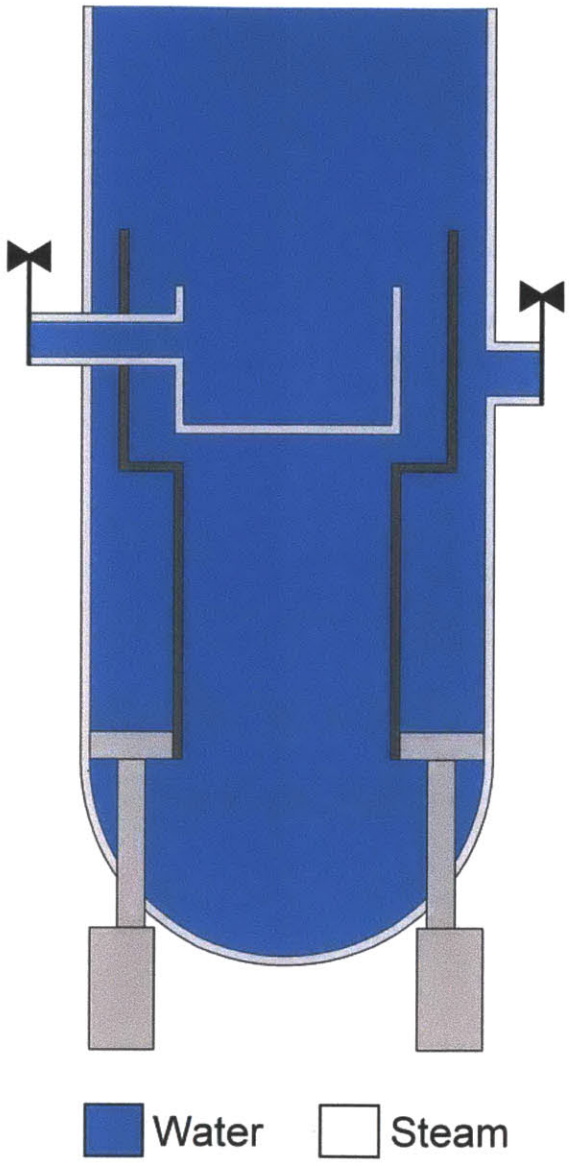

Figure 5-29 Startup of the ASBWR (step 1)

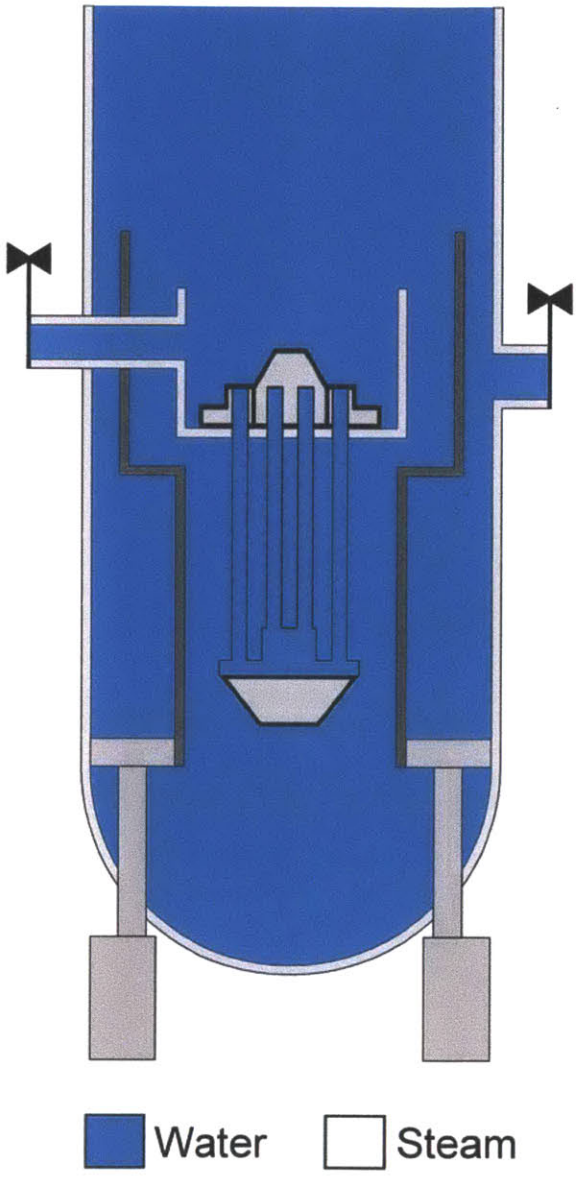

Figure 5-30 Startup of the ASBWR (step 2)

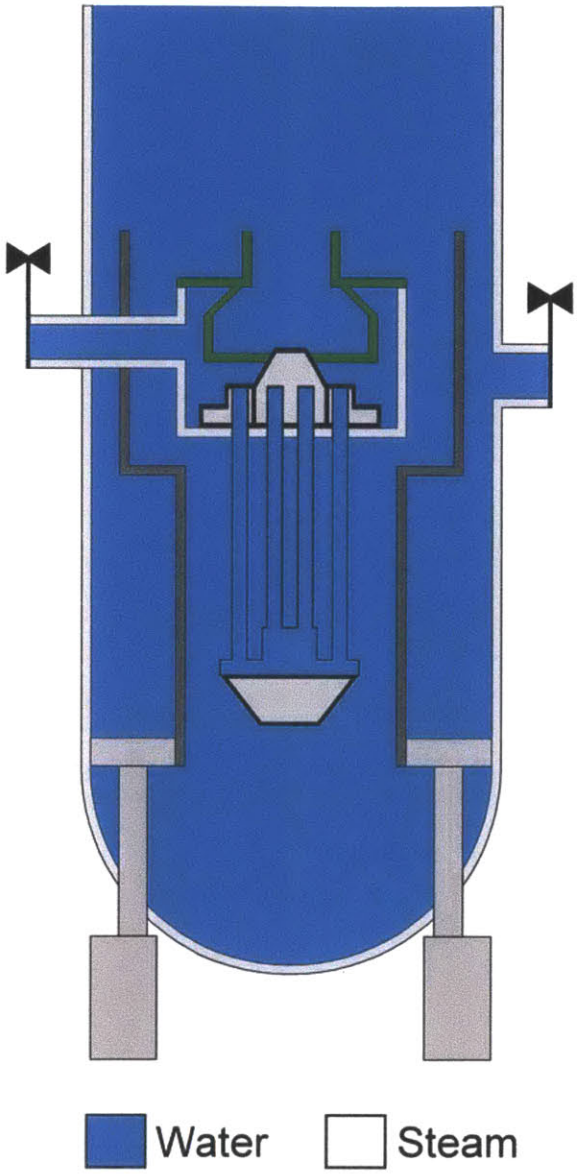

Figure 5-31 Startup of the ASBWR (step 3)

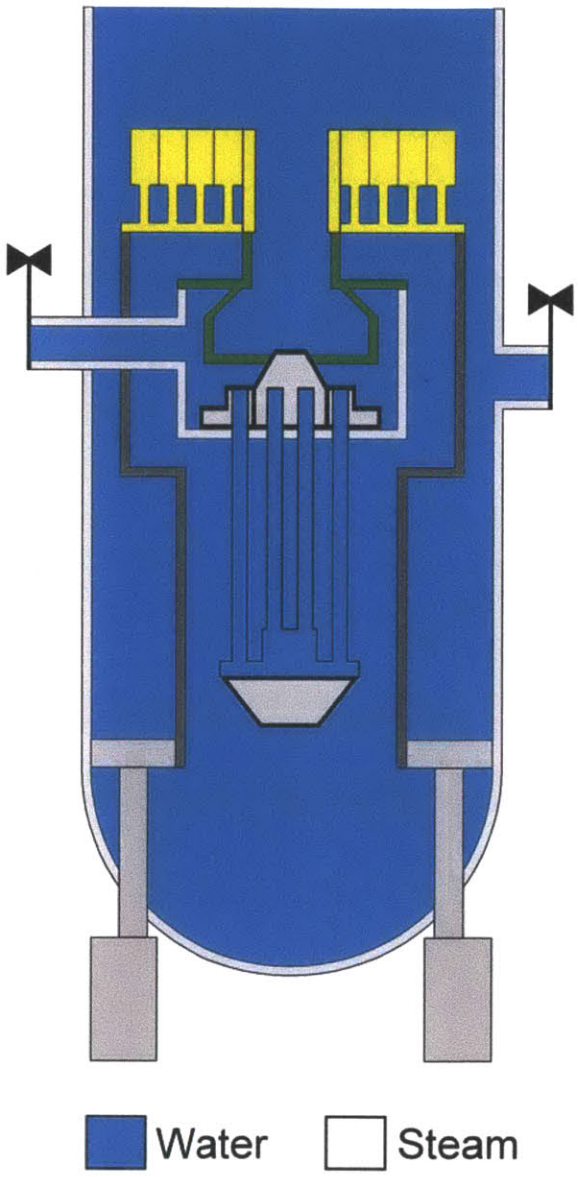

Figure 5-32 Startup of the ASBWR (step 4)

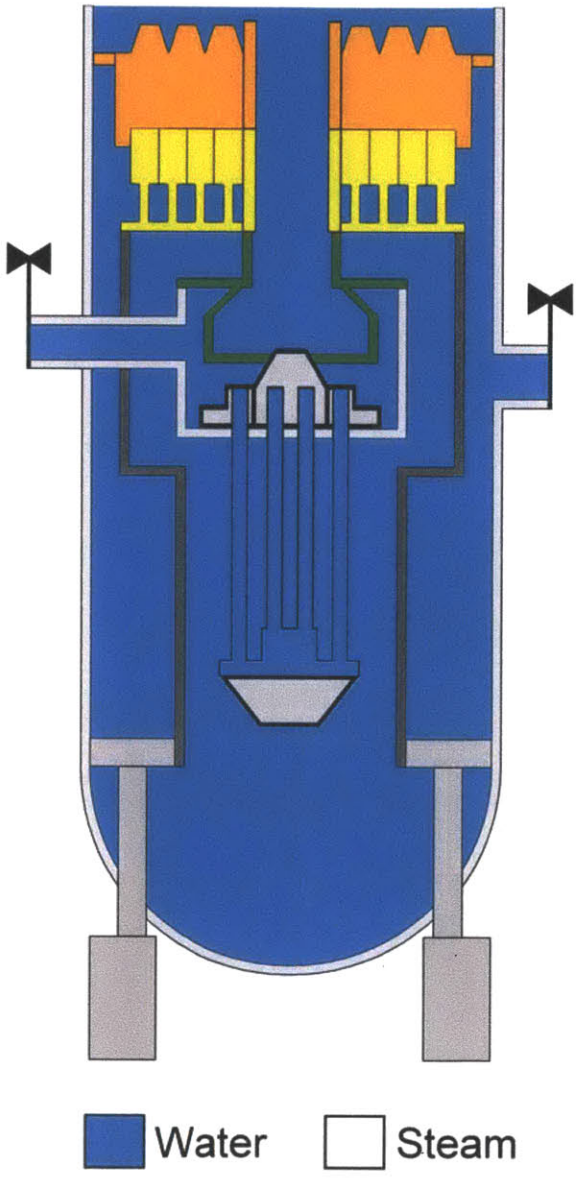

Figure 5-33 Startup of the ASBWR (step 5)

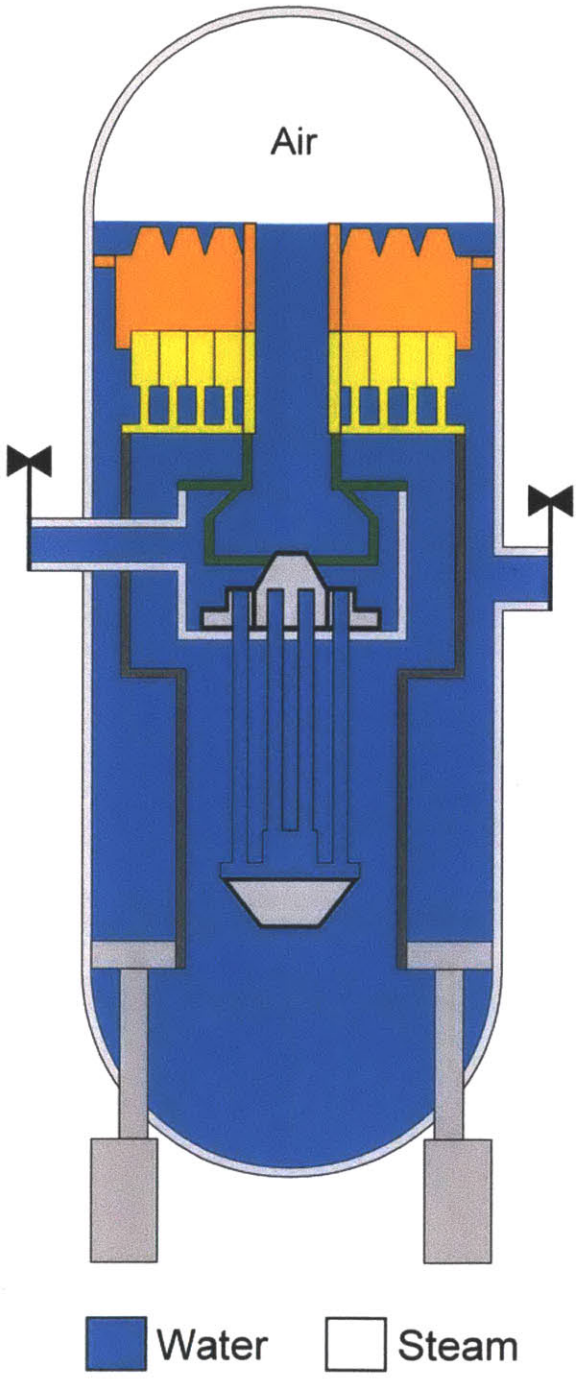

Figure 5-34 Startup of the ASBWR (step 6)

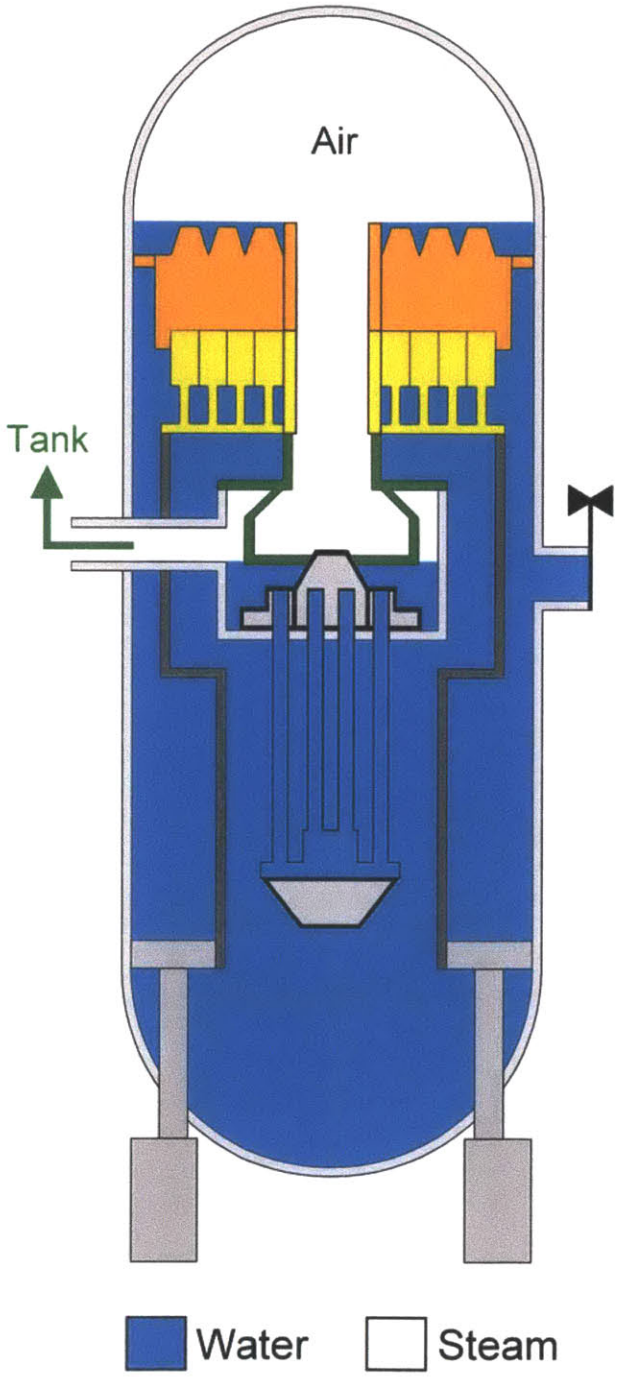

Figure 5-35 Startup of the ASBWR (step 7)

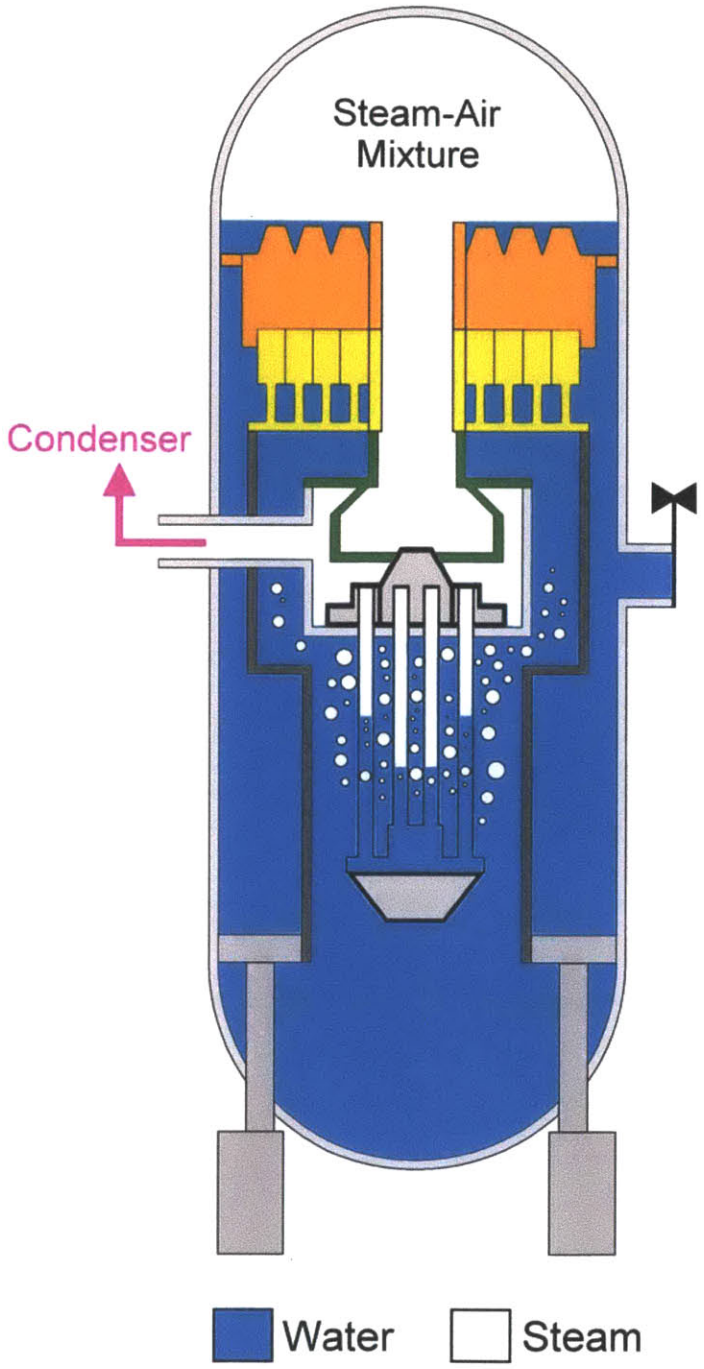

Figure 5-36 Startup of the ASBWR (step 8)

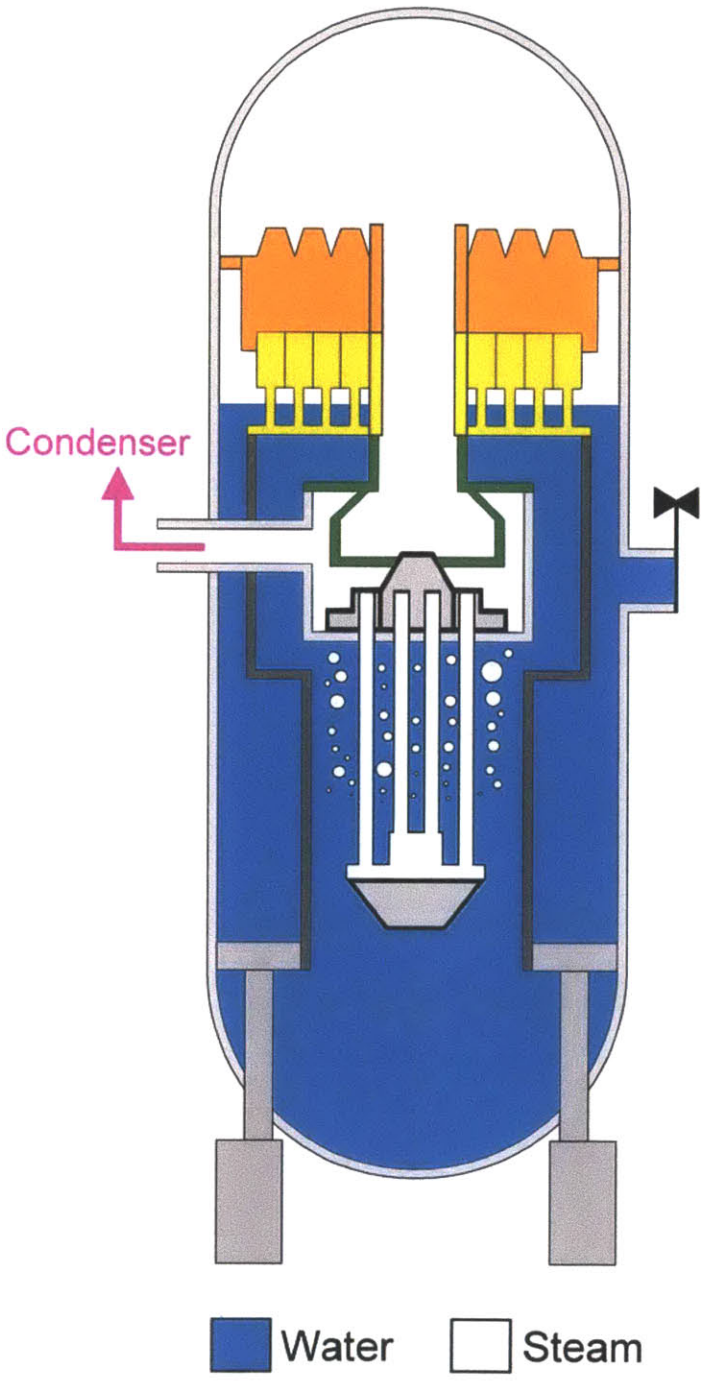

Figure 5-37 Startup of the ASBWR (step 9)

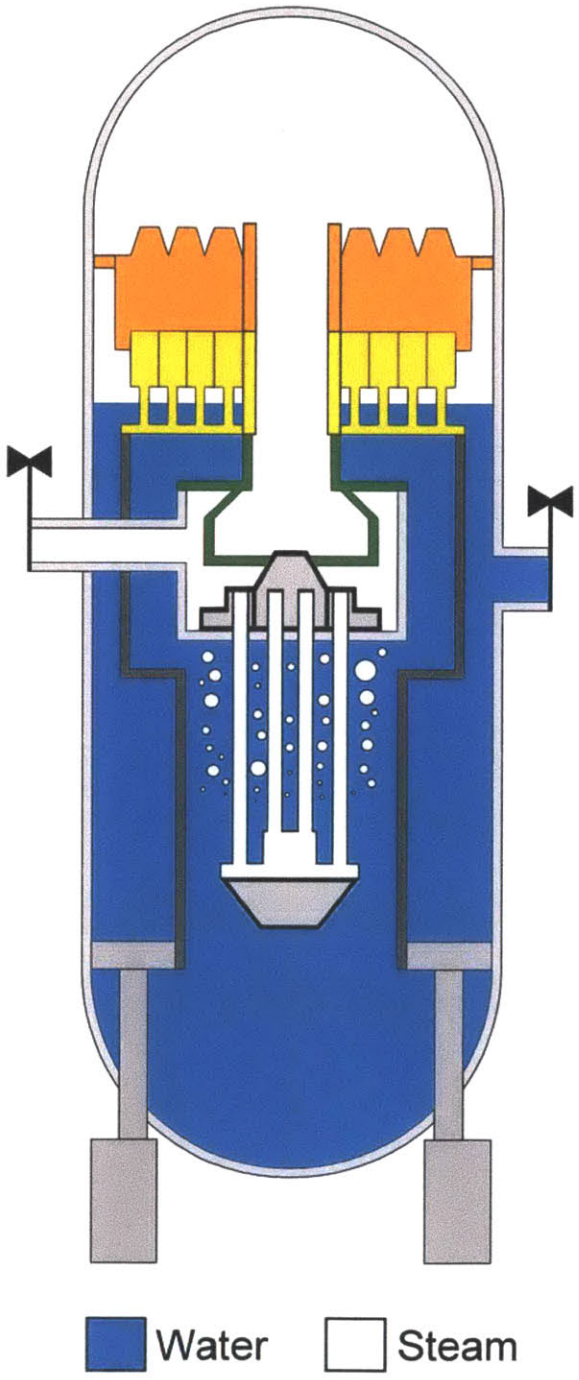

Figure 5-38 Startup of the ASBWR (step 10)

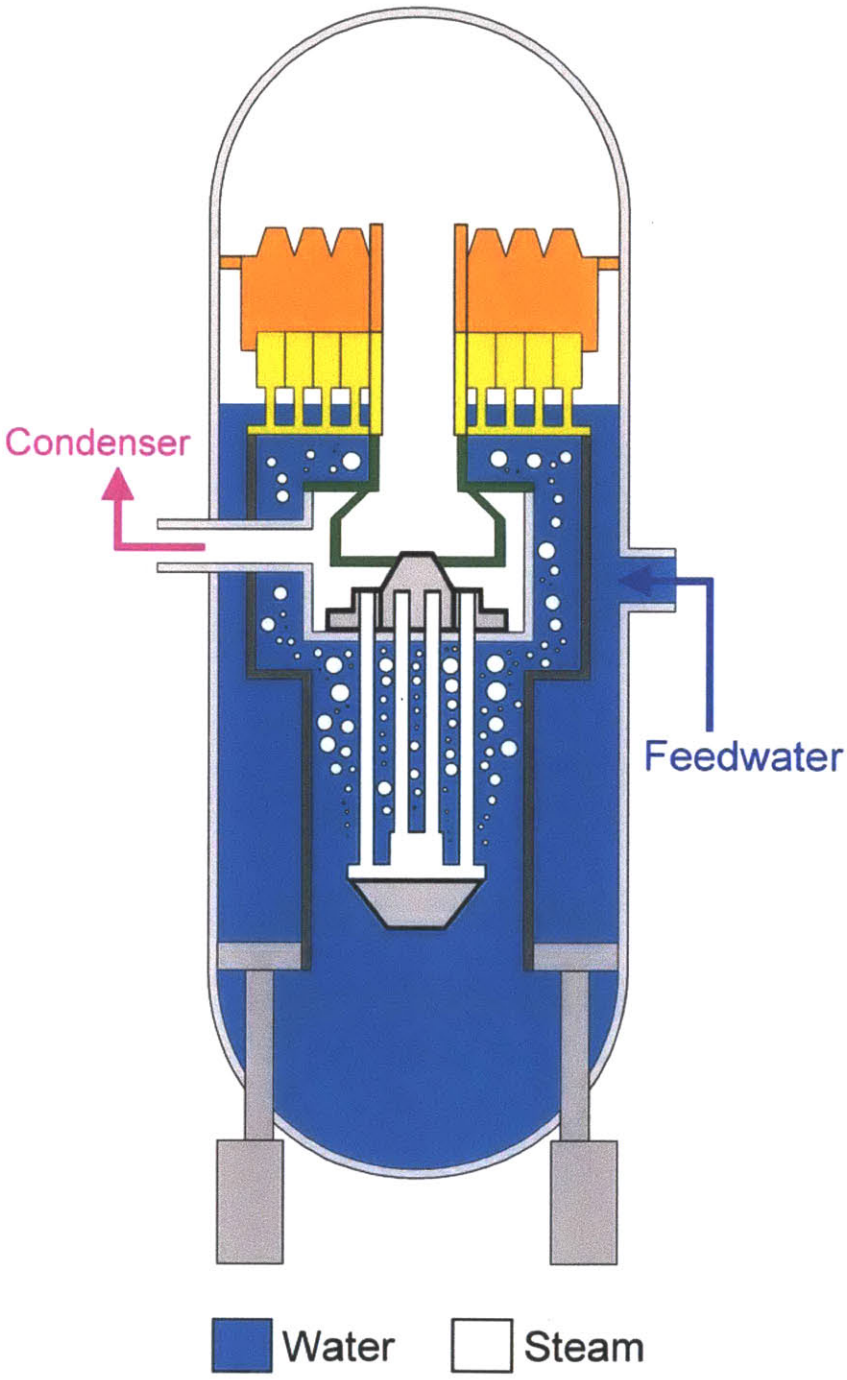

Figure 5-39 Startup of the ASBWR (step 11)

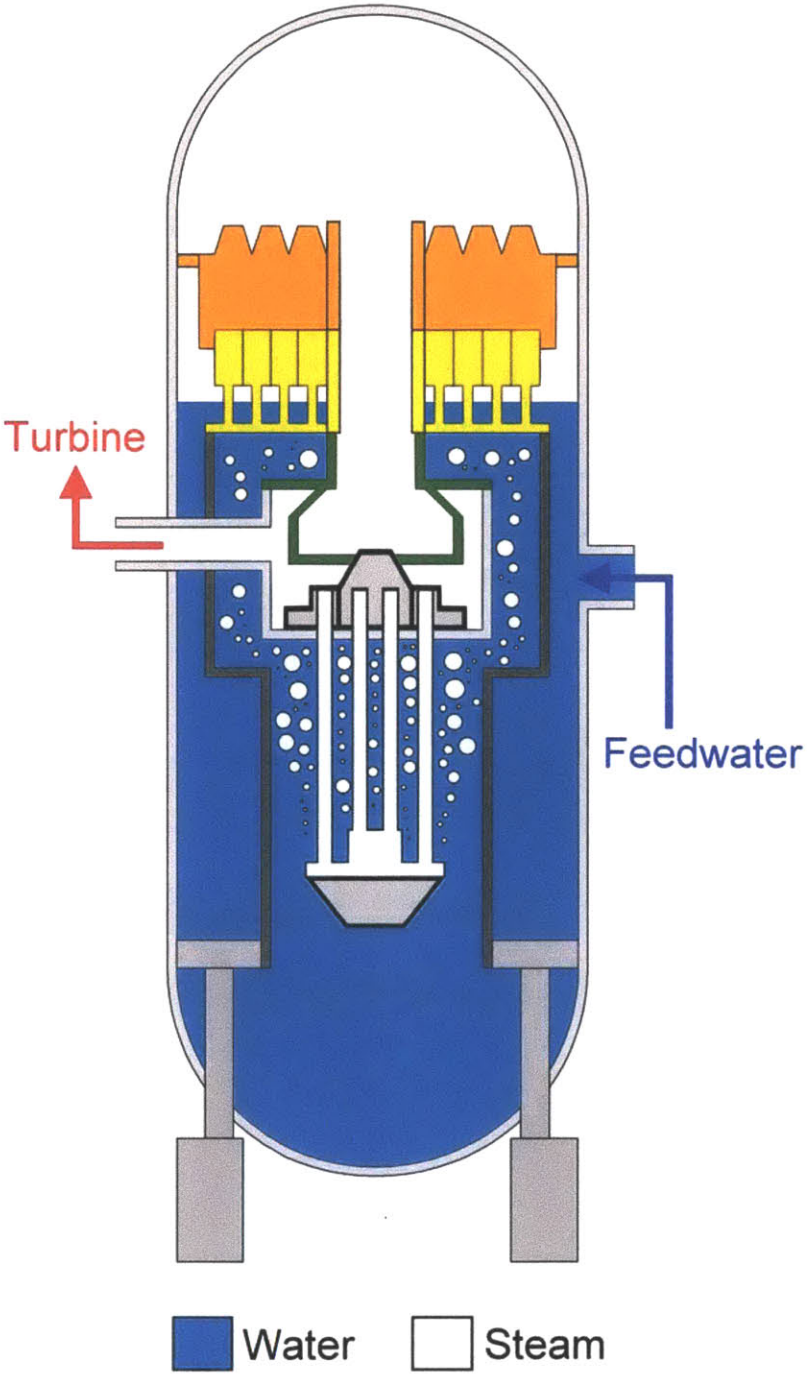

Figure 5-40 Startup of the ASBWR (step 12)

Chapter 6

Preliminary Thermal Expansion and Stress Analyses

6.1 Assumptions and Cladding Properties

Preliminary thermal expansion and stress analyses have been done for a fresh ASBWR fuel element. The purpose of these analyses is to investigate the stress distribution and thermal expansion of the cladding in the initial phase of operation. All assumptions applied to the analyses are listed in Table 6-1. Young's modulus and linear thermal expansion coefficients of the cladding materials are listed in Tables 6-2 and 6-3, respectively.

Table 6-1 Assumptions adopted in the thermal expansion and stress analyses

(1)	Steady state analysis for the fresh fuel element with T91 cladding
(2)	The hot steam up-flow channel is analyzed
(3)	Hot channel factor is 1.45 and the power density is 50 kW/L for the base case
(4)	Poisson's ratios are 0.3 and 0.29 for T91 and Inconel 718, respectively
(5)	Gap pressure is assumed to be 12.5 bar at full power operation

Table 6-2 Young's modulus of the cladding materials

Temperature (°C)	Young's modulus (GPa)	
	T91	Inconel 718
20	206.0	201.2
100	199.5	197.5
200	194.4	192.2
300	187.9	186.3
400	181.5	179.7
500	175.0	172.4
600	151.0	164.4
700	127.0	155.8
Reference	[111]	[99]

Table 6-3 Linear thermal expansion coefficients of the cladding materials

Temperature (°C)	Linear thermal expansion coefficient (10^{-6}/K)*	
	T91	Inconel 718
20	---	---
100	10.8	13.2
200	11.2	13.5
300	11.6	13.9
400	11.9	14.2
500	12.2	14.5
600	12.5	14.9
700	12.7	15.5
Reference	[111]	[99]

* Mean coefficient between 20 °C and T

6.2 Stresses Caused by Pressure

Figure 6-1 illustrates the pressure acting on the inner and outer cladding of the fresh fuel. Figure 6-2 shows the force balance for calculation of the axial stresses. Stresses caused by pressure can be expressed as the following equations [128].

For the inner cladding:

$$\sigma_r^i = \frac{-(P_{st} + P_{gap})}{2} \tag{6-1}$$

$$\sigma_\vartheta^i = \frac{r_1 P_{st} - r_2 P_{gap}}{r_2 - r_1} \tag{6-2}$$

$$\sigma_z^i = \frac{(r_3^2 - r_2^2)P_{gap} - (r_4^2 - r_1^2)P_{fw}}{(r_4^2 - r_3^2) + (r_2^2 - r_1^2)} \tag{6-3}$$

For the outer cladding:

$$\sigma_r^o = \frac{-(P_{fw} + P_{gap})}{2} \tag{6-4}$$

$$\sigma_\vartheta^o = \frac{r_3 P_{gap} - r_4 P_{fw}}{r_4 - r_3} \tag{6-5}$$

$$\sigma_z^o = \frac{(r_3^{\,2} - r_2^{\,2})P_{gap} - (r_4^{\,2} - r_1^{\,2})P_{fw}}{(r_4^{\,2} - r_3^{\,2}) + (r_2^{\,2} - r_1^{\,2})} \tag{6-6}$$

where the superscripts o, i, refer to outer and inner claddings respectively; P_{st}, P_{gap} and P_{fw} refer to steam, gap and water pressures, respectively; σ_r, σ_θ, σ_z refer to radial, hoop and axial stresses, respectively.

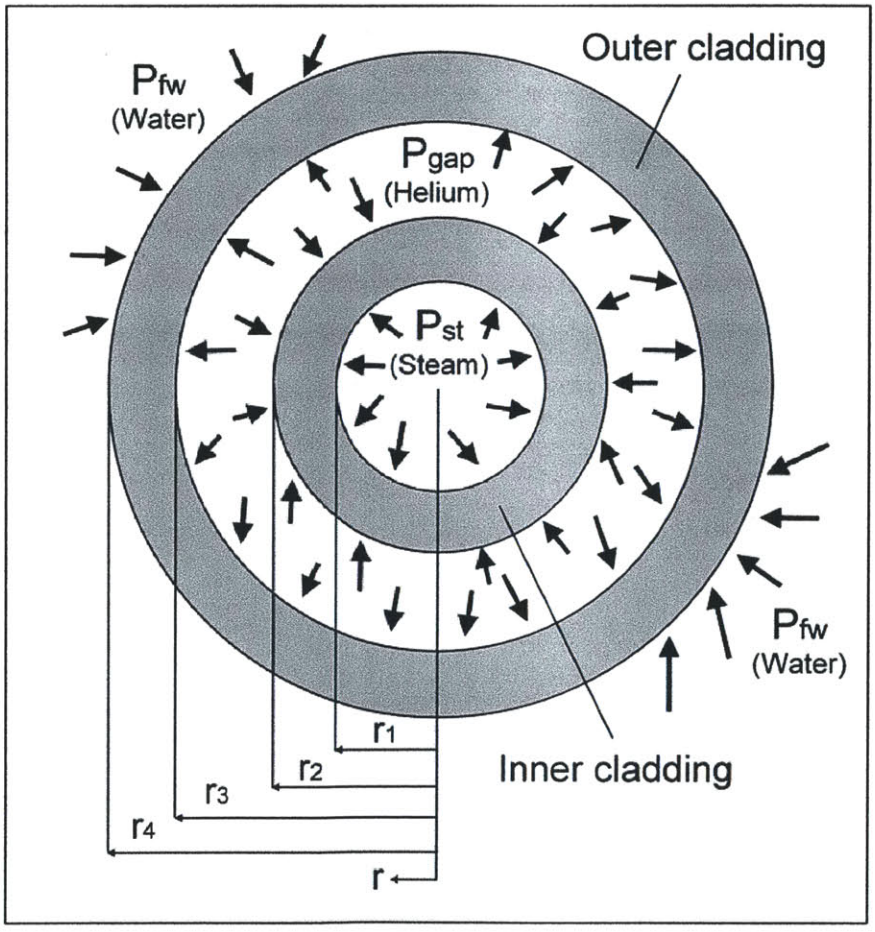

Figure 6-1 Illustration of the pressures acting on cladding

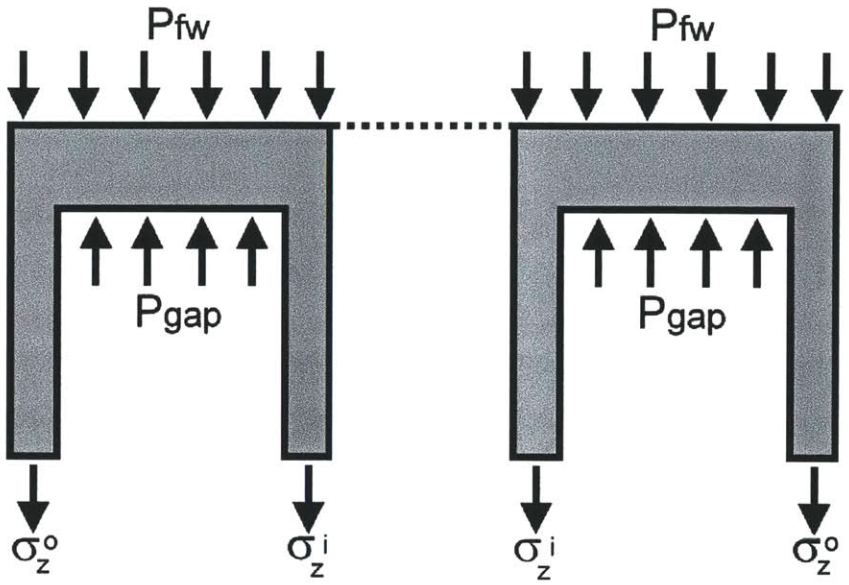

Figure 6-2 Balance of the axial forces

Table 6-4 summarizes the calculation results. It can be found that the inner cladding is subject to tensile hoop stress while the outing is subject to compressive hoop stress at the beginning of cycle. However, after the fuel burnup increases, the fuel internal pressure will increase considerably due to the release of fission gas from the fuel pellets. The plenum pressure will eventually be higher than the system pressure, and then the inner and outer claddings will be subject to compressive and tensile stresses, respectively.

Table 6-4 Calculation results of the stresses caused by pressure at the beginning of fuel life in core

	σ_r (MPa)	σ_θ (MPa)	σ_z (MPa)
Inner cladding	-3.94	32.41	-18.91
Outer cladding	-4.19	-73.35	-18.91

6.3 Calculation of Thermal Stresses

If the wall of a long hollow cylinder is heated non-uniformly through its thickness, its elements would not expand uniformly and thermal stresses are induced due to this mutual interference. Considering the cladding structure as a long, hollow cylinder, its thermal stresses can be expressed as [128]:

$$\sigma_r^T = \frac{\alpha E}{(1-\nu)r^2}\left[\frac{r^2-a^2}{b^2-a^2}\int_a^b T(r)rdr - \int_a^r T(r)dr\right] \tag{6-7}$$

$$\sigma_\vartheta^T = \frac{\alpha E}{(1-\nu)r^2}\left[\frac{r^2+a^2}{b^2-a^2}\int_a^b T(r)rdr + \int_a^r T(r)dr - T(r)r^2\right] \tag{6-8}$$

$$\sigma_z^T = \frac{\alpha E}{(1-\nu)}\left[\frac{2}{b^2-a^2}\int_a^b T(r)rdr - T(r)\right] \tag{6-9}$$

where the superscripts T refer to thermal stresses; α, ν and E are thermal expansion, Poisson ratio and Young's modulus, respectively; a and b are inner and outer radii, respectively. This analysis assumes the long cylinder to be axially unconstrained.

Figure 6-3 shows the peak thermal stresses on the steam side (inner) cladding. The maximum radial thermal stress (σ_r^T) is about 1.33 MPa which is negligible compared to σ_θ^T and σ_z^T. Figure 6-4 shows the maximum thermal stresses on the water side (outer) of the cladding. Compared with Figure 6-3, the water side cladding has slightly higher maximum thermal stresses because its radial temperature distribution is less uniform than that of the steam side cladding.

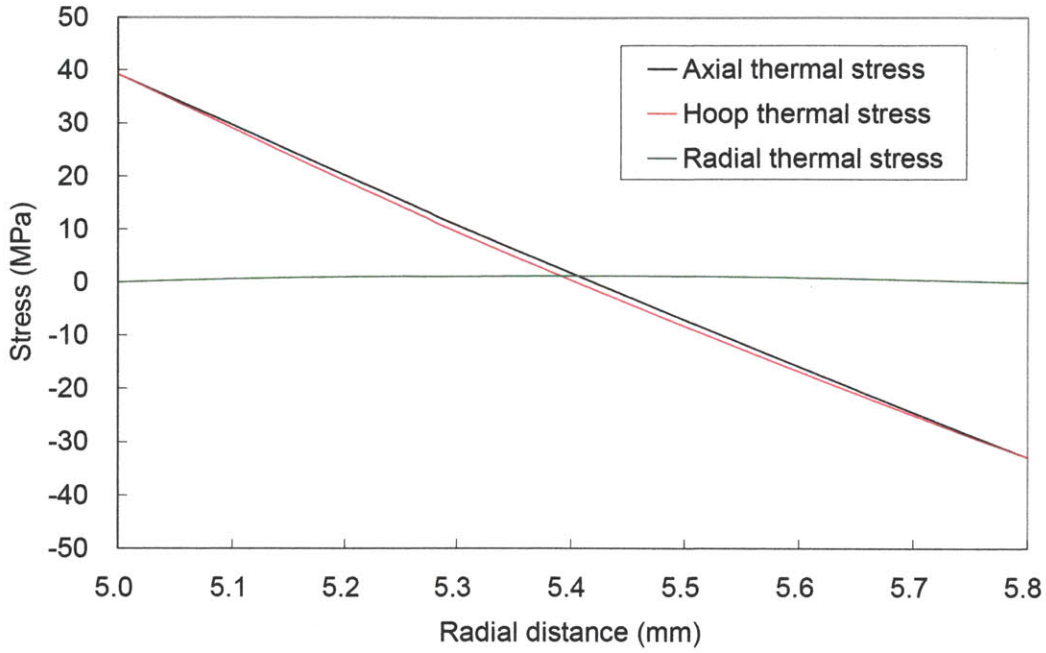

Figure 6-3 Peak thermal stresses on the steam side (inner) cladding

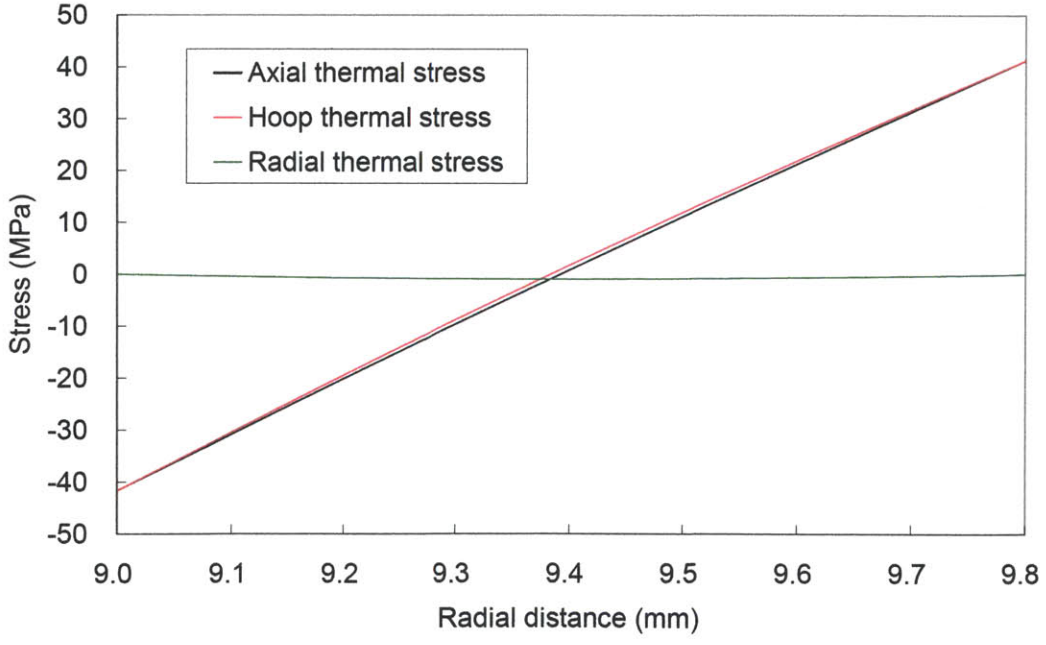

Figure 6-4 Peak thermal stresses on the water side (outer) cladding

6.4 Calculation of Strains and Thermal Expansion

During plant operation, cladding deforms gradually due to pressure, thermal expansion and irradiation effects etc. In this section, deformation of fresh fuel cladding caused by pressure and thermal expansion is evaluated.

Strains caused by pressure and thermal expansion can be expressed as [128]:

$$\varepsilon_r = \frac{1}{E}[\sigma_r - \nu(\sigma_z + \sigma_\vartheta)] + \int_{T_0}^{T} \alpha_r dT \qquad (6\text{-}10)$$

$$\varepsilon_\vartheta = \frac{1}{E}[\sigma_\vartheta - \nu(\sigma_r + \sigma_z)] + \int_{T_0}^{T} \alpha_\vartheta dT \qquad (6\text{-}11)$$

$$\varepsilon_z = \frac{1}{E}[\sigma_z - \nu(\sigma_r + \sigma_\vartheta)] + \int_{T_0}^{T} \alpha_z dT \qquad (6\text{-}12)$$

where ε_r, ε_θ, ε_z,, are radial, hoop and axial strains, respectively; T_o is the reference temperature (20 °C).

In this evaluation, the cladding material is assumed to expand isotropically, therefore $\alpha_r = \alpha_\vartheta = \alpha_z = \alpha$.

Table 6-5 summarizes the calculation results of strains, radial displacement, and axial and radial growths due to pressure and thermal expansion for the hot channel. The steam down-flowing and up-flow channels have different axial growths of the inner cladding since steam temperature is higher in the up-flow channels. For the axial growth of the outer cladding, the results between the steam down-flow and up-flow channels are about the same. Although the radial strain is about the same magnitude as the axial strain, the radial growth in cladding is very small due to the thin cladding thickness.

In addition, it can be seen from Table 6-5 that there is a noticeable difference in axial growth between the inner and outer claddings. For the steam up-flow channel, the axial growth of the inner cladding is 20.0 mm and is 10.46 mm for the outer cladding. The

difference is about 1 cm. On the other hand, the difference in axial growth between the inner and outer claddings of the steam down-flow channel is only 0.4 cm.

Table 6-6 summarizes the calculation results of axial growth due to pressure and thermal expansion. Results of the average and hot channels are also compared. It is found that the results of axial growth between the average and hot channels are approximately within a difference of 2 mm. Furthermore, Inconel 718 has larger overall axial growth and larger difference in axial growth between the inner and outer claddings due to its higher thermal expansion coefficient. Given the power density of 50 kW/L, for Inconel 718 the maximum axial growth is 25.18 mm while for T91 it is 20.03 mm.

Table 6-7 shows the results of axial growth due to pressure and thermal expansion with various power densities. As shown in Table 6-7, as the power density increases, the overall axial growth and the difference in axial growth between the inner and outer claddings also increase. The overall axial growth is expected to be accommodated by the spring ends as mentioned in Chapter 3. The difference in axial growth between the inner and outer claddings is expected to be compensated by bellows. Further studies are needed to investigate the long term fuel performance and the reliability of the proposed spring ends and bellows.

Table 6-5 Results of strain calculation of the base case (T91 cladding)

	Axial strain	Axial growth* (mm)	Radial strain	Radial growth* (mm)	Hoop strain	Radial displacement* (mm)
Steam down-flowing channel						
Inner cladding	0.0048	14.36	0.0043	0.0035	0.0052	0.0279
Outer cladding	0.0035	10.35	0.0035	0.0028	0.0030	0.0286
Steam up-flowing channel						
Inner cladding	0.0067	20.03	0.0071	0.0057	0.0071	0.0381
Outer cladding	0.0035	10.46	0.0035	0.0028	0.0031	0.0290

*Growth / displacement due to pressure and thermal expansion

Table 6-6 Calculation results of axial growth due to pressure and thermal expansion

			T91	Inconel 718
			Axial growth (mm)	
Average channel	Steam down-flow	Inner cladding	13.79	17.00
		Outer cladding	10.09	12.63
	Steam up-flow	Inner cladding	18.55	23.15
		Outer cladding	10.18	12.80
Hot channel	Steam down-flow	Inner cladding	14.36	17.78
		Outer cladding	10.35	13.09
	Steam up-flow	Inner cladding	20.03	25.18
		Outer cladding	10.46	13.29
Note: power density = 50 kW/L				

Table 6-7 Impact of power density on the axial growth

Power density (kW/L)	T91	Inconel 718	T91	Inconel 718
	Maximum axial growth (mm)		Difference of axial growth between inner and outer claddings (mm)	
40	19.0	--	8.73	--
45	19.6	--	9.17	--
50	20.0	25.2	9.57	11.88
55	20.4	25.8	9.91	12.34
60	20.8	26.3	10.22	12.75
65	21.2	26.9	10.50	13.13
70	21.5	27.3	10.76	13.48
75	--	27.8	--	13.80
80	--	28.2	--	14.10

* Axial growth is caused by pressure and thermal expansion

Chapter 7
Stability Analysis

7.1 Introduction

According to literature, the most important instability type in the BWR operation is the density wave oscillation (DWO) [119]. In general, there are three kinds of DWO instability: 1) single channel, 2) region wide (or out-of-phase) and 3) core wide (or in-phase) instabilities.

For the single channel instability, only one channel or a small fraction of the parallel channels oscillates, while the other channels remain steady. For the out-of-phase instability, about half of the core behaves out-of-phase from the other half. During this so-called out-of-phase oscillation, half of the core rises in power while the other half decreases alternately to maintain a nearly constant total core power. For the in-phase stability, the flow and power in all channels oscillate in phase throughout the whole core.

In this study, the single channel and core-wide in-phase stability analyses are performed for the reference BWR and ASBWR. Results are compared and reported in this chapter.

7.2 Computational Tool

An MIT in-house code is used to perform stability analysis for the ASBWR. The code, called SAB (Stability Analysis of BWR), was initially developed by Zhao [129] in 2005 and then modified by Hu [119] in 2007. The SAB code is programmed in MATLAB compiler and is capable of estimating the susceptibility of BWRs to two-phase flow oscillations of the density wave type. The numerical solver was developed based on the linearization and Laplace-transformation of the mass, momentum and energy equations, along with the constitutive relations in the frequency domain. The main output of the code is the Decay Ratio (DR) for a perturbation, which indicates whether the oscillations grow in time (DR>1) or are dampened (DR<1). The SAB code has the capability to

model in-phase and out-of-phase oscillations in the whole core with or without the neutronic feedback.

7.3 Modeling of the Annular Fuel for the Stability Analysis Code

A lumped fuel dynamics model with the temperature distribution in the fuel pin developed at Brookhaven National Laboratory [130] was initially used in the SAB code. The fuel dynamics model was then coupled to the coolant thermal-hydraulics model through the fluctuation of the fuel rods surface heat flux [119]. However, for the ASBWR this lumped fuel dynamics model is not applicable due to the use of annular fuel in the ASBWR assemblies.

In this study, a lumped annular fuel dynamics model has been developed based on the lumped modeling approach [130]. The SAB code has been modified to incorporate the lumped annular fuel dynamics model to capture the annular fuel features. Details of the derivation and modification of the SAB code are described in Appendix D.

7.4 Single Channel Thermal-hydraulic Stability Analysis

7.4.1 Assumptions

During the single channel flow stability, only one channel oscillates while the bulk flow remains at steady state. Therefore, a constant pressure drop boundary condition can be imposed on that single channel. Figure 7-1 illustrates this constant pressure drop boundary condition.

Due to the small fraction of the single channel flow compared to that of the whole reactor core, the neutronic feedback caused by the flow fluctuation of a single channel will not affect the whole core neutronics too much. Therefore, neutronic feedback is not considered in the single channel instability analysis.

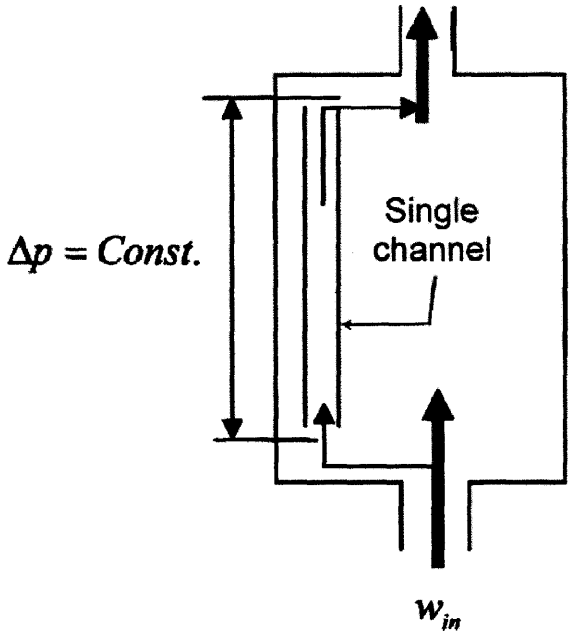

Figure 7-1 Illustration of the single channel instability loop

Assumptions adopted in the analysis of single channel instability are listed in Table 7-1. In this preliminary study, the water power split ratio, as defined in Chapter 5, is assumed to be constant during the oscillation. This assumption is reasonable since the water power split ratio can not be changed quickly unless there is a considerable change in the steam coolant flow rate. In addition, the perturbation feedback from the steam side is considered negligible because pressure oscillations from the water side are likely to be highly attenuated due to the tortuous path of steam in the separators/dryers region.

Table 7-1 Assumptions adopted in the thermal expansion and stress analyses

(1)	The lumped annular fuel dynamics model is used for the ASBWR
(2)	Power splits are 0.72 and 0.70 and remain constant during the oscillation for the T91 and Inconel 718 claddings, respectively.
(3)	Hot channel factor is 1.45 and the power density is 50 kW/L for the base case
(4)	The total fuel length is assumed to be 3.8 m
(5)	The hot channel flow disparity is 0.9 for both reference BWR and ASBWR*

*Water flow in the hot channel is assumed to be only 90% of that in the average channel

Table 7-2 Results of the single channel stability analysis

	Assembly power (MWt)	Assembly flow rate (kg/s)	Exit quality	Decay ratio
Reference BWR	6.30	15.24	0.244	0.1311
ASBWR (T91 cladding)	6.82	17.06	0.242	0.1219
ASBWR (Inconel 718 cladding)	6.64	17.06	0.235	0.1126

7.4.2 Results

Results of the single channel stability analysis are summarized in Table 7-2. As shown in Table 7-2, the ASBWR has smaller decay ratios than the reference BWR, which is desirable since a smaller decay ratio means the oscillation will be dampened faster than the reference BWR. The main reason for the larger decay ratio is the somewhat lower exit quality and larger hydraulic diameter of the ASBWR.

7.5 In-Phase Stability Analysis

7.5.1 Assumptions

Figure 7-2 illustrates the in-phase stability model [119]. In an in-phase oscillation, flow and power in all channels oscillate in the same mode throughout the whole core. The density wave is assumed to transit in a closed loop. The in-phase stability model only takes into account the water loop because the pressure oscillations are likely to be highly attenuated due to the tortuous path of steam in the separators/dryers region, which acts only on 15% of the flow. The oscillations in the path of water return are considered more important for the core flow loop. The oscillation in the core flow loop will affect the production of steam and thus the cooling in the annular fuel inner channels. This effect is taken into account by the water power split ratio in the lumped annular fuel dynamics model (Appendix D).

Table 7-3 shows the assembly grouping for the in-phase stability analysis. As shown in Table 7-3, the ASBWR is assumed to have the same power factors as the reference BWR. The pressure loss coefficients are listed in Table 5-9. Neutronic parameters related to the point kinetics model used in the analysis are given in Table 7-4. Since the full core study has not yet done for the ASBWR, the ASBWR is assumed to have the same temperature and void coefficients as the reference BWR.

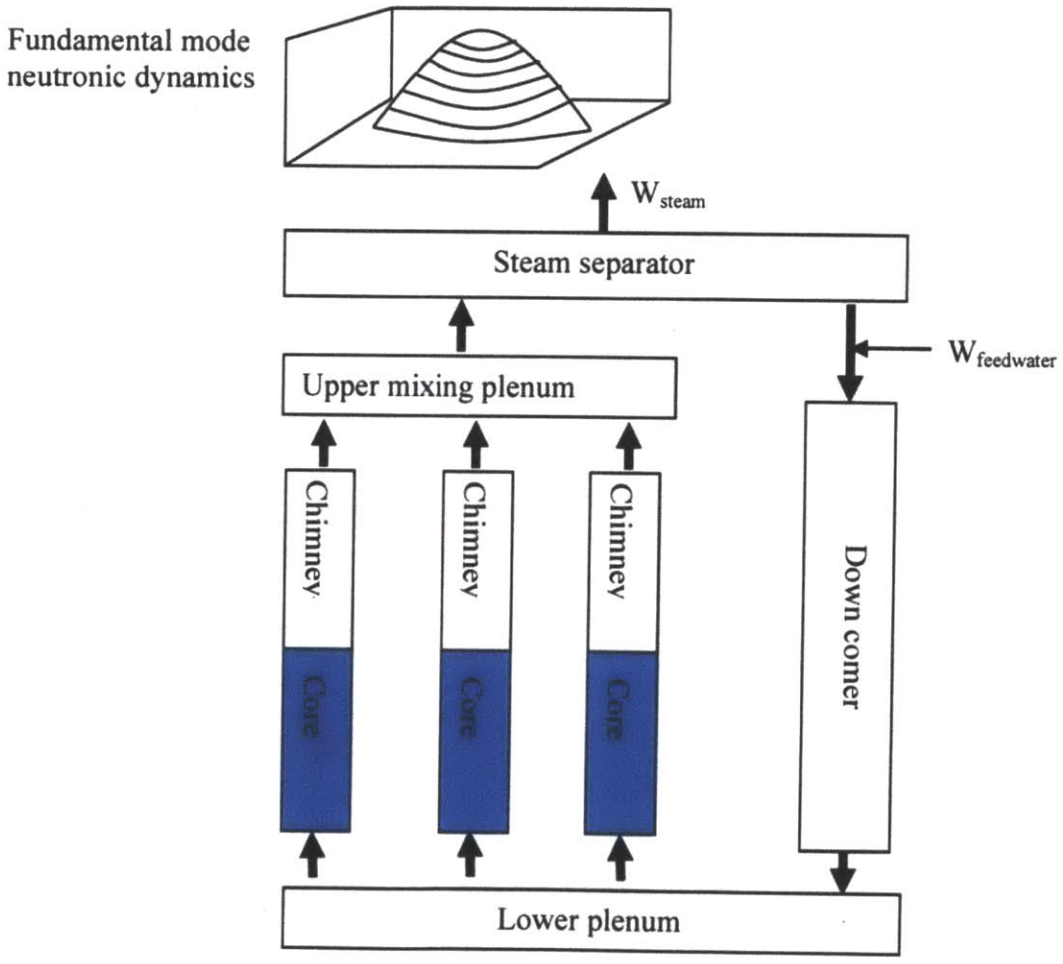

Figure 7-2 Illustration of in-phase stability model [119]

Table 7-3 Assembly grouping for the in-phase stability analysis

Assembly Type	Peaking Factor	# of Assemblies (Reference BWR)	# of Assemblies (ASBWR)
Hot	1.30	148	38
Average power	1.004	500	127
Low power	0.60	116	30

Table 7-4 Neutronic parameters for the in-phase stability analysis

Six group delayed neutron fraction		Six group decay constants (sec^{-1})	
β_1	2.21E-04	λ_1	2.21E-04
β_2	1.47E-03	λ_2	1.47E-03
β_3	1.31E-03	λ_3	1.31E-03
β_4	2.65E-03	λ_4	2.65E-03
β_5	7.71E-04	λ_5	7.71E-04
β_6	2.81E-04	λ_6	2.81E-04

Table 7-5 Results of the in-phase stability analysis

	Power density (kW/L)	Core average exit quality	Decay ratio
Reference BWR	50.5	0.140	0.2882
ASBWR (T91 cladding)	50.0	0.141	0.2363
ASBWR (Inconel 718 cladding)	50.0	0.140	0.2387
Void coefficient (pcm/ % void) = -144 Fuel temperature coefficient (pcm/K) = -1.7			

7.5.2 Results

Results of the in-phase stability analysis are summarized in Table 7-5. As shown in Table 7-5, the ASBWR has smaller decay ratios than the reference BWR. Compared with the results in Table 7-2, it is found that Inconl 718 has a lower single channel stability decay ratio but a slightly higher in-phase stability decay ratio than T91. The possible reasons are that for the single channel oscillation, the local exit quality of the analyzed channel has a great effect on the fluid compressibility. Therefore, a lower exit quality implies a lower single channel stability decay ratio. On the other hand, the in-phase oscillation takes into account the global properties, such as core flow rate, void coefficient, fuel and cladding material properties. The relatively low thermal conductivity of Inconel 718 results in a slower fuel response time, and thus its in-phase stability decay ratio is lower than T91.

7.6 Sensitivity Studies

The sensitivity studies have been performed to investigate the impact of steam side conditions on the stability decay ratio. The power split has been artificially adjusted such that the water side power and exit quality remain the same while the steam side conditions are changed. For example, a decrease in power split represents that more heat is transferred to the steam side and thus the steam, inner cladding and fuel temperatures become higher.

Table 7-6 summarizes the results of the power split sensitivity study. It is observed that the stability decay ratio is not very sensitive to the power split within the range of 0.66 to 0.76.

Table 7-6 Results of the power split sensitivity study

	Single channel stability decay ratio		In-phase stability decay ratio	
Power split	T91	Inconel 718	T91	Inconel 718
0.66	0.1145	0.1074	0.2381	0.2400
0.68	0.1171	0.1101	0.2375	0.2393
0.70	0.1195	0.1126	0.2369	0.2387
0.72	0.1219	0.1150	0.2363	0.2381
0.74	0.1242	0.1174	0.2358	0.2375
0.76	0.1263	0.1197	0.2354	0.2370

Chapter 8
Summary and Recommendations for Future Work

8.1 Summary

Summary of the Proposed Design

A conceptual design of an annular-fueled superheat boiling water reactor (ASBWR) has been presented in this work. By employing annular fuel elements, the ASBWR localizes a combined boiler and superheater regions around each fuel rod. This approach differs from those US designed superheat reactors in the 1960s, which had the core divided into two separate regions, one for boiling and one for superheating. This approach was the basis for a design of a German designed superheat reactor. But the ASBWR and that reactor have several important differences which are discussed in Chapter 3.

In the ASBWR, each annular fuel element, or fuel tube, is cooled internally by steam and externally by water. Fuel pellets are made of commercially viable enriched (< 20 weight percent) UO_2. T91 and Inconel 718 are selected as candidates for the cladding material in consideration of their excellent physical properties and corrosion resistance at high temperatures. The fuel cladding gap is filled with pressurized helium gas like the existing LWR fuels. The ASBWR fuel assembly contains sixty annular fuel elements and one square water rod (occupying a space of four fuel elements) in an 8 by 8 square array. Annular separators and steam dryers are utilized and located above the core in the reactor vessel. Water from the core exit is recirculated to the core inlet region by flowing near the reactor vessel, just as a typical BWR. Reactor internal pumps are used to adjust the core flow rate like typical ABWRs. Cruciform control rods, inserted from the reactor bottom, are used to control the reactivity of the core.

The coolant flow configuration of the ASBWR is a unique design. The externally circulating feedwater flows into the downcomer region through nozzles and combines with the saturated water exiting from the separators and flowing in the downcomer region,

as in the traditional BWRs. Then the combined water coolant flows upward into the fuel assemblies. In each fuel assembly, water is heated by the outer surface of the annular fuel elements and the steam-water mixture is formed in the heated paths. The two-phase mixture, composed of about 14% saturated steam, exits the fuel assemblies and continues to flow upward and enters the annular separator and dryer. The separated steam then makes a 180-degree turn and flows down through the central void region of the annular separator and dryer to enter the steam coolant distributor, where it is preheated by the surrounding superheated steam plenum. The steam distributor is well connected to the fuel assemblies so that the preheated steam coolant can flow into the inner channels of the annular fuel elements. In each fuel assembly, the steam coolant first flows down into the 28 central fuel elements and enters a steam box at the bottom end of the fuel element. In the steam box, the steam coolant is redirected to the 32 peripheral fuel elements where it flows upward until exiting the assembly. Finally, the steam coolant is collected in the superheated steam plenum above the core and is directed to the turbine.

The goal of this design is to generate superheated steam at a temperature of 520 °C or higher under similar pressure conditions to the existing BWRs. With an outlet steam temperature of 520 °C, the plant efficiency can be enhanced to above 40%, which is a substantial improvement over the plant efficiency of 33 to 35% that an advanced LWR can achieve nowadays. Although thermal power of the ASBWR is currently set to 1250 MWt, which is equivalent to an electric power output 500 MWe, the reactor core size is flexible to expand or shrink for a specific power demand.

Key advantages of the Proposed Design

The ASBWR has many distinguished advantages. First, the annular fuel alleviates the concern about emergency cooling of the superheating region internal to the fuel element. In the event of reactor scram or loss of the steam coolant, the reactor core will not be excessively overheated as long as the residual thermal energy can be transferred to the external side of the fuel. Second, the water and steam coolants are separated by the fuel, and thus heat losses from the superheated to the boiling side is prevented. Third, there

is no need for additional neutron moderation in the superheating region. Forth, the distribution of the superheating regions in the core is extremely uniform, which leads to a homogenized neutron spectrum across the entire core and greatly simplifies the reactor control. Fifth, the ASBWR uses only one type of fuel element and control rod, which is convenient for manufacture, spare element storage and fuel reshuffling. Most importantly, the ASBWR is well supported by the currently available technologies. The design and operation of the ASBWR can draw support from available data of the existing BWRs. The ASBWR can also benefit from the abundant experience in operating fossil-fueled superheat plants, since the temperature levels of steam entering the turbine are close. Furthermore, the issues of annular fuel application in LWRs have also been recently studied at both MIT and within industrial research organization such as Westinghouse and Korea Atomic Energy Research Institute. These all help to lower the technical barriers to achieve the ASBWR concept.

Main Challenges of the Proposed Design

On the other hand, the concept of the combined boiling-superheating fuel element involves a complicated fuel assembly design and raises several technological problems. The major challenges for the ASBWR design are: 1) the potential for excessive stresses due to different thermal expansion between the inner and outer claddings; 2) the uncertainty about achieving a desirable power split to the external and internal coolant channels; 3) a need for a higher enrichment UO_2 to achieve a comparable burnup to the BWRs arising from the larger clad volume fraction and higher absorption cross section of the clad materials; 4) higher manufacturing difficulty and associated cost of the fuel assembly; 5) potential for water flooding of the superheating regions, which would result in a reactivity insertion accident; and 6) reliable fuel performance during the fuel cycle. Further investigation and analyses are needed to solve these challenges. However, the ASBWR design is still promising since the advantages offered by this concept justify the efforts required to solve the problems involved.

Results of the Preliminary Study for the Proposed Design

Two-dimensional neutronic analysis at the assembly level has been performed using CASMO-4. The results indicate that the ASBWR's neutron economy is not as good as

the existing BWRs due to the almost doubled cladding material in the core and the higher cladding absorption cross section. Compared with the reference BWR, which has an average enrichment of 4.32 w/o, the enrichment of the ASBWR fuel has to be raised to 6.35 w/o and 7.28 w/o for T91 and Inconel 718 claddings, respectively, to achieve a comparable burnup to the reference BWR. It is also found that the neutron spectrum of the ASBWR is somehow harder than the reference BWR due to the higher enrichment and the cladding absorptions. Thus, gadolinium in the ASBWR fuel is not burned as efficiently as the reference BWR, which imposes a limit on the gadolinium enrichment and the number of poison rods for the assembly design. The preliminary study shows that the optimized assembly design can achieve a desirable burnup with a local peaking of 1.25, which is close to that of the reference BWR.

The void and fuel temperature reactivity coefficients of the ASBWR are both slightly more negative than the reference BWR. Because of the more negative void coefficient, the larger assembly dimension, and harder spectrum, the ASBWR requires either stronger control materials or a higher control rod number density to obtain a desirable shutdown margin. The K-lattice control rod pattern, which is proposed for the ABWR-II, is considered applicable to the ASBWR. If the conventional N-lattice is used, the ASBWR would need enriched boron carbide with appropriate blade length for the control rod design. The fuel cycle length has also been estimated. The results show that the ASBWR is able to achieve a 24-month cycle for a three-batch core with a power density of 50 kW/L.

Results of the preliminary economic analysis indicate that the uranium purchase and enrichment cost of the ASBWR is increased by 24 ~ 45% due to the higher enrichment. The cost of electricity generation is reduced by 9 ~ 12% given the assumed plant efficiency. The reduction in the cost of electricity generation might be slightly overestimated since the ASBWR fuel fabrication cost is expected to be higher than the reference BWR.

Steady state thermal-hydraulic analysis has been performed using the widely used code

VIPRE-01 and a specially written code during this work, MASCAC. The ASBWR has been designed to meet the requirements in the following thermal-hydraulic and safety considerations: 1) Minimum Critical Heat Flux Ratio (MCHFR), 2) maximum cladding temperature, 3) thermal-nuclear coupled stability and 4) moderate core pressure drop. In fact, the moderate core pressure drop requirement implies a limit on the exit steam velocity, and thus mitigates the potential erosion and vibration damage to the fuel.

Applying radial and axial peaking factors comparable to the traditional BWR, the results of a single channel analysis indicate that at the low heat generation region, which is near both ends of the active fuel, a particular situation of "reverse heating" (i.e., steam is heating the fuel) may occur. If the power density is lower than 50 kW/L, the outlet steam temperature would be below 520 °C and the desired plant efficiency of 40% may not be obtained. Therefore, the power density of 50 kW/L is selected as the base case for this preliminary study.

Given the power density of 50 kW/L, the maximum cladding temperatures in the hot channels would be 616.2 and 626.5 °C for the T91 and Inconel 718 claddings, respectively. These temperatures are well within the cladding working limits. The maximum fuel temperature would be around 950 °C, which is much lower than the typical solid fuel temperature of 1800 °C. The maximum steam velocity would be about 78 m/s and the steam core pressure drop would be around 485 ~ 500 kPa. It is found that the steam side pressure drop is much higher than the water side (about seven times higher) primarily due to the doubled flowing path length in the core and the higher acceleration pressure drop. For both T91 and Inconel 718, the power split (the fraction of power rejected to the external water-cooled side) is about 0.70 for the hot channel and 0.74 for the average channel. An increase in power density leads to a higher steam velocity, and thus the power split is reduced because the heat transfer coefficient of steam is increased and more heat is absorbed by the steam coolant.

Given the same power density, the ASBWR has a larger dryout margin than the reference BWR. The MCHFR is 1.226 for the reference BWR and is 1.408 ~ 1.441 for the

ASBWR, depending on the cladding material. Regarding the total pressure drop, additional pumping power may be incurred if the power density is higher than 50 kW/L. This may lead to the use of pumps which have higher capacity than those used in the existing BWRs.

For the startup of the ASBWR, it is proposed to void the superheater by vaporizing all the water in the inner channel of the annular fuel element. A startup analysis which assumes an insulated steam side has been performed. The results show that the maximum cladding temperature remains below 580 °C at the 25% rated power and 30% rated core flow. The actual cladding temperature should be lower since in reality the steam side is not insulated during the startup. Therefore, this dryout approach is considered feasible for the startup of the ASBWR.

Preliminary thermal expansion and stress analyses have been done for the fresh ASBWR fuel. The results indicate that there is a noticeable difference in the axial expansion between the inner and outer claddings. For T91, the maximum axial thermal growth of the inner cladding is 20.03 mm, which is about 9.8 mm more than the outer cladding. For Inconel 718, the results are 25.18 mm and 11.9 mm, respectively. The overall axial expansion is expected to be accommodated by springs at the fuel element upper end. The uneven axial expansion between the inner and outer claddings is expected to be compensated by bellows. Further studies are needed to investigate the long term fuel performance and the reliability of the proposed end springs and bellows.

A stability analysis has been done using the MIT in-house code, SAB. Single channel and in-phase stability decay ratios have been calculated. The results show that the ASBWR has a lower decay ratio than the reference BWR mainly due to its lower exit quality, larger hydraulic diameter and shorter core length.

Table 8-1 lists the results of the preliminary study regarding the major thermal-hydraulic constraints and design goals for the base case. As shown in Table 8-1, the ASBWR with a power density of 50 kW/L meets all the design requirements and goals. Therefore, it is

concluded that the ASBWR is promising to achieve a power density of 50 kW/L. Comparison of the main design specifications between the reference BWR and ASBWR are shown in Table 8-2.

Table 8-1 Comparison of the goals and ASBWR preliminary design conditions for the base case power density of 50 kW/L

	Requirement or goal	ASBWR results*
Steam outlet temperature (°C)	> 520	520.8 ~ 524.6
Minimum critical heat flux ratio	> 1.226	1.408 ~ 1.441
Maximum cladding temperature (°C)	< 650 (for T91) < 850 (for Inconel 718)	616.2 (T91) 626.5 (Inconel 718)
Single channel stability decay ratio	< 0.1311	0.1126 ~ 0.1219
In-phase stability decay ratio	< 0.2882	0.2363 ~ 0.2387
Pumping power required to compensate the total core pressure drop (kW)	< 388.0	377.7 ~ 387.4

Table 8-2 Comparison of design specifications between BWR and ASBWR

	Conventional BWR	ASBWR
Operating pressure (bar)	71.4	71.4
Power (MWth)	3,323	1,250
Core diameter (m)	4.9	3.3
Active core height (m)	3.7	3.0
Power density (kW/L)	50.5	50.0
Specific power (kW/kg U)	24.6	26.0
Fuel element geometry	Solid	Annular
Cladding material	Zircaloy-2	T91 or Inconel 718
Fuel average enrichment (w/o) to achieve 24 month fuel cycle length	4.32	6.35 (T91) 7.28 (Inconel 718)
Coolant type	Water	Steam (inner channel) Water (outer channel)
# of fuel assembly	764	192
Assembly outer dimension (mm)	137.58	193.68
Fuel array	9 x 9	8 x 8
# of fuel rods	56,536	11,520
Cladding thickness (mm)	0.71	0.8
Gap thickness (mm)	0.1	Steam side: 0.1 Water side: 0.1
Fuel rod diameter (mm)	11.18	19.6 (outer diameter) 10.0 (inner diameter)
Pitch to diameter ratio	1.279	1.174
Core inlet temperature (°C)	278.3	278.3
Steam outlet temperature (°C)	287.2	520.8 ~ 524.6
Core exit quality (%)	14.0	14.1
Hydrogen to heavy metal ratio	4.47	4.42
Hot assembly power (MWth)	6.30	9.48 (6.82 for water side 2.66 for steam side)
Hot assembly power peaking factor	1.45	1.45
Hot assembly mass flow rate (kg/s)	15.2	17.1 (water side)
Hot assembly mass flux (kg/m^2-s)	1644	1086 (water side)
Assembly local peaking factor	1.29	1.25
Minimum critical heat flux ratio	1.226	1.408
Efficiency (%)	33	40 ~ 40.5 (expected)

8.2 Conclusions

Compared with other advanced reactor concepts, the ASBWR is distinguished because it is well supported by currently available technologies. The experiences in operating BWRs and fossil-fueled superheaters are abundant. The annular fuel application has also been recently studied. Therefore, the technical barrier is relatively lower in order to realize this concept.

The major design constraints have been identified and evaluated in this work. The performance of the fuel cladding at the high temperatures in a radiation environment remains to be verified. For the selection of cladding materials, although Inconel 718 has higher thermal neutron absorption cross section, lower thermal conductivity and larger thermal expansion coefficient, Inconel 718 is still considered more promising than T91 due to its much higher allowable working temperature. It is essential to have sufficient margin for the maximum cladding temperature to prevent the cladding failure due to overheating in an operational transient or accident. However, the qualification of cladding materials should also take into account their long term irradiation resistance under the ASBWR operating conditions. Further analyses of the Inconel 718 and T91 performance and investigation of the other feasible cladding materials are perhaps the most important future works.

According to the calculation results, the ASBWR is promising to achieve a power density of 50 kW/L and meet all the main safety requirements. Given this power density, the ASBWR is capable of generating superheated steam at 520 °C. The plant efficiency is expected to be above 40%, which is substantially greater than the plant efficiency of 33 to 35% that an advanced LWR can achieve nowadays. In addition to generating electricity, the ASBWR may also be useful for process heat applications, hydrogen production (especially with electrolysis at the higher plant efficiency) and in turn hydrogen use for liquid fuel production.

8.3 Future Work

The following tasks are recommended for future work.

Fuel performance analysis

Due to the lack of experimental data, the ASBWR fuel currently cannot be modeled using an appropriately validating existing computer code for fuel performance analysis. It is recommended to perform irradiation tests for T91 and Inconel 718 to investigate their performance under the designed operating conditions. The uneven axial thermal expansion between the inner and outer claddings is the other important issue for the ASBWR fuel. This work has proposed to use bellows to compensate the uneven axial expansion. Further studies should be performed to assess the reliability of the bellows for service throughout the fuel irradiation time. If advanced welding techniques become available, the use of two different materials for inner and outer cladding should also be studied further.

Assessment of power split variation during the fuel cycle

Power split is one of the key parameters that have a great impact on the overall reactor performance. Due to material degradation, closure of gap, cladding oxidation, deposition of crud on the cladding surface and many other reasons, variation of power split is expected during the fuel cycle. The variation of power split should be assessed in conjunction with the fuel performance analysis.

Full core modeling and three-dimensional neutronic analysis

A full core model should be developed to calculate the core-wide void coefficient and assembly radial peaking factor. Three-dimensional neutronic analysis should be performed to estimate the core axial power profile. Design of the control rod system should be finalized in accordance with the shutdown margin requirement.

Assessment of the ASBWR economics

The fabrication cost of the ASBWR fuel assembly is expected to be higher than that of a traditional BWR, mainly due to the complicated assembly design and higher uranium enrichment. It is recommended to assess the ASBWR economics to see if the additional

fuel cost and the neutronic penalty can be justified by the enhanced plant efficiency.

Analysis of transients and accidents

Analysis of transients and accidents (e.g., LOCA, LOFA, loss of feedwater flow, turbine trip, anticipated transient without scram, and main steam line break) has to be performed thoroughly for the ASBWR. The ASBWR should perform well during these transients since the fuel has the same power density but higher surface-to-volume ratio than conventional BWRs; however, there is no natural circulation path for the inner channels. In any case, the plant safety has to be proven quantitatively with a system code, such as RELAP5 [134]. In addition, the reactivity insertion accident due to flooding of the superheating region should also be studied further. Detailed neutronic analyses must be performed to evaluate the reactivity response during such events.

Evaluation of the nitrogen-16 concentration in the turbine and balance of plant

The outlet superheated steam is expected to carry more radioactivity than BWRs since the duration of steam in the core is longer. In the inner cladding fails, the release of fission products could be much greater than a similar release from a BWR fuel element because the steam coolant has no effective scrubbing action like water. Consistent with the BWR experience, the dominant nuclide contributing to the ASBWR coolant radioactivity at full power is N-16, which is produced by an (n, p) reaction on O-16 [135]. It is essential to evaluate the N-16 concentration in the turbine and balance of plant and investigate the associated shielding requirements.

A thorough analysis of the uncertainties in all important parameters

A thorough analysis of the uncertainties in all important parameters is recommended. In particular, the ASBWR should be able to allow a possible maldistribution of flow in the channels, and leakages from the high pressure, but cooler side of the steam into the lower pressure but hotter steam due to imperfections in leak tightness which may develop with time due to differential expansion between the two sides. In addition, structural analysis of the fitting of the steam pipe carrying the superheated steam in a vessel, which will have a much cooler temperature, should be performed in the future.

References

[1] C. R. Braun, "Superheat and the BWR," *Nuclear Engineering,* vol. 5, pp. 393~399, Sep. 1960.

[2] J. E. O'Brian et al., "Analysis of Commercial Scale Implementation of HTE to Oil Sands Recovery," DOE Milestone Report, Idaho National Laboratory, 2006

[3] J. E. O'Brian et al. "High Temperature Electrolysis for Hydrogen Production from Nuclear Energy – Technology Summary," Idaho National Laboratory, INL/EXT-09-16140, Feb. 2010.

[4] C. M. Stoots, "High-Temperature Co-Electrolysis of H_2O and CO_2 for Syngas Production," *2006 Fuel Cell Seminar*, Idaho National Laboratory, Nov. 2006.

[5] Alfred G. Dale, "Nuclear Power Development in the United States to 1960," *Arno Press – A New York Times Company*, 1979

[6] US Atomic energy Commission, "Small power reactors; current status, research and development program, and economic potential," USAEC Report, TID-8535, June 1960

[7] US Atomic energy Commission, "Small power reactor projects of the United States Atomic Energy Commission," USAEC Report, TID-8538, Sep.1961

[8] M. Novick et al., "Developments in nuclear superheat," Proceedings of the third international conference on the peaceful uses of atomic energy, Geneva, Aug. 31 – Sep. 9, 1964.

[9] Argonne National Laboratory, "Design, and Hazards Summary Report – Boiling Water Reactor Experiment V (BORAX-V)," USAEC Report, MaANL-6302, 1962.

[10] C. B. Burtoff et al.,, "Pathfinder – the long road toward decommissioning", *Radwaste Solutions*, American Nuclear Society, March/April 2008

[11] General Nuclear Engineering Corp., "Analysis of the initial nuclear superheat critical experiments," USAEC Report, GNEC 153, Jan. 1961

[12] US Department of Energy, "Environmental Assessment for Authorizing the Puerto Rico Electric Power Authority (PREPA) to allow Public Access to the Boiling Nuclear Superheat (BONUS) Reactor Building, Ricon, Puerto Rico," DOE/EA-1394, Jan. 2003.

[13] John Barnard, "The Esada Vallecitos Experimental Superheat Reactor," Power Apparatus and Systems, Part III. *Transactions of the American Institute of Electrical Engineers*, Vo. 80, Issue 3, pp. 708-710, 1961

[14] Chicago Operations Office, "Nuclear Superheat Meeting No. 8," Idaho Falls, Idaho, USAEC Report, March 1963.

[15] International Atomic Energy Agency, "Power Reactor Projects in Member States," IAEA General Conference, GC(07)/INF/62, Sep. 1963

[16] E. R. Appleby, "Review of power and heat reactor designs, domestic and foreign, revision 2," USAEC Report, HW-66666 REV 2, Oct. 1963.

[17] H. Kornbichler, "Superheat reactor development in the federal republic of Germany," Proceedings of the third international conference on the peaceful uses of atomic energy, Geneva, Aug. 31 – Sep. 9, 1964.

[18] P. H. Margen, L. Leine and R. Nilson, "The design of the Marviken boiling heavy-water reactor with nuclear superheat," Proceedings of the third international

conference on the peaceful uses of atomic energy, Geneva, Aug. 31 – Sep. 9, 1964.

[19] Wikipedia, "Introduction of the R4 nuclear reactor," available from World Wide Web: http://en.wikipedia.org/wiki/R4_nuclear_reactor

[20] N.A. Dollezhal et al., "Uranium-Graphite Reactor with Superheated High Pressure Steam," Proceedings of the second international conference on the peaceful uses of atomic energy," Geneva, Sep., 1958.

[21] N. A. Dollezhal, Uranium-graphite reactors for power stations using superheated steam," *Atomic Energy*, Vol. 3, Number 5, Nov. 1957.

[22] A. G. Samoilov, A. V. Pozdnyakova and V. S. Volkov, "Steam-superheating fuel elements of the reactors in the I. V. Kurchatov Beloyarsk nuclear power station," *Atomic Energy*, Vol. 40, Number 5, May 1976.

[23] P. E. Florido, J. E. and A. Clausse, "Economics of combined nuclear–gas power generation," *Nuclear Engineering and Design*, Vol 195, pp. 109-115, 2000

[24] W. R. Dunbarl, S. D. Moody and N. Lior "Exergy analysis of an operating boiling water reactor nuclear power station," *Energy Conversion and Management*, Vol. 36, pp. 149-159, Mar. 1995.

[25] N. Lior, "Energy, exergy and thermoeconomic analysis of the effects of fossil-fuel superheating in nuclear power plants," *Energy Conversion and Management*, Vol. 38, pp. 1585-1593, Oct. 1997.

[26] G. Tsikauri, "CCGT+LWR: the power plant of the future?," *Nuclear Engineering International*, Vol. 41, pp. 22-25, 1996

[27] G. Bodvarsson and D.E. Eggers, "The exergy of thermal water," *Geothermics*, Vol. 1, Issue 3, pp. 93-95, Sep. 1972.

[28] M. Kanoglua, I. Dincerb, and M. A. Rosenb, "Understanding energy and exergy efficiencies for improved energy management in power plants," *Energy Policy*, Vol. 37, Issue 7, pp. 3967-3978, July 2007.

[29] H. E. Metcalf, "Method and means of producing steam in neutronic reactors," United States Patent # 2787593, April 1957.

[30] E. P. Wigner, "Neutronic reactor," United States Patent # 2806820, Sep. 1957.

[31] J. H. Ammon, "Boiling coolant reactor with integral vapor separation and nuclear superheat," United States Patent # 3185630, May 1965.

[32] K. W. Campbell, "Steam producing reactor and fuel therefore," United States Patent # 3243351, Mar. 1966.

[33] A. Huet, "Nuclear reactor supplying superheated steam," United States Patent # 3156626, Nov. 1964.

[34] H. Kluge et al., "Boiling water nuclear reactor producing superheated steam," United States Patent # 3206372, Sep. 1965.

[35] S. N. Tower et al., "Integral boiling and superheating nuclear reactor and pressure tube assembly," United States Patent # 3311540, Mar. 1967.

[36] R. T. Bryan, "Boiling water nuclear reactor with breeder blanket superheater," United States Patent # 3228846, Jan. 1966.

[37] J. H. Ammon et al., "Integral boiler nuclear reactor," United States Patent # 3245881, Jul. 1962.

[38] S. Hackney, "Boiling liquid nuclear reactor," United States Patent # 3253998, May 1966.

[39] U.S. Atomic Energy Commission. Reactor Engineering Division, Chicago

Operations Office. "Small nuclear power plants," Division of Technical Information, USAEC, COO-284 TID-4500, Vol. 1, Oct. 1966

[40] J. C. Linsenmeyer, "Nuclear reactor," United States Patent # 3132999, May 1964.

[41] S. M. Valter, "Boiling water-superheat nuclear reactor," United States Patent # 3284310, Nov. 1966.

[42] L. O. T. Wadmark, "Integral boiling water-superheat nuclear reactor," United States Patent # 3454467, Jul. 1969.

[43] J. M. Harrer et al., "Direct-cycle, boiling-water nuclear reactor," United States Patent # 3049487, Aug. 1962.

[44] C. W. Wheelock, "Nuclear reactor fuel assembly," United States Patent # 3121666, Feb. 1964.

[45] D. H. Lennox et al., "An Evaluation of Reactor Concepts for Use As Separate Steam Superheaters," Argonne National Laboratory, ANL-6437, Oct. 1961.

[46] M. Treshow, "Superheating in a boiling water reactor," United States Patent # 2938845, May 1960.

[47] T. P. Heckman, "Boiler-superheater reactor," United States Patent # 2982712, May 1961.

[48] IAEA Power Reactor Information System – PRIS data base, "Operational data of the Elk River Reactor," available from World Wide Web: Operational data of the Elk River Reactor, http://0rz.tw/IBQGh

[49] USNRC Data base http://www.nrc.gov/info-finder/decommissioning/power-reactor/indian-point-unit-1.html

[50] Wikipedia, "Introduction of the Carolinas-Virginia Tube Reactor," available from World Wide Web: http://en.wikipedia.org/wiki/Carolinas-Virginia_Tube_Reactor

[51] U.S. Department of Energy, "Nuclear Reactors Built, Being Built, or Planned: 2003 in the United States," U.S. Department of Energy, DOE/NE-0118, Dec. 2003

[52] Argonne National Laboratory - West data base, available from World Wide Web: http://0rz.tw/RacsE

[53] V. A. Sidorenko, "Nuclear power in the Soviet Union and in Russia," *Nuclear Engineering and Design,* Vol. 173, pp. 3-20, Oct. 1997

[54] N. Oshikanov, "Beloyarsk NPP," The Magazine of the World Association of Nuclear Operators, Vol. 12, No. 3, 2004.

[55] N. A. Dollezhal et al., "Development of Superheating Power Reactors of the Beloyarsk Nuclear Power Station Type," Atomic Energy, Vol. 17, No. 5, Nov. 1964.

[56] IAEA Power Reactor Information System – PRIS data base, "Nuclear Power Reactor Details - HDR," available from World Wide Web: http://0rz.tw/DEk4Q

[57] M. B. Bader and G. L. O'Neilla, "EVESR Power Distribution and Thermal-hydraulic Analysis," *Nuclear Engineering and Design*, Vol. 6, Issue 2, pp. 115-133, Sep. 1967.

[58] OECD Nuclear Energy Agency, Radioactive Waste Management Committee (RWMC), "Management Board of the Co-operative Programme for the Exchange of Scientific and Technical Information concerning Nuclear Installations Decommissioning Projects, Progress During 1995-2005," NEA/RWM/CPD(2006)3, Oct. 2006.

[59] Nuclear facilities in Germany

http://www.bfs.de/en/kerntechnik/Kernanlagen_Stilllegung_Jan_2010engl.pdf
[60] "Heavy Water Reactors: Status and Projected Development," Technical Reports Series No. 407, International Atomic Energy Agency, 2002
[61] A. W. Eitz et al., "HDR – Heißdampfreaktor Großwelzheim," Atomwirt., Atomtech., Vol. 14, pp. 526-556, Nov. 1969.
[62] M. Treshow, "Nuclear Reactor," United States Patent # 2999059, Sep. 1961.
[63] R. J. Holl, R. W. Klecker and C. Graham, "Nuclear superheater for boiling water reactor," United States Patent # 3034977, May 1962.
[64] D. J. Stoker, L. S. Mims and S. Siegel, "Steam superheat boiling water nuclear reactor," United States Patent # 3150052, Sep. 1964.
[65] J. A. DE Felice, "Method of operating boiling coolant reactor with positive reactivity coefficient," United States Patent # 3153617, Oct. 1964.
[66] D. J. Stoker et al., "Fuel Element for A Steam Superheat Boiling Water Nuclear Reactor," United States Patent # 3218237, Nov. 1965.
[67] C. F. Leyse, "Single Pass Superheat Reactor," United States Patent # 3276965, Nov. 1965.
[68] P. H. E. Margen, "Tubular fuel element for a nuclear reactor," United States Patent # 3331746, Jul. 1967.
[69] L. E. Fennern, "Nuclear Reactor With Bi-Level Core," United States Patent # 5116567, May 1992.
[70] J. H. Germer, "Steam-cooled Reactor," United States Patent # 3634189, Jan. 1972.
[71] J. H. Germer, "Liquid moderated vapor superheat reactor," United States Patent # 3085959, Apr. 1963.
[72] F. Nettel and T. Nakanishi, "Power plant using a steam-cooled nuclear reactor," United States Patent # 3108938, Oct. 1963.
[73] K. Heinz, F. Erhard and K. Hans, "Superheater reactor," United States Patent # 3188277, Jun. 1965.
[74] R. T. Pennington, "Three tank separate superheat reactor," United States Patent # 3212986, Oct. 1965.
[75] R. E. Vuia, "combination fossil fuel and superheated steam nuclear power plant," United States Patent # 3575002, Apr. 1971.
[76] M. Treshow, "A Preliminary Study of superheating Boiling Reactors", *Nuclear Science and Engineering*, Vol. 1, pp. 167–173, 1956.
[77] Z. Ferrara and L.E. Hochreiter , "Conceptual Design of a Superheat Boiling Water Reactor", ANS international winter meeting, Washington D.C., USA, Nov. 2007
[78] R. L. Loftness, "Nuclear power plants: design, operating experience, and economics," Van Nostrand, 1964.
[79] International Atomic Energy Agency, "Nuclear Power Reactors in the World," IAEA-RDS-2/26, ISBN 92–0–106906–5, 2006.
[80] U.S. Atomic Energy Commission. Reactor Engineering Division, Chicago Operations Office. "Small nuclear power plants," Division of Technical Information, USAEC, COO-284 TID-4500, Vol. 3, March. 1967
[81] Wikipedia, "Introduction of the Obninsk Nuclear Power Plant," available from World Wide Web: http://en.wikipedia.org/wiki/Obninsk_Nuclear_Power_Plant
[82] G. N. Ushkov et al., "Operating Experience with the World's First Atomic Power Station," *Atomic Energy*, Vol. 16, No. 6, pp. 601-605, 1964.

[83] N. A. Dollezhal et al., "Operating Experience with the Beloyarsk Nuclear Power Station," *Atomic Energy*, Vol. 27, No. 5, pp. 1153-1161, 1969.

[84] W. J. Kelly, H. L. Shaffer, and J. K. Thompson, "The Economics of Nuclear Power in the Soviet Union," *Soviet Studies*, Vol. 34, No. 1, pp. 43-68, Jan., 1982.

[85] D. J. Bradley , "Radioactive Waste Management in the USSR: A Review of Unclassified Sources, Vol. II," Pacific Northwest Laboratory, PNL-7645, 1991.

[86] Wikipedia, "Introduction of the Beloyarsk Nuclear Power Plant," available from World Wide Web: http://en.wikipedia.org/wiki/Beloyarsk_Nuclear_Power_Station

[87] G. R. Milne, S. M. Stroller and F. R. Ward, "The Consolidated Edison Company of New York Nuclear Electric Generating Station," Proceedings of the second international conference on the peaceful uses of atomic energy, Geneva, Sep. 1958.

[88] U.S. NRC data base of the Indian Point, available from World Wide Web: http://www.nrc.gov/info-finder/decommissioning/power-reactor/indian-point-unit-1.html

[89] S. M. Stacy, "Proving the Principle: A History of The Idaho National Engineering and Environmental Laboratory, 1949-1999," Idaho Operations Office of the Department of Energy, DOE/ID-10799, 2000.

[90] U.S. Department of Energy, "Guidelines For Preparing Criticality Safety Evaluations at Department of Energy Non-reactor Nuclear Facilities," US Department of Energy, DOE-STD-3007-93, 1998.

[91] U. S. Atomic Energy Commission, "Civilian Power Reactor Program. Part III. Book 5. Status Report on Boiling Water Reactors Technology as of 1959," TID-8518(5), USAEC, Jan. 1960.

[92] I. Bredberg et al., "State and Development of Nuclear Energy Utilization in the Federal Republic of Germany 2008," Department of Nuclear Safety, (The Federal Office for Radiation Protection, Germany), BfS-SK-13/10, 2010.

[93] T. Schulenberg, J. Starflinger and J. Heinecke "Three pass core design proposal for a high performance light water reactor," *Progress in Nuclear Energy*, Vol. 50, Issues 2-6, pp.526-531, 2008.

[94] J. Hofmeister et al., "Fuel assembly design study for a reactor with supercritical water," *Nuclear Engineering and Design*, Vol. 237, Issue 14, pp 1513-1521, Aug. 2007

[95] Yi Yuan, "The Design of High Power Density Annular Fuel for LWRs," MIT Thesis, 2004.

[96] K. Ehrlich, J. Konys and L. Heikinheimo, "Materials for high performance light water reactors," *Journal of Nuclear Materials*, Vol. 327, Issues 2-3, pp. 140-147, May 2004.

[97] Benjamin M. Ma, "Nuclear reactor materials and applications," Van Nostrand Reinhold Company Inc., 1983.

[98] G. Guntz et al., "The T91 book. Ferritic tubes and pipe for high temperature use in boilers," France, Vallourec Industries,1990.

[99] "Inconel 718 Properties," On-line resource, available from World Wide Web: http://www.espimetals.com/tech/inconel718.pdf http://www.espimetals.com/technicaldata.htm

[100] J. N. Sweet, E. P. Roth and M. Moss, "Thermal conductivity of Inconel 718 and 304 stainless steel," *International Journal of Thermophysics*, Vol. 8, No. 5, pp 593-606,

Sep. 1987.
[101] J. J. Duderstadt and L. J. Hamilton, "Nuclear Reactor Analysis," Wiley, ISBN: 0471223638, Jan. 1976
[102] G. A. Greene and C. C. Finfrock, "Oxidation of Inconel 718 in Air at High Temperatures," *Oxidation of Metals*, Vol. 55, pp 505-521, Jun. 2001.
[103] D. Sapundjiev, A. Al Mazouzi and S. Van Dyck, "A study of the neutron irradiation effects on the susceptibility to embrittlement of A316L and T91 steels in lead–bismuth eutectic," *Journal of Nuclear Materials*, Vol. 356, Issues 1-3, pp 229-236, Sep. 2006.
[104] Y. Chen, K. Sridharan and T. Allen, "Corrosion behavior of ferritic–martensitic steel T91 in supercritical water," *Corrosion Science*, Vol. 48, Issue 9, pp 2843-2854, Sep. 2006.
[105] R. Fazzolare, "Gas-cooled fast breeder reactor designs with advanced fuel and cladding," *Nuclear Engineering and Design*, Vol. 40, Issue 1, pp 191-201, Jan. 1977.
[106] M. S. Kazimi et al., "Annular Fuel Special Issue," *Nuclear Technology*, Vol. 160, No.1, Oct. 2007.
[107] T. W. Eagar, Professor of Materials Science and Engineering, Massachusetts Institute of Technology, *Personal Communication*, Oct. 5, 2009.
[108] G. Dooley, President of DCS SYSTEMS INC., *Personal Communication*, Aug. 2, 2010.
[109] M. S. Kazimi et al., "High Performance Fuel Design for Next Generation PWRs: Final Report," MIT CANES report, MIT-NFC-PR-082, Jan. 2006
[110] A. Karahan, "An Evolutionary Fuel Assembly Design for High Power Density BWRs," Master Thesis, Massachusetts Institute of Technology, Dec. 2006.
[111] M. Ashrafi-Nik, "Thermo hydraulic optimisation of the EURISOL DS target," Issue 2, TM-34-06-04, Dec. 2006.
[112] G. A. Berna et al., "FRAPCON-3: A Computer Code for the Calculation of Steady-State, Thermal-Mechanical Behavior of Oxide Fuel Rods for High Burnup, Volume 2," Pacific Northwest National Laboratory, , NUREG/CR-6534, PNNL-11513, Dec. 1997
[113] Y. Long, "Modeling the Performance of High Burnup Thoria and Urania PWR Fuel," Ph.D. Thesis, Department of Nuclear Science of Engineering, Massachusetts Institute of Technology, 2002.
[114] P. G. Lucuta, H. S. Matzke, and I. J. Hastings, "A Pragmatic Approach to Modeling Thermal Conductivity of Irradiated UO_2 Fuel: Review and Recommendations," *Journal of Nuclear Material*, Vol. 232, pp. 166-180, 1996.
[115] J. H. Harding and D. G. Martin, "Recommendation for the Thermal Conductivity of UO2," *Journal of Nuclear Materials*, Issue 166, pp. 223-226, 1989.
[116] R. E. Boraks, "Thermal aspects of a boiling water reactor with integral superheater for ship propulsion," MIT MS thesis, 1959.
[117] M. S. Kazimi and N. E. Todreas, "Nuclear Systems, Vol. I," Taylor & Francis, 1993.
[118] S. Kakac, R. K. Shah and W. Aung, "Handbook of single-phase convective heat transfer," John Wiley & Sons Inc., 1987.
[119] R. Hu, "Stability Analysis of Natural Circulation in BWRs at High Pressure Conditions," MIT MS thesis, Sep. 2007.
[120] D. Knott, B. H. Forssen and M. Edenius, "CASMO-4, A Fuel Assembly Burnup

Program, Methodology," Studsvik/SOA-95/2, Studsvik of America, Inc., 1995.
[121] J. F. Briesmeister (Editor), "MCNP-- A general Monte Carlo N-particle transport code," Los Alamos National Laboratory Report LA-12625-M, Los Alamos, NM, 1993.
[122] T. Ellis, "Advanced Design Concepts for PWR and BWR High-Performance Annular Fuel Assemblies," MIT MS Thesis, Jun. 2006.
[123] M. J. Driscoll, T. J. Downar and E. E. Pilat, "The Linear Reactivity Model for Nuclear Fuel Management," American Nuclear Society, ISBN: 0894480359, Feb. 1991.
[124] IAEA TECDOC-1391, "Status of Advanced Light Water Designs 2004," International Atomic Energy Agency, IAEA-TECDOC-1391, 2004.
[125] J. M. Cuta, et al., "VIPRE-01 A Thermal-Hydraulic Code for reactor Cores," Volumes 1-3, EPRI, NP-2511CCM, 1985.
[126] J. H. Rust, "Nuclear Power Plant Engineering," Haralson Pub Co, June 1979.
[127] Taiwan Power Company, "Preliminary Safety Analysis Report for Lungmen Plant Units 1 and 2," Taiwan Power Company, June 2002.
[128] J. F. Harvey, "Theory And Design of Pressure Vessels," Springer; Sep. 1991.
[129] J. Zhao, "Stability Analysis of Supercritical Water Cooled Reactors," MIT PhD Thesis, Jul. 2005.
[130] W. Wulff, H. S. Cheng and A. N. Mallen, "Analytical modeling techniques for efficient heat transfer simulation in nuclear power plant transients," BNL-NUREG-35944, National heat transfer conference, Denver, CO, USA, Aug. 1985.
[131] F. M. White, "Fluid Mechanics," Mcgraw-Hill College; 4th edition, Dec. 1998.
[132] "UxC Nuclear Fuel Price Indicators," On-line resource, available from World Wide Web: http://www.uxc.com/review/uxc_Prices.aspx
[133] NEA/OECD, "Trends in the Nuclear Fuel Cycle, Economic, Environmental and Social Aspects," Paris, 2001.
[134] The RELAP5 Code Development Team, "RELAP5/MOD3 Code Manual," USA: Idaho National Engineering Laboratory, 1995.
[135] B. Fischer, M. Smolinski and J. Buongiorno, "Nitrogen-16 Generation and Transport and Associated Shielding Requirements in a Supercritical-water-cooled Reactor," *Nuclear Technology*, Vol. 147, pp. 269-283, Aug. 2004.

Appendix A

Review of Historical Superheat Nuclear Reactors

A.1 Nuclear Power Plants with Fossil Fuel-fired Superheaters

A.1.1 The Elk River Reactor

General

The Elk River Reactor (ERR) was a natural-circulation, indirect-cycle boiling water reactor with a separate coal-fired superheater, owned by AEC and operated by the Rural Cooperative Power Association (RCPA) of Elk River, Minnesota. This project was part of the second invitation of the AEC's Power Demonstration Reactor Program and was used for power production. It was the first boiling water reactor operating on a wholly indirect cycle and the first to add a fossil fuel superheater to the nuclear plant cycle. The reactor was rated at 58.2 MWt and its coal-fired superheater at 14.8 MWt; the plant net electrical output was 22.5 MW [39].

Summary of Plant History

On June 16, 1958, the American Car and Foundry Industries (ACF) signed a contract with the AEC to design, develop fabricate, construct, start up and test operate a closed-cycle boiling water reactor with a separate fossil-fuel-fired superheater. Plant construction began in August 1958. In May 1959, ACF transferred its nuclear reactor business (including the ERR project) to the Allis-Chalmers Manufacturing Company. On November 19, 1962, ERR achieved the first criticality. Full power operation was achieved on February 10, 1964. The Elk River reactor was only operated from 1962 until 1968 before undergoing decommission in the following years, ending in the early 1970s.

Description of the Reactor

Table A-1 lists the design features of the Elk River reactor. The reactor core was a cylinder approximately 5 ft. in diameter and 5 ft. high. It had 148 fuel assemblies with

each assembly containing 25 fuel rods. The fuel consisted of a mixture of 4.3% enriched UO_2 (Urania) and ThO_2 (Thoria) in the form of pellets contained in borated stainless steel tubes. It was one of the first commercial nuclear power plants to use a urania-thoria mixture fuel. Reactor control was provided by 13 cruciform rods made of boron steels. Each control rod had a Zircaloy follower and was mounted below the reactor. Figure A-1 illustrates the pressure vessel of the Elk River reactor [39].

Plant Operation

The reactor was operated on an indirect cycle using an intermediate heat exchanger to eliminate the carry-over of any radioactivity into the turbine. The 450 °F feedwater entered the reactor vessel above the core level by natural circulation through two 8-inch nozzles and a distributing ring. The 538 °F, 950 psia saturated steam left the vessel through two 10-inch outlet nozzles and entered two steam generators where the 506 °F, 715 psia secondary steam was generated. A coal-fired superheater was used to improve the quality of the secondary steam to 825 °F in order to permit the use of a preferred standard efficiency turbine. Figure A-2 shows the schematic flow diagram of the Elk River reactor [7].

Table A-1 Design features of the Elk River reactor [7, 45]

Location	Elk River, Minnesota, USA
Owner/Operator	USAEC/RCPA
Type	Indirect cycle boiling-water reactor, with conventional fuel fired superheater
Power Gross thermal Electrical Overall efficiency	 Boiler: 58.2 MW; Superheater: 14.8 MW Net: 22.5 MW 30.8 %
Fuel element Type Fuel	 25 rod clusters, stainless steel cladding containing boron as burnable poison 4.3 % U-235, 0.3 % U-238, 95.4 % Th; in form of dioxide
Core Dimensions Number of fuel assemblies Power density	 5 ft diameter, 5 ft high 148, room for 16 more 39.6 kW/liter
Pressure vessel	7 ft diameter, 25 ft high, carbon steel with SS cladding
Control rods Type Number	 Cruciform 13
Turbine steam conditions Temperature Pressure Mass flow rate	 825 °F 620 psig 225,000 lb/hr
Construction schedule [39] Start of construction Initial criticality achieved Full power achieved	 August 1958 November 1962 February 1964

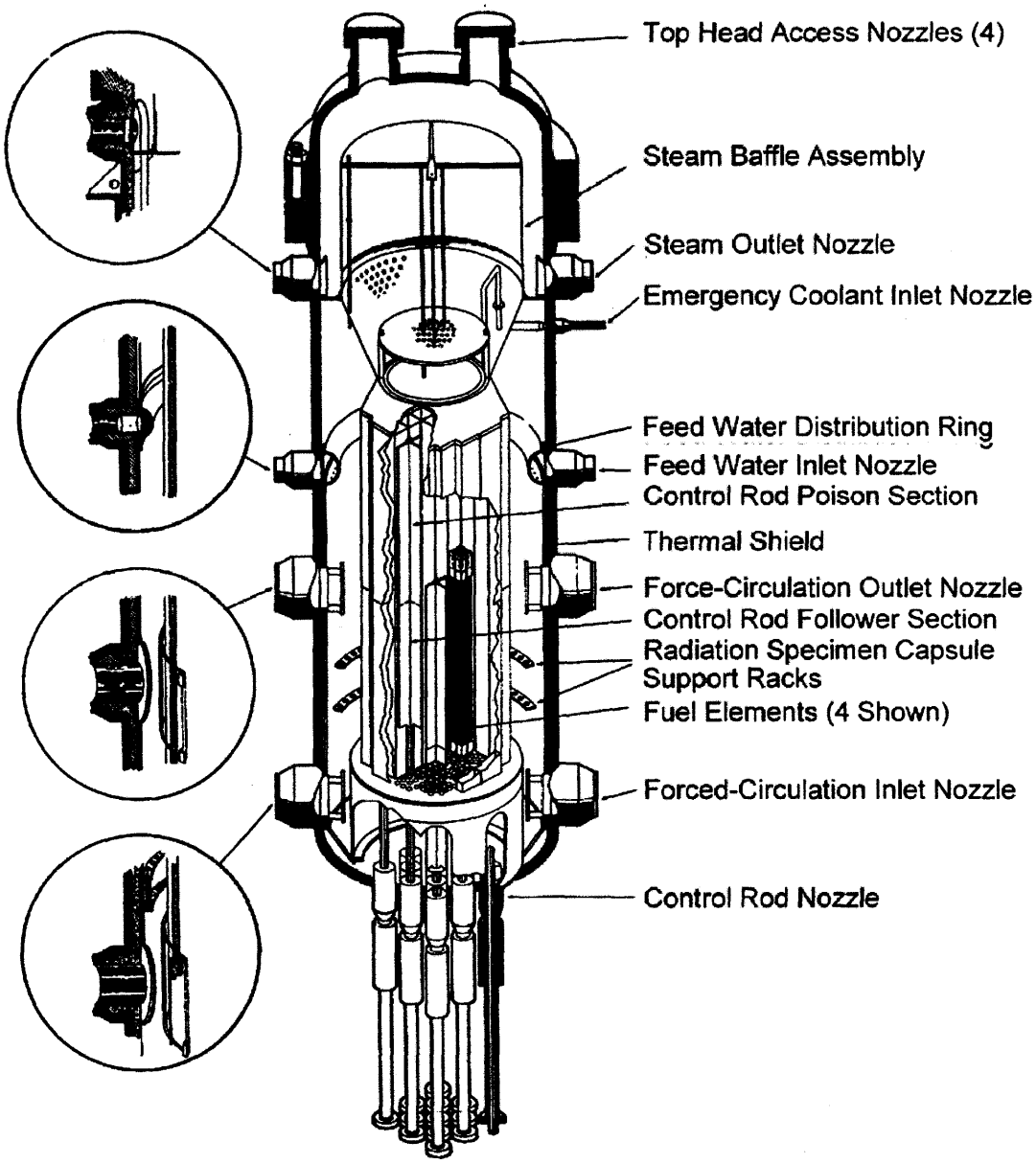

Figure A-1 Elk River reactor pressure vessel [39]

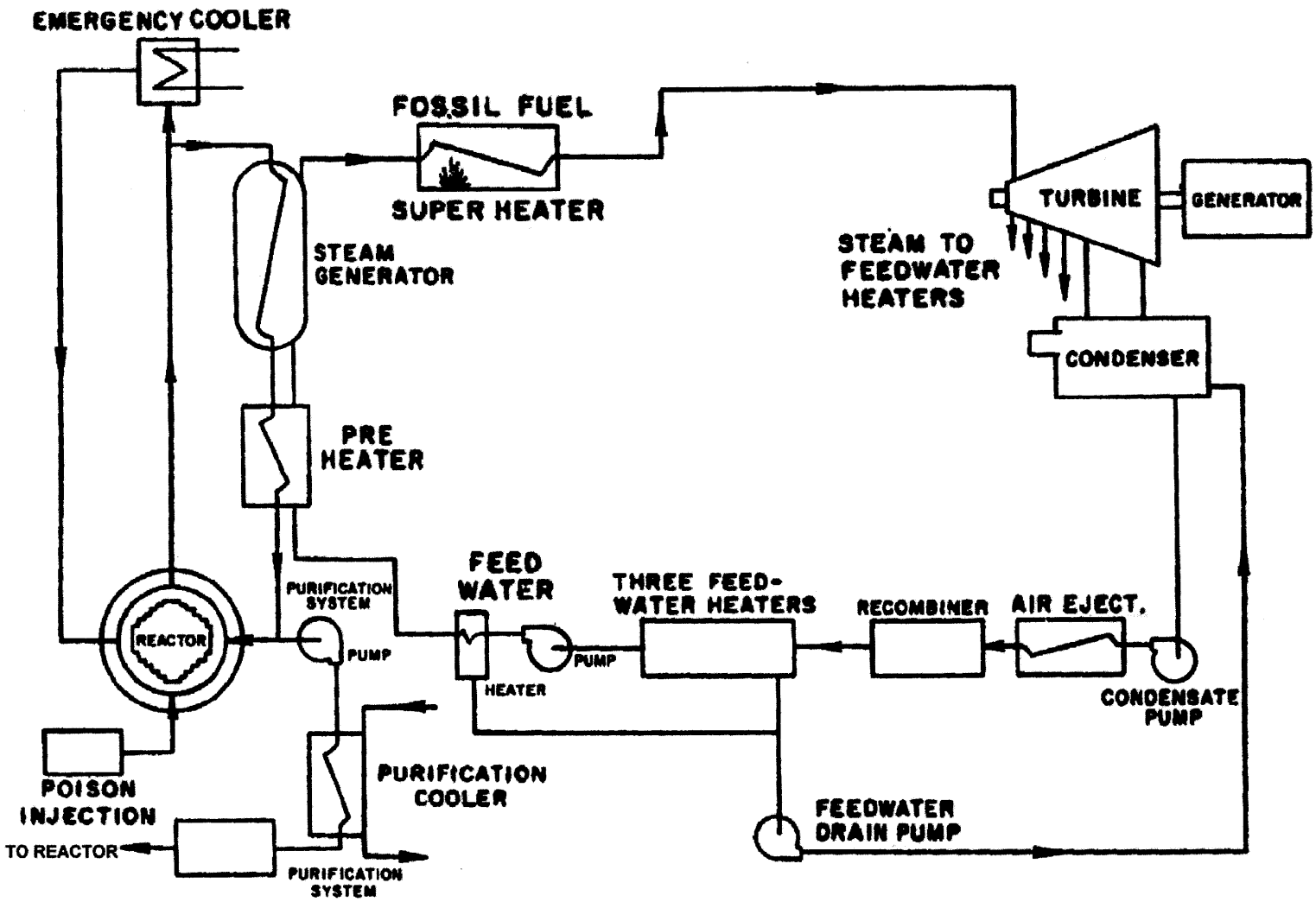

Figure A-2 Schematic flow diagram of the Elk River reactor [7]

A.1.2 Indian Point Nuclear Power Plant Unit 1

General

Indian Point unit 1 was a pressurized water reactor with a separate oil-fired superheater, designed by B&W and owned and operated by Consolidated Edison. The plant was located at Buchanan, New York on the east bank of the Hudson River, 24 miles north of New York City. The thermal power of the Indian Point unit 1 and its oil-fired superheater were 585 and 215 MWt, respectively [45]. Its net electric power out was 275 MWe, composed of 163 MWe from the reactor and 112 MWe from the oil-fired superheater [78].

Summary of Plant History

The reactor was issued an operating license on March 26, 1962. The first criticality was achieved on August 2, 1962 [78] and the reactor started operations on September 16, 1962. The full power operation was achieved on January 29, 1963. The Indian Point unit 1 was shut down on October 31, 1974 because the emergency core cooling system did not meet regulatory requirements. All spent fuel was removed from the reactor vessel by January 1976 [88].

Description of the Reactor

Table A-2 lists the design features of the Indian Point unit 1. The reactor core was a 6.5 ft. in diameter and 8 ft. high. It had 120 fuel assemblies and 21 cruciform-type, bottom-mounted hafnium control rods. Each fuel assembly comprised 196 fuel rods. The fuel was made of a mixture of UO_2 and ThO_2 with 93 percent enrichment. Fuel composition was varied within the rods in a single assembly as well as in various zones of the core. Burnable poison was also included as 200 to 225 ppm boron in the stainless steel cladding [78]. Figure A-3 shows the schematic flow diagram of the Indian Point unit 1 [7].

Table A-2 Design features of the Indian Point unit 1 [78]

Location	Buchanan, New York, USA
Owner/Operator	Consolidated Edison
Type	Pressurized water reactor, with conventional oil-fired superheater
Power Gross thermal Electrical Overall efficiency	 Boiler: 585 MW; Superheater: 215 MW Net: 255 MW 32.0 %
Fuel element Type Fuel	 196 fuel rods per assembly, stainless steel cladding containing boron as burnable poison 93 % UO_2-ThO_2
Core Dimensions Number of fuel assemblies Power density	 6.5 ft diameter, 8 ft high 120 76 kW/liter
Pressure vessel	9.75 ft diameter, 36.8 ft high, carbon steel with SS cladding
Control rods Type Number	 Cruciform-shape, hafnium rods 21
Turbine steam conditions Temperature Pressure Mass flow rate	 1000 °F 420 psig 2,200,000 lb/hr
Construction schedule Construction permitted Initial criticality achieved Full power achieved	 May 1956 August 1962 January 1963

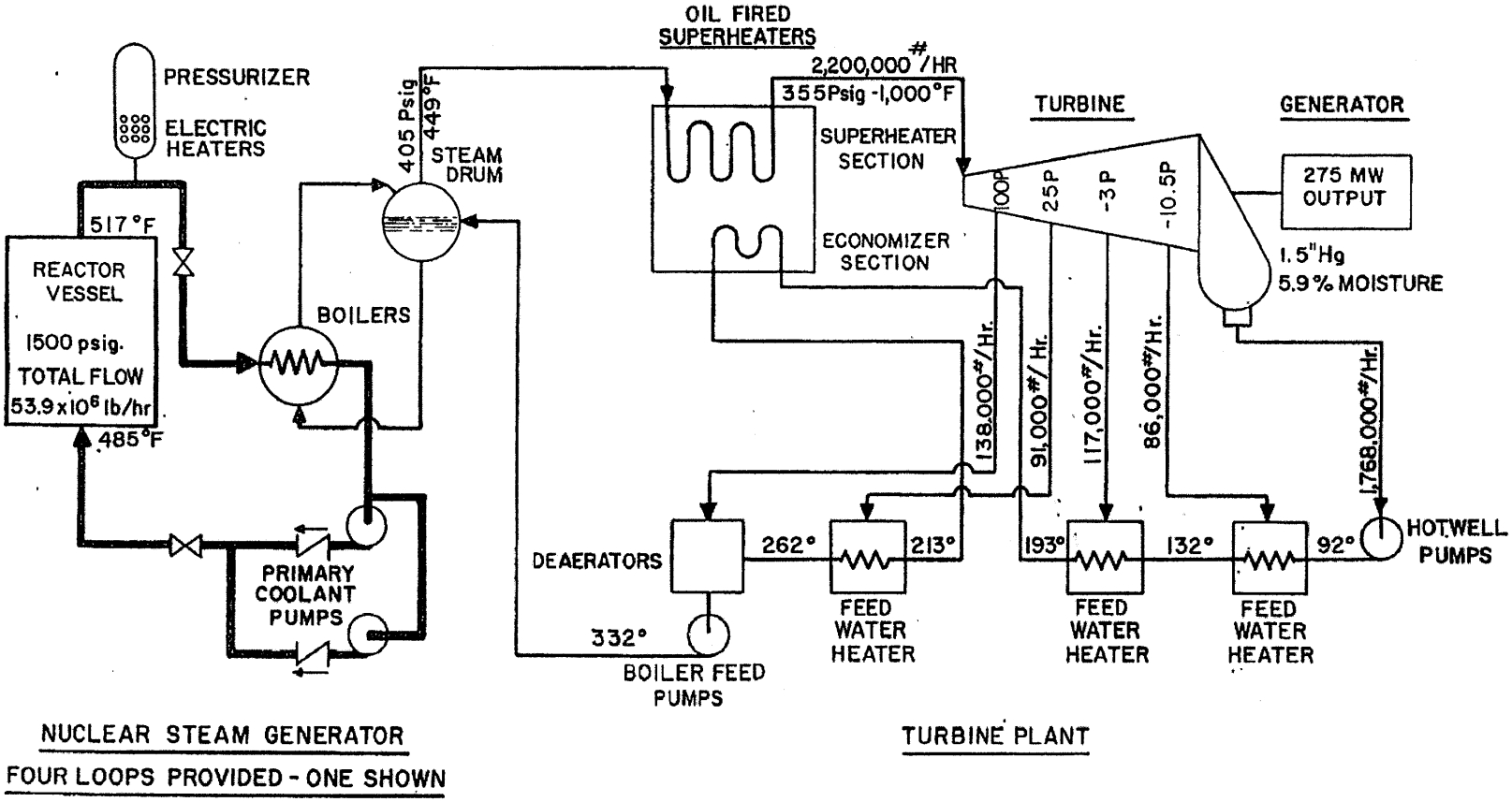

Figure A-3 Schematic flow diagram of the Indian Point unit 1 [86]

A.1.3 The Carolinas–Virginia Tube Reactor (CVTR)

General

The Carolinas–Virginia tube reactor (CVTR), located at Parr, South Carolina, was the first heavy water reactor in the United States. It was built to demonstrate the concept of a heavy water moderated and cooled pressurized tube reactor for civilian power. The CVTR featured a pressurizer and an oil-fired superheater to upgrade the quality of the steam being fed to the turbine. It had an electrical output of 19 MW. The outlet superheated steam conditions were 385°C and 28 kg/cm^2. Table A-3 lists the design features of the CVTR.

Summary of Plant History

Construction of the plant started in 1960 and completed in 1963. The first criticality was achieved on March 30, 1963. After about four years of operation (1963 ~1967), the CVTR completed the planned test programs and was shut down. In 2009, decommission of the site was in complete and the site returned to a green field [50].

Description of the Reactor

Figure A-4 shows the flow diagram of the CVTR circuits [60]. Figures A-5 and A-6 show the vertical and horizontal sections of the CVTR core, respectively. The fuel assembly consisted of 36 U-tube fuel channels. The reactor was fueled with slightly enriched uranium. One third of the core utilized the 1.5% enriched U-235, and the other two thirds used the 2% enriched U-235 fuel assemblies. The fuel cladding was made of Zircaloy-2 with a 1.25 cm outside diameter and a 0.58 mm wall thickness. Control of the CVTR was provided by 12 boron stainless steel control rods and 16 stainless steel rods. The reactor and primary system were housed in a steel containment shell 58 feet in diameter and 119 feet high [78].

Plant Operation

During power operation, heavy water flowed through the U-tubes containing the fuel

assemblies which heated the water. The heated water then flowed through an inverted U-tube steam generator where the heat was transferred to the secondary side light water which turns to steam. The steam flowed from the steam generator to an oil-fired superheater which increased the steam temperature before the steam entered the turbine.

Table A-3 Design features of the Carolinas–Virginia tube reactor [60,78]

Location	Parr, South Carolina, USA
Owner/Operator	Carolinas–Virginia Nuclear Power Associates
Type	Pressure tube, heavy water cooled and moderated reactor, with conventional oil-fired superheater
Power Gross thermal Electrical Overall efficiency	 65 MW Net: 19 MW 29.2 %
Fuel element Type Fuel	 19 rod cluster, Zir-4 cladding 1.5 and 2.0 % UO_2
Core Dimensions Power density	 6.9 ft diameter, 8 ft high 15 kW/liter
Pressure vessel	9 ft diameter, 16 ft high
Control rods Type Number	 Boron steel rods 32
Turbine steam conditions Temperature Pressure	 385 °C 2.75 MPa
Construction schedule Construction permitted Initial criticality achieved Reactor shutdown	 1960 March 1963 1967

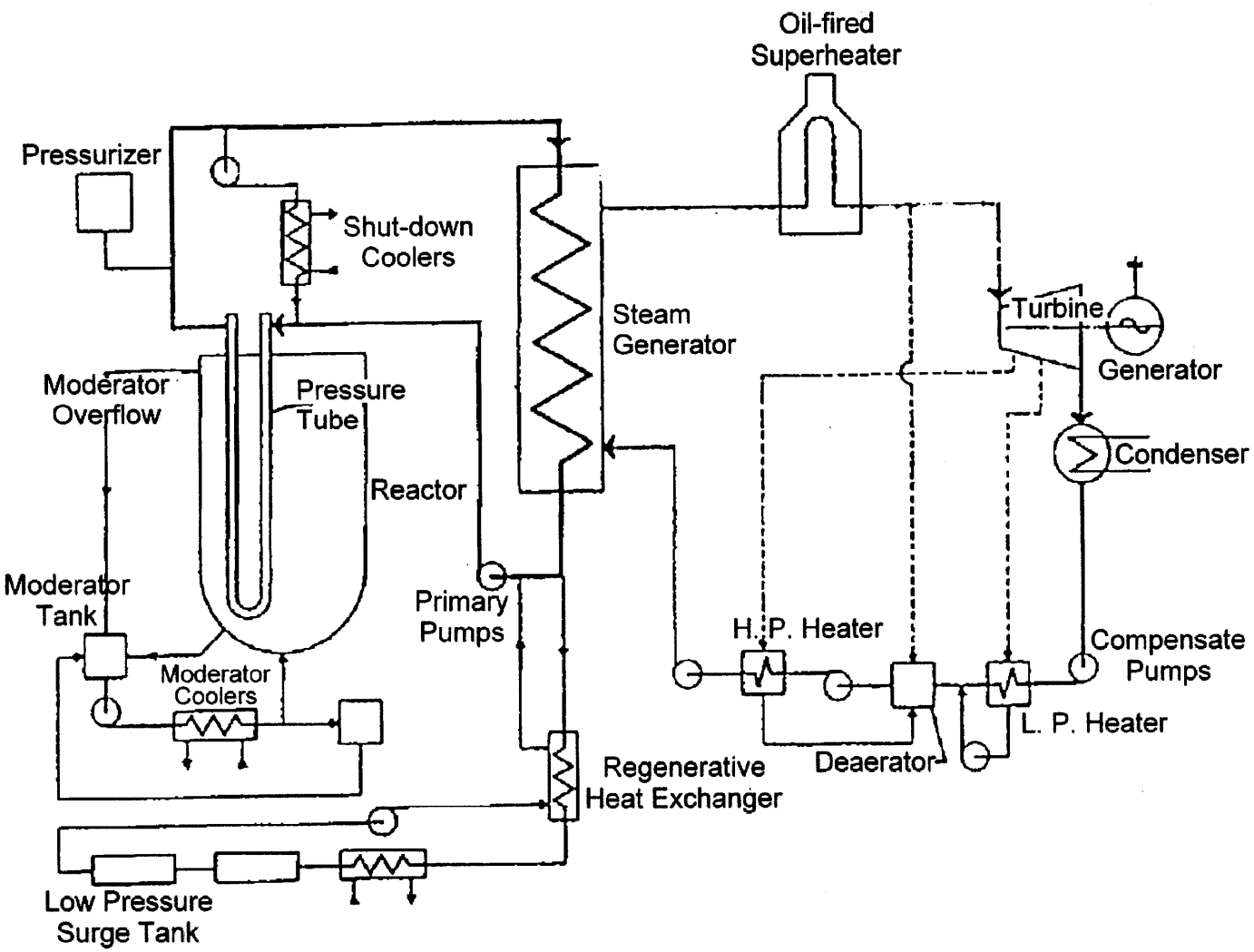

Figure A-4 Schematic flow diagram of the Carolinas–Virginia tube reactor [60]

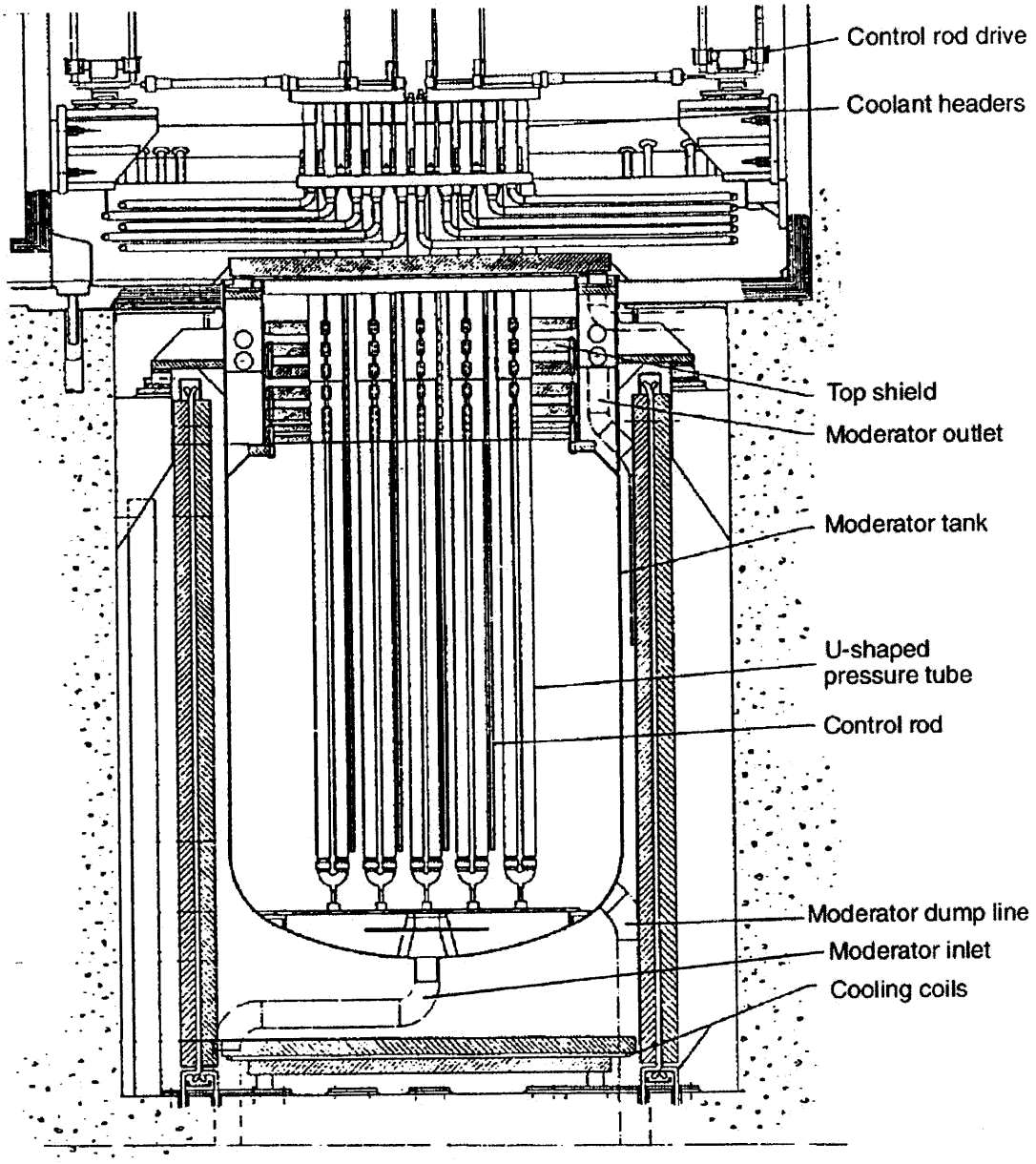

Figure A-5 Vertical section of the CVTR core [60]

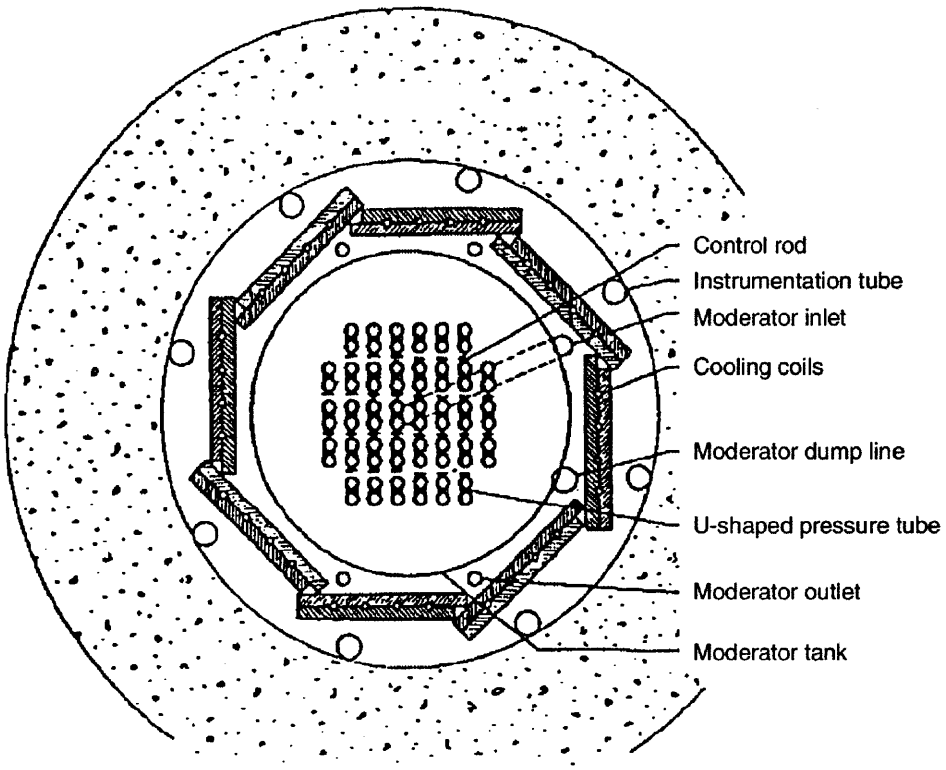

Figure A-6 Horizontal section of the CVTR core [60]

A.2 Nuclear Power Plants with Non-integral Nuclear Superheaters

A.2.1 The Vallecitos Experimental Superheat Reactor (VESR)

General

The ESADA Vallecitos Experimental Superheat Reactor (EVESR or VESR), located at Pleasanton, California, was the first separate-superheat reactor in the world [78]. The objective of the VESR was to investigate the technical and economic feasibility of the separate nuclear superheater concept. Steam from the Vallecitos boiling water reactor (VBWR) was piped to the VESR where it was superheated to 828 °F at 934 psig. The construction of VEBR was a joint program of the Empire State Atomic Development Associates (ESADA) and the General Electric Company. The VESR was a light water moderated, steam cooled reactor with a 17 MW thermal power [57].

Summary of Plant History

The first criticality was achieved in the fall of 1962 [13]. The VESR was started up in 1963 and permanently shut down in February 1967 [51].

Description of the Reactor

The reactor was housed in a pressure vessel 7 feet in diameter and 32 feet long. The core consisted of 36 fuel bundles within process tubes. Each fuel bundle consisted of nine fuel elements in a 3 by 3 array. The tubular fuel element was made from two concentric stainless steel tubes sealed on the end and filled with hollow uranium dioxide pellets. The enrichment of UO_2 was about 3.6 percent [13]. Steam flow distribution in the reactor core was controlled by a combination of fuel bundle orificing and external valves of the superheated steam lines.

Design features of the VESR are listed in Table A-4. Figures A-7 and A-8 show the vertical cross section and the fuel bundle of the VESR, respectively.

Table A-4 Design features of the Vallecitos experimental superheat reactor [13,78]

Location	Pleasanton, California, USA
Owner/Operator	GE and ESADA
Type	Light water-moderated and steam-cooled non-integral nuclear superheater
Power	
Gross thermal	17 MW
Electrical	NA
Overall efficiency	NA
Fuel element	
Type	9 tube cluster, SS cladding
Fuel	3.6 % UO_2
Core	
Dimensions	4 ft diameter, 5 ft high
Power density	2.9 kW/liter
Pressure vessel	7 ft diameter, 32 ft high
Control rods	
Type	Cruciform rods made of B_4C in SS
Number	12
Turbine steam conditions	
Temperature	828 °F
Pressure	934 psig
History	
Initial criticality achieved	1962
Reactor operation started	1963
Reactor shutdown	1967

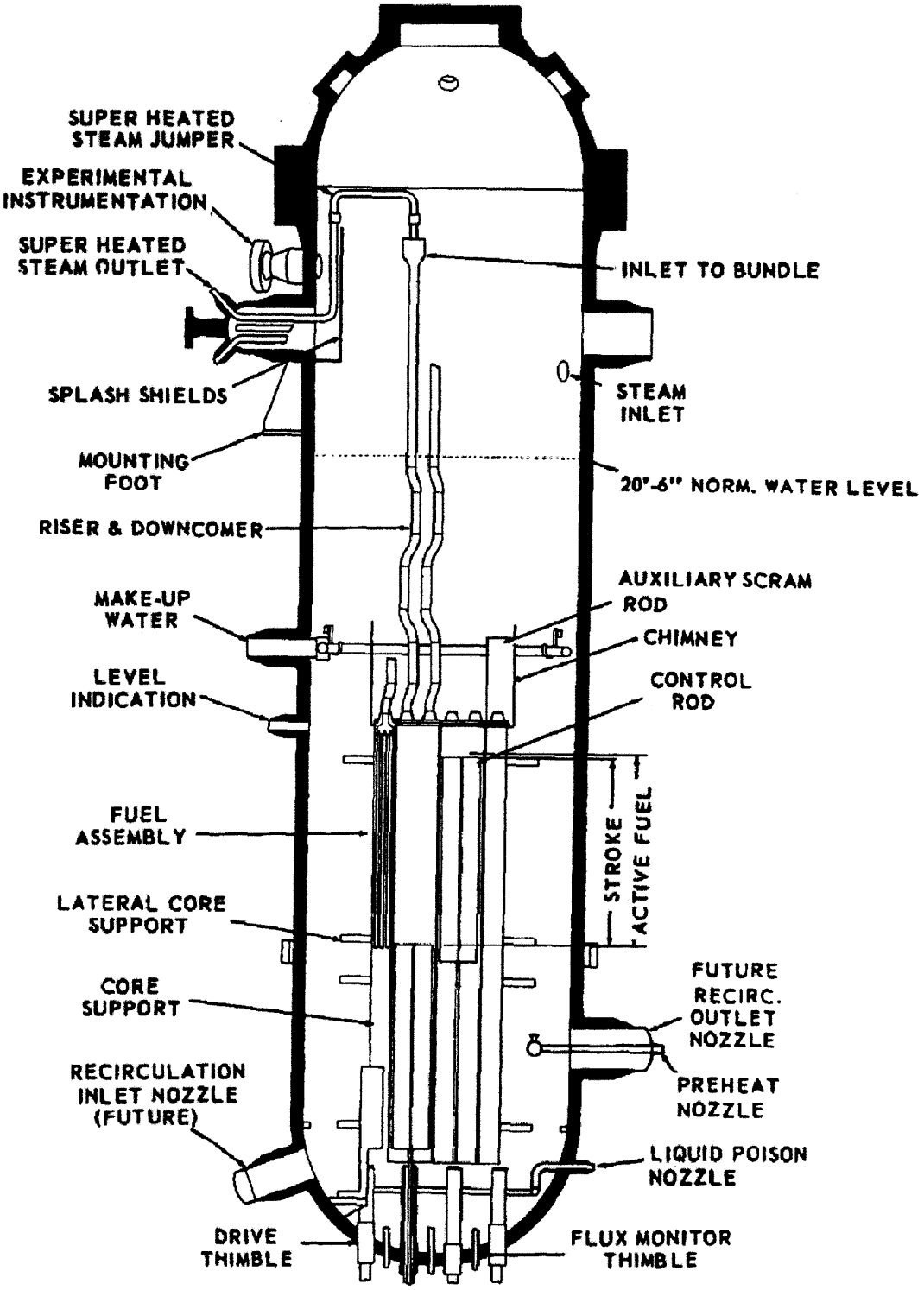

Figure A-7 Vertical cross section of the Vallecitos experimental superheat reactor [57]

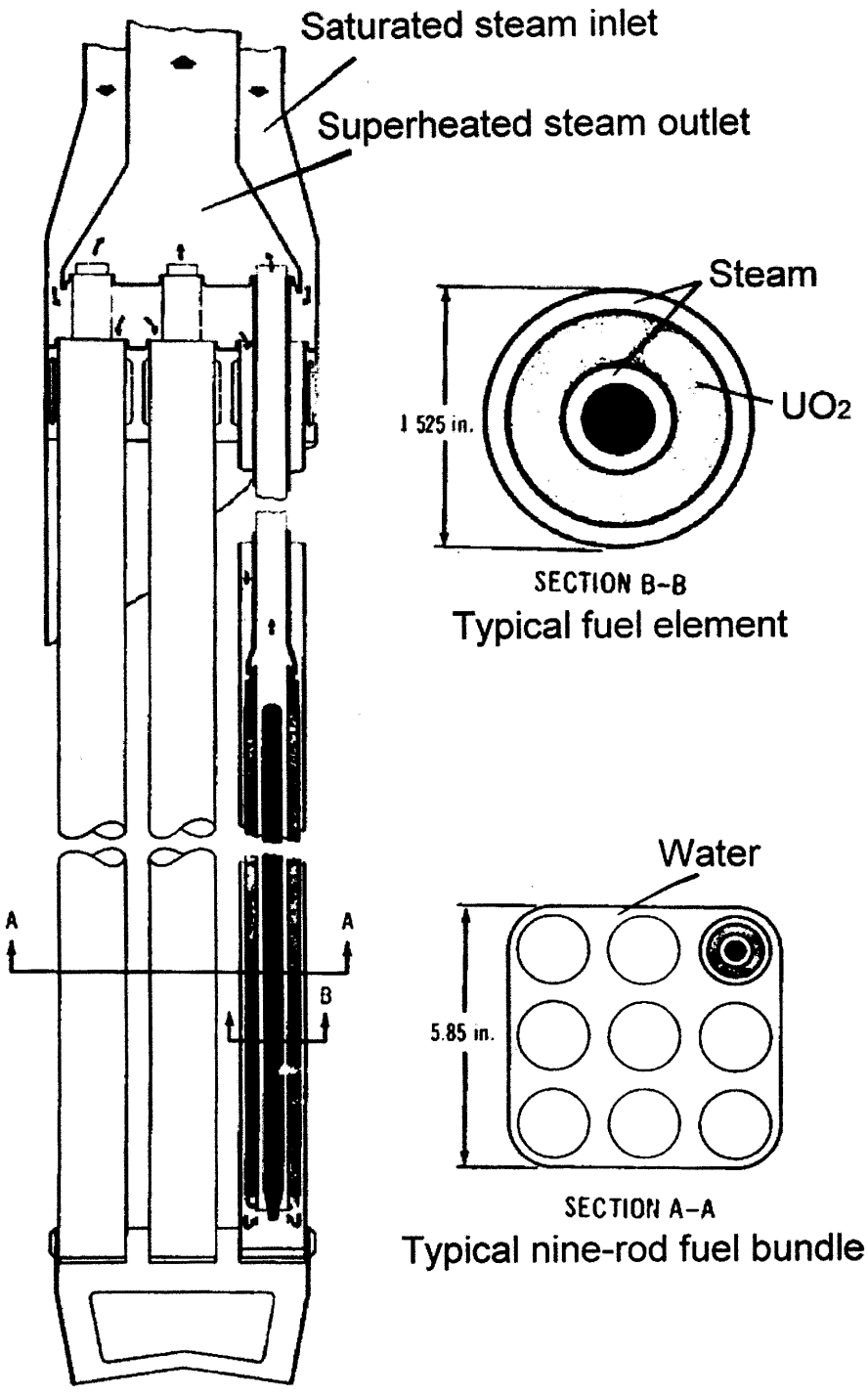

Figure A-8 Fuel bundle of the Vallecitos experimental superheat reactor [57]

A.3 Nuclear Power Plants with Integral Nuclear Superheaters

A.3.1 The Atomic Power Station 1 (APS-1)

General

The Atomic Power Station 1 (APS-1) was the first civilian nuclear power station in the world. It was located at Obninsk, about 110 km southwest from Moscow. The reactor was initially designed as a graphite-moderated, light water-cooled, pressure tube-type pressurized water reactor. However, due to the incentives of boiling superheat operation, the APS-1 had been used to provide information for the design of the subsequent superheat reactors at Beloyarsk. The electric power of the APS-1 was 5 MW [78].

Summary of Plant History

Construction of the APS-1 started on January 1, 1951. The APS-1 was connected to the grid on June 26, 1954. For around ten years, The APS-1 remained the only nuclear power reactor in the Soviet Union. After morn than 45 years of operation, it was finally shut down in April, 2002 [81].

Description of the Reactor

The reactor vessel was made of carbon steel and operates at a pressure of about 20 psig of nitrogen. The reactor core was 67 inches high and 59 inches in diameter. The graphite moderator was pierced by 128 thimble-type pressure tubes. The light water coolant flowed into the thimbles, where it was partially vaporized. The steam-water mixture was directed into a centrifugal separator [82]. Then the separated steam was directed to the superheating channels where it was converted to superheated steam.

A.3.2 The BORAX-V Reactor

General

During 1953 ~ 1964, the Argonne National Laboratory (ANL) initiated a series of boiling water reactor experiments (BORAX) to demonstrate the feasibility of using boiling water as a moderator and coolant for nuclear reactors. A considerable amount of data and operating experience were generated from these experiments. BORAX-V, the fifth in the celebrated series of experimental reactors, was designed as an exceedingly flexible boiling-plus-superheating facility. The primary purpose of the BORAX-V reactor was to test the nuclear superheating concepts, safety and economic feasibility of an integral nuclear superheater. Design features of BORAX-V are listed in Table A-5.

Summary of Plant History

BORAX-V achieved its first criticality on February 9, 1962. Reactor operation started on September 2, 1962 [78]. From 1962 to 1964, BORAX-V was used with an integral nuclear superheat system. On October 10, 1963, it produced superheated (dry) steam entirely by nuclear means for the first time. The BORAX-V project was terminated at the end of August 1964 after the planned tests and experiments were completed.

Description of the Reactor

BORAX-V was designed as a very flexible system so that any one of the three core support structures could be installed in the vessel to permit central superheat, peripheral superheat or straight boiling operation [78]. Figure A-9 illustrates the central and peripheral superheat operation of BORAX-V [9]. Two types of fuel elements were used: (a) 5 %-enriched, UO_2 rod-type element clad in stainless steel for the boiling portion of the reactor core and (b) 93 %-enriched, UO_2-stainless steel cermet, dispersion-type element plate clad in stainless steel for the superheating portion of the core. Figures A-10 and A-11 show a 4 x 4 array of the BORAX-V superheater fuel assemblies and subassemblies, respectively [90]. Each superheater fuel assembly consisted of five subassemblies with intervening water gaps. Each subassembly contained four superheater fuel plates. The boiler assembly could accommodate up to 49 fuel rods in a

7x7 array. The boiler assembly was made up of a bottom cylindrical-to-square-transition fitting and a square tube made of Al X-8001 [9].

Plant Operation

The superheat assemblies were placed in individual pipes, through which the saturated steam would be taken from the top of the vessel, in a downward direction for superheating. The outlet steam conditions were 600 psig and 850 °F, and the peak reactor power was around 40 MWt. Startup and shutdown during superheating operation were handled by procedures involving draining and flooding of the superheating section. The reactor was started with superheater elements flooded. After sufficient steam was produced in the boiler elements to cool the superheater elements, the superheater section was drained and the steam flow was allowed to enter [78].

Table A-5 Design features of BORAX-V [9, 78]

Location	Idaho Falls, Idaho, USA
Owner/Operator	USAEC/ANL
Type	Integral boiling nuclear superheater
Power Gross thermal Electrical Overall efficiency	 35.7 MW Net: 3.5 MW NA (Experimental facility)
Fuel element Type Fuel	 Boiler: 49-rod clusters, stainless steel cladding Superheater: Plate, stainless steel cladding Boiler: 5 %-enriched, UO_2 Superheater: 90 %-enriched, UO_2-SS
Core Dimensions Power density	 3.25 ft diameter, 2 ft high Boiler: 95 kW/liter Superheater: 80 kW/liter
Pressure vessel	5.5 ft diameter, 16 ft high
Control rods Type Number	 Cruciform and T rods 5 (Cruciform) and 4 (T)
Turbine steam conditions Temperature Pressure Mass flow rate	 850 °F 540 psig 49,200 lb/hr
History Initial criticality achieved Start of operation End of operation	 February 1962 September1962 1964

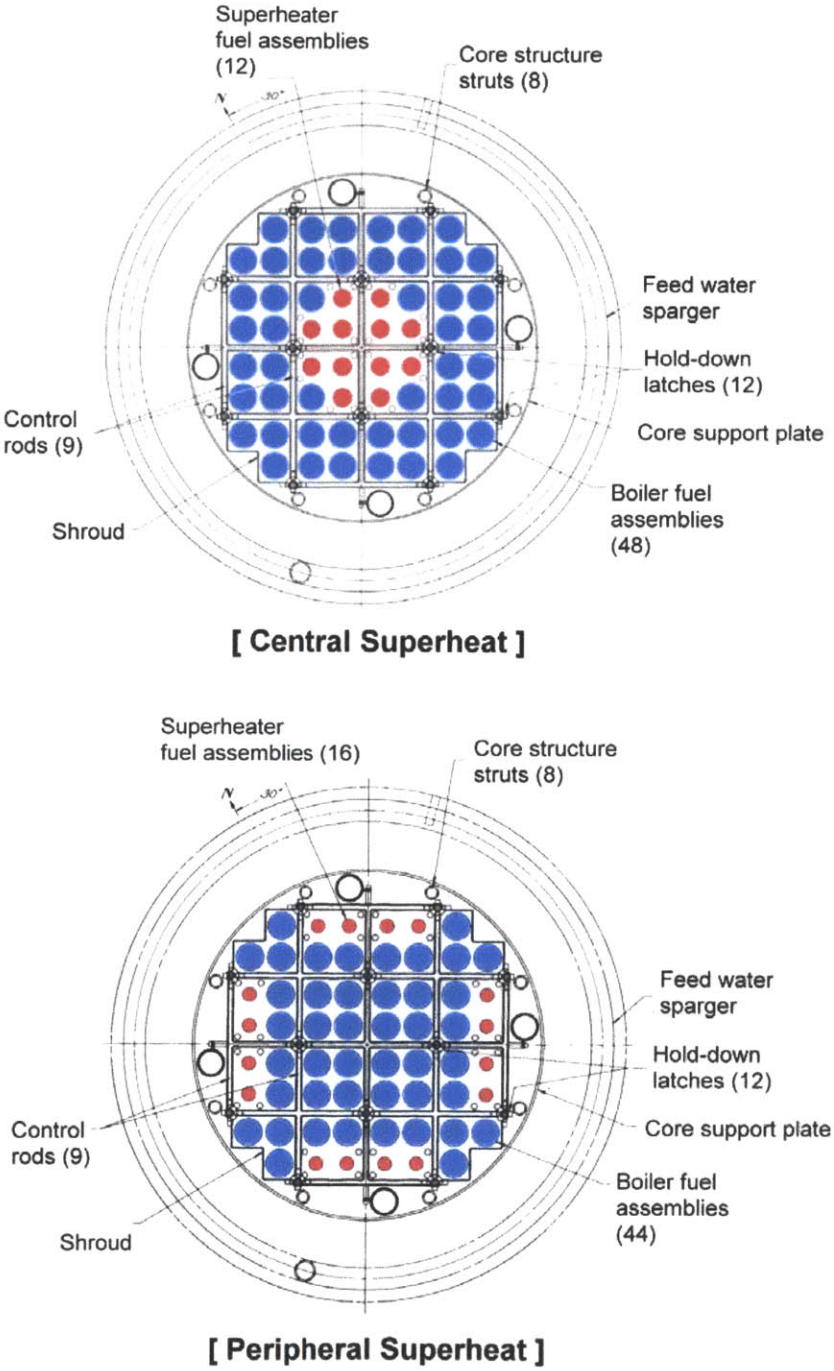

Figure A-9 Central and peripheral superheat operation of BORAX-V [9]

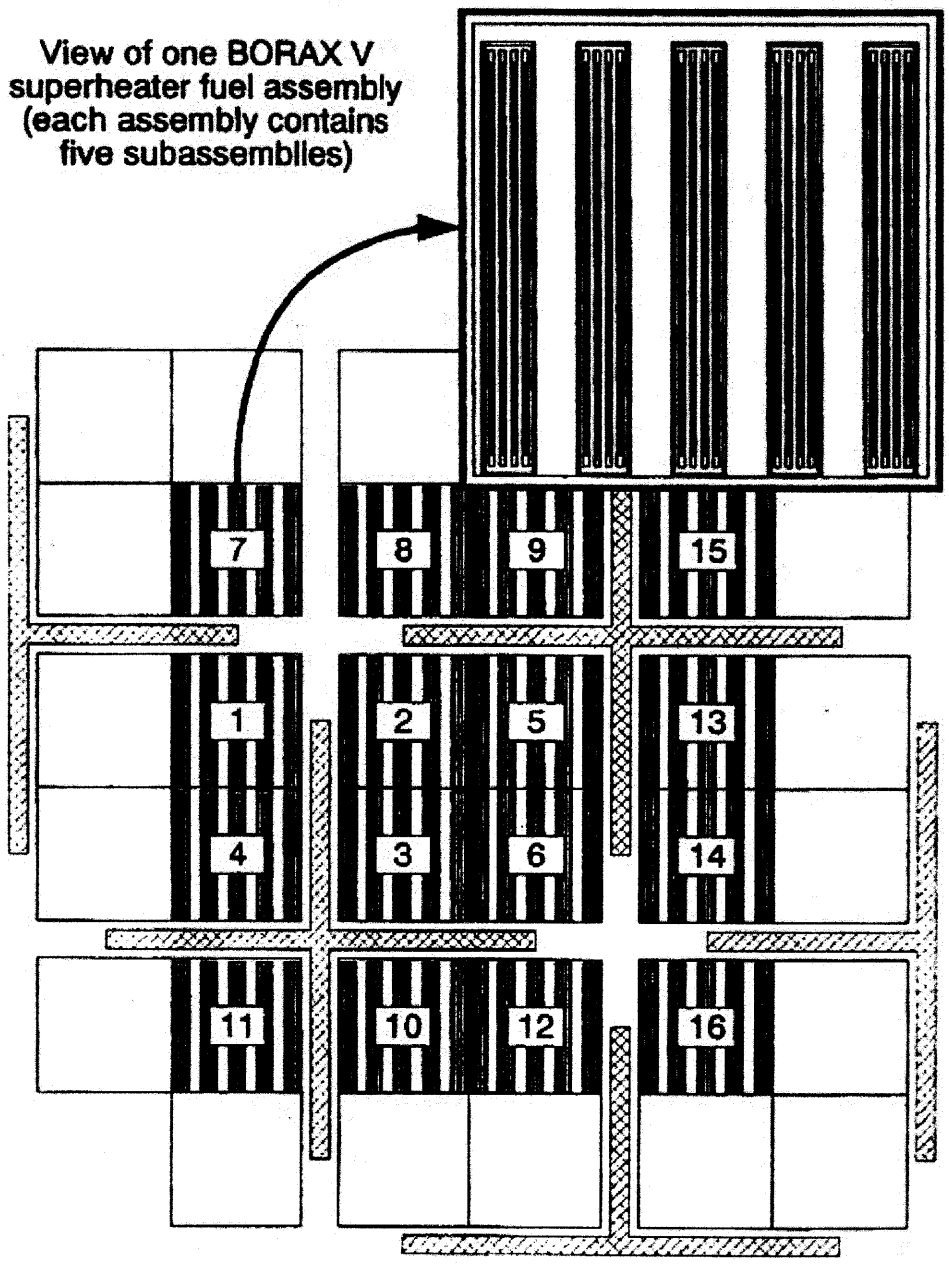

Figure A-10 The BORAX-V superheater fuel assembly [90].

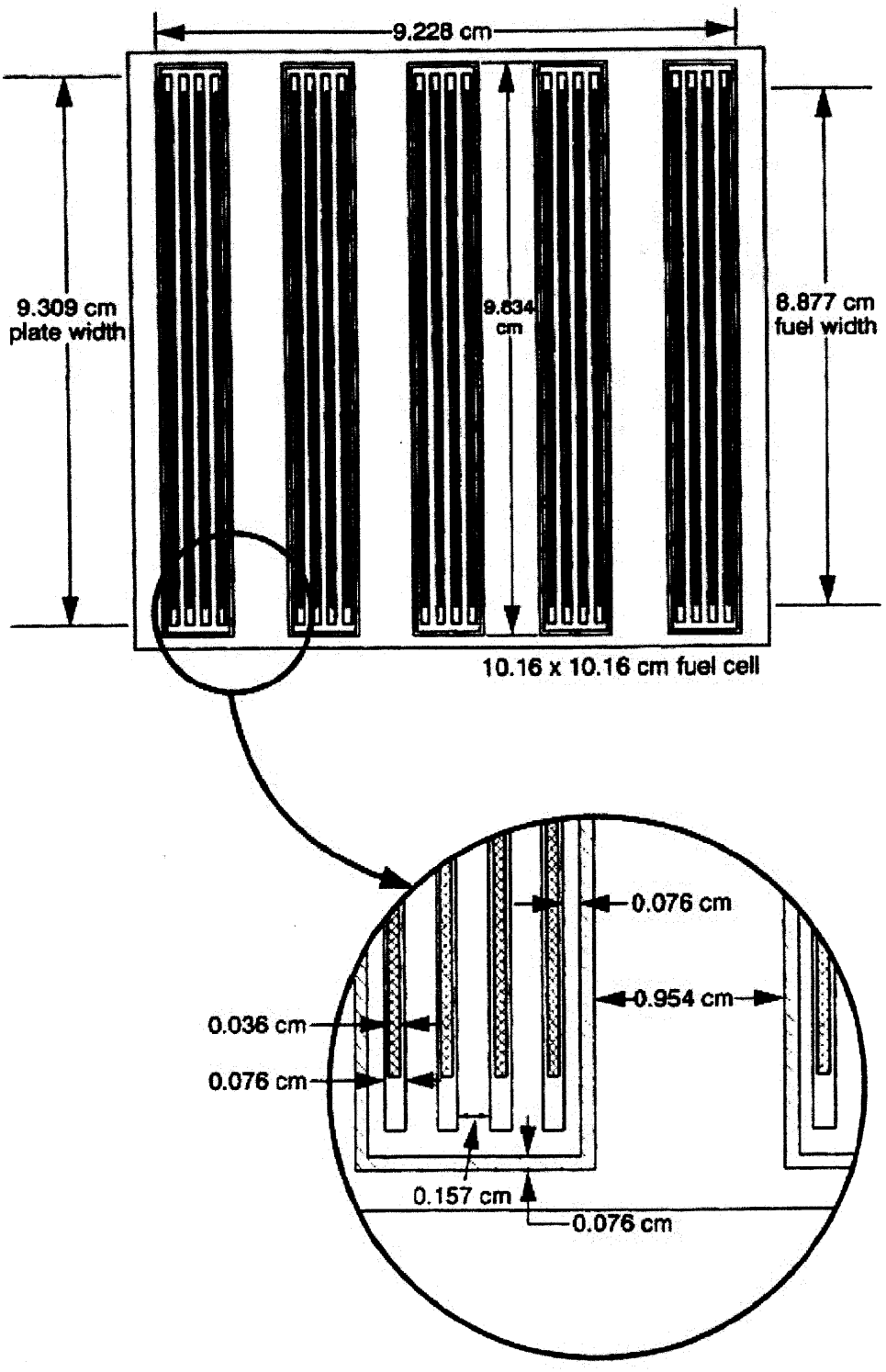

Figure A-11 The BORAX-V superheater fuel subassembly [90].

A.3.3 The Pathfinder Reactor

General

The Pathfinder plant was situated on the south bank of Big Sioux River, 3.5 miles north east of Sioux Falls, South Dakota. It was owned and operated by the Northern States Power Company (NSPC). Pathfinder was a light-water moderated and cooled, controlled recirculation boiling water reactor having an integral nuclear superheater. It was the first reactor which uses variable coolant flow rates for controlling the reactor power [39].

Summary of Plant History

Pathfinder was designed by the Allis-Chalmers Manufacturing Company (AC) and construction began in August 1959. The plant achieved initial criticality in March 1964, and the first electrical energy was generated on July 25, 1966. Although commercial operations began on August 1, 1966, Pathfinder had never attained sustained full-power operation. A series of unfortunate events and an impractical design shortened Pathfinder's useful lifetime. Finally, the plant was shut down in 1967. The technical concern that shut down the plant was chloride stress corrosion cracking of the stainless steel cladding material and other stainless steel components in the reactor vessel [77]. Later on, the owner decided to convert the plant's heat source from nuclear to fossil. Conversion, as an acceptable decommission option at that time, began on December 13, 1968. Commercial operation of the Pathfinder fossil plant commenced in May 1969 and continued until July 2000 [10, 39, 51].

Description of the Reactor

The plant's thermal rating was 199.6 MW with 157.2 MWt from the boiler and 42.2 MWt from the superheater [39]. The electrical output of Pathfinder was 62 MWe. The schematic diagram of the Pathfinder power plant is shown in Figure A-12. Design features of the Pathfinder reactor are listed in Table A-6.

The reactor core consisted of two concentrically located separate regions, the boiler and superheater. Figure A-13 illustrates the cross section of the core. In contrast to the BONUS reactor, Pathfinder had its boiler located on the periphery and the superheater located in the center of the core. The core was 6 ft in diameter and 6 ft in height. The central superheater region had a diameter of 32 inches. The active length of the entire core was about 55 inches. The power density was 46 kW/L in the boiling region, and was 50 kW/L in the superheating region.

The surrounding boiler section had 96 fuel assemblies made of low enrichment (2.2 to 3.2%) UO_2. Each fuel assembly was divided into four fuel sections. Each fuel section consisted of 81 fuel rods in a 9 by 9 array. The active length of the boiler fuel was about 17 inches. Aluminum was originally proposed for the cladding, but the substitution of Zircaloy-2 for the aluminum alloy cladding was made because of the aluminum corrosion problems.

The superheater had 415 highly enriched (about 93 %) tubular fuel assemblies, which were also made of UO_2. Annular fuel was used to increase heat transfer area. As shown in Figure A-14, there were three passages for superheated steam. Thermal isolation of the high temperature superheater from the rest of the core was accomplished by mounting each superheater element in a double-walled, stainless steel tube. A 53-mil annular gap between the double tube walls was filled with stagnant steam which acted as a thermal barrier to prevent excessive heat loss to the water surrounding the superheater tubes. Burnable Poison was placed in the center of the fuel rod to offset power shift late in the cycle.

The reactor could be controlled by manual operation of the control rods and/or by the recirculation flow rate. Recirculation flow was controlled by butterfly valves located in each of the three recirculating lines. Sixteen cruciform-shaped, boron stainless steel control rods using plate type blades were used in the boiler region. Forty-eight boron stainless steel control rods (0.75 inch diameter) were used in the superheater region.

Figure A-15 is the sectional view of the pressure vessel. It was an 11-foot inside diameter right cylinder with an overall height of 36 feet. The vessel was made of carbon steel clad with 0.25-inch thick stainless steel.

Plant Operation

Figure A-16 shows the simplified flow diagram of the Pathfinder reactor. Steam was produced initially in an annular boiling region surrounding the central superheater. After flowing up through the moisture separators located above the boiler, steam made a single pass downward through the superheater, emerging at 825 °F into a collection plenum beneath the core which was in turn connected directly to the main steam line.

Table A-6 Design features of the Pathfinder reactor [7]

Location	Sioux Falls, South Dakota, USA
Owner/Operator	Northern States Power Company
Type	Boiling water reactor with integral nuclear superheater
Power Gross thermal Electrical Overall efficiency	 Boiler: 157 MW; Superheater: 42 MW Net: 62 MW 31 %
Fuel element Type Fuel	 Boiler: 81 rods per assembly Superheater: two concentric tubes with centered burnable poison rod Boiler: 2.2% enriched UO_2 Superheater: 93% enriched UO_2-SS cermet
Core Dimensions Number of fuel elements Power density Fuel clad	 6 ft diameter, 6 ft high with central superheater region of 32 in. in diameter Boiler: 96; Superheater: 415 Boiler: 46 kW/L; Superheater: 50 kW/L Boiler: Zircaloy-2; Superheater: SS
Pressure vessel	11 ft 6 in. outer diameter, 36 ft high, carbon steel with SS cladding
Control rods Type Number	 Boiler: cruciform plate Superheater: cruciform cluster Boiler: 16; Superheater: 4
Turbine steam conditions Temperature Pressure Mass flow rate	 825 °F 540 psig 616,125 lb/hr
History [79] Initial criticality achieved Start of operation End of operation	 March 1964 July 1966 October 1967

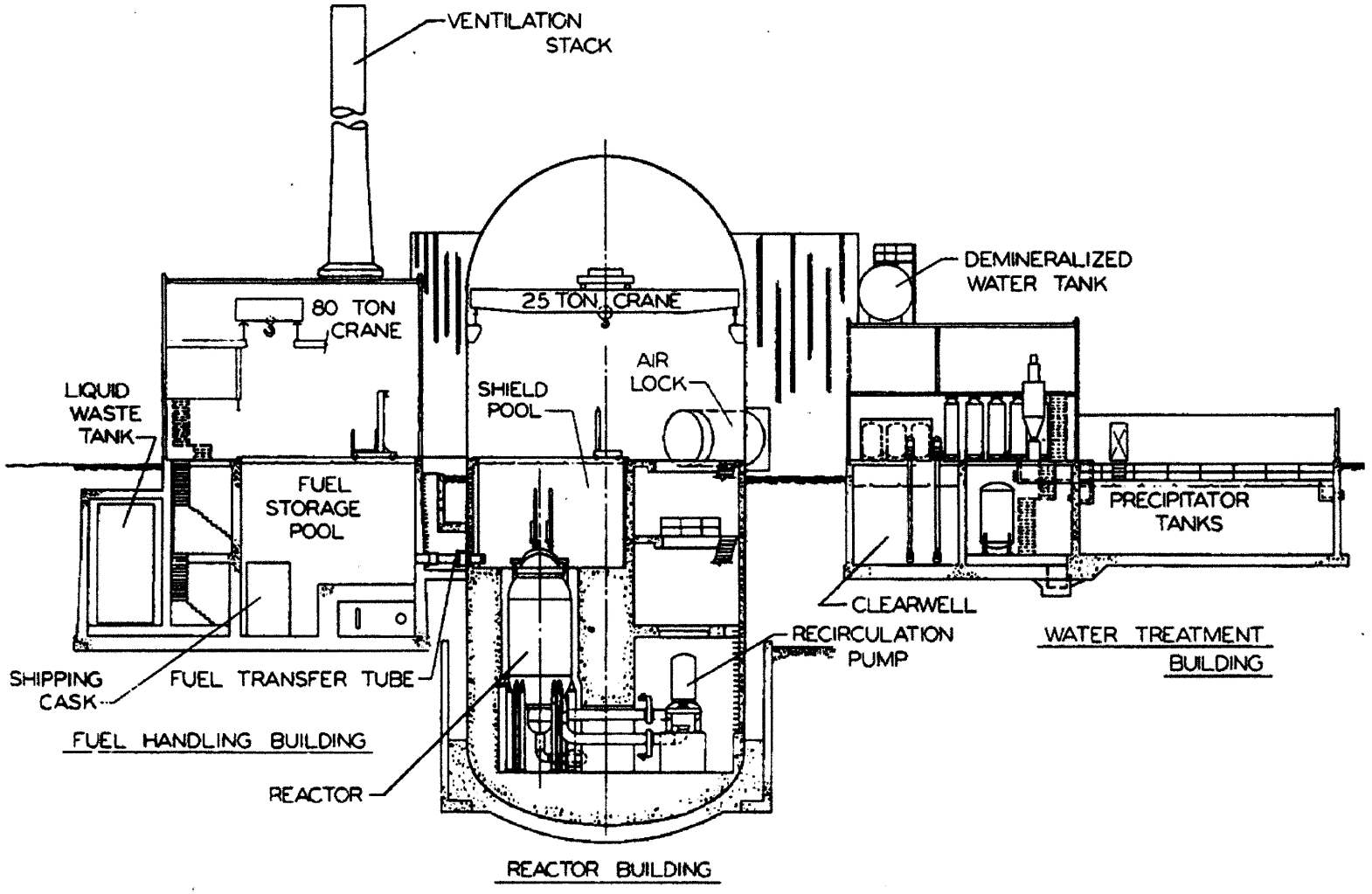

Figure A-12 The schematic diagram of the Pathfinder power plant [39]

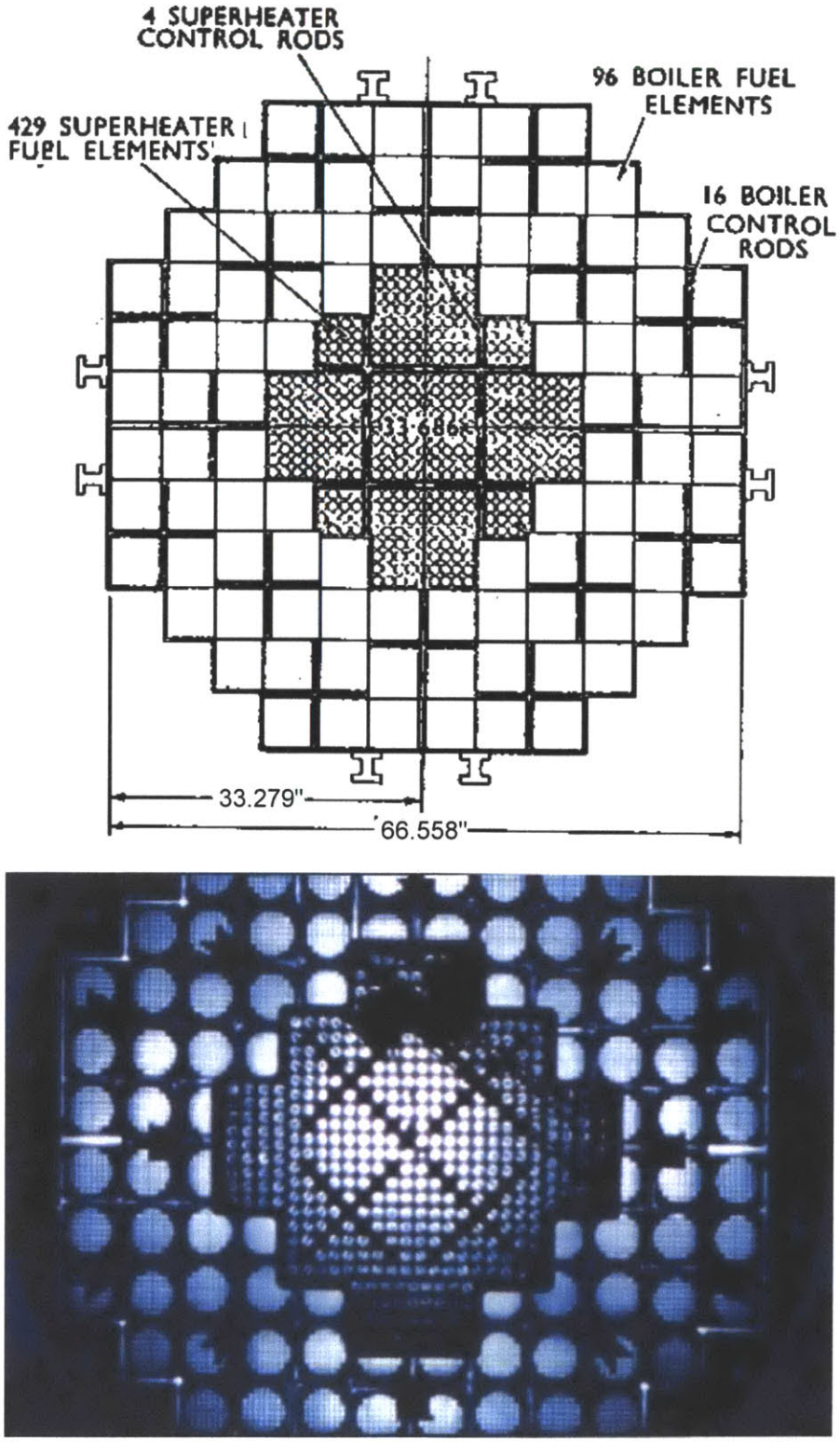

Figure A-13 Cross section of the Pathfinder reactor core [1,10]

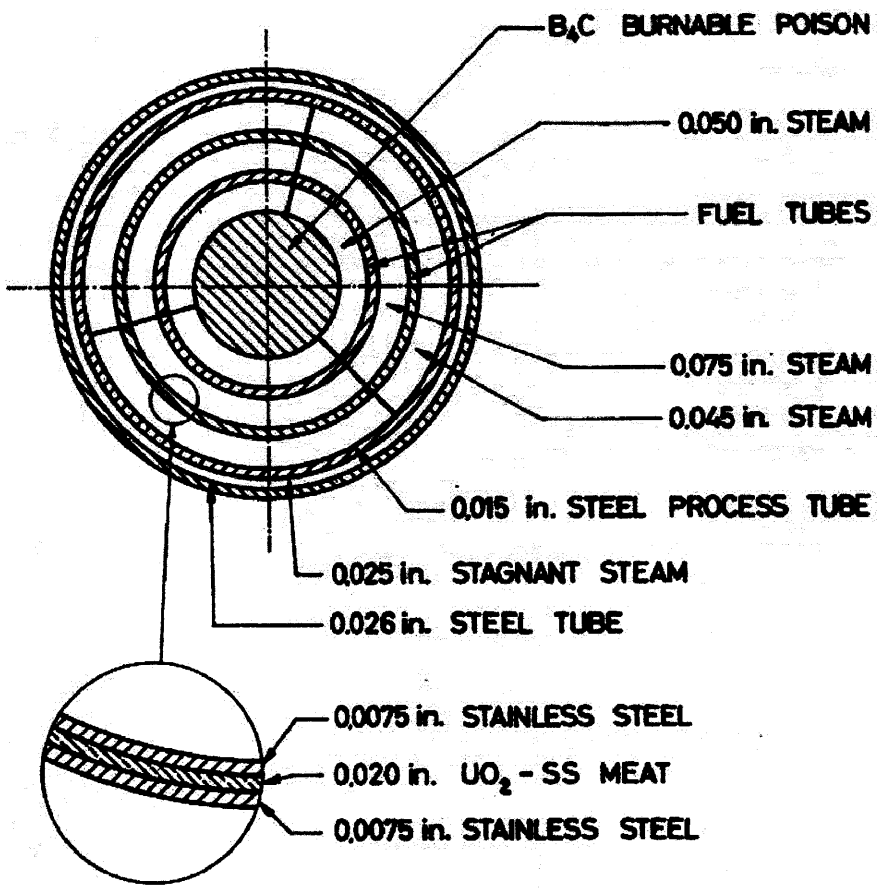

Figure A-14 The Pathfinder superheater fuel element [77]

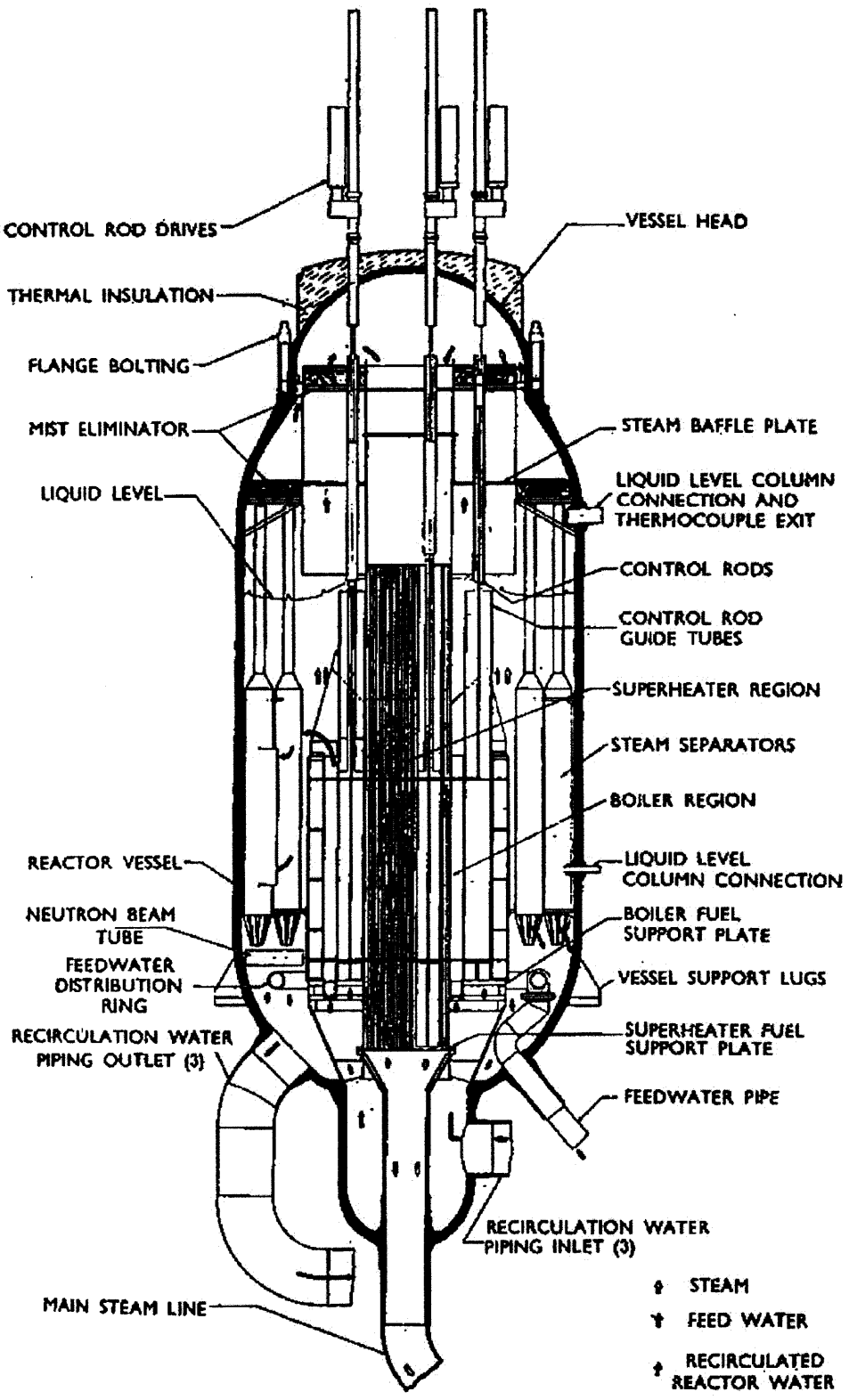

Figure A-15 Sectional view of the Pathfinder reactor vessel [39]

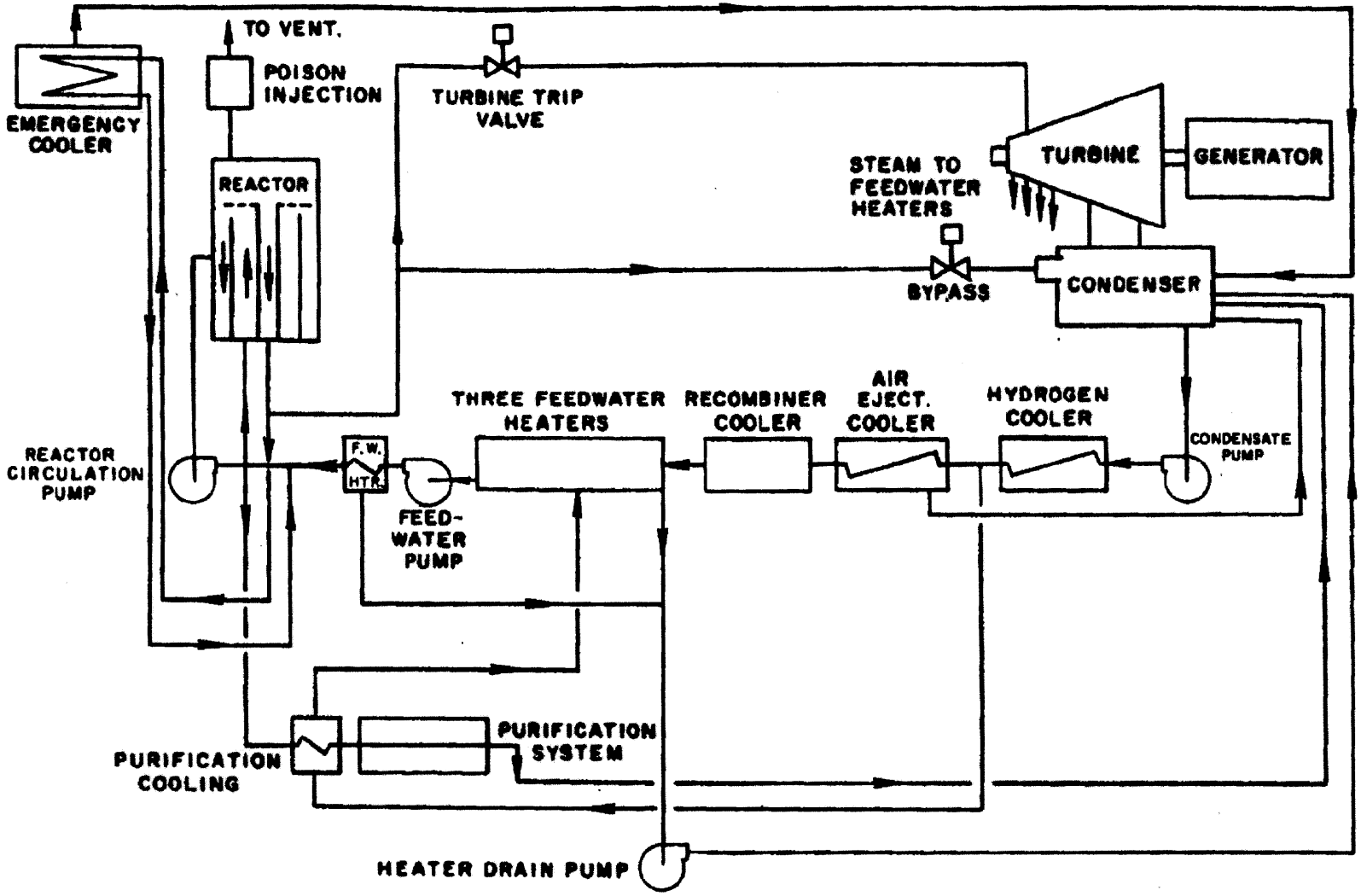

Figure A-16 Simplified flow diagram of the Pathfinder reactor [91]

A.3.4 The Boiling Nuclear Superheater (BONUS)

General

The Boiling Nuclear Superheater (BONUS) was located at Punta Higuera on the seacoast at the westernmost tip of Puerto Rico. It was a boiling-water reactor with an integral nuclear superheater. The BONUS reactor was a joint project of the U.S. Atomic Energy Commission and the Puerto Rico Water Resources Authority (PRWRA). The BONUS reactor and Pathfinder were the only two boiling water superheater reactors ever developed in the United States. Design features of the BONUS reactor are summarized in Table A-7.

Summary of Plant History

In 1960, the Atomic Energy Commission entered into a contract with the PRWRA (predecessor of the Puerto Rico Electric Power Authority, PREPA), for the construction and operation of the BONUS power station. Startup and initial operations were performed by Combustion Engineering, Inc., and the PRWRA had responsibility for long-term operation. Construction of the facility occurred from 1960 to 1962. The BONUS reactor first went critical on April 13, 1964. The reactor underwent a series of criticality tests, and then was operated experimentally at various power levels, first as a boiler and later as an integral boiler superheater. Full power was achieved on November 9, 1965, and tests demonstrated satisfactory operation at 10% over-power in November 1965. Operation of the BONUS facility was terminated in June 1968, and decommissioning of the facility was conducted from 1968 to 1970 [12].

Description of the Reactor

The reactor was designed to deliver 152,000 lbs/hr of steam at 850 psig and 900 °F, producing 50 MWt and 16.3 MWe net with a plant efficiency of 32%. Of the 50 MWt heat output, 38.6 MWt was generated in the central boiler region and 11.4 MWt in the superheating region.

The BONUS reactor had its integral nuclear superheater located on the periphery and the

boiler located in the center of the core. Figure A-17 shows the horizontal cross section of the BONUS reactor core. The boiler region was a 35.5-inch square and the total area of the entire core was equivalent to a circle having a diameter of 56 inches. The active length of the entire core was about 55 inches. The power density was 32.9 kW/L in the central boiling region, and was 11.6 kW/L in the superheating region.

Figures A-18 and A-19 show the perspective of the boiler, and superheater fuel assemblies, respectively. As shown in Figure A-18, the boiling region contained 64 fuel assemblies in an 8 by 8 array. Each boiler fuel assembly consisted of 32 fuel rods in a 6 x 6 square array with the 4 central rods omitted. Each fuel rod was made of sintered UO_2 compacts (2.4 % enriched), which were contained in a Zircaloy tube. Figure A-20 shows the boiler and superheater fuel rods. Each boiler fuel rod had an inner diameter of 0.4553 inch, outer diameter of 0.5035 inch, and the central UO_2 pellets had a diameter of 0.445 inch.

As shown in Figure A-17, there were 32 fuel assemblies in the peripheral superheating region. Each assembly also consisted of 32 fuel rods, which were made of sintered UO_2 (3.25 % enriched), contained in Inconel-600 free-standing tubes. As shown in Figure A-20, each superheater fuel rod was surrounded by a 0.012-inch thick stainless steel coolant tube and then by a 0.018-inch thick stainless steel pressure tube.

The BONUS reactor was controlled by 17 boron-stainless steel rods. The nine control rods located in the boiling region were 0.125-inch thick cruciforms with a 7.75-inch span. The eight control slabs located between the boiling and superheating regions were 0.125-inch thick and 14.25-inch wide. There were no control rods in the superheating region.

The pressure vessel was made of 2.75-inch thick carbon steel clad internally with 0.25-inch thick stainless steel. It had an internal diameter of 7 feet, a height of 27.5 feet and a weight of 57 tons. The pressure vessel was designed to withstand 1150 psig at 600 °F, but the normal operating conditions were 950 psig and 540 °F. The perspective

of the BONUS pressure vessel is shown in Figure A-21.

Plant Operation

Figure A-22 shows the schematic diagram of the BONUS reactor. Water with a flow rate of 7,500 gpm was circulated through the 64 fuel elements in the boiler section by forced circulation. The water coolant entered the boiler at 532 °F, generating steam at 540 °F, which was separated from the water by gravitation. Before entering the superheater, the steam, with 5 % moisture, passed through the conventional steam driers which reduced the steam moisture to below 0.1 %. The dry steam at 540 °F made four passes through the superheater elements and was superheated to 900 °F [39].

Table A-7 Design features of the BONUS reactor [7, 78]

Location	Punta Higuera, Puerto Rico
Owner/Operator	USAEC/ Puerto Rico Water Resources Authority
Type	Boiling water reactor with integral nuclear superheater
Power	
Gross thermal	Boiler: 38.4 MW; Superheater: 11.6 MW
Electrical	Net: 16.5 MW
Overall efficiency	33 %
Fuel element	
Type	Boiler: solid pin with Zircaloy cladding Superheater: solid pin with Inconel cladding in a double-walled SS tube
Fuel	Boiler: 1.85% enriched UO_2 and natural uranium Superheater: 3.5% enriched UO_2
Core	
Dimensions	Boiler: 35.6 × 35.6 × 55 in.; Superheater: 4 adjacent slabs 8.95 in. thick, 55 in. high
Number of fuel elements	Boiler: 64; Superheater: 32
Power density	Boiler: 33.6 kW/L; Superheater: 11.5 kW/L
Structural metal	Boiler: Zircaloy-2 ; Superheater: SS and Zircaloy-2
Fuel clad	Boiler: Zircaloy-2 ; Superheater: Inconel-600
Pressure vessel	11 ft 6 in. outer diameter, 36 ft high, carbon steel with SS cladding
Control rods	
Type	Boiler: cruciform; Superheater: plates
Material	Boron steel
Number	Boiler: 9; Superheater: 8
Turbine steam conditions	
Temperature	900 °F
Pressure	850 psig
Mass flow rate	152,000 lb/hr
History [51]	
Start of construction	August 1959
Initial criticality achieved	March 1964 (with boiler fuel only) November 1964 (with both boiler and superheater fuel)
Start of operation	1964
End of operation	June 1968

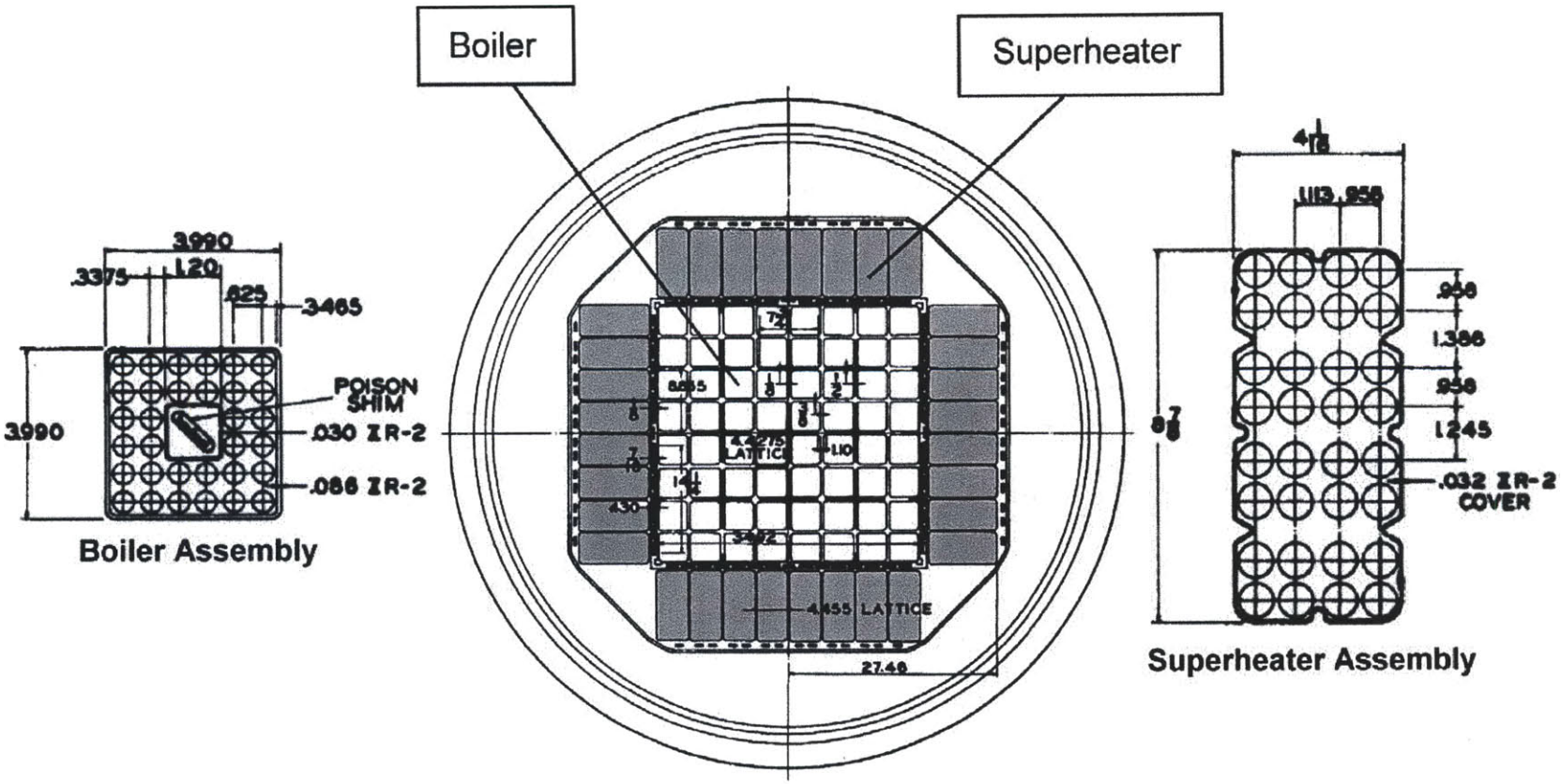

Figure A-17 Horizontal cross section of the BONUS reactor core [39]

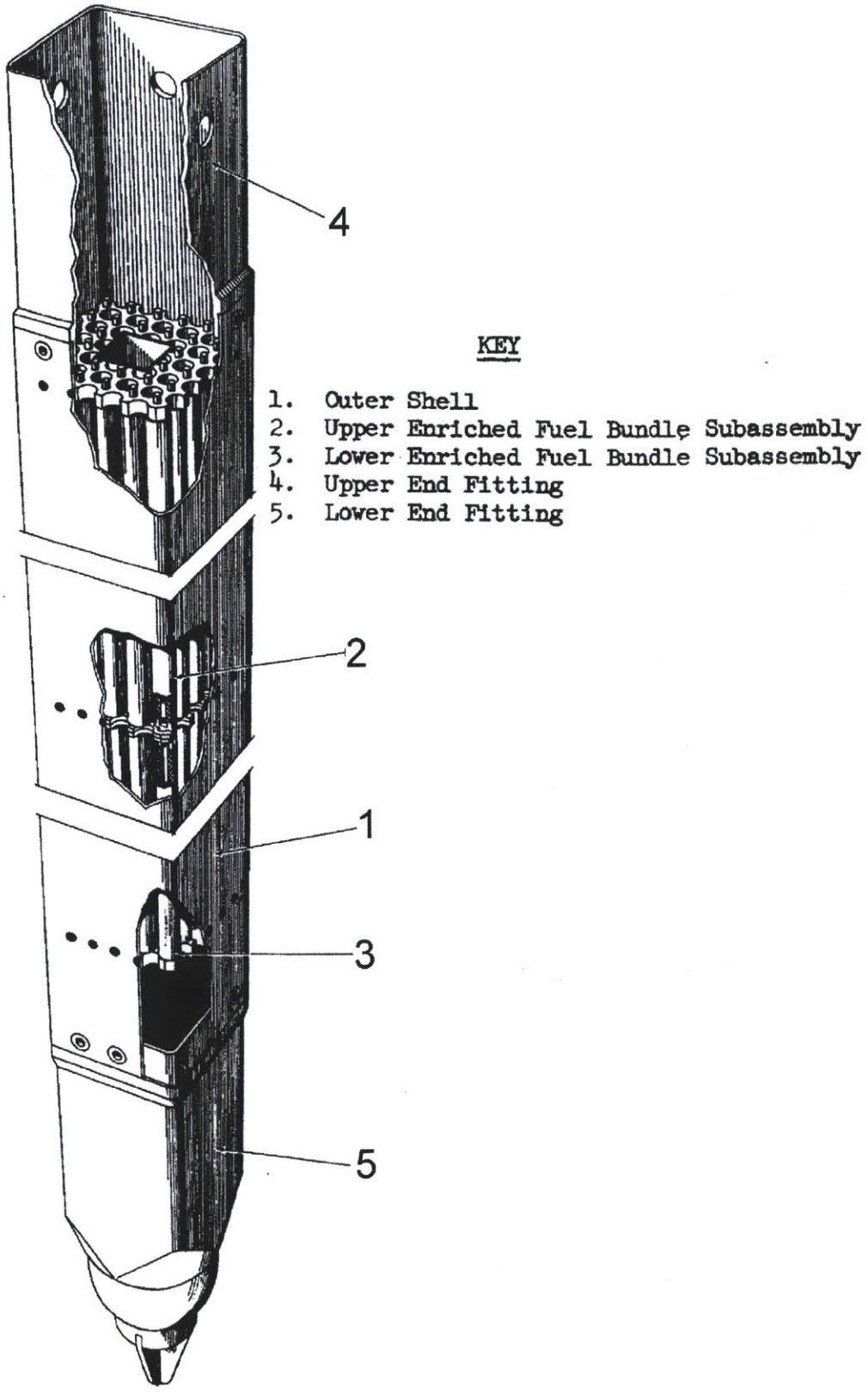

Figure A-18 Perspective of the BONUS boiler fuel assembly [39]

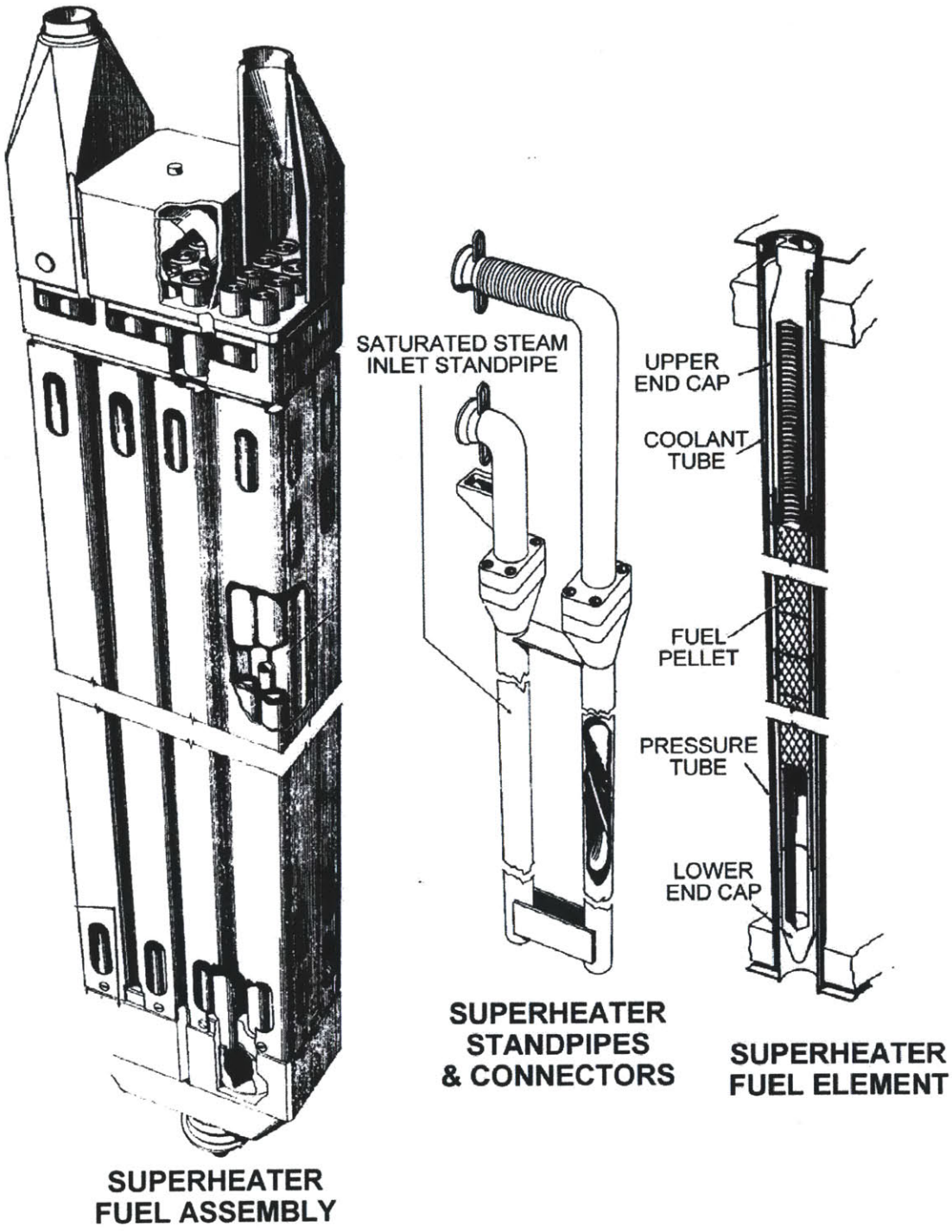

Figure A-19 Perspective of the BONUS superheater fuel assembly [39]

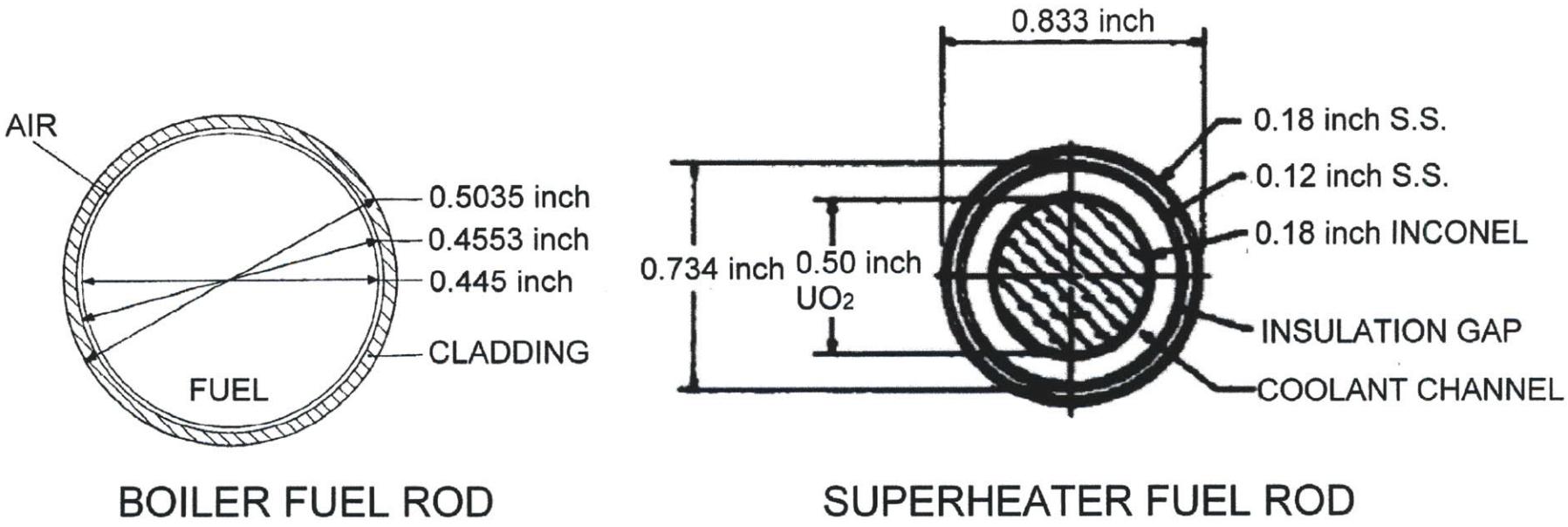

Figure A-20 BONUS boiler and superheater fuel rods [39]

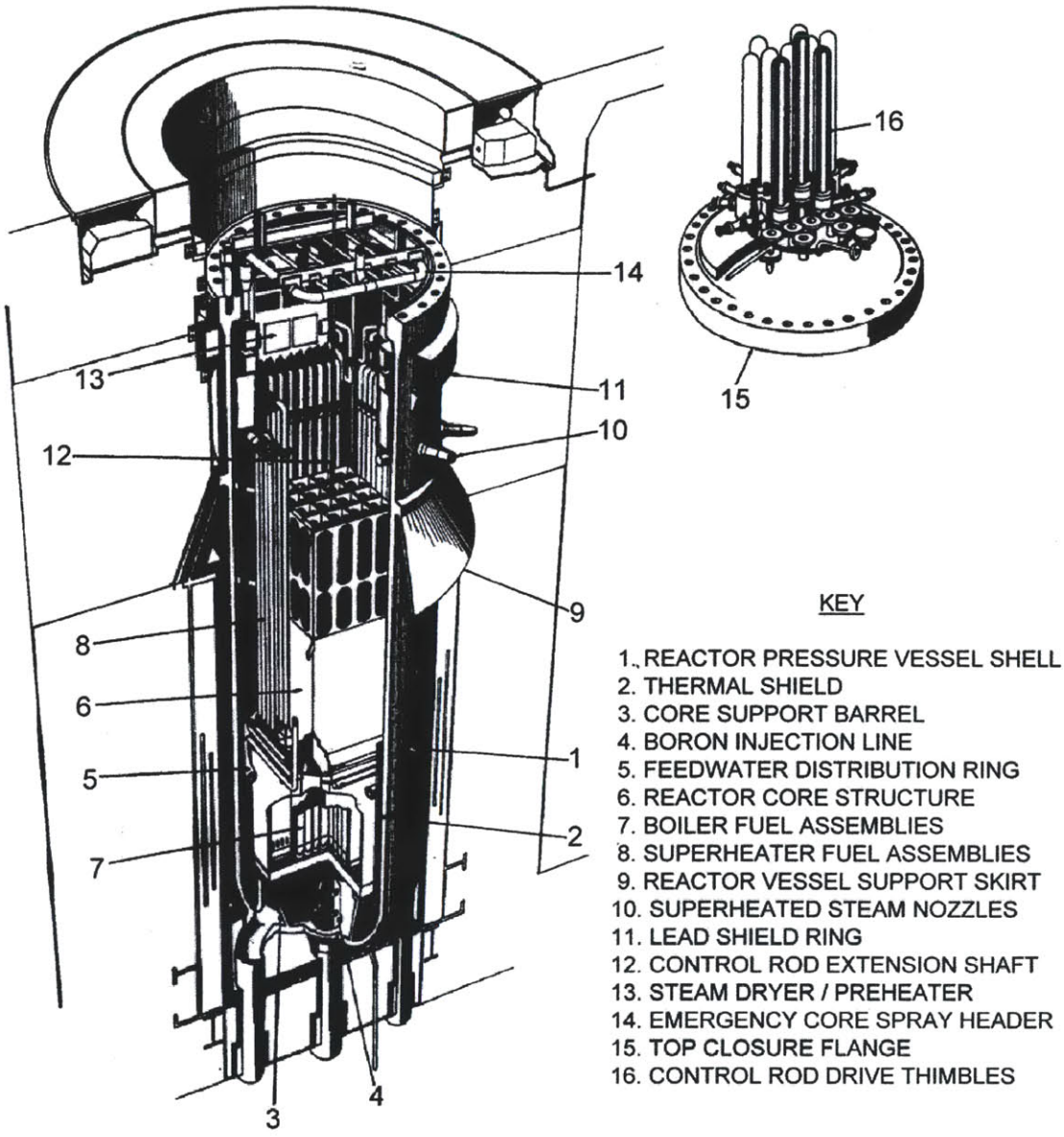

Figure A-21 Perspective of the BONUS reactor pressure vessel [39]

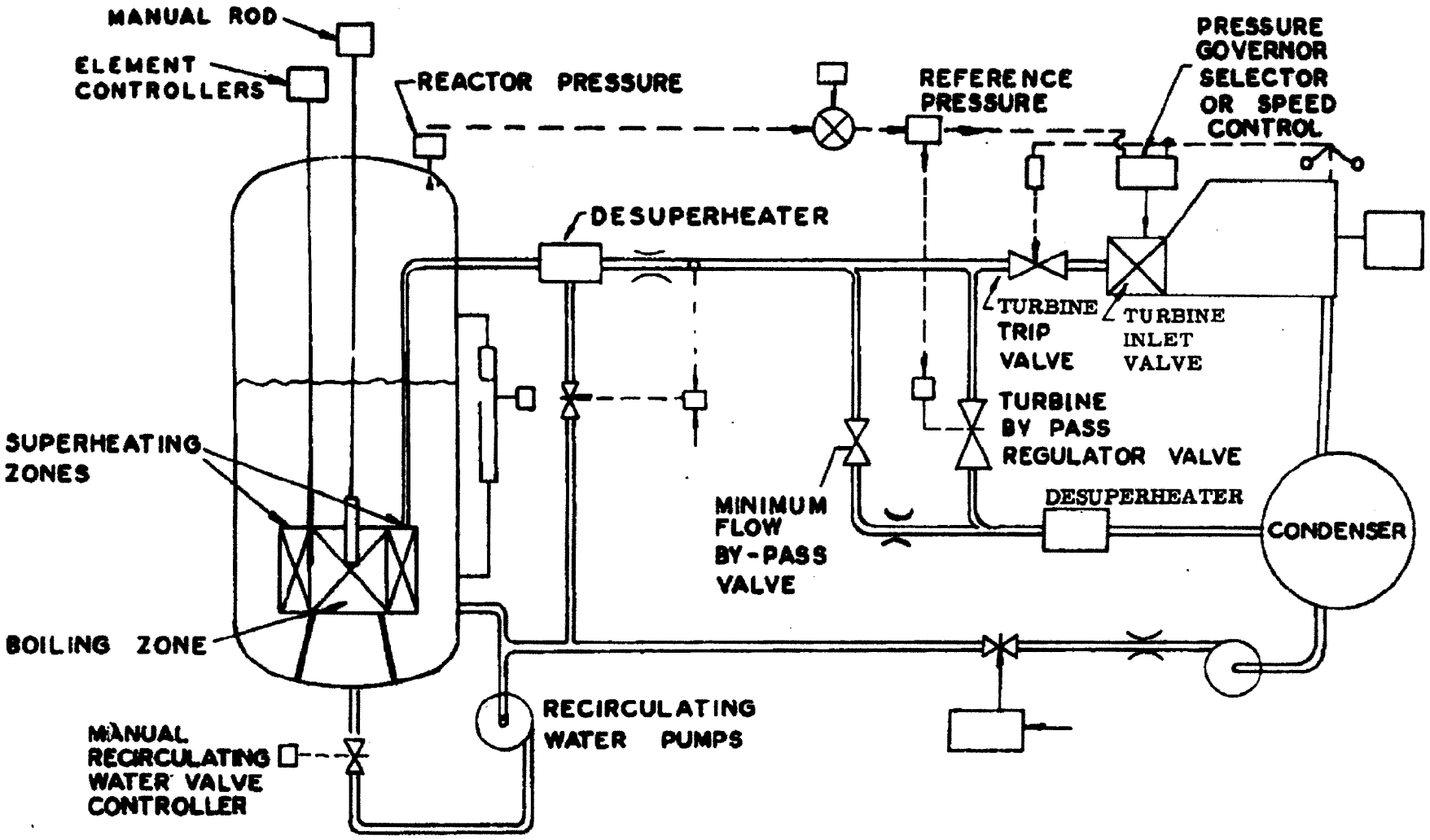

Figure A-22 Simplified schematic diagram of the BONUS power reactor [7]

A.3.5 The Beloyarsk Nuclear Power Station

General

The Beloyarsk Nuclear Power Station (NPS) is situated by Zarechny in Sverdlovsk Oblast, Russia. The two boiling superheat reactors at Beloyarsk, AMB-100 and AMB-200, were based on the successful experience obtained with the APS-1 reactor. The Beloyarsk NPS was the first to operate graphite-moderated pressure-tube-type superheat reactors to produce electrical power in the world. In addition, AMB-100 was the first commercial nuclear power unit in Russia [54]. Successful operation of the Beloyarsk prototype channel BWRs led to the creation of the first Soviet series-produced, high-power BWR — the RBMK-1000 (1000 MW capacity). These RBMK reactors are similar to AMB-200 at Beloyarsk, but do not incorporate the superheating feature [84].

Summary of Plant History

Construction of AMB-100 started in 1958. The first criticality was achieved in September 1963. The AMB-100 reactor had been operated from 1964 to 1983. Construction of AMB-200 started in January 1962. The AMB-200 reactor first went critical in October 1967 and was connected to the grid in December of the same year [79]. In 1977, half of the fuel rods melted down in the ABM-200 reactor. Operators were exposed to severe radiation doses and the repair work took more than a year. In December 1978, ABM-200 caught fire and the reactor went out of control. Eight people who assisted in securing cooling of the reactor core were exposed to very high radiation doses [86]. After 22 years of operation, the AMB-200 reactor was finally shut down in 1990.

Description of the Reactor

AMB-100 was a graphite-moderated, pressure-tube-type reactor with an electric output of 100 MW. Figure A-23 shows the Simplified flow diagram of the AMB-100 reactor. AMB-200 was the same design with an electric output of 200 MW but eliminated the secondary loop in the coolant system; that is, steam produced in the reactor core was fed directly to the turbine [84]. The AMB-100 reactor core was 24 feet in diameter and 20 feet high with an additional 2 0r 3 feet of graphite around the core to serve as reflector. The core was enclosed in a sealed, cylindrical,

carbon-steel tank under one atmosphere of nitrogen [79]. A fuel assembly, which was a combination of pressure tube and fuel element, was installed vertically in the core region. Each fuel assembly contained six tubular fuel elements which were made of U-Mg (1.3% enriched) canned inside and outside with stainless steel surrounded a seventh centrally located stainless steel coolant tube [91].

Plant Operation

As shown in Figure A-23, the coolant was allowed to boil as it flowed through the boiler fuel elements. The exit steam-water mixture was taken to a steam separator and then the primary steam was used to generate the saturated secondary steam in a heat exchanger. This secondary steam was returned to the superheat fuel elements, where it was superheated and sent directly to the turbine [91].

The pressure tubes in which the superheating was done were located at an intermediate radius such that the reactivity was affected very little by interchanging water with steam inside the tubes. This "intermediate superheater" design was distinct from the BONUS and the Pathfinder reactors, which have their integral superheaters on the periphery and in the center, respectively.

At start up, the superheater tubes were filled with water. With the reactor operating at 30% of full power, the secondary steam from the steam generator was used to force the water exiting from the superheater tubes.

The turbine inlet conditions were 1320 psig and 930 °F, which were better than conditions achieved in the U.S. reactors at that time [91].

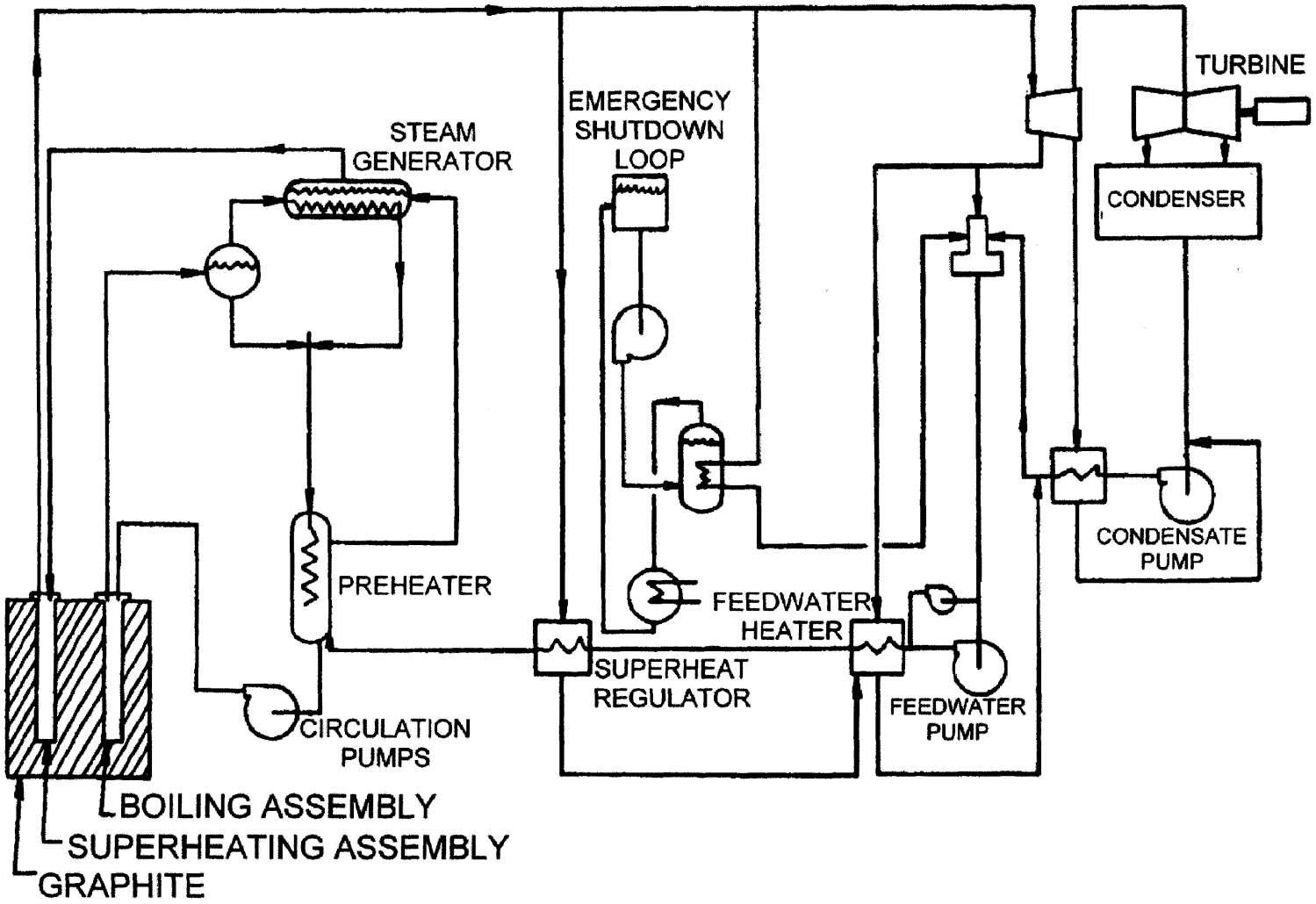

Figure A-23 Simplified flow diagram of the AMB-100 reactor [91]

A.3.6 The Marviken Boiling Heavy-water Superheat Reactor (R4)

General and the Plant History

The Marviken or R4 reactor was a boiling heavy water reactor built at Marviken and the fourth nuclear reactor built in Sweden [19]. The Marviken reactor was designed as heavy water cooled and moderated with an electric output of 200 MWe [18]. Construction of the Marviken reactor started in 1962. Commission in 1968 was planned; however, due to serious problems, the R4 project was canceled in 1970 before the fuel loading. The plant site was subsequently used for an oil-fired power station. The pressure vessel and containment building were subsequently used for experiments into reactor behavior under accident conditions [19].

Description of the Reactor

The design of the Marviken reactor was published at the international conference on the peaceful uses of atomic energy in Geneva, 1964 [18]. Slightly subcooled heavy water at the inlet plenum flowing upwardly into the boiling channels at 49.5 bar pressure, left as a steam-water mixture and entered the separator. The separated steam then flowed downwardly into the superheater channels where it was heated to 475 °C [18]. Both the boiler and superheater utilized slightly enriched UO_2 fuel (1.3% and 1.6%), with Zircaloy and Inconel cladding, respectively. Other design features of the Marviken reactor are summarized in Table 2-5.

A.3.7 The German Superheat Nuclear Reactor (HDR)

General

In Germany, the first studies on the nuclear superheat concept were made in 1960. In 1961, the Federal Ministry of Scientific Research started a three-year project which included the selection of the reactor type and a detailed layout for a prototype plant. After some studies, the superheat heat reactor with tubular type fuel elements was selected to be the most promising concept [17]. Based on this research project, the Heissdampfreaktor (HDR) was designed and constructed. The HDR, located in Großwelzheim, Germany, was the first reactor in the world that incorporated annular fuel elements to demonstrate the concept of nuclear superheat. It was light water cooled and moderated with a thermal output of 100 MWt. Design features of the HDR are listed in Table A-8.

Summary of Plant History

Construction of HDR started in January 1965. The initial criticality was achieved in October 1969. After a series of tests, the reactor was commercially operated in August 1970. Due to deformations at the cladding tubes of the novel superheat fuel elements, HDR was permanently shut down in April 1971 [92]. In total the reactor was operated only for the equivalent of five full power days [58]. The spent fuel elements were reprocessed in the Karlsruhe nuclear fuel reprocessing plant (WAK). The reactor internals were removed, and the facility was decontaminated.

From 1974 to 1991, the reactor building was used for various safety related experiments, such as the performance of nuclear power plant behavior in case of severe accidents or earthquakes. New equipment was installed specifically in the plant for reactor blowdown simulations in a small but authentic containment facility.

The decommissioning of HDR started on 16 February 1983. The plant was entirely dismantled [59]. The residual conventional dismantling work was completed in October 1998.

Description of the Reactor

Figure A-24 shows the fuel assembly of the original HDR design [17]. Each assembly consisted of 64 annular fuel rods in an 8×8 array. Each annular fuel was cooled internally by steam and externally by boiling water. The annular fuel element was made of powder UO_2 fuel (5% enrichment and 85% TD) with tool steel as outer cladding and Inconel as inner cladding to accommodate the uneven axial expansion between the claddings.

Figure A-25 and A-26 show the reactor vessel and flow configuration of the original HDR design, respectively. The reactor core consisted of 45 fuel assemblies which were divided into to groups; one comprising 25 and the other 20 fuel assemblies. Since the reactor core was very small, the steam must pass four times through the core in order to attain the desirable temperature level (500°C). The saturated steam made the first two passes through the inner group of 25 fuel assemblies and the third and fourth passage through the outer group of 20 fuel assemblies. A Chimney was set in the vessel to achieve gravitational separation of the steam-water mixture [17].

However, when the prototype reactor was built at Großwelzheim, the fuel assembly and flow configuration were revised [61]. As shown in Figure A-27, the actual fuel assembly of HDR consisted of four sub-assemblies. Each sub-assembly contained six annular fuel elements. The actual flow configuration of HDR, as shown in Figure A-28, was simplified so that the steam coolant would pass only two times through the core.

Table A-8 Design features of the HDR [56, 59, 61]

Location	Großwelzheim, Germany
Owner/Operator	Germany
Type	Integral boiling nuclear superheater with annular fuel elements
Power	
Gross thermal	100 MW
Electrical	Net: 25 MW
Overall efficiency	25 %
Fuel element	
Type	Annular fuel made of VIPAC fuel with Inconel inner cladding and tool steel outer cladding
Fuel	5% enriched UO_2, 85 % TD
Reactor	
Pressure	90 bar
Specific power	15 kW/kg U
Number of fuel assemblies	52
Number of control rods	21
Fuel active length	1.8 m
Pressure vessel	6.95 m high, 2.96 m in diameter
Turbine steam conditions	
Temperature	457 °C
Pressure	72 bar
Mass flow rate	157,000 kg/hr
History	
Start of construction	January 1965
Initial criticality achieved	October 1969
Start of commercial operation	August 1970
End of operation	April 1971
Start of decommission	1983
End of decommission	1998

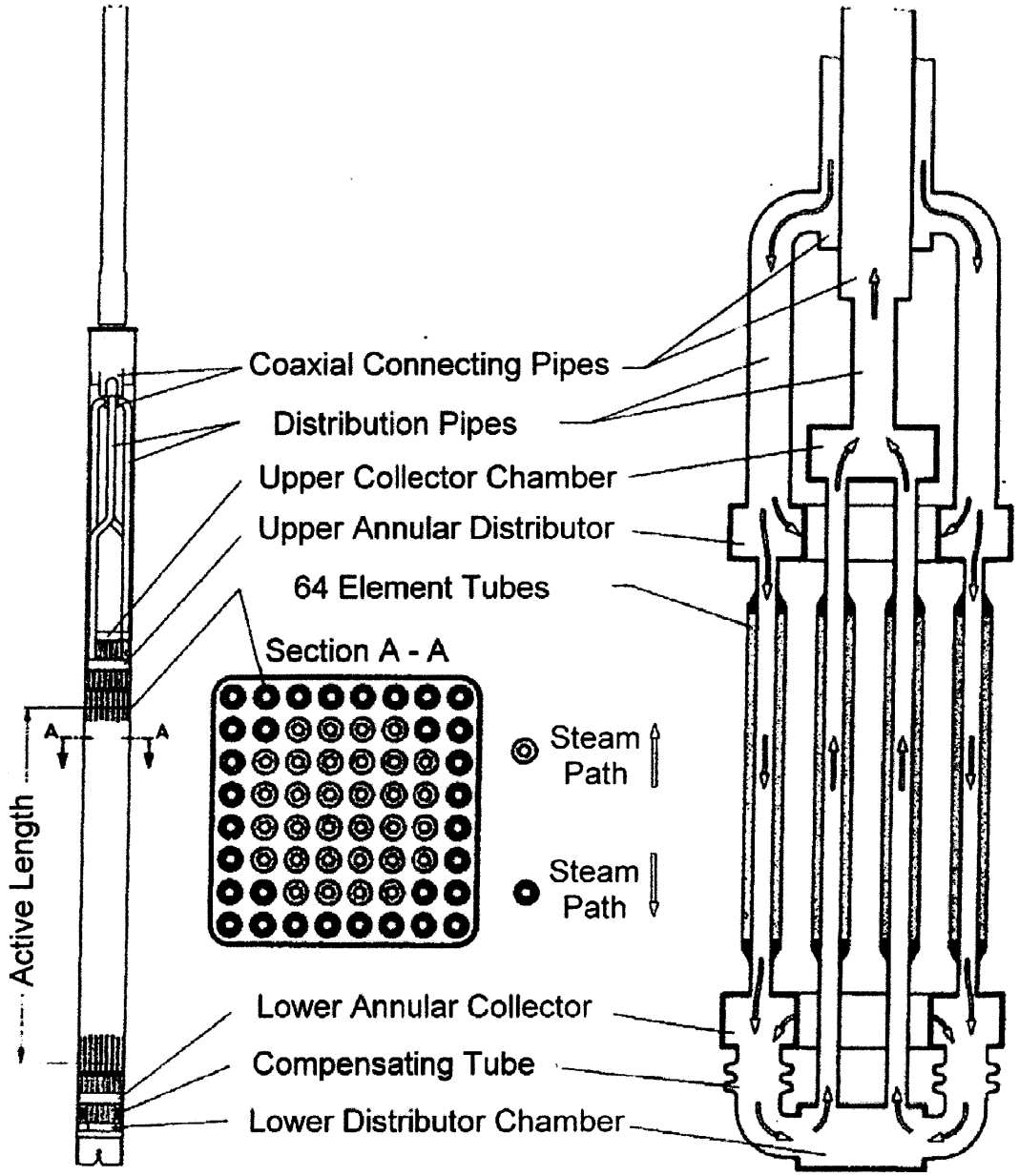

Figure A-24 The original HDR fuel assembly design [17]

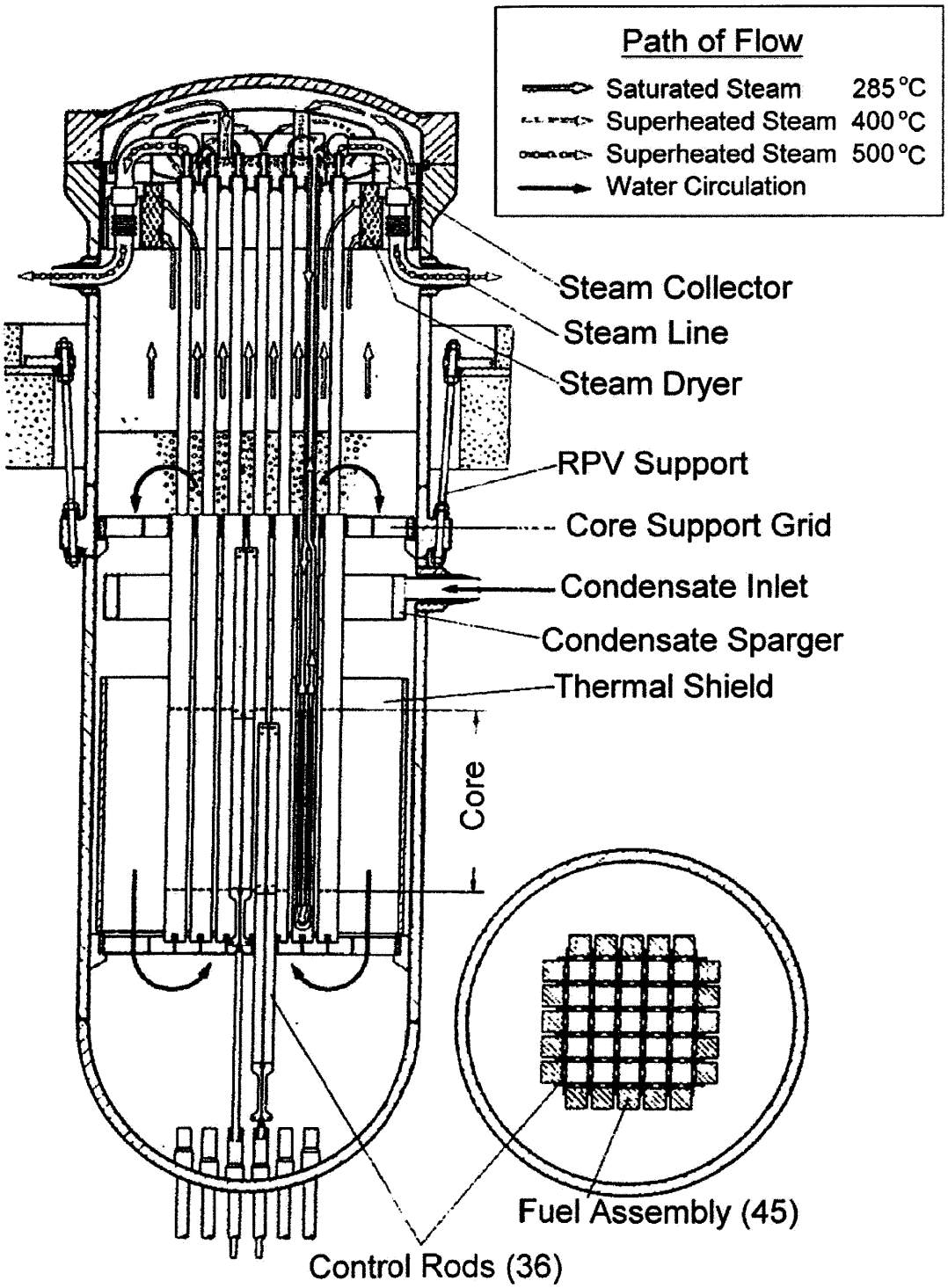

Figure A-25 The HDR reactor vessel (original design) [17]

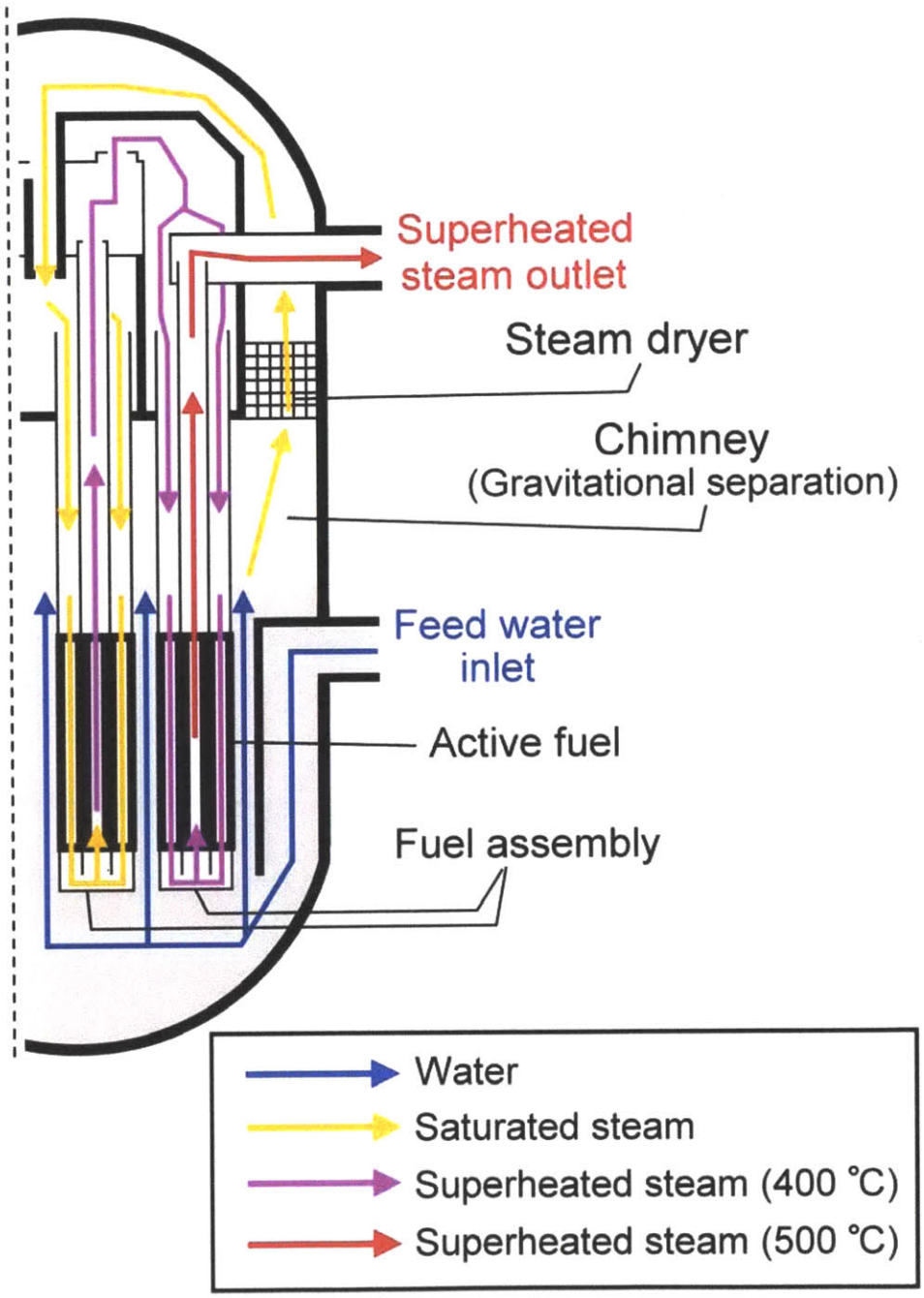

Figure A-26 Flow Configuration of the HDR (original design)

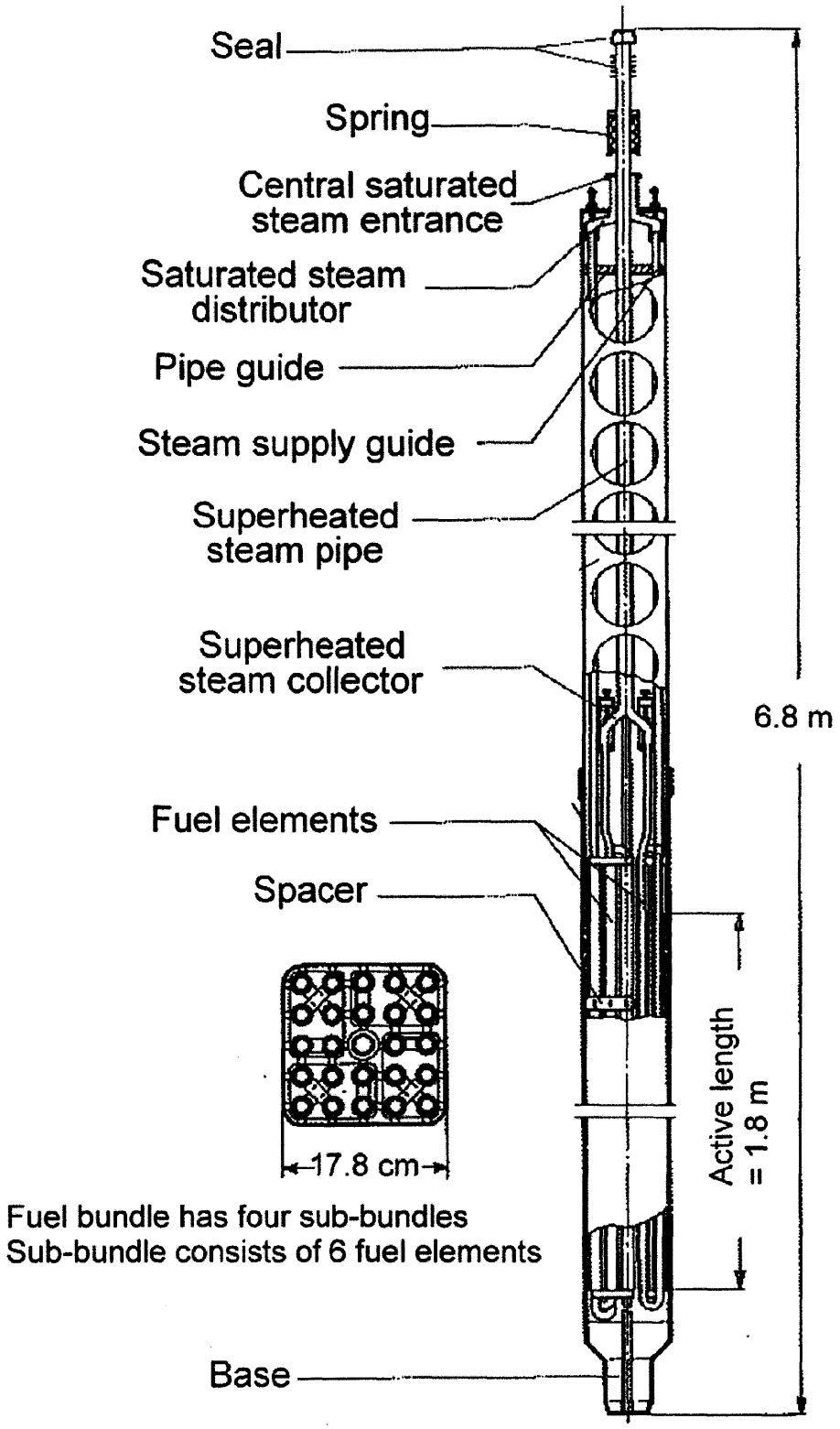

Figure A-27 The revised HDR fuel assembly design [61]

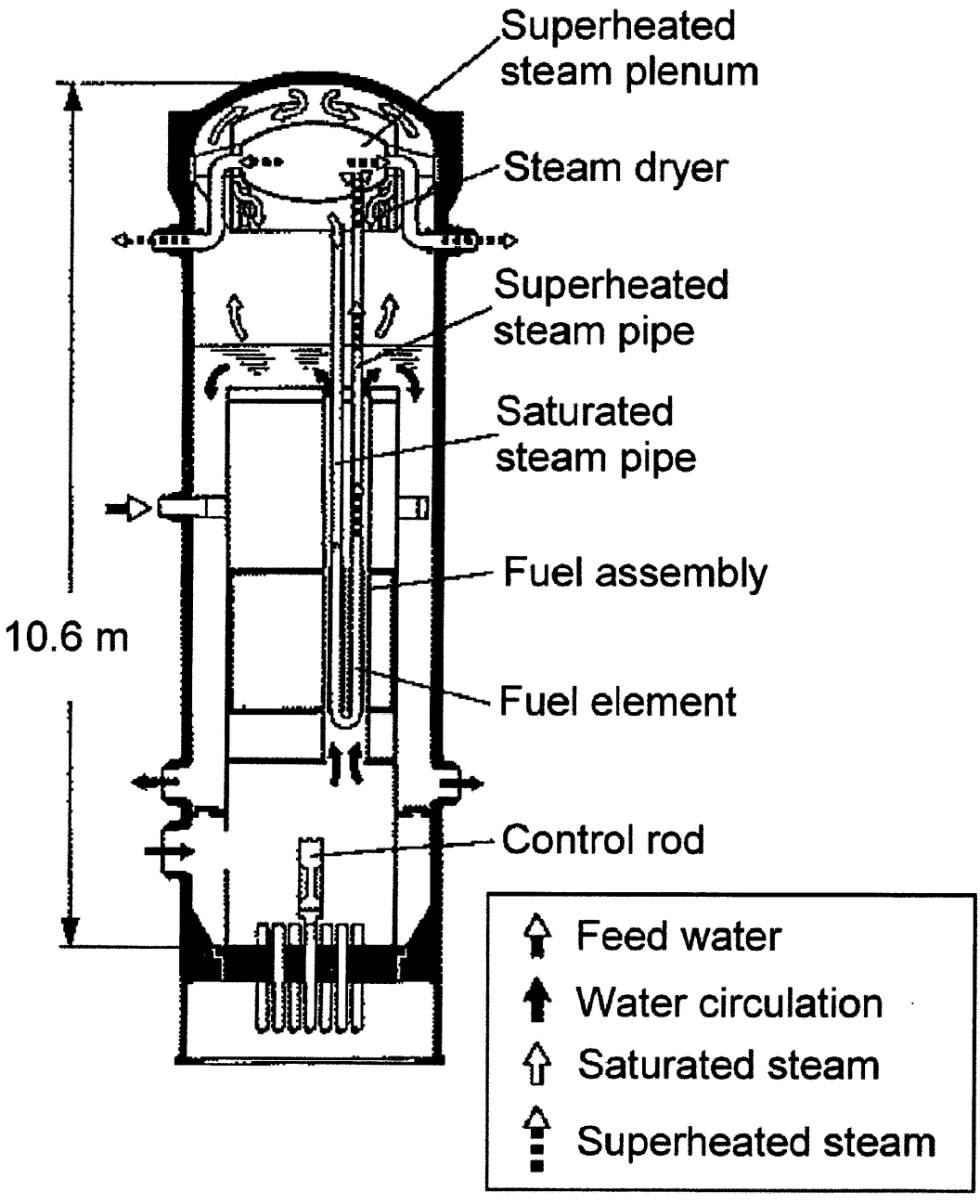

Figure A-28 The revised HDR flow configuration [61]

Appendix B

The MIT ASBWR Single Channel Analysis Code

B.1 Objectives of the MIT ASBWR Single Channel Analysis Code

On account of the unique design of the superheater annular fuel elements and flow configuration, it is difficult to find an existing commercial code which can be directly used for preliminary thermal-hydraulic calculations for the ASBWR. As a result, the MIT ASBWR Single Channel Analysis Code (MASCAC) has been developed in order to serve this purpose. MASCAC is programmed in the MATLAB compiler. The objectives of MASCAC are to accomplish the following tasks:

1. To compute steady-state axial and radial temperature profiles for both the average channel and hot channel under fresh fuel conditions.
2. To investigate the magnitude and location of the peak cladding and fuel temperatures.
3. To estimate the steam pressure drop through the heating channel.
4. To calculate the power split between the water and steam sides.
5. Given different power densities, estimating the steam outlet temperature and steam velocity.
6. To provide the results of single channel analysis as an input for VIPRE to perform assembly subchannel analysis.

B.2 Code Structure and Assumptions

MASCAC is a steady-state, two-dimensional numerical solver, which uses a finite difference approach to calculate the temperature distribution in the fuel region. The simplified flowchart of MASCAC is illustrated in Figure B-1. The calculation begins by processing input data. Initial guess of the power split is given to calculate the steam and water coolant temperatures and film drops. Then the temperature distribution

throughout the fuel and the cladding is calculated at each axial node. MASCAC calculates these temperatures iteratively until the calculated power split is within 1% difference from the initial guess.

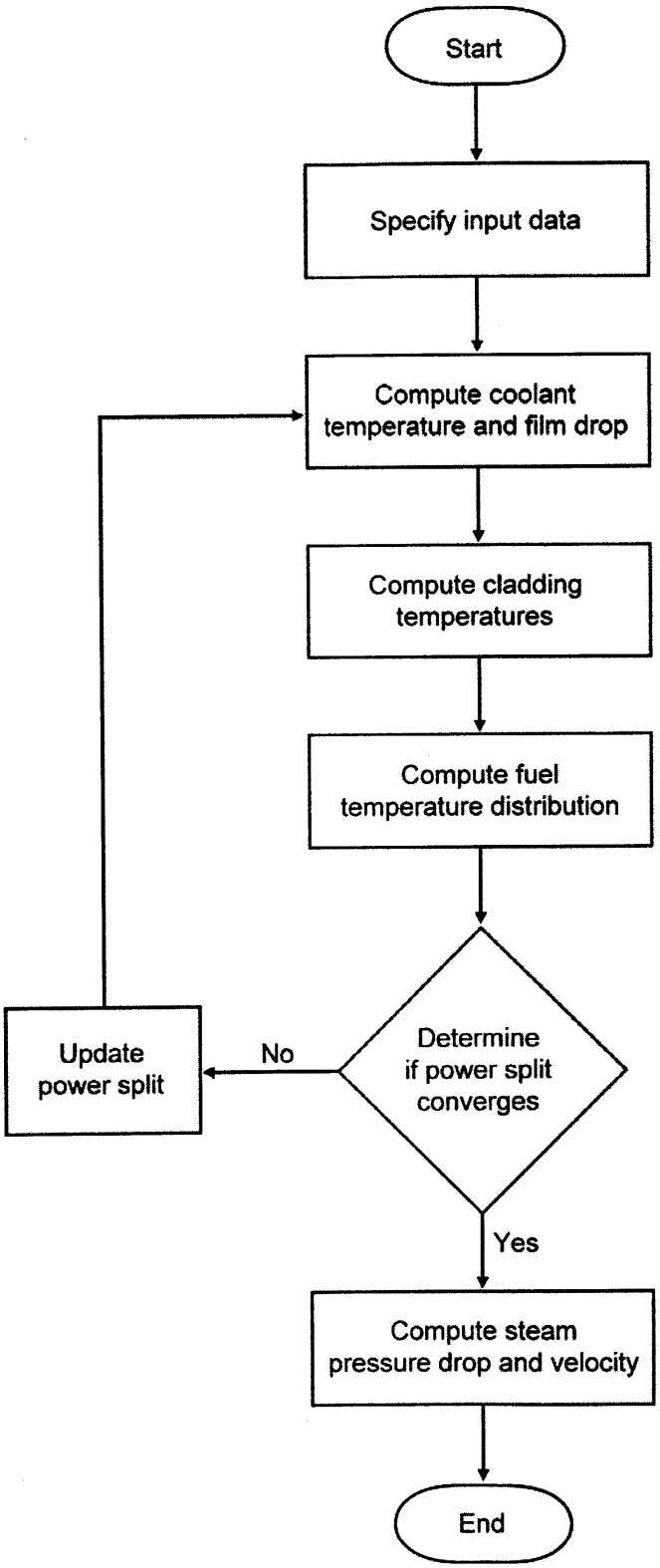

Figure B-1 Simplified MASCAC flow chart

After the calculation of temperatures is converged, the steam pressure drop throughout the inner heating channels and the steam outlet velocity are calculated.

Figure B-2 shows the single channel model of the ASBWR. As shown in Figure B-2, the single channel model is divided into seven regions, where only regions 2 and 6 are heated, in other words, only regions 2 and 6 contain annular fuel pellets. Figure B-3 shows the simplified single channel model, which is used in MASCAC. Compared Figure B-2 with Figure B-3, it can be observed that regions 1, 4 and 7 are not modeled in MASCAC. Region 1 is neglected because the inlet steam coolant has approximately the same temperature as the surrounding steam-water mixture. Region 4 is ignored due to its short length relative to regions 3 and 5. Heat exchange in region 7 is also considered negligible because it is near the bellows region (see Figure 3-12 in Chapter 3), where the fission gas plenum can provide effective insulation. Figure B-4 illustrates the detailed model for the fuel active region and unheated region. In the fuel active region, cladding, gap and fuel meat are modeled, while the unheated region only contains cladding material.

Figures B-5 and B-6 are thermal conductivity variation under different temperatures of T91 and Inconel 718, respectively [100, 111]. For simplicity, constant T91 thermal conductivity has been assumed in MASCAC. According to the expected cladding temperature, 28.5 W/m-K is assumed for both inner and outer claddings if T91 is adopted. For Inconel 718, however, thermal conductivity is treated as a function of cladding temperature and is calculated using Eq. B-1 in MASCAC.

$$k_{Inconel\,718} = 11.45 + 1.156\times10^{-2}T + 7.72\times10^{-6}T^2 \qquad \text{(B-1)}$$

where $k_{Inconel\ 718}$ is in W/m-K and T is in °C.

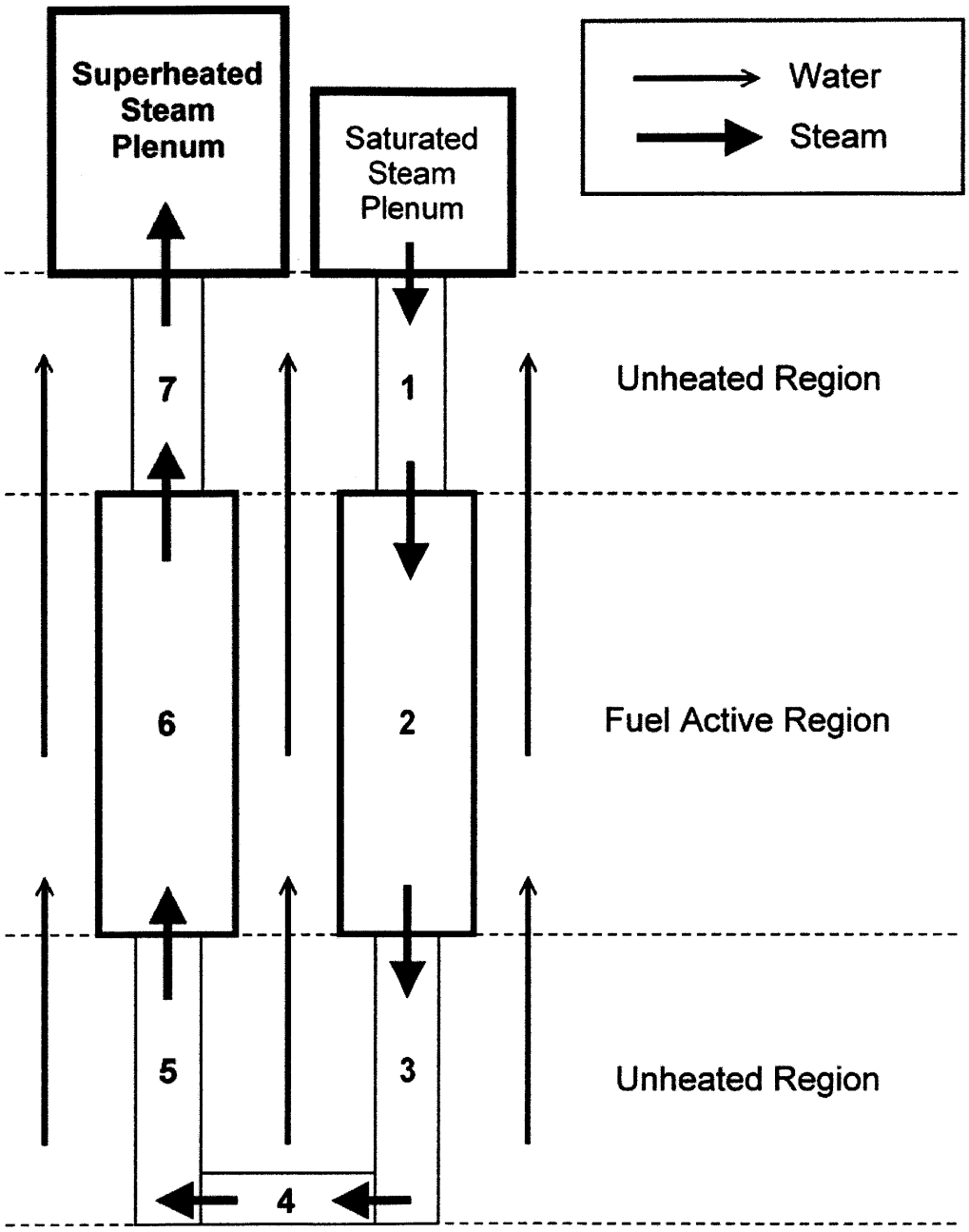

Figure B-2 Single channel model of the ASBWR

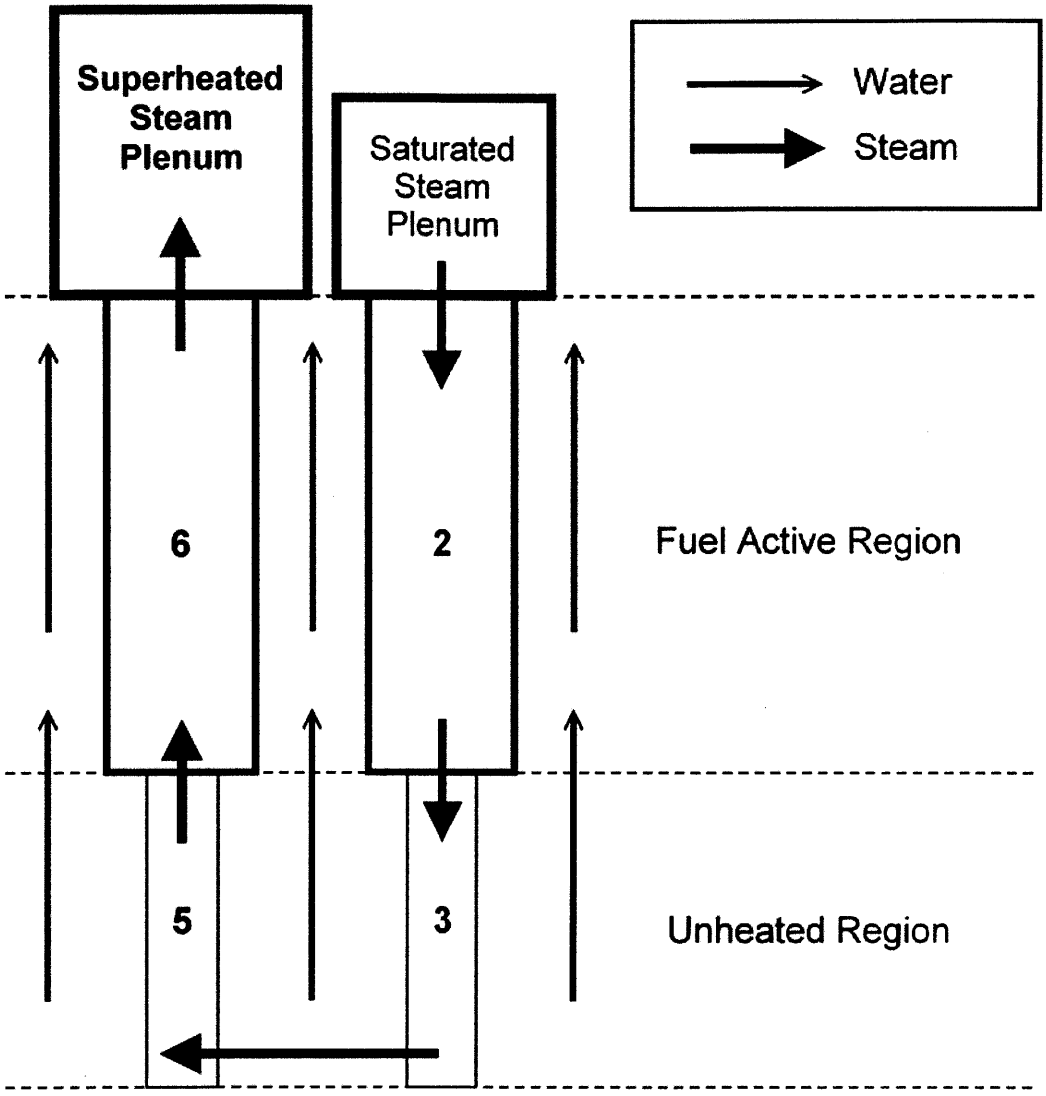

Figure B-3 Simplified single channel model of the ASBWR used in MASCAC

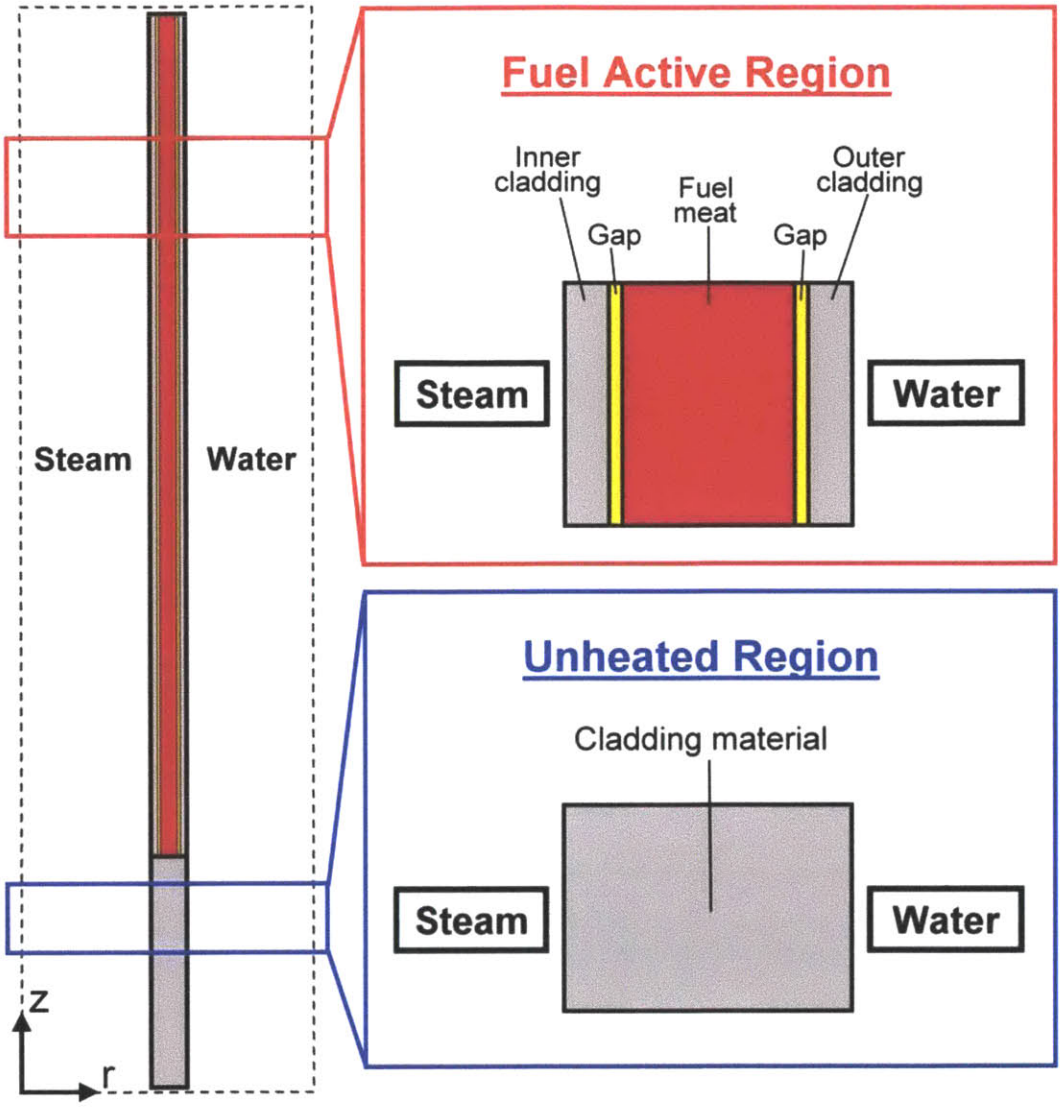

Figure B-4 Illustration of the fuel active and unheated regions

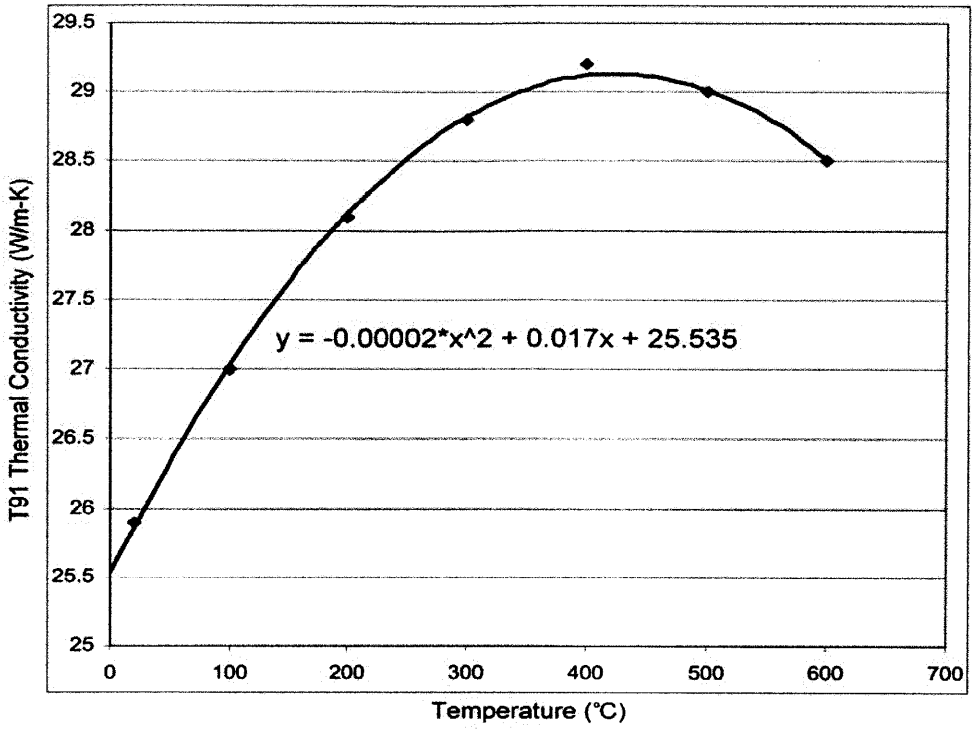

Figure B-5 Thermal conductivity of T91 [111]

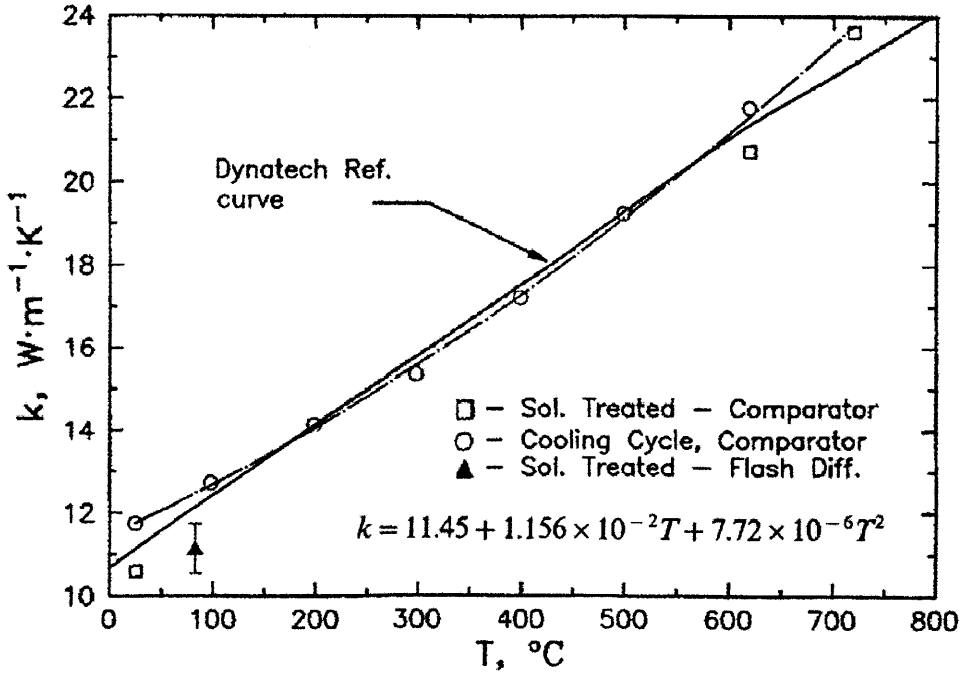

Figure B-6 Thermal conductivity of Inconel 718 [100]

In addition, the models used for the calculations in MASCAC include a number of assumptions:

1. Steady-state heat flux is assumed.
2. Heat conduction in the axial direction is considered negligible relative to radial heat conduction and is ignored.
3. Heat conduction in the azimuthal direction is ignored.
4. The annular fuel element is a right circular tube surrounded externally by water and internally by steam.
5. Onset of nucleate boiling occurs at 5 °C wall superheat.
6. Crud and oxidation layer on the cladding surfaces are ignored.

B.3 Models for the Temperature Calculation

B.3.1 Coolant Conditions

MASCAC computes bulk steam and water coolant temperatures according to

$$T_{b,i}(z) = T_{in,i} + \int_0^z \left[\frac{4q''_i(z)}{C_{p,i}G_iD_{e,i}}\right] \qquad \text{(B-2)}$$

where

i	=	subscript, indicating coolant types (i.e., water or steam)
$T_b(z)$	=	bulk coolant temperature at elevation z on the rod axis (K)
T_{in}	=	inlet coolant temperature (K)
q"(z)	=	heat flux at elevation z on the rod axis (W/m)
C_p	=	heat capacity of the coolant (J/kg-K)
G	=	coolant mass flux (kg/s-m^2)

D_e = coolant channel heated diameter (m).

B.3.2 Cladding Surface Temperature

The cladding surface temperature at axial elevation z is calculated as the following:

$$T_{w,i}(z) = T_{b,i}(z) + \frac{q''_i(z)}{h_i} \qquad \text{(B-3)}$$

where

$T_w(z)$ = cladding surface temperature at elevation z on the rod axis (K)

h = heat transfer coefficient (W/m^2-K).

The heat transfer coefficient (h) is calculated by different correlations according to the local heat transfer mechanism at elevation z. Table B-1 lists the heat transfer correlations used in MASCAC.

Table B-1 Heat transfer correlations used in MASCAC

Heat transfer mechanism	**Heat transfer correlation**
For water side	
Single phase forced convection	Dittus-Boelter correlation [117]
Subcooled and saturated nucleate boiling	Chen correlation [117]
For steam side	
Single phase forced convection	Gnielinski correlation [118]

B.3.3 Cladding Temperature Drop

The cladding temperature drop for each axial location is calculated by Eq. B-4 for steady-state heat transfer through a cylinder with uniform thermal conductivity.

$$\Delta T_{c,i}(z) = q''_i(z)\, r_{o,i}\, \ln(r_{o,i}/r_{i,i})/k_{c,i} \qquad \text{(B-4)}$$

where

ΔT_c = cladding temperature drop (K)

r_o = cladding outside radius (m)

r_i = cladding inside radius (m)

k_c = cladding thermal conductivity (W/m-K).

B.3.4 Fuel-Cladding Gap Temperature Drop

The fuel cladding gap temperature drop is calculated using the cladding outer surface heat flux at elevation z and the fuel-cladding gap conductance for both the water-side and steam-side claddings. The fuel-cladding gap conductance is the sum of three components: 1) the conductance due to radiation, 2) the conduction through the gas, and 3) the conduction through regions of fuel-cladding contact.

$$\Delta T_{gap,i}(z) = \frac{q''_i(z)}{h_{gap}} \qquad \text{(B-5)}$$

$$h_{gap} = h_r + h_{gas} + h_{solid} \qquad \text{(B-6)}$$

where

ΔT_{gap} = fuel-cladding gap temperature drop (K)

h_{gap} = fuel-cladding gap conductance (W/m^2-K)

h_r = conductance due to radiation (W/m^2-K)

h_{gas} = conductance of the gas gap (W/m^2-K)

h_{solid} = conductance due to fuel-cladding contact (W/m^2-K).

The equations and models for each of these three components are given in Ref. [112]. FRAPCON-3 uses detailed models for each component to calculate the fuel-cladding gap conductance. In MASCAC, however, a constant fuel-cladding gap conductance is assumed with a magnitude of 0.36 W/m^2-K. This assumption is made based on the calculation results of FRAPCON-3 under the same operating conditions and fuel element dimensions.

B.3.5 Fuel Pellet Temperature Distribution

Finite differences are used to calculate the temperature distribution in the fuel region. The steady-state integral form of the heat conduction equation is

$$\iint_S k(T,\bar{x})\,\vec{\nabla}T(\bar{x})\cdot\vec{n}\,ds = \iiint_V q'''(\bar{x})\,dV \qquad \text{(B-7)}$$

where

k = thermal conductivity (W/m-K).

s = surface of the control volume (m^2)

$\vec{n}$ = surface normal unit vector

q''' = volumetric heat generation (W/m^3)

T = temperature (K)

V = control volume (m^3)

$\bar{x}$ = the space coordinates (m).

Two boundary conditions are needed to calculate the temperature profile in the fuel. The boundary conditions are prescribed temperatures at the inner and outer surfaces of the fuel. The fuel surface temperatures can be obtained from the following equation

$$T_{f,i}(z) = T_{w,i}(z) + \Delta T_{c,i}(z) + \Delta T_{gap,i}(z) \qquad \text{(B-7)}$$

where

T_f = fuel surface temperature (K).

B.4 Benchmark Studies

The radial temperature profiles predicted by MASCAC have been benchmarked against the results of the modified FRAPCON-ANNULAR code.

B.4.1 The Modified FRAPCON-ANNULAR Code

FRAPCON fuel rod modeling code was developed by the Pacific Northwest National Laboratory for use by the Nuclear Regulatory Commission in evaluation of Light Water Reactor (LWR) fuel rod behavior up to a burnup of 65 MWd/kg. FRAPCON models the fuel and cladding of a single solid fuel rod under steady-state conditions. The code is capable of calculating temperature distributions, stress and strain, fission gas release, cladding oxidation, and other physical behavior as a function of an input power history and core conditions [112].

In 2004, the FRAPCON-ANNULAR code was developed at MIT [95]. The code was developed based on FRAPCON and can be used to perform steady-state fuel performance analysis for the annular fuel design. However, FRAPCON-ANNULAR can only be used for annular fuels with zircaloy cladding under LWR operating conditions.

In this work, FRAPCON-ANNULAR has been modified to incorporate T91 and Inconel 718 properties. Superheated steam properties and Gnielinski heat transfer correlation are also included in the modified FRAPCON-ANNULAR code. Due to the fact that the behavior of T91 and Inconel 718 contacting boiling water and high temperature steam in a high irradiation environment is still under investigation, the modified FRAPCON -ANNULAR code currently cannot be used to evaluate the long term fuel performance of the ASBWR fuel.

B.4.2 Assumptions

Main differences between the modified FRAPCON-ANNULAR code and MASCAC are listed in Table B-2.

Assumptions adopted by the benchmark studies include:

1. Fresh fuel conditions
2. Uniform axial power profile
3. Fuel element linear power = 46.7 (kW/m)
4. Same operating conditions and fuel element dimensions for both codes.
5. Water power split ratio is defined as the heat transferred by the water coolant divided by the total heat generation

Table B-2 Differences between the modified FRAPCON-ANNULAR and MASCAC

	Modified FRAPCON-ANNULAR	MASCAC
Cladding thermal conductivity	For T91 cladding: $k_{T91} = 25.535 + 1.7\times10^{-2}T - 2.0\times10^{-5}T^2$ where k_{T91} is in W/m-K and T is in °C.	For T91 cladding: $k_{T91} = 28.5$ (W/m-K)
Gap conductance	h_{gap} is calculated by detailed models*	$h_{gap} = 0.36$ (W/m-K)
UO_2 thermal conductivity	k_{UO_2} is calculated by detailed models*	$k_{UO_2} = 3.0$ (W/m-K)
Heat transfer correlation for nucleate boiling	Jens-Lottes formulation*	Chen correlation [117]

*See Ref. [112]

B.4.3 Results

Figure B-7 and Table B-3 summarizes the results of benchmark study in which T91is used as cladding material. It can be seen in Figure B-7 and Table B-3 that the results predicted by MASCAC are in good agreement with the results calculated by the modified FRAPCON-ANNULAR. MASCAC predicts higher cladding and fuel temperatures than the modified FRAPCON-ANNULAR. The differences are about 10 °C in the peak cladding temperature and 50 °C in the peak fuel temperature. The two codes predict roughly the same water power split ratios.

Figure B-8 and Table B-4 summarizes the results of benchmark study in which Inconel 718 is used as cladding material. These results have a similar trend to that in Figure B-7 and Table B-3.

The results of benchmark study indicate that MASCAC predicts a radial temperature profile which has higher peak cladding and fuel temperatures. Therefore, MASCAC is considered more conservative than the modified FRAPCON-ANNULAR. For a preliminary study, MASCAC is selected to evaluate the steady-state thermal-hydraulic performance of the ASBWR concept.

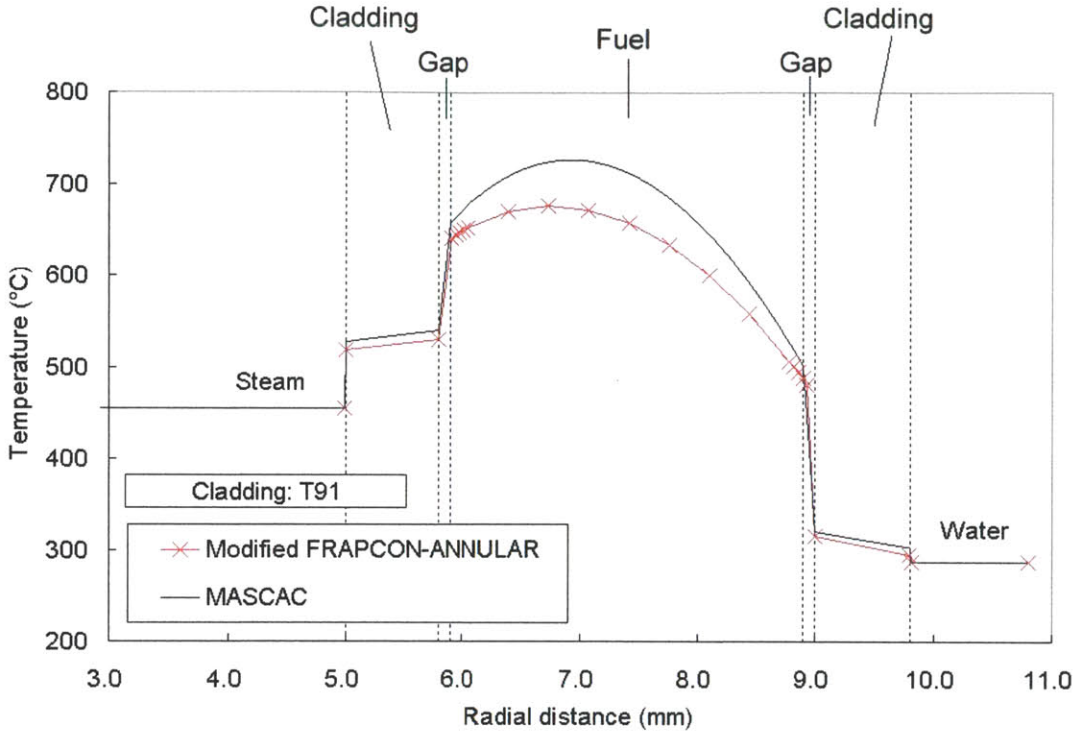

Figure B-7 FRAPCON and MASCAC radial temperature profiles (T91)

Table B-3 Summary of benchmark study (with T91 cladding)

	Modified FRAPCON-ANNULAR	MASCAC
Steam temperature (°C)	426.6	426.6
Water temperature (°C)	287.2	287.2
Peak cladding temperature (°C)	529.7	540.0
Peak fuel temperature (°C)	676.5	726.6
Water power split ratio	0.719	0.716

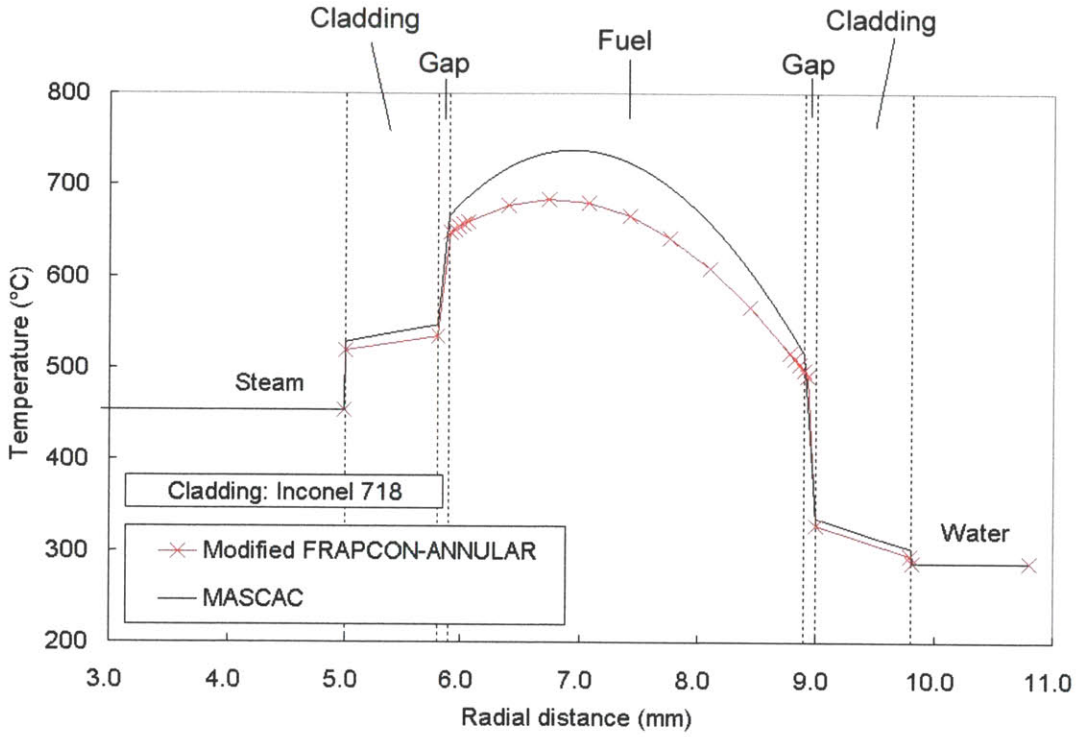

Figure B-8 FRAPCON and MASCAC radial temperature profiles (Inconel 718)

Table B-4 Summary of benchmark study (with Inconel 718 cladding)

	Modified FRAPCON-ANNULAR	MASCAC
Steam temperature (°C)	426.6	426.6
Water temperature (°C)	287.2	287.2
Peak cladding temperature (°C)	534.9	547.0
Peak fuel temperature (°C)	684.2	737.8
Water power split ratio	0.716	0.712

B.5 Source Code

```
%Annular fuel solver version 4.0   20081122
%This solver has different cladding and gap
%                    BC1 IBC2 IBC3        IBC4 IBC5   BC6
%dimensions: ------+--------+----+--------------+----+--------+-------
%Region                  I      II      III      IV      V
%           steam    clad    gap    fuel meat   gap   clad   water
%                (T91 or Inconel)                (T91 or Inconel)
%Thickness (mm): fuel meat =3.0; clad=0.8; gap=0.1
%inner channel radius (mm) = 5.0
clear; clf;
%=========================================================
% Constants
%=========================================================
gravity=9.81 ;                %(m/s2)
%=========================================================
% Input parameter
%=========================================================
%FW=fluid = Feed water; ST=Gas = steam
%_____________________________________________
%HALF CORE Approach See NOTE H1 - 081111
%Core A (steam IN) and Core B (steam OUT)
%_____________________________________________
%                    Goal
%_____________________________________________
RTP=1250E6; %Reactor Thermal Power (W) = 1250 (MWth)
% Target efficiency = 40% => Electric power = 500 MWe
%_____________________________________________
%                    Operating conditions
%_____________________________________________
%---   HOT CHANNEL   ----
HCF=1.45;                      %Hot channel Factor
%HCF=1.0;                      %If AVE channel
FD=1.0;                        %Hot channel FLOW Disparity factor
OHOT=0.205;                    %Orifice-adjusted HOT channel m_ST
PPR=1.4;                       %Power multiplier
MPR=1.4;                       %Flowrate multiplier
```

```
NofD=28;                        %# of steam downward flow tubes
DFF=30/NofD;                    % down flow factor   (after/before)
UFF=30/(60-NofD);                       % up flow factor   (after/before)
power = 77.8*1000*HCF*PPR;      % power per rod (W)
pressure=71.36;                   %Operating pressure = (bar) => Tsat = 287 C
m_FW=0.22*MPR*FD    ;           %mass flow rate/rod =   (kg/s)
%_____________________________________________
%                          Rod Geometry
%_____________________________________________
C_H=3.0E3;                                  %Active Core height = 3000 (mm) = 3 (m)
F_m_t= 3.0;                                 %Fuel meat thickness (mm)
I_c_t= 0.8 ;                                %Inner cladding thickness -- SS (mm)
O_c_t= 0.8;                                 %outer cladding thickness -- Zr (mm)
I_g_t= 0.10;                                %Inner (Steam side) gap thickness -- He (mm)
O_g_t= 0.10;                                %Outer (Water side) gap thickness -- He (mm)
Rv=5.0 ;                                    %annular fuel inner radius (mm)
Rfo=Rv+F_m_t+I_c_t+O_c_t+I_g_t+O_g_t;       %annular fuel outer radius (mm)
pitch=23.;                                  %Pitch = 23 (mm)
p_over_d=pitch/(2*Rfo);                     %Pitch to diameter ratio
fA_FW=(pitch*pitch-Rfo*Rfo*pi);             %Water flow area /rod (mm2)
fA_ST=Rv*Rv*pi ;                            %Steam flow area /rod (mm2)
hA_FW=2*Rfo*pi*C_H;                         %Water heat transfer area /rod (mm2)
hA_ST=2*Rv*pi*C_H   ;                       %Steam heat transfer area /rod (mm2)
Pw_FW=2*Rfo*pi ;                            %Water wetted parimeter (mm)
Pw_ST=2*Rv*pi       ;                       %Steam wetted parimeter (mm)
Ph_FW=2*Rfo*pi ;                            %Water heated parimeter (mm)
Ph_ST=2*Rv*pi   ;                           %Steam heated parimeter (mm)
De_FW=4*fA_FW/Pw_FW   ;                             %Water hydraulic equivalent dia (mm)
De_ST=4*fA_ST/Pw_ST   ;                             %Steam hydraulic equivalent dia (mm)
Dh_FW=4*fA_FW/Ph_FW    ;                            %Water heated equivalent dia (mm)
Dh_ST=4*fA_ST/Ph_ST    ;                            %Steam heated equivalent dia (mm)
%_____________________________________________
%                          Assembly Geometry
%_____________________________________________
O=4;   %clearance between duct and peripheral rods (mm)
J=2.54; %Box Wall thickness (mm)
H=7*pitch+2*(Rfo+O);   % CASMO CHW, assembly inner distance
```

```
GAW=7.5; %Wide water gap (mm)
GAN=7.5; %Narrow water gap (mm)
AOD = (H+2*J);  %Assembly Outer Dimension (mm)
UCD=(H+2*J+2*GAW)*(H+2*J+2*GAW);  %Unit Cell Dimension (mm2)
%_____________________________________________________
%                    Core Geometry
%_____________________________________________________
N_R = RTP/power*HCF;                  %  Number of annular rods
N_R_A=N_R/60;                  %  Number of assemblies (60 elements/assembly)
C_D=(  (N_R_A*UCD)*4/pi  )^0.5;        %Core diameter (mm)
n=round(100*(F_m_t+I_c_t+O_c_t+I_g_t+O_g_t));  %meshes => dr=0.01(mm) => n+1 radial nodes
j=round(C_H);                                  %dx =0.01(mm)=> j+1 axial nodes
dr=(Rfo-Rv)/n;                                 %radial node length (mm)
dx=C_H/j;                                      %axial   node length (mm)
extra_d=100;                                   %Extrapolation distance (mm) = 10 (cm)
C_H_extra=C_H+2*extra_d;                       %length over which n flux is nonzero (mm)
T_C_V=C_D*C_D*pi/4*C_H;                        %Total Core volume (mm3)
%_____________________________________________________
%                    Properties
%_____________________________________________________
k_SS=28.5E-3 ;                                 %T91 Thermal conductivity%(W/mmk)
k_gap=0.36E-3 ;   %Gap Thermal conductivity (W/mmk), adjusted based on FRAPCON model 08-15-10
k_UO2=3.0E-3 ;                                 %UO2 Thermal conductivity (W/mmk)
UO2_d=10.7E-6;                                 %UO2 density = 10.7 (g/cm3)= 10.7E-6(kg/mm3)
enrich=0.0635;                                 %enrichment
%=====================================================
%                    Pre-Calculations
%=====================================================
%  Reactor Core and power
%_____________________________________________________
T_F_V=((Rv+I_c_t+I_g_t+F_m_t)^2-(Rv+I_c_t+I_g_t)^2)*pi*C_H*N_R;  %Total Fuel volume (mm3)
T_F_M=T_F_V*UO2_d;                             %Total Fuel Mass (kg)
power_d=RTP/1000/T_C_V*1.0E6;          %power density (kW/L)
S_power=RTP/(T_F_M/1000*(235*enrich+238*(1-enrich)/(16*2+235*enrich+238*(1-enrich))))          ;
%Specific power (W/g); Definitaion see T&K P33
qqq=power/(T_F_V/N_R);                 %Volumetric heat generation of fuel meat (W/mm3)
qqq_p(j+1)=0.;                 %Axial power profile (default=cos)
```

```
%==========================================================
%                Matrix
%==========================================================
h_FW(j+1)=0.;                    %Fluid heat transfer coe.
h_ST(j+1)=0.;                    %Steam heat transfer coe.
h_FC(j+1)=0.;                    %Subcooled boiling, 2 phase FC
h_NB(j+1)=0.;                    %Subcooled boiling, NB
T_FW(j+1)=0.;                    %Feed water temp. (C)
T_ST(j+1)=0.;                    %Steam temp. (C)
%T_FW(1)=277 ;                   %Feed Water inlet temp. = 277 C =550K
%T_ST(1)=290 ;                   %Steam inlet temp. = 290 C= 563K
T_W_FW(j+3)=0.;                  %T wall, Feed water side temp. (C)
T_W_ST(j+1)=0.;                  %T wall, Steam side temp. (C)
H_FW(j+1)=0.;                    %Fluid enthalpy (KJ/Kg)
%H_FW(1)=XSteam('h_pT',pressure,T_FW(1));          %Fluid enthalpy (KJ/Kg)
H_ST(j+1)=0.;                    %Steam enthalpy (KJ/Kg)
HM=T_F_M*1000/(235*enrich+238*(1-enrich)+16*2);          %moles of UO2; Refer to Xu's thesis
(4.3) P95
Hydro_ST(j+1)=0.;                %moles of hydrogen in steam channel
Hydro_FW(j+1)=0.;                %moles of hydrogen in water channel
H_over_HM(j+1)=0.;
%H_ST(1)=XSteam('h_pT',pressure,T_ST(1));          %Steam enthalpy (KJ/Kg)
qua(j+1)=0.;                     %Fluid quality
Xe(j+1)=0.;                      %Equilebrium quality
Xc(j+1)=0.;                      %Critical quality
phi_fo2(j+1)=1.;                 % 2 phase friction factor multiplier
rho_ST(j+1)=0.;                  %Steam channel density (kg/m3)
rho_FW(j+1)=0.;                  %Water channel density (kg/m3)
%rho_FW(1)=XSteam('rho_pT',pressure,T_FW(1));
rho_ST_AVG(j+1)=0.;                    %Steam channel (AVG of Core A & B) density (kg/m3)
rho_FW_AVG(j+1)=0.;                    %Water channel (AVG of Core A & B) density (kg/m3)
% rho_m_S = rho_m_D if HEU model is used, see T&K p488
V_ST(j+1)=0.;                    %Steam velocity
V_FW(j+1)=0.;                    %Water velovity
vo_A(j+1)=0.;                    %Void fraction of Core A
vo_B(j+1)=0.;                    %Void fraction of Core B
%==========================================================
```

```
%Set up equations
%=========================================================
r=Rv:dr:Rfo;                    %radius for each mesh
A=zeros(n+1,n+1);               %Solve Ax=B
x=zeros(n+1,1);                 %x=temp. distribution
B=zeros(1,n+1);                 %Source term
% Set up thermal conductivity K (W/mm-k)
K(n)=0. ;                       %Thermal conductivity (W/mk)
K(1:round(I_c_t*100))=k_SS ;                %K_SS-306=21.5
K(round(I_c_t*100)+1:round((I_c_t+I_g_t)*100))=k_gap ;      %K_Gap (He)=0.15
K(round((I_c_t+I_g_t)*100)+1:round((I_c_t+I_g_t+F_m_t)*100))=k_UO2                ;
%K_UO2=3 [can be f(T)]
K(round((Rfo-Rv-O_g_t-O_c_t)*100)+1:round((Rfo-Rv-O_c_t)*100))=k_gap  ;          %K_Gap
(He)=0.15
%K(381:430)=k_zr ;              %K_Zir2=16.8
K(round((Rfo-Rv-O_c_t)*100)+1:n)=k_SS ;          %Use only SS for cladding 092008 yko
%-----------------------------------------------------------
% Set up matrix A
for i=2:n
    A(i,i-1)=K(i-1)/dr*(r(i-1)+0.5*dr);
    A(i,i)=-1.0/dr*(K(i-1)*(r(i-1)+0.5*dr)+K(i)*(r(i+1)-0.5*dr));
    A(i,i+1)=K(i)/dr*(r(i+1)-0.5*dr);
end
%Solution
TEMP=zeros(j+2,n+1); %TEMP=zeros(3001,431)
TEMP(1,:)=r ;
%=========================================================
%Units conversion (mm) -> (m) for heat transfer correlations
%=========================================================
De_FWc=De_FW/1000.  ;                   %Fluid hydraulic equivalent dia (m)
De_STc=De_ST/1000.  ;                   %Gas hydraulic equivalent dia (m)
Dh_FWc=Dh_FW/1000.  ;                   %Fluid heated equivalent dia (m)
Dh_STc=Dh_ST/1000.  ;                   %Gas heated equivalent dia (m)
pitchc=pitch/1000.;                     %Pitch = 0.024 (m)
Rfoc=Rfo/1000.;                         %Rod radius (m)
%=========================================================
% SET UP Power profile
```

```
%==========================================================
%Axial power profile Switch
%APPS = 3; %1=chopped cos; 2= uniform; 3=BWR profile
% if APPS ==1; %Chopped COS
% for z=1:j+1;
% %Calculate axial power profile
% %1.  %cosine shape
% %qqq_p(z)=pi*qqq*cos(((z-1)/C_H-0.5)*pi)/2;     %cosine shape
% qqq_p(z)=qqq*(C_H/C_H_extra)*(pi/2)/sin(pi/2*C_H/C_H_extra)...
% *cos((((z-1)-0.5*C_H)/C_H_extra)*pi);     %chopped cosine => see note P1
% %=> For chopped cos => Output_B(1974,52));   %Max cladding
% end
% end
% if APPS==2;          %2.  %Uniform profile
% for z=1:j+1;
% qqq_p(z)=qqq;   %Uniform profile
% % Remember to change the PEAK cladding temp tracking location!!!!
% %=> For Uniform Profile => Output_B(3002,52));   %Max cladding
% end
% end
%if APPS==3;%3. Typical BWR
% Remember to change the PEAK cladding temp tracking location!!!!
%=> For BWR Profile => Output_B(2436,52));   %Max cladding
qqq_p(1)=0.0;     %BWR profile
qqq_p(63)=0.38;     %BWR profile
qqq_p(188)=0.69;     %BWR profile
qqq_p(313)=0.93;     %BWR profile
qqq_p(438)=1.1;     %BWR profile
qqq_p(563)=1.21;     %BWR profile
qqq_p(688)=1.3;     %BWR profile
qqq_p(813)=1.47;     %BWR profile
qqq_p(938)=1.51;     %BWR profile
qqq_p(1063)=1.49;     %BWR profile
qqq_p(1188)=1.44;     %BWR profile
qqq_p(1313)=1.36;     %BWR profile
qqq_p(1438)=1.28;     %BWR profile
qqq_p(1563)=1.16;     %BWR profile
```

```
qqq_p(1688)=1.06;     %BWR profile
qqq_p(1813)=1.01;     %BWR profile
qqq_p(1938)=0.97;     %BWR profile
qqq_p(2063)=0.94;     %BWR profile
qqq_p(2188)=0.97;     %BWR profile
qqq_p(2313)=0.96;     %BWR profile
qqq_p(2438)=0.91;     %BWR profile
qqq_p(2563)=0.77;     %BWR profile
qqq_p(2688)=0.59;     %BWR profile
qqq_p(2813)=0.38;     %BWR profile
qqq_p(2938)=0.12;     %BWR profile
qqq_p(3001)=0.;     %BWR profile

for z=2:63;
    qqq_p(z)=(0.38/62+qqq_p(z-1));
end
for uu=1:1:23;
for z=1:1:125;

qqq_p(63+(uu-1)*125+z)=((qqq_p(63+uu*125)-qqq_p(63+(uu-1)*125))/125+qqq_p(63+(uu-1)*125+z-1));
end
end
for z=2939:3001;
    qqq_p(z)=(-0.12/63+qqq_p(z-1));
end

qqq_p=qqq_p/2984.31*3001*qqq;
%end
%end
%=================================================
%Calculate Core A (1st half)
%=================================================
Heat_FW=0.66;    %Initial guess of power split: % of heat transferred by FW
T_FW_inlet=278.3; %Initial guess of FW inlet temp
T_FW(j+1)=XSteam('Tsat_p',pressure);
T_ST(j+1)=290.; %Assume the inlet steam has been preheated to this temp
H_ST(j+1)=XSteam('h_pT',pressure,T_ST(j+1));
```

```
T_W_FW(j+2)=XSteam('Tsat_p',pressure)+3.; %Guess delta T is close to 3 degree C
        %This is reasonable because outlet T_FW is known = TSat
        %Inlet T_ST is also known = 290 (assumed preheated)
        %With these two knowns the 3 degree C is a good guess
T_W_FW(j+3)=T_W_FW(j+2);
T_SUB=XSteam('Tsat_p',pressure)+5;   %Assume 5 degree c for onset of subcooled boiling
%-------------------------------------
%   Calculate heat transfer coef. => BCs for linear equations
%-------------------------------------
for y=1:10;

SUB=1.0; %indicator to distinguish single phase, subcooled and saturated booiling
hhh(j+1)=0.;   %Heat transfer mode indicator: 1=SP, 2=suncooled, 3=saturated
guess_heat_FW = Heat_FW*power/1000; %(kW)
H_FW(j+1)=guess_heat_FW/m_FW+XSteam('h_pT',pressure,T_FW_inlet);   %(kJ/kg)
% Converge if calculated T_FW(1) = guessed T_FW(1)
Xe(j+1)=(H_FW(j+1)-XSteam('hL_p',pressure))/(XSteam('hV_p',pressure)-XSteam('hL_p',pressure));
%m_ST=m_FW/(1-USCF)*(Xe(j+1)+0.141)/2; %(kg/s), full core flow rate * exit quality
                                    %Need to take into account the qaulity of
                                    %other half of core
 m_ST=2*m_FW*OHOT;    %Assumed m_FW controled by orifice   ! TWO passes for steam flow
 m_ST=m_ST*DFF;         % up/down factor   07/20/2010
 m_STd=m_ST;   %Down flow of steam

for z=j+1:-1:1;
%Equilibrium quality
Xe(z)=(H_FW(z)-XSteam('hL_p',pressure))/(XSteam('hV_p',pressure)-XSteam('hL_p',pressure));
if Xe(z)<0.; %single phase or subcooled boiling
    qua(z)=0.; %No saturated boiling
    if   T_W_FW(min(j+1,(z+1)))<T_SUB-2.; %Assume Subcooled boiling will cool down T_wall to +3
superheat
        SUB =0.1; %single phase
    end
    h_FC(z)=D_B(pressure,T_FW(z),De_FWc,Dh_FWc,m_FW,1);
    h_NB(z)=0.;
    h_FW(z)=h_FC(z)+h_NB(z);
    hhh(z)=1.0;
```

```
    if SUB>0.5;
    h_FC(z)=Chen_h_2(pressure,qua(z),T_FW(z),max(T_SUB,T_W_FW(z+1)),De_FWc,m_FW,1);
    h_NB(z)=Chen_h_NB(pressure,qua(z),T_FW(z),max(T_SUB,T_W_FW(z+1)),De_FWc,m_FW,1);
    h_FW(z)=h_FC(z)+h_NB(z);
    hhh(z)=2.0;
    end

else %Saturated boiling
    qua(z)=Xe(z);

h_FC(z)=Chen_h_2(pressure,qua(z),T_FW(z),(T_W_FW(z+1)+T_W_FW(z+2))/2,De_FWc,m_FW,1);

h_NB(z)=Chen_h_NB(pressure,qua(z),T_FW(z),(T_W_FW(z+1)+T_W_FW(z+2))/2,De_FWc,m_FW,1);
    h_FW(z)=h_FC(z)+h_NB(z);
    hhh(z)=3.0;

end
    h_FW(z)=h_FW(z)/1.0E6;          %unit conversion (W/m2-K)->(W/mm2-K)
    h_FC(z)=h_FC(z)/1.0E6;          %unit conversion (W/m2-K)->(W/mm2-K)
    h_NB(z)=h_NB(z)/1.0E6;          %unit conversion (W/m2-K)->(W/mm2-K)
    h_ST(z)=Gni(pressure,T_ST(z),De_STc,Dh_STc,m_ST,1);   %Gnielinski
    h_ST(z)=h_ST(z)/1.0E6;          %unit conversion (W/m2-K)->(W/mm2-K)
%-----------------------------------------------------------------
%Set up source term
%-----------------------------------------------------------------
for i=2:n
B(i)=-qqq_p(z)*r(i)*dr;   % Set up matrix B
end
% Interface Boundary condition (IBC 2&5)
B(1:round((I_c_t+I_g_t)*100))=0;
B(round((I_c_t+I_g_t+F_m_t)*100)+2:n+1)=0;
% Interface Boundary condition (IBC 3&4)
B(round((I_c_t+I_g_t)*100)+1)=-qqq_p(z)*dr/4*(2*r(round((I_c_t+I_g_t)*100)+1)+0.5*dr);
B(round((I_c_t+I_g_t+F_m_t)*100)+1)=-qqq_p(z)*dr/4*(2*r(round((I_c_t+I_g_t+F_m_t)*100)+1)-0.5*dr
);
% Boundary condition 1: given steam h and temp.
A(1,1)=-K(1)/dr*(r(1)+0.5*dr)-h_ST(z)*r(1);
```

```
A(1,2)=K(1)/dr*(r(1)+0.5*dr);
B(1)=-h_ST(z)*r(1)*T_ST(z);
% Boundary condition 6: given water h and temp.
A(n+1,n)=K(n)/dr*(r(n)+0.5*dr);
A(n+1,n+1)=-K(n)/dr*(r(n)+0.5*dr)-(h_FC(z)+h_NB(z))*r(n+1);
B(n+1)=-(h_NB(z)*XSteam('Tsat_p',pressure)+h_FC(z)*T_FW(z))*r(n+1);
%Solution = save in TEMP
x=A\B';
%TEMP(j+2-z,:)=x'; %X-direction upwards
TEMP(z+1,:)=x';   %X-direction downwards
T_W_ST(z)=x(1);
T_W_FW(z)=x(n+1);
%CORE A => Steam flows downwards => "-"
if (z-1)>0;
H_ST(z-1)=H_ST(z)+h_ST(z)*(x(1)-T_ST(z))*2*Rv*pi*dx/(m_ST/1)/1.0E3; %"+" HERE
H_FW(z-1)=H_FW(z)-(h_FC(z)*(T_W_FW(z)-T_FW(z))+h_NB(z)*(T_W_FW(z)-XSteam('Tsat_p',pressu
re)))*2*Rfo*pi*dx/(m_FW/1)/1.0E3;
T_ST(z-1)=XSteam('T_ph',pressure,H_ST(z-1));
T_FW(z-1)=XSteam('T_ph',pressure,H_FW(z-1));
end
qq_ST(z)=h_ST(z)*(T_W_ST(z)-T_ST(z))*1.0E6; %(W/m2)    steam side heat flux
qq_FW(z)=(h_FC(z)*(T_W_FW(z)-T_FW(z))+h_NB(z)*(T_W_FW(z)-XSteam('Tsat_p',pressure)))*1.0E6;
%(W/m2)    water side heat flux
%qq_CHF3(z)=CHF_03(pressure,Xe(z),277,qq_FW(z),De_FWc,m_FW,N_R);    %EPRI-1 CHF, assume
T_FW inlet = 277
%----------Calculate velocity----------
V_ST(z)=m_ST/fA_ST/XSteam('rho_pT',pressure,T_ST(z))*1.0E6;    %(m/s)
%----------Calculate velocity----------
end
if abs(T_FW_inlet-T_FW(1))>1.5;
    if T_FW_inlet<T_FW(1);%Boiling length too long => need to reduce heat into FW
        Heat_FW=Heat_FW-0.01;
    else                        %Boiling length too short => need to add heat into FW
        Heat_FW=Heat_FW+0.01;
    end
else
    break;
```

```
end
end

if abs(T_FW_inlet-T_FW(1))<1.5;
%-------------[     Output CORE A RESULTS    ]--------------------------
%Output T_ST, TEMP and T_FW:12345=ST; 91011=FW
Output=[12345 T_ST(1:j+1);91011 T_FW(1:j+1)]; %no need T_ST(j+2)& T_FW(j+2)
Output=Output';       %   Output_A = Core A results
Output_A=[Output(:,1) TEMP Output(:,2)]; %output axial temp
Out_A=Output_A';                                    %output radial temp
h_ST_A=h_ST'*1.0E6;       %output ST heat transfer coe.   (W/m2)
h_FW_A=h_FW'*1.0E6;       %output FW heat transfer coe.   (W/m2)
qq_ST_A=qq_ST'/1000;% (W/m2)=> (kW/m2);          %output steam side heat flux
qq_FW_A=qq_FW'/1000;% (W/m2)=> (kW/m2);          %output water side heat flux
q_ST_A=(H_ST(j+1)-H_ST(1))*N_R*NofD/60*m_ST/1.0E3*(-1);   %output ST heat transfer (MW) "-"
HERE
q_FW_A=(H_FW(j+1)-H_FW(1))*N_R*NofD/60*m_FW/1.0E3;   %output FW heat transfer (MW)
qua_A=qua';
V_ST_A=V_ST';   %output steam velovity (m/s)
H_ST_A=H_ST';

for z=1:j+1;
     if Xe(z)>0.;
vo_A(z)=EPRI_v(pressure,Xe(z),De_FWc,m_FW);
     else
          vo_A(z)=0.;
     end
rho_FW(z)=XSteam('rhoV_p',pressure)*vo_A(z)+(1-vo_A(z))*XSteam('rhoL_p',pressure);
rho_ST(z)=XSteam('rho_pT',pressure,T_ST(z));
end
vo_A=vo_A';
Xe_A=Xe';
Xc_A=Xc';
hhh=hhh';
rho_FW_A=rho_FW';   %kg/m3
rho_ST_A=rho_ST';   %kg/m3
```

```
else
    return;
end

%$$$$$$$$$$$$$$$$$$$$$$$$$$$$$$$$$$$$$$$$$$$$$$$$$$$$$$$$$$$$$$$$$$$$$$$$
%   Calculating HEAT LOSS in the non-active region
%$$$$$$$$$$$$$$$$$$$$$$$$$$$$$$$$$$$$$$$$$$$$$$$$$$$$$$$$$$$$$$$$$$$$$$$$
C_H_n = 200.;                       %Non-active length (mm)
w=round(C_H_n);                     %dx =0.01(mm)=> j+1 axial nodes
%=====================================================================
%                 Matrix
%=====================================================================
h_FWn(w+1)=0.;                      %Fluid heat transfer coe.
h_STn(w+1)=0.;                      %Steam heat transfer coe.
T_FWn(w+1)=0.;                      %Feed water temp. (C)
T_STn(w+1)=0.;                      %Steam temp. (C)
T_W_FWn(w+1)=0.;                    %T wall, Feed water side temp. (C)
T_W_STn(w+1)=0.;                    %T wall, Steam side temp. (C)
H_FWn(w+1)=0.;                      %Fluid enthalpy (KJ/Kg)
H_STn(w+1)=0.;                      %Steam enthalpy (KJ/Kg)
rho_STn(w+1)=0.;                    %Steam channel density (kg/m3)
rho_FWn(w+1)=0.;                    %Water channel density (kg/m3)
V_STn(w+1)=0.;                      %Steam velocity
V_FWn(w+1)=0.;                      %Water velovity
%=====================================================================
%Set up equations
%=====================================================================
r=Rv:dr:Rfo;                        %radius for each mesh
A=zeros(n+1,n+1);                   %Solve Ax=B
x=zeros(n+1,1);                     %x=temp. distribution
B=zeros(1,n+1);                     %Source term
% Set up thermal conductivity K (W/mm-k)
K(n)=0. ;                           %Thermal conductivity (W/mk)
K(1:n)=k_SS ;                       %K_SS-306=21.5
%-----------------------------------------------------------------
% Set up matrix A
for i=2:n
```

```
    A(i,i-1)=K(i-1)/dr*(r(i-1)+0.5*dr);
    A(i,i)=-1.0/dr*(K(i-1)*(r(i-1)+0.5*dr)+K(i)*(r(i+1)-0.5*dr));
    A(i,i+1)=K(i)/dr*(r(i+1)-0.5*dr);
end
%Solution
TEMPn=zeros(w+2,n+1);
TEMPn(1,:)=r ;
%=========================================================
%Calculate NON-active Core A (1st half)
%=========================================================
T_FWn(w+1)=T_FW(1)-0.0174;   %temp difference in the first axial node
T_STn(w+1)=T_ST(1)-0.0437;   %temp difference in the first axial node
H_STn(w+1)=XSteam('h_pT',pressure,T_STn(w+1));
H_FWn(w+1)=XSteam('h_pT',pressure,T_FWn(w+1));   %(kJ/kg)
%---------------------------------
%   Calculate heat transfer coef. => BCs for linear equations
%---------------------------------
for i=2:n
    A(i,i-1)=K(i-1)/dr*(r(i-1)+0.5*dr);
    A(i,i)=-1.0/dr*(K(i-1)*(r(i-1)+0.5*dr)+K(i)*(r(i+1)-0.5*dr));
    A(i,i+1)=K(i)/dr*(r(i+1)-0.5*dr);
end

%for z=j+1:-1:1;
for z=w+1:-1:1;
% Calculate heat transfer coef.
     h_FWn(z)=D_B(pressure,T_FWn(z),De_FWc,Dh_FWc,m_FW,1);
     h_FWn(z)=h_FWn(z)/1.0E6;                %unit conversion (W/m2-K)->(W/mm2-K)
     h_STn(z)=Gni(pressure,T_STn(z),De_STc,Dh_STc,m_ST,1);   %Gnielinski
     h_STn(z)=h_STn(z)/1.0E6;                %unit conversion (W/m2-K)->(W/mm2-K)
%-----------------------------------------------------------------
%Set up source term
%-----------------------------------------------------------------
for i=2:n
B(i)=0.;   % Set up matrix B
end
% Interface Boundary condition (IBC 2&5)
```

```
B(1:round((l_c_t+l_g_t)*100))=0;                %No source; non-active region
B(round((l_c_t+l_g_t+F_m_t)*100)+2:n+1)=0; %No source; non-active region
% Interface Boundary condition (IBC 3&4)
B(round((l_c_t+l_g_t)*100)+1)=0;                %No source; non-active region
B(round((l_c_t+l_g_t+F_m_t)*100)+1)=0;          %No source; non-active region
% Boundary condition 1: given steam h and temp.
A(1,1)=-K(1)/dr*(r(1)+0.5*dr)-h_STn(z)*r(1);
A(1,2)=K(1)/dr*(r(1)+0.5*dr);
B(1)=-h_STn(z)*r(1)*T_STn(z);
% Boundary condition 6: given water h and temp.
A(n+1,n)=K(n)/dr*(r(n)+0.5*dr);
A(n+1,n+1)=-K(n)/dr*(r(n)+0.5*dr)-(h_FWn(z))*r(n+1);
B(n+1)=-(h_FWn(z)*T_FWn(z))*r(n+1);
%Solution = save in TEMP
x=A\B';
%TEMP(j+2-z,:)=x'; %X-direction upwards
TEMPn(z+1,:)=x';   %X-direction downwards
T_W_STn(z)=x(1);
T_W_FWn(z)=x(n+1);
%CORE A => Steam flows downwards => "-"
if (z-1)>0;
H_STn(z-1)=H_STn(z)-h_STn(z)*(T_STn(z)-x(1))*2*Rv*pi*dx/(m_ST/1)/1.0E3; %"-" HERE
H_FWn(z-1)=H_FWn(z)-(h_FWn(z)*(T_W_FWn(z)-T_FWn(z)))*2*Rfo*pi*dx/(m_FW/1)/1.0E3;
T_STn(z-1)=XSteam('T_ph',pressure,H_STn(z-1));
T_FWn(z-1)=XSteam('T_ph',pressure,H_FWn(z-1));
end
qq_STn(z)=h_STn(z)*(T_W_STn(z)-T_STn(z))*1.0E6; %(W/m2)    steam side heat flux
qq_FWn(z)=(h_FWn(z)*(T_W_FWn(z)-T_FWn(z)))*1.0E6; %(W/m2)    water side heat flux
%--------------Calculate velocity------------
V_STn(z)=m_ST/fA_ST/XSteam('rho_pT',pressure,T_STn(z))*1.0E6;    %(m/s)
%--------------Calculate velocity------------
end

%-------------[     Output CORE A RESULTS    ]--------------------------
%Output T_ST, TEMP and T_FW:12345=ST; 91011=FW
Outputn=[12345 T_STn(1:w+1);91011 T_FWn(1:w+1)]; %no need T_ST(j+2)& T_FW(j+2)
Outputn=Outputn';       %    Output_A = Core A results
```

```
Output_An=[Outputn(:,1) TEMPn Outputn(:,2)]; %output axial temp
Out_An=Output_An';                                  %output radial temp
h_ST_An=h_STn'*1.0E6;      %output ST heat transfer coe.   (W/m2)
h_FW_An=h_FWn'*1.0E6;      %output FW heat transfer coe.   (W/m2)
qq_ST_An=qq_STn'/1000;% (W/m2)=> (kW/m2);          %output steam side heat flux
qq_FW_An=qq_FWn'/1000;% (W/m2)=> (kW/m2);          %output water side heat flux
q_ST_An=(H_STn(w+1)-H_STn(1))*N_R*NofD/60*m_ST/1.0E3*(-1);   %output ST heat transfer (MW)
"-" HERE
q_FW_An=(H_FWn(w+1)-H_FWn(1))*N_R*NofD/60*m_FW/1.0E3;   %output FW heat transfer (MW)
V_ST_An=V_STn';   %output steam velovity (m/s)
H_ST_An=H_STn';
H_FW_An=H_FWn';

for z=1:w+1;
rho_FWn(z)=XSteam('rho_pT',pressure,T_FWn(z));
rho_STn(z)=XSteam('rho_pT',pressure,T_STn(z));
end
rho_FW_An=rho_FWn';   %kg/m3
rho_ST_An=rho_STn';   %kg/m3

%=========================================================
%Calculate NON-active Core B (2nd half)
%=========================================================
%---------------------------------
%   Calculate heat transfer coef. => BCs for linear equations
%---------------------------------
H_FW(j+1)=XSteam('h_pT',pressure,T_FW(j+1));   %(kJ/kg)
 m_ST=m_ST/DFF*UFF;   %adusted flowrate
 m_STu=m_ST;          %up steam flow

for z=1:1:w+1;
     h_FWn(z)=D_B(pressure,T_FWn(z),De_FWc,Dh_FWc,m_FW,1);
     h_FWn(z)=h_FWn(z)/1.0E6;                %unit conversion (W/m2-K)->(W/mm2-K)
     h_STn(z)=Gni(pressure,T_STn(z),De_STc,Dh_STc,m_ST,1);   %Gnielinski
     h_STn(z)=h_STn(z)/1.0E6;                %unit conversion (W/m2-K)->(W/mm2-K)
%-------------------------------------------------------------
%Set up source term
```

```
%-------------------------------------------------------------
for i=2:n
B(i)=0.;   % Set up matrix B
end
% Interface Boundary condition (IBC 2&5)
B(1:round((I_c_t+I_g_t)*100))=0;
B(round((I_c_t+I_g_t+F_m_t)*100)+2:n+1)=0;
% Interface Boundary condition (IBC 3&4)
B(round((I_c_t+I_g_t)*100)+1)=0;
B(round((I_c_t+I_g_t+F_m_t)*100)+1)=0;
% Boundary condition 1: given steam h and temp.
A(1,1)=-K(1)/dr*(r(1)+0.5*dr)-h_STn(z)*r(1);
A(1,2)=K(1)/dr*(r(1)+0.5*dr);
B(1)=-h_STn(z)*r(1)*T_STn(z);
% Boundary condition 6: given water h and temp.
A(n+1,n)=K(n)/dr*(r(n)+0.5*dr);
A(n+1,n+1)=-K(n)/dr*(r(n)+0.5*dr)-(h_FWn(z))*r(n+1);
B(n+1)=-(h_FWn(z)*T_FWn(z))*r(n+1);
%Solution = save in TEMP
x=A\B';
%TEMP(j+2-z,:)=x'; %X-direction upwards
TEMPn(z+1,:)=x';   %X-direction downwards
T_W_STn(z)=x(1);
T_W_FWn(z)=x(n+1);
%CORE A => Steam flows downwards => "-"
H_STn(z+1)=H_STn(z)-h_STn(z)*(T_STn(z)-x(1))*2*Rv*pi*dx/(m_ST/1)/1.0E3; %"-" HERE
H_FWn(z+1)=H_FWn(z)+(h_FWn(z)*(T_W_FWn(z)-T_FWn(z)))*2*Rfo*pi*dx/(m_FW/1)/1.0E3;
T_STn(z+1)=XSteam('T_ph',pressure,H_STn(z+1));
T_FWn(z+1)=XSteam('T_ph',pressure,H_FWn(z+1));
qq_STn(z)=h_STn(z)*(T_W_STn(z)-T_STn(z))*1.0E6; %(W/m2)    steam side heat flux
qq_FWn(z)=(h_FWn(z)*(T_W_FWn(z)-T_FWn(z)))*1.0E6; %(W/m2)    water side heat flux
%---------------Calculate velocity-------------
V_STn(z)=m_ST/fA_ST/XSteam('rho_pT',pressure,T_STn(z))*1.0E6;    %(m/s)
%---------------Calculate velocity-------------
end
%-------------[     Output CORE A RESULTS    ]--------------------------
Outputn=[12345 T_STn(1:w+1);91011 T_FWn(1:w+1)]; %no need T_ST(j+2)& T_FW(j+2)
```

```
Outputn=Outputn';      %   Output_A = Core A results
Output_Bn=[Outputn(:,1) TEMPn Outputn(:,2)]; %output axial temp
Out_Bn=Output_Bn';                                    %output radial temp
h_ST_Bn=h_STn'*1.0E6;      %output ST heat transfer coe.   (W/m2)
h_FW_Bn=h_FWn'*1.0E6;      %output FW heat transfer coe.   (W/m2)
qq_ST_Bn=qq_STn'/1000;% (W/m2)=> (kW/m2);        %output steam side heat flux
qq_FW_Bn=qq_FWn'/1000;% (W/m2)=> (kW/m2);        %output water side heat flux
q_ST_Bn=(H_STn(w+1)-H_STn(1))*N_R*(60-NofD)/60*m_ST/1.0E3;   %output ST heat transfer (MW)
"-" HERE
q_FW_Bn=(H_FWn(w+1)-H_FWn(1))*N_R*(60-NofD)/60*m_FW/1.0E3;   %output FW heat transfer
(MW)
V_ST_Bn=V_STn';   %output steam velovity (m/s)
H_ST_Bn=H_STn';
H_FW_Bn=H_FWn';

for z=1:w+1;
rho_FWn(z)=XSteam('rho_pT',pressure,T_FWn(z));
rho_STn(z)=XSteam('rho_pT',pressure,T_STn(z));
end
rho_FW_Bn=rho_FWn';   %kg/m3
rho_ST_Bn=rho_STn';   %kg/m3
%else
 %     return;
%end

%$$$$$$$$$$$$$$$$$$$$$$$$$$$$$$$$$$$$$$$$$$$$$$$$$$$$$$$$$$$$$$$$$$$$$$$$$$$$

%==================================================================
%Calculate Core B (2nd half)
%______________________________________________________
%==================================================================
%                 Matrix
%==================================================================
h_FW(:)=0.;                      %Fluid heat transfer coe.
h_ST(:)=0.;                      %Steam heat transfer coe.
h_FC(:)=0.;                      %Subcooled boiling, 2 phase FC
h_NB(:)=0.;                      %Subcooled boiling, NB
```

```
T_FW(:)=0.;                    %Feed water temp. (C)
T_ST(:)=0.;                    %Steam temp. (C)
T_W_FW(:)=0.;                  %T wall, Feed water side temp. (C)
T_W_ST(:)=0.;                  %T wall, Steam side temp. (C)
H_FW(:)=0.;                    %Fluid enthalpy (KJ/Kg)
H_ST(:)=0.;                    %Steam enthalpy (KJ/Kg)
Hydro_ST(:)=0.;                %moles of hydrogen in steam channel
Hydro_FW(:)=0.;                %moles of hydrogen in water channel
H_over_HM(:)=0.;
qua(:)=0.;                     %Fluid quality
Xe(:)=0.;                      %Equilebrium quality
Xc(:)=0.;                      %Critical quality
rho_ST_AVG(:)=0.;              %Steam channel (AVG of Core A & B) density (kg/m3)
rho_FW_AVG(:)=0.;              %Water channel (AVG of Core A & B) density (kg/m3)
phi_fo2(:)=1.;                 % 2 phase friction factor multiplier
rho_ST(:)=0.;                  %Steam channel density (kg/m3)
rho_FW(:)=0.;                  %Water channel density (kg/m3)
%================================================================
%Set up equations
%================================================================
A=zeros(n+1,n+1);              %Solve Ax=B
x=zeros(n+1,1);                %x=temp. distribution
B=zeros(1,n+1);                %Source term
%----------------------------------------------------------------
% Set up thermal conductivity K (W/mm-k)
K(1:round(I_c_t*100))=k_SS ;                    %K_SS-306=21.5
K(round(I_c_t*100)+1:round((I_c_t+I_g_t)*100))=k_gap ;          %K_Gap (He)=0.15
K(round((I_c_t+I_g_t)*100)+1:round((I_c_t+I_g_t+F_m_t)*100))=k_UO2                              ;
%K_UO2=3 [can be f(T)]
K(round((Rfo-Rv-O_g_t-O_c_t)*100)+1:round((Rfo-Rv-O_c_t)*100))=k_gap  ;                  %K_Gap
(He)=0.15
%K(381:430)=k_zr ;              %K_Zir2=16.8
K(round((Rfo-Rv-O_c_t)*100)+1:n)=k_SS ;                 %Use only SS for cladding 092008 yko
%----------------------------------------------------------------
% Set up matrix A
for i=2:n
    A(i,i-1)=K(i-1)/dr*(r(i-1)+0.5*dr);
```

```
    A(i,i)=-1.0/dr*(K(i-1)*(r(i-1)+0.5*dr)+K(i)*(r(i+1)-0.5*dr));
    A(i,i+1)=K(i)/dr*(r(i+1)-0.5*dr);
end
%Solution
TEMP=zeros(j+2,n+1); %TEMP=zeros(3001,431)
TEMP(1,:)=r ;
%=================================================
%Solve Core B
%=================================================
T_ST(1)=T_STn(w+1)+0.0437;   %temp difference in the first axial node;
%!!!!!!!!!   ST inlet temp From the non-active CORE B
H_ST(1)=XSteam('h_pT',pressure,T_ST(1));          %Steam enthalpy (KJ/Kg)
T_FW(1)=T_FWn(w+1)+0.0174;          %!!!!!!!!!   FW inlet temp From the non-active CORE B
H_FW(1)=XSteam('h_pT',pressure,T_FW(1));          %Steam enthalpy (KJ/Kg)

%-------------------------------------
%   Calculate heat transfer coef. => BCs for linear equations
%-------------------------------------
SUB=0.1; %indicator to distiguish single phase, subcooled and saturated booiling
T_SUB=XSteam('Tsat_p',pressure)+5;   %Assume 5 degree c for onset of subcooled boiling
for z=1:j+1;
Xe(z)=(H_FW(z)-XSteam('hL_p',pressure))/(XSteam('hV_p',pressure)-XSteam('hL_p',pressure));
if Xe(z)<0; %single phase or subcooled boiling
    qua(z)=0.; %No saturated boiling
    if   T_W_FW(max(1,(z-1)))>T_SUB
        SUB =1.0; %subcooled phase
    end
    h_FC(z)=D_B(pressure,T_FW(z),De_FWc,Dh_FWc,m_FW,1);
    h_NB(z)=0.;
    h_FW(z)=h_FC(z)+h_NB(z);
     hhh(z)=1.0;
    if SUB>0.5;

h_FC(z)=Chen_h_2(pressure,qua(z),T_FW(z),max(T_SUB,max(T_W_FW(max(1,(z-1))),T_W_FW(max(1
,(z-2)))),De_FWc,m_FW,1);

h_NB(z)=Chen_h_NB(pressure,qua(z),T_FW(z),max(T_SUB,max(T_W_FW(max(1,(z-1))),T_W_FW(ma
```

```
x(1,(z-2))))),De_FWc,m_FW,1);
      h_FW(z)=h_FC(z)+h_NB(z);
       hhh(z)=2.0;
      end
else %Saturated boiling
 %
h_FW(z)=Chen(pressure,qua(z),T_FW(z),max(T_SUB,max(T_W_FW(max(1,(z-1))),T_W_FW(max(1,(z-
2))))),De_FWc,m_FW,N_R);
    qua(z)=Xe(z);
   hhh(z)=3.0;
      h_FC(z)=Chen_h_2(pressure,qua(z),T_FW(z),(T_W_FW(z-1)+T_W_FW(z-2))/2,De_FWc,m_FW,1);

h_NB(z)=Chen_h_NB(pressure,qua(z),T_FW(z),(T_W_FW(z-1)+T_W_FW(z-2))/2,De_FWc,m_FW,1);
      h_FW(z)=h_FC(z)+h_NB(z);

end
      h_FW(z)=h_FW(z)/1.0E6;                %unit conversion (W/m2-K)->(W/mm2-K)
      h_FC(z)=h_FC(z)/1.0E6;                %unit conversion (W/m2-K)->(W/mm2-K)
      h_NB(z)=h_NB(z)/1.0E6;                %unit conversion (W/m2-K)->(W/mm2-K)
      h_ST(z)=Gni(pressure,T_ST(z),De_STc,Dh_STc,m_ST,1);   %Gnielinski
      h_ST(z)=h_ST(z)/1.0E6;                %unit conversion (W/m2-K)->(W/mm2-K)

%-----------------------------------------------------------------
%Set up source term
%-----------------------------------------------------------------
for i=2:n
B(i)=-qqq_p(z)*r(i)*dr;   % Set up matrix B
end
% Interface Boundary condition (IBC 2&5)
B(1:round((I_c_t+I_g_t)*100))=0;
B(round((I_c_t+I_g_t+F_m_t)*100)+2:n+1)=0;
% Interface Boundary condition (IBC 3&4)
B(round((I_c_t+I_g_t)*100)+1)=-qqq_p(z)*dr/4*(2*r(round((I_c_t+I_g_t)*100)+1)+0.5*dr);
B(round((I_c_t+I_g_t+F_m_t)*100)+1)=-qqq_p(z)*dr/4*(2*r(round((I_c_t+I_g_t+F_m_t)*100)+1)-0.5*dr
);
% Boundary condition 1: given steam h and temp.
A(1,1)=-K(1)/dr*(r(1)+0.5*dr)-h_ST(z)*r(1);
```

```
A(1,2)=K(1)/dr*(r(1)+0.5*dr);
B(1)=-h_ST(z)*r(1)*T_ST(z);
% Boundary condition 6: given water h and temp.
A(n+1,n)=K(n)/dr*(r(n)+0.5*dr);
A(n+1,n+1)=-K(n)/dr*(r(n)+0.5*dr)-(h_FC(z)+h_NB(z))*r(n+1);
B(n+1)=-(h_NB(z)*XSteam('Tsat_p',pressure)+h_FC(z)*T_FW(z))*r(n+1);
%Solution = save in TEMP
x=A\B';
%TEMP(j+2-z,:)=x'; %X-direction upwards
TEMP(z+1,:)=x';   %X-direction downwards
%CORE B => Steam flows upwards => "+"
T_W_ST(z)=x(1);
T_W_FW(z)=x(n+1);
H_ST(z+1)=H_ST(z)+h_ST(z)*(x(1)-T_ST(z))*2*Rv*pi*dx/(m_ST/1)/1.0E3; %"+" HERE
H_FW(z+1)=H_FW(z)+(h_FC(z)*(T_W_FW(z)-T_FW(z))+h_NB(z)*(T_W_FW(z)-XSteam('Tsat_p',press
ure)))*2*Rfo*pi*dx/(m_FW/1)/1.0E3;
T_ST(z+1)=XSteam('T_ph',pressure,H_ST(z+1));
T_FW(z+1)=XSteam('T_ph',pressure,H_FW(z+1));
qq_ST(z)=h_ST(z)*(T_W_ST(z)-T_ST(z))*1.0E6; %(W/m2)   steam side heat flux
qq_FW(z)=h_FW(z)*(T_W_FW(z)-T_FW(z))*1.0E6; %(W/m2)   water side heat flux
%--------------Calculate velocity-----------
V_ST(z)=m_ST/fA_ST/XSteam('rho_pT',pressure,T_ST(z))*1.0E6;   %(m/s)

end
for z=1:j+1;
    if Xe(z) >= 0.
        Zsat=z; %Onset of saturated boiling (mm)
        break;
    end
end

%-------------[    Output CORE B RESULTS   ]-------------------------------
Output=[12345 T_ST(1:j+1);91011 T_FW(1:j+1)]; %no need T_ST(j+2)& T_FW(j+2)
Output=Output';      %   Output_A = Core A results
Output_B=[Output(:,1) TEMP Output(:,2)]; %output axial temp

h_ST_B=h_ST'*1.0E6;      %output ST heat transfer coe.   (W/m2)
```

```
h_FW_B=h_FW'*1.0E6;      %output FW heat transfer coe.  (W/m2)
qq_ST_B=qq_ST'/1000;% (W/m2)=> (kW/m2);          %output steam side heat flux
qq_FW_B=qq_FW'/1000;% (W/m2)=> (kW/m2);          %output water side heat flux
q_ST_B=(H_ST(j+1)-H_ST(1))*N_R*(60-NofD)/60*m_ST/1.0E3;   %output ST heat transfer (MW)
q_FW_B=(H_FW(j+1)-H_FW(1))*N_R*(60-NofD)/60*m_FW/1.0E3;   %output FW heat transfer (MW)
qua_B=qua';
V_ST_B=V_ST';   %output steam velovity (m/s)
H_ST_B=H_ST';
for z=1:j+1;
    if Xe(z)>0.;
vo_B(z)=EPRI_v(pressure,Xe(z),De_FWc,m_FW);
    else
        vo_B(z)=0.;
    end
rho_FW(z)=XSteam('rhoV_p',pressure)*vo_B(z)+(1-vo_B(z))*XSteam('rhoL_p',pressure);
rho_ST(z)=XSteam('rho_pT',pressure,T_ST(z));
end
vo_B=vo_B';
Xe_B=Xe';
Xc_B=Xc';
hhh=hhh';
rho_FW_B=rho_FW'; %kg/m3
rho_ST_B=rho_ST'; %kg/m3

%--------------[    Combine active and non-active cores      ]----------------
Output_A(1,:)=[]; %output axial temp
Output_A=[Output_An
          Output_A];
Out_A=Output_A';                                %output radial temp
Output_B(1,:)=[]; %output axial temp
Output_B=[Output_Bn
          Output_B];
Out_B=Output_B';                                %output radial temp
%--------------[    Combine active and non-active cores      ]----------------
%=============================
%Calculate steam channel dP
%=============================
```

```
G_STd=(m_STd/(De_STc^2*pi/4)/1); %Mass Flux of ST, (kg/m2-s)
G_STu=(m_STu/(De_STc^2*pi/4)/1); %Mass Flux of ST, (kg/m2-s)
for z=j+w+2:-1:2;
f_ST=SP_f(pressure,Output_A(z,1),De_STc,m_STd,1);
dP_fri_ST(2)=f_ST*dx/De_ST*0.5*G_STd^2/XSteam('rho_pT',pressure,Output_A(z,1));
dP_fri_ST(1)=dP_fri_ST(1)+dP_fri_ST(2);
dP_gra_ST(2)=XSteam('rho_pT',pressure,Output_A(z,1))*gravity*dx/1000; %(mm)=>(m)
dP_gra_ST(1)=dP_gra_ST(1)+dP_gra_ST(2);
end
dP_gra_ST(1)=-1*dP_gra_ST(1); %Pressure increase in the first half of the channel
for z=2:j+w+2;
f_ST=SP_f(pressure,Output_B(z,1),De_STc,m_STu,1);
dP_fri_ST(2)=f_ST*dx/De_ST*0.5*G_STu^2/XSteam('rho_pT',pressure,Output_B(z,1));
dP_fri_ST(1)=dP_fri_ST(1)+dP_fri_ST(2);
dP_gra_ST(2)=XSteam('rho_pT',pressure,Output_B(z,1))*gravity*dx/1000; %(mm)=>(m)
dP_gra_ST(1)=dP_gra_ST(1)+dP_gra_ST(2);
end
% single-phase dP_acc_ST, see T&K p401
dP_acc_ST(1)=G_STu^2*1/XSteam('rho_pT',pressure,Output_B(j+w+2,1))-G_STd^2*1/XSteam('rho_pT',
pressure,Output_A(j+w+2,1));
dP_ST=dP_acc_ST(1)+dP_fri_ST(1)+dP_gra_ST(1);     %(pa)
%=============================
%Calculate Power Split
%=============================
q_ST_A=q_ST_A+q_ST_An;
q_ST_B=q_ST_B+q_ST_Bn;
q_FW_A=q_FW_A+q_FW_An;
q_FW_B=q_FW_B+q_FW_Bn;
HSA=(q_FW_A)/(q_FW_A+q_ST_A);   %Power split A
HSB=(q_FW_B)/(q_FW_B+q_ST_B) ;%Power split B
q_TOTAL=q_FW_A+q_ST_A+q_FW_B+q_ST_B;   %Total energy (MW) , must be equal RTP*HCF
q_LOSS=(q_ST_An+q_ST_Bn);   %Total heat loss from the steam side (MW)
%===
qqq_p=qqq_p';
fid = fopen('OUTPUT.txt', 'wt+'); %Open or create new file ASBWR_SPx.txt -- See manual function F_O
p336
fprintf(fid, '%10.3f\n',m_FW);
```

```
fprintf(fid, '%10.3f\n',m_ST);
fprintf(fid, '%10.3f\n',max(qua_A));
fprintf(fid, '%10.3f\n',max(qua_B));
fprintf(fid, '%10.3f\n',(max(qua_B)+max(qua_A))*0.5 ); %Quality AVG
fprintf(fid, '%10.3f\n',HSA);
fprintf(fid, '%10.3f\n',HSB);
fprintf(fid, '%10.3f\n',(HSA*NofD+HSB*(60-NofD))/60 ); %Ave Heat split : water
fprintf(fid, '%10.3f\n',q_LOSS ); %Ave Heat split : water
fprintf(fid, '%10.3f\n',q_LOSS/(q_ST_A+q_ST_B+q_LOSS)); %Ave Heat split : water
fprintf(fid, '%10.3f\n',(Output_A(200,1)-Output_B(200,1))); %Loss in steam temp (C)
fprintf(fid, '%10.2f\n',Output_B(2174,80));   %Max cladding temp = Chopped COS Shape
fprintf(fid, '%10.2f\n',Output_B(1391,80));   %Max cladding temp for BWR Axial Profile
fprintf(fid, '%10.2f\n',Output_B(j+w+2,80));   %Max cladding temp for Uniform Profile
fprintf(fid, '%10.2f\n',Output_B(j+w+2,1));   %Steam outlet temp =
fprintf(fid, '%10.3f\n',V_ST_B(j+1) );   %Steam velocity =
fprintf(fid, '%10.3f\n',OHOT );   %   OAVG, steam flow ratio
fprintf(fid, '%10.3f\n',OHOT/OHOT );   %   OAVG/OHOT
fprintf(fid, '%10.3f\n',PPR );
fprintf(fid, '%10.3f\n',MPR );
fprintf(fid, 'OHOT, = %10.3f\n',OHOT );
fprintf(fid, '%10.3f \n',power_d); %Power density =
fprintf(fid, '%10.3f\n',dP_ST ); %steam pressure drop
fprintf(fid, '-----------------------------------------\n');
fprintf(fid, '# of downward tubes = %10.3f\n',NofD );
fprintf(fid, '-----------------------------------------\n');
fprintf(fid, 'm_FW =     %10.3f\n',m_FW);
fprintf(fid, 'm_ST = %10.3f\n',m_ST);
fprintf(fid, 'qua_A = %10.3f\n',max(qua_A));
fprintf(fid, 'qua_B = %10.3f\n',max(qua_B));
fprintf(fid, 'qua = %10.3f\n',(max(qua_B)+max(qua_A))*0.5 ); %Quality AVG
fprintf(fid, 'HSA = %10.3f\n',HSA);
fprintf(fid, 'HSB = %10.3f\n',HSB);
fprintf(fid, 'Power split = %10.3f\n',(HSA*NofD+HSB*(60-NofD))/60 ); %Ave Heat split : water
fprintf(fid, 'Heat loss = %10.3f\n',q_LOSS ); %Ave Heat split : water
fprintf(fid, 'Heat loss ratio = %10.3f\n',q_LOSS/(q_ST_A+q_ST_B+q_LOSS)); %Ave Heat split :water
fprintf(fid, 'Loss in steam temp (C) = %10.3f\n',(Output_A(200,1)-Output_B(200,1))); %LOSS in temp
fprintf(fid, '%10.2f\n',Output_B(2174,80));   %Max cladding temp = Chopped COS Shape
```

```
fprintf(fid, '%10.2f\n',Output_B(1391,80));   %Max cladding temp for BWR Axial Profile
fprintf(fid, '%10.2f\n',Output_B(j+w+2,80));   %Max cladding temp for Uniform Profile
fprintf(fid, '%10.2f\n',Output_B(j+w+2,1));   %Steam outlet temp =
fprintf(fid, '%10.3f\n',V_ST_B(j+1) );   %Steam velocity =
fprintf(fid, '%10.3f\n',OHOT );   %   OAVG, steam flow ratio
fprintf(fid, '%10.3f\n',OHOT/OHOT );   %   OAVG/OHOT
fprintf(fid, '%10.3f\n',PPR );
fprintf(fid, '%10.3f\n',MPR );
%fprintf(fid, 'OAVG, = %10.3f\n',OAVG );
fprintf(fid, 'OHOT, = %10.3f\n',OHOT );
fprintf(fid, '%10.3f \n',power_d); %Power density =
%fprintf(fid, '%10.3f\n',I_g_t ); %Inner gap thickness
fprintf(fid, '%10.3f\n',dP_ST ); %steam pressure drop
fprintf(fid, '-----------------------------------------------\n');
fclose(fid);
type OUTPUT.txt
```

Appendix C

Subroutine for Generating VIPRE Input Files

```
% Generate VIPRE Input files
% Yu-Chih Ko   08-21-2010
% Reference: 091116 VIPRE /Inputs/Modeling.xls & Modeling.PDF
% i=1, 2, 3, 4, 5, 6, 7;
% C = Corner; E = Edge; F=Full; W1 = Water rod1; W2 = Water rod2
% gia = GEOM 4, R-7 = gap width
% gib = GEOM 4, R-8 = distance between centroids
% Unit = (mm) if not specified
% Denotation refers to 091111 Dimensions/CELL091111a.jpg
clear; clf;
%==========================================
RTP=1250E6; %thermal power (Wt) = 1250 (MWt)
pressure=71.36;   %Operating pressure = (bar) => Tsat = 287 C
%$$$$$$$$$$$$$$$$$$$$$$$$$$$$$$$$$$$$$$$$$$$$$$$$$$$$$$$$$$$$$$$$$$$$$$$$$$$$
%---   HOT CHANNEL   ----
HCF=1.45;                       %Hot channel Factor
FD=0.9;                         %Hot channel FLOW Disparity factor
%Hot channel flow disparity (assume min flow in the hot channel)
%---   HOT CHANNEL   ----
PPR=1.4;                        %Power multiplier
MPR=1.4;                        %Flowrate multiplier
NofD=28;                    %# of steam downward flow tubes
DFF=30/NofD;                % down flow factor   (after/before)
UFF=30/(60-NofD);                      % up flow factor   (after/before)
power = 108.92*1000*HCF*PPR;   % power per rod (W)   => equivalent to 50 kW/L
m_FW=0.308*MPR    ;          %mass flow rate/rod =   (kg/s)
m_FW=m_FW*2.2046;               %mass flow rate/rod =   (lbm/s)
HS=0.72;   %Heat split to water side
T_inlet = 280.2;             % FW inlet temp (C)
T_inlet = T_inlet*1.8+32;     % FW inlet temp (F)
%$$$$$$$$$$$$$$$$$$$$$$$$$$$$$$$$$$$$$$$$$$$$$$$$$$$$$$$$$$$$$$$$$$$$$$$$$$$$
%_________________________________________________
%                        Rod Geometry
%_________________________________________________
IC=0.8;    %Inner clad thickness
OC=0.8;    %Outer clad thickness
IG=0.1;    %Inner gap thickness
OG=0.1;    %Outer gap thickness
FT=3.0;    %Fuel pellet thickness
ID=10.0;   %Inner diameter
E=ID+2*(IC+IG+FT+OG+OC);    %Rod OD
M=23;        %Pitch
O=4;         %duct clearance
N=M-E;       %normal gap
R=42;        %water rod OD
Q=R-2;       %water rod ID, assume thickness = 2 mm
C_H=3.0E3;          %Active Core height = 3000 (mm) = 3 (m)
%_________________________________________________
%                        Assembly Geometry
%_________________________________________________
```

```
J=2.54; %Box Wall thickness (mm)
H=7*M+2*O+E;   % CASMO CHW, assembly inner distance
GAW=7.5; %Wide water gap (mm)
GAN=7.5; %Narrow water gap (mm)
AOD = (H+2*J);   %Assembly Outer Dimension (mm)
UCD=(H+2*J+2*GAW)*(H+2*J+2*GAW);   %Unit Cell Dimension (mm2)
mA=m_FW*(60+((2*M)^2-R*R)/(M*M-E*E*pi/4))*FD; %mass flow per assembly => 60 rods + water
rod clearance
%_____________________________________________
%                    Core Geometry
%_____________________________________________
N_R = RTP/power*HCF;                    %   Number of annular rods
N_R_A=N_R/60;                    %   Number of assemblies (60 elements/assembly)
C_D=(   (N_R_A*UCD)*4/pi   )^0.5;          %Core diameter (mm)
T_C_V=C_D*C_D*pi/4*C_H;                    %Total Core volume (mm3)
power_d=RTP/1000/T_C_V*1.0E6;          %power density (kW/L)
% ***************************************
% Conversion (mm) => (inch)
% ***************************************
IC=IC/25.4;
OC=OC/25.4;
IG=IG/25.4;
OG=OG/25.4;
FT=FT/25.4;
E=E/25.4;    %Rod OD
M=M/25.4;       %Pitch
O=O/25.4;       %duct clearance
N=N/25.4;      %normal gap
R=R/25.4;       %water rod OD
Q=Q/25.4;
H=H/25.4;   %Assembly inner distance
power = power/1000.*HS;     % VIPRE Input power per rod on the water side (kW)
% ***************************************
% Input Radial Peakings (from CASMO results)
% ***************************************
%FOR DESIGN A - ASBWR Only
%Only peakings on the SW coner have to be entered.
%Source: 100823 CASMO_PHD - T91 - With Gd - TA3.out
% p01 p05 p09 p13
% p02 p06 p10 p14
% p03 p07 p11 p15
% p04 p08 p12 p16
p01=1.15;
p02=1.184;
%p03=1.245;
p03=1.29; %Adjust to be equal to BWR local peaking
p04=1.183;
p05=0.888;
p06=0.511;
p07=0.926;
p08=1.244;
p09=1.043;
p10=0.855;
p11=0.511;
p12=1.182;
p13=0.; %Water Rd
```

```
p14=1.042;
p15=0.888;
p16=1.148;
%---------
q01=p04;
q02=p03;
q03=p02;
q04=p01;
q05=p01;
q06=p02;
q07=p03;
q08=p04;
%--
q09=p08;
q10=p07;
q11=p06;
q12=p05;
q13=p05;
q14=p06;
q15=p07;
q16=p08;
%--
q17=p12;
q18=p11;
q19=p10;
q20=p09;
q21=p09;
q22=p10;
q23=p11;
q24=p12;
%--
q25=p16;
q26=p15;
q27=p14;
q28=p14;
q29=p15;
q30=p16;
% ***************************************
% Flow area (FA), Pw and Ph
% ***************************************
FA_C=(O+E/2)^2-E*E*pi/4/4; %Corner
Pw_C=2*(O+E/2)+E*pi*0.25;   %Corner
Ph_C=E*pi*0.25;   %Corner
FA_E=M*(O+E/2)-E*E*pi/4/2; %Edge
Pw_E=M+E*pi*0.5;   %Edge
Ph_E=E*pi*0.5;   %Edge
FA_F=M*M-E*E*pi/4; %Full
Pw_F=E*pi;   %Full
Ph_F=E*pi;   %Full
FA_W1=M*M-E*E*pi/4*0.75-((R-M)/2)^2; %Water rod 1
Pw_W1=E*pi*0.75+(R-M);   %Water rod 1
Ph_W1=E*pi*0.75;   %Water rod 1
FA_W2=M*M-E*E*pi/4*0.5-(R-M)/2*M; %Water rod 1
Pw_W2=E*pi*0.5+M;   %Water rod 1
Ph_W2=E*pi*0.5;   %Water rod 1
% ***************************************
```

```
%   Gap width and distance between centroids
% ***************************************
g1a = O;% C-E
g1b = M/2+(O+E/2)*0.5+E/4/1.4142;% C-E
g2a = O;% E-E
g2b = M;% E-E
g3a = N;% E-F
g3b = M/2+(O+E/2)*0.5+E/4/1.4142;% E-F
g4a = N;% F-F
g4b = M;% F-F
g5a = N;% F-W1
g5b = M-((1.4142*M-E)/2-1.4142*(M-R/2))/2/1.4142;% F-W1
g6a = N;% F-W2
g6b = M/2+(M-(R-M)/2)/2;% F-W2
g7a = M-E/2-(R-M)/2;% W1-W2
g7b = M+((1.4142*M-E)/2-1.4142*(M-R/2))/2/1.4142;% W1-W2
% ***************************************
% Water rod & Wall connection -- for RODS 9, (#61~65),
% Reference: 091116 VIPRE /Inputs/Modeling.PDF
% ***************************************
R_W1=(R-M)/(4*R); % fraction of W1 connected to water rod
R_W2=(M)/(4*R); % fraction of W2 connected to water rod
R_C=(O+E/2)/H; % fraction of C connected to wall
R_E=M/H; % fraction of E connected to wall
% ***************************************
fid = fopen('INPUT', 'wt+'); %Open or create new file ASBWR_SPx.txt -- See manual function F_O p336
fprintf(fid, '*    A-SBWR Assembly with one square water rod\n');
fprintf(fid, '*                \n');
fprintf(fid, '*    Yu-Chih Ko 12/20/09 \n');
fprintf(fid, '*                \n');
fprintf(fid, '************************************************************************** \n');
fprintf(fid,'*A-SBWR Assembly with one square water rod                                    \n');
fprintf(fid,'1,0,0,                                                                  *vipre.1 \n');
fprintf(fid,'A-SBWR Assembly                                                            *vipre.2 \n');
fprintf(fid,'*                                                                                \n');
fprintf(fid,'geom,80,80,60,0,0,0,     *80 channels, 60 axial nodes                        \n');
fprintf(fid,'*                                                                                \n');
fprintf(fid,'118.11,0.0,0.5,          *geom.2     3 m = 118.11 inches                        \n');
fprintf(fid,'*                                                                                \n');
fprintf(fid,'* START of geom 4                                                               \n');
fprintf(fid,'*                                                                                \n');
fprintf(fid,'1,%6.4f,%6.4f,%6.4f,2,2,%6.4f,%6.4f,10,%6.4f,%6.4f,\n',FA_C,Pw_C,Ph_C,g1a,g1b,g1a,g1b);
fprintf(fid,'2,%6.4f,%6.4f,%6.4f,2,3,%6.4f,%6.4f,11,%6.4f,%6.4f, \n',FA_E,Pw_E,Ph_E,g2a,g2b,g3a,g3b);
fprintf(fid,'3,%6.4f,%6.4f,%6.4f,2,4,%6.4f,%6.4f,12,%6.4f,%6.4f, \n',FA_E,Pw_E,Ph_E,g2a,g2b,g3a,g3b);
fprintf(fid,'4,%6.4f,%6.4f,%6.4f,2,5,%6.4f,%6.4f,13,%6.4f,%6.4f, \n',FA_E,Pw_E,Ph_E,g2a,g2b,g3a,g3b);
fprintf(fid,'5,%6.4f,%6.4f,%6.4f,2,6,%6.4f,%6.4f,14,%6.4f,%6.4f, \n',FA_E,Pw_E,Ph_E,g2a,g2b,g3a,g3b);
fprintf(fid,'6,%6.4f,%6.4f,%6.4f,2,7,%6.4f,%6.4f,15,%6.4f,%6.4f, \n',FA_E,Pw_E,Ph_E,g2a,g2b,g3a,g3b);
fprintf(fid,'7,%6.4f,%6.4f,%6.4f,2,8,%6.4f,%6.4f,16,%6.4f,%6.4f, \n',FA_E,Pw_E,Ph_E,g2a,g2b,g3a,g3b);
fprintf(fid,'8,%6.4f,%6.4f,%6.4f,2,9,%6.4f,%6.4f,17,%6.4f,%6.4f, \n',FA_E,Pw_E,Ph_E,g1a,g1b,g3a,g3b);
fprintf(fid,'9,%6.4f,%6.4f,%6.4f,1,18,%6.4f,%6.4f,\n',FA_C,Pw_C,Ph_C,g1a,g1b);
fprintf(fid,'*                                                                                \n');
fprintf(fid,'10,%6.4f,%6.4f,%6.4f,2,11,%6.4f,%6.4f,19,%6.4f,%6.4f,\n',FA_E,Pw_E,Ph_E,g3a,g3b,g2a,g2b
);
fprintf(fid,'11,%6.4f,%6.4f,%6.4f,2,12,%6.4f,%6.4f,20,%6.4f,%6.4f,\n',FA_F,Pw_F,Ph_F,g4a,g4b,g4a,g4b);
fprintf(fid,'12,%6.4f,%6.4f,%6.4f,2,13,%6.4f,%6.4f,21,%6.4f,%6.4f,\n',FA_F,Pw_F,Ph_F,g4a,g4b,g4a,g4b)
;
```

```
fprintf(fid,'13,%6.4f,%6.4f,%6.4f,2,14,%6.4f,%6.4f,22,%6.4f,%6.4f,\n',FA_F,Pw_F,Ph_F,g4a,g4b,g4a,g4b)
;
fprintf(fid,'14,%6.4f,%6.4f,%6.4f,2,15,%6.4f,%6.4f,23,%6.4f,%6.4f,\n',FA_F,Pw_F,Ph_F,g4a,g4b,g4a,g4b)
;
fprintf(fid,'15,%6.4f,%6.4f,%6.4f,2,16,%6.4f,%6.4f,24,%6.4f,%6.4f,\n',FA_F,Pw_F,Ph_F,g4a,g4b,g4a,g4b)
;
fprintf(fid,'16,%6.4f,%6.4f,%6.4f,2,17,%6.4f,%6.4f,25,%6.4f,%6.4f,\n',FA_F,Pw_F,Ph_F,g4a,g4b,g4a,g4b)
;
fprintf(fid,'17,%6.4f,%6.4f,%6.4f,2,18,%6.4f,%6.4f,26,%6.4f,%6.4f,\n',FA_F,Pw_F,Ph_F,g3a,g3b,g4a,g4b)
;
fprintf(fid,'18,%6.4f,%6.4f,%6.4f,1,27,%6.4f,%6.4f,\n',FA_E,Pw_E,Ph_E,g2a,g2b);
fprintf(fid,'*                                                                \n');
fprintf(fid,'19,%6.4f,%6.4f,%6.4f,2,20,%6.4f,%6.4f,28,%6.4f,%6.4f,\n',FA_E,Pw_E,Ph_E,g3a,g3b,g2a,g2b
);
fprintf(fid,'20,%6.4f,%6.4f,%6.4f,2,21,%6.4f,%6.4f,29,%6.4f,%6.4f,\n',FA_F,Pw_F,Ph_F,g4a,g4b,g4a,g4b)
;
fprintf(fid,'21,%6.4f,%6.4f,%6.4f,2,22,%6.4f,%6.4f,30,%6.4f,%6.4f,\n',FA_F,Pw_F,Ph_F,g4a,g4b,g4a,g4b)
;
fprintf(fid,'22,%6.4f,%6.4f,%6.4f,2,23,%6.4f,%6.4f,31,%6.4f,%6.4f,\n',FA_F,Pw_F,Ph_F,g4a,g4b,g5a,g5b)
;
fprintf(fid,'23,%6.4f,%6.4f,%6.4f,2,24,%6.4f,%6.4f,32,%6.4f,%6.4f,\n',FA_F,Pw_F,Ph_F,g4a,g4b,g6a,g6b)
;
fprintf(fid,'24,%6.4f,%6.4f,%6.4f,2,25,%6.4f,%6.4f,33,%6.4f,%6.4f,\n',FA_F,Pw_F,Ph_F,g4a,g4b,g5a,g5b)
;
fprintf(fid,'25,%6.4f,%6.4f,%6.4f,2,26,%6.4f,%6.4f,34,%6.4f,%6.4f,\n',FA_F,Pw_F,Ph_F,g4a,g4b,g4a,g4b)
;
fprintf(fid,'26,%6.4f,%6.4f,%6.4f,2,27,%6.4f,%6.4f,35,%6.4f,%6.4f,\n',FA_F,Pw_F,Ph_F,g3a,g3b,g4a,g4b)
;
fprintf(fid,'27,%6.4f,%6.4f,%6.4f,1,36,%6.4f,%6.4f,\n',FA_E,Pw_E,Ph_E,g2a,g2b);
fprintf(fid,'*                                                                \n');
fprintf(fid,'28,%6.4f,%6.4f,%6.4f,2,29,%6.4f,%6.4f,37,%6.4f,%6.4f,\n',FA_E,Pw_E,Ph_E,g3a,g3b,g2a,g2b
);
fprintf(fid,'29,%6.4f,%6.4f,%6.4f,2,30,%6.4f,%6.4f,38,%6.4f,%6.4f,\n',FA_F,Pw_F,Ph_F,g4a,g4b,g4a,g4b)
;
fprintf(fid,'30,%6.4f,%6.4f,%6.4f,2,31,%6.4f,%6.4f,39,%6.4f,%6.4f,\n',FA_F,Pw_F,Ph_F,g5a,g5b,g4a,g4b)
;
fprintf(fid,'31,%6.4f,%6.4f,%6.4f,2,32,%6.4f,%6.4f,40,%6.4f,%6.4f,\n',FA_W1,Pw_W1,Ph_W1,g7a,g7b,g
7a,g7b);
fprintf(fid,'32,%6.4f,%6.4f,%6.4f,1,33,%6.4f,%6.4f,\n',FA_W2,Pw_W2,Ph_W2,g7a,g7b);
fprintf(fid,'33,%6.4f,%6.4f,%6.4f,2,34,%6.4f,%6.4f,41,%6.4f,%6.4f,\n',FA_W1,Pw_W1,Ph_W1,g5a,g5b,g
7a,g7b);
fprintf(fid,'34,%6.4f,%6.4f,%6.4f,2,35,%6.4f,%6.4f,42,%6.4f,%6.4f,\n',FA_F,Pw_F,Ph_F,g4a,g4b,g4a,g4b)
;
fprintf(fid,'35,%6.4f,%6.4f,%6.4f,2,36,%6.4f,%6.4f,43,%6.4f,%6.4f,\n',FA_F,Pw_F,Ph_F,g3a,g3b,g4a,g4b)
;
fprintf(fid,'36,%6.4f,%6.4f,%6.4f,1,44,%6.4f,%6.4f,\n',FA_E,Pw_E,Ph_E,g2a,g2b);
fprintf(fid,'*                                                                \n');
fprintf(fid,'37,%6.4f,%6.4f,%6.4f,2,38,%6.4f,%6.4f,45,%6.4f,%6.4f,\n',FA_E,Pw_E,Ph_E,g3a,g3b,g2a,g2b
);
fprintf(fid,'38,%6.4f,%6.4f,%6.4f,2,39,%6.4f,%6.4f,46,%6.4f,%6.4f,\n',FA_F,Pw_F,Ph_F,g4a,g4b,g4a,g4b)
;
fprintf(fid,'39,%6.4f,%6.4f,%6.4f,2,40,%6.4f,%6.4f,47,%6.4f,%6.4f,\n',FA_F,Pw_F,Ph_F,g6a,g6b,g4a,g4b)
;
fprintf(fid,'40,%6.4f,%6.4f,%6.4f,1,48,%6.4f,%6.4f,\n',FA_W2,Pw_W2,Ph_W2,g7a,g7b);
fprintf(fid,'41,%6.4f,%6.4f,%6.4f,2,42,%6.4f,%6.4f,50,%6.4f,%6.4f
\n',FA_W2,Pw_W2,Ph_W2,g6a,g6b,g7a,g7b);
```

```
fprintf(fid,'42,%6.4f,%6.4f,%6.4f,2,43,%6.4f,%6.4f,51,%6.4f,%6.4f,\n',FA_F,Pw_F,Ph_F,g4a,g4b,g4a,g4b)
;
fprintf(fid,'43,%6.4f,%6.4f,%6.4f,2,44,%6.4f,%6.4f,52,%6.4f,%6.4f,\n',FA_F,Pw_F,Ph_F,g3a,g3b,g4a,g4b)
;
fprintf(fid,'44,%6.4f,%6.4f,%6.4f,1,53,%6.4f,%6.4f,\n',FA_E,Pw_E,Ph_E,g2a,g2b);
fprintf(fid,'*                                                    \n');
fprintf(fid,'45,%6.4f,%6.4f,%6.4f,2,46,%6.4f,%6.4f,54,%6.4f,%6.4f,\n',FA_E,Pw_E,Ph_E,g3a,g3b,g2a,g2b
);
fprintf(fid,'46,%6.4f,%6.4f,%6.4f,2,47,%6.4f,%6.4f,55,%6.4f,%6.4f,\n',FA_F,Pw_F,Ph_F,g4a,g4b,g4a,g4b)
;
fprintf(fid,'47,%6.4f,%6.4f,%6.4f,2,48,%6.4f,%6.4f,56,%6.4f,%6.4f,\n',FA_F,Pw_F,Ph_F,g5a,g5b,g4a,g4b)
;
fprintf(fid,'48,%6.4f,%6.4f,%6.4f,2,49,%6.4f,%6.4f,57,%6.4f,%6.4f,\n',FA_W1,Pw_W1,Ph_W1,g7a,g7b,g
5a,g5b);
fprintf(fid,'49,%6.4f,%6.4f,%6.4f,2,50,%6.4f,%6.4f,58,%6.4f,%6.4f,\n',FA_W2,Pw_W2,Ph_W2,g7a,g7b,g
6a,g6b);
fprintf(fid,'50,%6.4f,%6.4f,%6.4f,2,51,%6.4f,%6.4f,59,%6.4f,%6.4f,\n',FA_W1,Pw_W1,Ph_W1,g5a,g5b,g
5a,g5b);
fprintf(fid,'51,%6.4f,%6.4f,%6.4f,2,52,%6.4f,%6.4f,60,%6.4f,%6.4f,\n',FA_F,Pw_F,Ph_F,g4a,g4b,g4a,g4b)
;
fprintf(fid,'52,%6.4f,%6.4f,%6.4f,2,53,%6.4f,%6.4f,61,%6.4f,%6.4f,\n',FA_F,Pw_F,Ph_F,g3a,g3b,g4a,g4b)
;
fprintf(fid,'53,%6.4f,%6.4f,%6.4f,1,62,%6.4f,%6.4f,\n',FA_E,Pw_E,Ph_E,g2a,g2b);
fprintf(fid,'*                                                    \n');
fprintf(fid,'54,%6.4f,%6.4f,%6.4f,2,55,%6.4f,%6.4f,63,%6.4f,%6.4f,\n',FA_E,Pw_E,Ph_E,g3a,g3b,g2a,g2b
);
fprintf(fid,'55,%6.4f,%6.4f,%6.4f,2,56,%6.4f,%6.4f,64,%6.4f,%6.4f,\n',FA_F,Pw_F,Ph_F,g4a,g4b,g4a,g4b)
;
fprintf(fid,'56,%6.4f,%6.4f,%6.4f,2,57,%6.4f,%6.4f,65,%6.4f,%6.4f,\n',FA_F,Pw_F,Ph_F,g4a,g4b,g4a,g4b)
;
fprintf(fid,'57,%6.4f,%6.4f,%6.4f,2,58,%6.4f,%6.4f,66,%6.4f,%6.4f,\n',FA_F,Pw_F,Ph_F,g4a,g4b,g4a,g4b)
;
fprintf(fid,'58,%6.4f,%6.4f,%6.4f,2,59,%6.4f,%6.4f,67,%6.4f,%6.4f,\n',FA_F,Pw_F,Ph_F,g4a,g4b,g4a,g4b)
;
fprintf(fid,'59,%6.4f,%6.4f,%6.4f,2,60,%6.4f,%6.4f,68,%6.4f,%6.4f,\n',FA_F,Pw_F,Ph_F,g4a,g4b,g4a,g4b)
;
fprintf(fid,'60,%6.4f,%6.4f,%6.4f,2,61,%6.4f,%6.4f,69,%6.4f,%6.4f,\n',FA_F,Pw_F,Ph_F,g4a,g4b,g4a,g4b)
;
fprintf(fid,'61,%6.4f,%6.4f,%6.4f,2,62,%6.4f,%6.4f,70,%6.4f,%6.4f,\n',FA_F,Pw_F,Ph_F,g3a,g3b,g4a,g4b)
;
fprintf(fid,'62,%6.4f,%6.4f,%6.4f,1,71,%6.4f,%6.4f,\n',FA_E,Pw_E,Ph_E,g2a,g2b);
fprintf(fid,'*                                                    \n');
fprintf(fid,'63,%6.4f,%6.4f,%6.4f,2,64,%6.4f,%6.4f,72,%6.4f,%6.4f,\n',FA_E,Pw_E,Ph_E,g3a,g3b,g1a,g1b
);
fprintf(fid,'64,%6.4f,%6.4f,%6.4f,2,65,%6.4f,%6.4f,73,%6.4f,%6.4f,\n',FA_F,Pw_F,Ph_F,g4a,g4b,g3a,g3b)
;
fprintf(fid,'65,%6.4f,%6.4f,%6.4f,2,66,%6.4f,%6.4f,74,%6.4f,%6.4f,\n',FA_F,Pw_F,Ph_F,g4a,g4b,g3a,g3b)
;
fprintf(fid,'66,%6.4f,%6.4f,%6.4f,2,67,%6.4f,%6.4f,75,%6.4f,%6.4f,\n',FA_F,Pw_F,Ph_F,g4a,g4b,g3a,g3b)
;
fprintf(fid,'67,%6.4f,%6.4f,%6.4f,2,68,%6.4f,%6.4f,76,%6.4f,%6.4f,\n',FA_F,Pw_F,Ph_F,g4a,g4b,g3a,g3b)
;
fprintf(fid,'68,%6.4f,%6.4f,%6.4f,2,69,%6.4f,%6.4f,77,%6.4f,%6.4f,\n',FA_F,Pw_F,Ph_F,g4a,g4b,g3a,g3b)
;
fprintf(fid,'69,%6.4f,%6.4f,%6.4f,2,70,%6.4f,%6.4f,78,%6.4f,%6.4f,\n',FA_F,Pw_F,Ph_F,g4a,g4b,g3a,g3b)
;
```

```
fprintf(fid,'70,%6.4f,%6.4f,%6.4f,2,71,%6.4f,%6.4f,79,%6.4f,%6.4f,\n',FA_F,Pw_F,Ph_F,g3a,g3b,g3a,g3b)
;
fprintf(fid,'71,%6.4f,%6.4f,%6.4f,1,80,%6.4f,%6.4f,\n',FA_E,Pw_E,Ph_E,g1a,g1b);
fprintf(fid,'*                                                    \n');
fprintf(fid,'72,%6.4f,%6.4f,%6.4f,1,73,%6.4f,%6.4f,\n',FA_C,Pw_C,Ph_C,g1a,g1b);
fprintf(fid,'73,%6.4f,%6.4f,%6.4f,1,74,%6.4f,%6.4f,\n',FA_E,Pw_E,Ph_E,g2a,g2b);
fprintf(fid,'74,%6.4f,%6.4f,%6.4f,1,75,%6.4f,%6.4f,\n',FA_E,Pw_E,Ph_E,g2a,g2b);
fprintf(fid,'75,%6.4f,%6.4f,%6.4f,1,76,%6.4f,%6.4f,\n',FA_E,Pw_E,Ph_E,g2a,g2b);
fprintf(fid,'76,%6.4f,%6.4f,%6.4f,1,77,%6.4f,%6.4f,\n',FA_E,Pw_E,Ph_E,g2a,g2b);
fprintf(fid,'77,%6.4f,%6.4f,%6.4f,1,78,%6.4f,%6.4f,\n',FA_E,Pw_E,Ph_E,g2a,g2b);
fprintf(fid,'78,%6.4f,%6.4f,%6.4f,1,79,%6.4f,%6.4f,\n',FA_E,Pw_E,Ph_E,g2a,g2b);
fprintf(fid,'79,%6.4f,%6.4f,%6.4f,1,80,%6.4f,%6.4f,\n',FA_E,Pw_E,Ph_E,g1a,g1b);
fprintf(fid,'80,%6.4f,%6.4f,%6.4f,\n',FA_C,Pw_C,Ph_C);
fprintf(fid,'*                                                    \n');
fprintf(fid,'* END of geom.4                                      \n');
fprintf(fid,'*                                                    \n');
fprintf(fid,'prop,0,1,2,1     *internal EPRI functions *prop.1 \n');
fprintf(fid,'*                                                    \n');
fprintf(fid,'rods,1,65,1,3,2,0,0,0,0,0,0   *3types of rod,two types of mat. *rods.1    \n');
fprintf(fid,'118.11,0.0,0,0                                                          *rods.2    \n');
fprintf(fid,'*                                                    \n');
fprintf(fid,'*                                                    \n');
fprintf(fid,'26                                                                *rods3 \n');
fprintf(fid,'*One axial profile only    (rods.4)      \n');
fprintf(fid,'0.00,0.00,?                                          \n');
fprintf(fid,'2.46,0.38,?                                          \n');
fprintf(fid,'7.38,0.69,?                                          \n');
fprintf(fid,'12.30,0.93,                                          \n');
fprintf(fid,'17.22,1.10,?                                         \n');
fprintf(fid,'22.14,1.21,?                                         \n');
fprintf(fid,'27.06,1.30,?                                         \n');
fprintf(fid,'31.97,1.47,                                          \n');
fprintf(fid,'36.89,1.51,?                                         \n');
fprintf(fid,'41.81,1.49,?                                         \n');
fprintf(fid,'46.73,1.44,?                                         \n');
fprintf(fid,'51.65,1.36,                                          \n');
fprintf(fid,'56.57,1.28,?                                         \n');
fprintf(fid,'61.49,1.16,?                                         \n');
fprintf(fid,'66.41,1.06,?                                         \n');
fprintf(fid,'71.33,1.01,                                          \n');
fprintf(fid,'76.25,0.97,?                                         \n');
fprintf(fid,'81.17,0.94,?                                         \n');
fprintf(fid,'86.09,0.97,?                                         \n');
fprintf(fid,'91.01,0.96,                                          \n');
fprintf(fid,'95.92,0.91,?                                         \n');
fprintf(fid,'100.84,0.77,?                                        \n');
fprintf(fid,'105.76,0.59,?                                        \n');
fprintf(fid,'110.68,0.38,                                         \n');
fprintf(fid,'115.6,0.12,?                                         \n');
fprintf(fid,'118.11,0.00,                                         \n');
fprintf(fid,'*                                                    \n');
fprintf(fid,'*                                                    \n');
fprintf(fid,'*                                                    \n');
fprintf(fid,'******rods geometry input                                                *rods.9      \n');
fprintf(fid,'* Radial peaking is based on CASMO Results \n');
fprintf(fid,'*091112 Control Rod and Gd, A12.out, zero burnup\n');
```

```
fprintf(fid,'*                                                    \n');
%Radial pwaking from CASMO 100207 Final CASMO, A30817b2z.out
fprintf(fid,'1,1,%5.3f,1,1,0.25,2,0.25,10,0.25,11,0.25,   \n',q01);
fprintf(fid,'2,1,%5.3f,1,2,0.25,3,0.25,11,0.25,12,0.25,   \n',q02);
fprintf(fid,'3,1,%5.3f,1,3,0.25,4,0.25,12,0.25,13,0.25,   \n',q03);
fprintf(fid,'4,1,%5.3f,1,4,0.25,5,0.25,13,0.25,14,0.25,   \n',q04);
fprintf(fid,'5,1,%5.3f,1,5,0.25,6,0.25,14,0.25,15,0.25,   \n',q05);
fprintf(fid,'6,1,%5.3f,1,6,0.25,7,0.25,15,0.25,16,0.25,   \n',q06);
fprintf(fid,'7,1,%5.3f,1,7,0.25,8,0.25,16,0.25,17,0.25,   \n',q07);
fprintf(fid,'8,1,%5.3f,1,8,0.25,9,0.25,17,0.25,18,0.25,   \n',q08);
fprintf(fid,'*                                                    \n');
fprintf(fid,'9,1,%5.3f,1,10,0.25,11,0.25,19,0.25,20,0.25,\n',q09);
fprintf(fid,'10,1,%5.3f,1,11,0.25,12,0.25,20,0.25,21,0.25,      \n',q10);
fprintf(fid,'11,1,%5.3f,1,12,0.25,13,0.25,21,0.25,22,0.25,      \n',q11);
fprintf(fid,'12,1,%5.3f,1,13,0.25,14,0.25,22,0.25,23,0.25,      \n',q12);
fprintf(fid,'13,1,%5.3f,1,14,0.25,15,0.25,23,0.25,24,0.25,      \n',q13);
fprintf(fid,'14,1,%5.3f,1,15,0.25,16,0.25,24,0.25,25,0.25,      \n',q14);
fprintf(fid,'15,1,%5.3f,1,16,0.25,17,0.25,25,0.25,26,0.25,      \n',q15);
fprintf(fid,'16,1,%5.3f,1,17,0.25,18,0.25,26,0.25,27,0.25,      \n',q16);
fprintf(fid,'*                                                    \n');
fprintf(fid,'17,1,%5.3f,1,19,0.25,20,0.25,28,0.25,29,0.25,      \n',q17);
fprintf(fid,'18,1,%5.3f,1,20,0.25,21,0.25,29,0.25,30,0.25,      \n',q18);
fprintf(fid,'19,1,%5.3f,1,21,0.25,22,0.25,30,0.25,31,0.25,      \n',q19);
fprintf(fid,'20,1,%5.3f,1,22,0.25,23,0.25,31,0.25,32,0.25,      \n',q20);
fprintf(fid,'21,1,%5.3f,1,23,0.25,24,0.25,32,0.25,33,0.25,      \n',q21);
fprintf(fid,'22,1,%5.3f,1,24,0.25,25,0.25,33,0.25,34,0.25,      \n',q22);
fprintf(fid,'23,1,%5.3f,1,25,0.25,26,0.25,34,0.25,35,0.25,      \n',q23);
fprintf(fid,'24,1,%5.3f,1,26,0.25,27,0.25,35,0.25,36,0.25,      \n',q24);
fprintf(fid,'*                                                    \n');
fprintf(fid,'25,1,%5.3f,1,28,0.25,29,0.25,37,0.25,38,0.25,      \n',q25);
fprintf(fid,'26,1,%5.3f,1,29,0.25,30,0.25,38,0.25,39,0.25,      \n',q26);
fprintf(fid,'27,1,%5.3f,1,30,0.25,31,0.25,39,0.25,40,0.25,      \n',q27);
fprintf(fid,'28,1,%5.3f,1,33,0.25,34,0.25,41,0.25,42,0.25,      \n',q28);
fprintf(fid,'29,1,%5.3f,1,34,0.25,35,0.25,42,0.25,43,0.25,      \n',q29);
fprintf(fid,'30,1,%5.3f,1,35,0.25,36,0.25,43,0.25,44,0.25,      \n',q30);
fprintf(fid,'*                                                    \n');
fprintf(fid,'31,1,%5.3f,1,37,0.25,38,0.25,45,0.25,46,0.25,      \n',q25);
fprintf(fid,'32,1,%5.3f,1,38,0.25,39,0.25,46,0.25,47,0.25,      \n',q26);
fprintf(fid,'33,1,%5.3f,1,39,0.25,40,0.25,47,0.25,48,0.25,      \n',q27);
fprintf(fid,'34,1,%5.3f,1,41,0.25,42,0.25,50,0.25,51,0.25,      \n',q28);
fprintf(fid,'35,1,%5.3f,1,42,0.25,43,0.25,51,0.25,52,0.25,      \n',q29);
fprintf(fid,'36,1,%5.3f,1,43,0.25,44,0.25,52,0.25,53,0.25,      \n',q30);
fprintf(fid,'*                                                    \n');
fprintf(fid,'37,1,%5.3f,1,45,0.25,46,0.25,54,0.25,55,0.25,      \n',q17);
fprintf(fid,'38,1,%5.3f,1,46,0.25,47,0.25,55,0.25,56,0.25,      \n',q18);
fprintf(fid,'39,1,%5.3f,1,47,0.25,48,0.25,56,0.25,57,0.25,      \n',q19);
fprintf(fid,'40,1,%5.3f,1,48,0.25,49,0.25,57,0.25,58,0.25,      \n',q20);
fprintf(fid,'41,1,%5.3f,1,49,0.25,50,0.25,58,0.25,59,0.25,      \n',q21);
fprintf(fid,'42,1,%5.3f,1,50,0.25,51,0.25,59,0.25,60,0.25,      \n',q22);
fprintf(fid,'43,1,%5.3f,1,51,0.25,52,0.25,60,0.25,61,0.25,      \n',q23);
fprintf(fid,'44,1,%5.3f,1,52,0.25,53,0.25,61,0.25,62,0.25,      \n',q24);
fprintf(fid,'*                                                    \n');
fprintf(fid,'45,1,%5.3f,1,54,0.25,55,0.25,63,0.25,64,0.25,      \n',q09);
fprintf(fid,'46,1,%5.3f,1,55,0.25,56,0.25,64,0.25,65,0.25,      \n',q10);
fprintf(fid,'47,1,%5.3f,1,56,0.25,57,0.25,65,0.25,66,0.25,      \n',q11);
fprintf(fid,'48,1,%5.3f,1,57,0.25,58,0.25,66,0.25,67,0.25,      \n',q12);
```

```
fprintf(fid,'49,1,%5.3f,1,58,0.25,59,0.25,67,0.25,68,0.25,      \n',q13);
fprintf(fid,'50,1,%5.3f,1,59,0.25,60,0.25,68,0.25,69,0.25,      \n',q14);
fprintf(fid,'51,1,%5.3f,1,60,0.25,61,0.25,69,0.25,70,0.25,      \n',q15);
fprintf(fid,'52,1,%5.3f,1,61,0.25,62,0.25,70,0.25,71,0.25,      \n',q16);
fprintf(fid,'*                                                  \n');
fprintf(fid,'53,1,%5.3f,1,63,0.25,64,0.25,72,0.25,73,0.25,      \n',q01);
fprintf(fid,'54,1,%5.3f,1,64,0.25,65,0.25,73,0.25,74,0.25,      \n',q02);
fprintf(fid,'55,1,%5.3f,1,65,0.25,66,0.25,74,0.25,75,0.25,      \n',q03);
fprintf(fid,'56,1,%5.3f,1,66,0.25,67,0.25,75,0.25,76,0.25,      \n',q04);
fprintf(fid,'57,1,%5.3f,1,67,0.25,68,0.25,76,0.25,77,0.25,      \n',q05);
fprintf(fid,'58,1,%5.3f,1,68,0.25,69,0.25,77,0.25,78,0.25,      \n',q06);
fprintf(fid,'59,1,%5.3f,1,69,0.25,70,0.25,78,0.25,79,0.25,      \n',q07);
fprintf(fid,'60,1,%5.3f,1,70,0.25,71,0.25,79,0.25,80,0.25,      \n',q08);
fprintf(fid,'*                                                  \n');
fprintf(fid,'*                                                  \n');
fprintf(fid,'*   *Water rod (ext)                           \n');
fprintf(fid,'*                                                  \n');
fprintf(fid,'61,2,0.0,1,31,%6.4f,33,%6.4f,48,%6.4f,50,%6.4f,?\n',R_W1,R_W1,R_W1,R_W1);
fprintf(fid,'32,%6.4f,40,%6.4f,41,%6.4f,49,%6.4f, \n',R_W2,R_W2,R_W2,R_W2);
fprintf(fid,'*                                                  \n');
fprintf(fid,'*   *Channel (Inner surface)          \n');
fprintf(fid,'*                                                  \n');
fprintf(fid,'-62,3,0.0,1,1,%7.5f,2,%7.5f,3,%7.5f,4,%7.5f,?\n',R_C,R_E,R_E,R_E);
fprintf(fid,'5,%7.5f,6,%7.5f,7,%7.5f,8,%7.5f,9,%7.5f,\n',R_E,R_E,R_E,R_E,R_C);
fprintf(fid,'*                                                  \n');
fprintf(fid,'-63,3,0.0,1,1,%7.5f,10,%7.5f,19,%7.5f,28,%7.5f,?\n',R_C,R_E,R_E,R_E);
fprintf(fid,'37,%7.5f,45,%7.5f,54,%7.5f,63,%7.5f,72,%7.5f,\n',R_E,R_E,R_E,R_E,R_C);
fprintf(fid,'*                                                  \n');
fprintf(fid,'-64,3,0.0,1,9,%7.5f,18,%7.5f,27,%7.5f,36,%7.5f,?\n',R_C,R_E,R_E,R_E);
fprintf(fid,'44,%7.5f,53,%7.5f,62,%7.5f,71,%7.5f,80,%7.5f,\n',R_E,R_E,R_E,R_E,R_C);
fprintf(fid,'*                                                  \n');
fprintf(fid,'-65,3,0.0,1,72,%7.5f,73,%7.5f,74,%7.5f,75,%7.5f,?\n',R_C,R_E,R_E,R_E);
fprintf(fid,'76,%7.5f,77,%7.5f,78,%7.5f,79,%7.5f,80,%7.5f,\n',R_E,R_E,R_E,R_E,R_C);
fprintf(fid,'*                                                  \n');
fprintf(fid,'*                                                  \n');
fprintf(fid,'*                                                  \n');
fprintf(fid,'0              *End of rods.9          \n');
fprintf(fid,'*                                                  \n');
fprintf(fid,'*                                                  \n');
fprintf(fid,'*fuel geometry                                 \n');
fprintf(fid,'1,nucl,%6.4f,%6.4f,12,%6.4f,%6.4f                                                  *rods.62
\n',E,(E-2*OC-2*OG),(E-2*OC-2*OG-2*FT),OC);
fprintf(fid,'0,0,2,0,0,1056.66,0.955,0.0,       *rods 63 T91 or Inconel cladding in RODs 70 =2     \n');
fprintf(fid,'*constant radial power in the pellet, no power in the clad \n');
fprintf(fid,'*                                                  \n');
fprintf(fid,'*water tube                                    \n');
fprintf(fid,'2,tube,%6.4f,%6.4f,1    *rods.68\n',((4*R*R/pi)^0.5),((4*Q*Q/pi)^0.5));
fprintf(fid,'3,1,%7.5f,1.0,      *rods.69   \n',((4*R*R/pi)^0.5-(4*Q*Q/pi)^0.5)/2);
fprintf(fid,'*wall                                          \n');
fprintf(fid,'3,wall,%6.4f,0.0,1     *rods.68   \n',H);
fprintf(fid,'3,1,0.1,1.0,   *rods.69   Assume wall thickness = 0.1" \n');
fprintf(fid,'*                                                  \n');
fprintf(fid,'*                                                  \n');
fprintf(fid,'1,1,409.7,clad,              *rods 70   Zir2       \n');
fprintf(fid,'662,0.076,10.05,             *rods 71\n');
fprintf(fid,'*T91 density=7.79 g/cm^3; specific heat = 560J/kg-K at 300 C; Thermal conductivity=29
```

```
W/mK \n');
fprintf(fid,'2,1,486.582,TT91,            *rods 70   T91        \n');
fprintf(fid,'662,0.1338,16.77,            *rods 71      \n');
fprintf(fid,'*Inconel 718 density=8.19 g/cm^3; specific heat = 435 J/kg-K; Thermal conductivity=15.5
W/mK \n');
fprintf(fid,'*2,1,511.57,I718,            *rods 70   Inconel 718 \n');
fprintf(fid,'*662,0.1039,8.956,           *rods 71      \n');
fprintf(fid,'***********************************     \n');
fprintf(fid,'*P,T                          \n');
fprintf(fid,'oper,1,1,0,1,0,1,0,0,0,                  *oper.1   /flow is specified \n');
fprintf(fid,'-1.0,0.0,2.0,0.005,                      *oper.2      \n');
fprintf(fid,'0                                              *oper.3      \n');
fprintf(fid,'1035.0,%6.2f,%6.3f,%6.2f,0.0      *oper.5 \n',T_inlet,mA,power);
fprintf(fid,'*                             \n');
fprintf(fid,'*Rod power got from total power divided total number of rods\n');
fprintf(fid,'0,                 *no forcing functions    *oper.12    \n');
fprintf(fid,'***********************************     \n');
fprintf(fid,'*correlations                 \n');
fprintf(fid,'corr,1,2,0,                                                                *corr.1 \n');
fprintf(fid,'epri,epri,epri,none,                                                     *corr.2 \n');
fprintf(fid,'0.2,                                                                            *corr.3 \n');
fprintf(fid,'ditb,chen,chen,epri,cond,g5.7,      *correlation for boiling curve     *corr.6 \n');
fprintf(fid,'epri,                               *corr.9,DNB Analysis \n');
fprintf(fid,'1,0,0.0,                            *corr.16,for epri       \n');
fprintf(fid,'***********************                \n');
fprintf(fid,'mixx,0,0,0,                    \n');
fprintf(fid,'0.8,0.0048,0.0,               \n');
fprintf(fid,'*************************************************************     \n');
fprintf(fid,'grid,0,7,                                    *grid.1 => seven local grid loss IDs \n');
fprintf(fid,'9.4609,1.203,0.3751,21.089,182.049,312.0,729.0 *grid2 value of the seven local grid loss IDs
\n');
fprintf(fid,'80,10,                                                     *grid.4 ; 80 rods, 10 axial
locations \n');
fprintf(fid,'1,2,3,4,5,6,7,8,9,10,11,12,13,14,15,16,                         *grid.5   \n');
fprintf(fid,'17,18,19,20,21,22,23,24,25,26,27,28,29,30,31,32,\n');
fprintf(fid,'33,34,35,36,37,38,39,40,41,42,43,44,45,46,47,48,\n');
fprintf(fid,'49,50,51,52,53,54,55,56,57,58,59,60,61,62,63,64,\n');
fprintf(fid,'65,66,67,68,69,70,71,72,73,74,75,76,77,78,79,80,\n');
fprintf(fid,'*grid.5                        \n');
fprintf(fid,'*                              \n');
fprintf(fid,'0.000,4,5.9063,1,15.7771,2,31.554,2,47.3314,2,63.1085,2,78.8856,2,94.6628,2            *grid6
\n');
fprintf(fid,'110.4399,2,115.6989,3
*grid6      \n');
fprintf(fid,'0,                                                    *End of Grid input       \n');
fprintf(fid,'*************************************************************     \n');
fprintf(fid,'cont,                                                                            *cont.1 \n');
fprintf(fid,'0.0,0,500,100,3,0,    *iterative solution                              *cont.2 \n');
fprintf(fid,'0.10,0.00001,0.001,0.05,0.01,0.9,1.5,1.0,                              *cont.3 \n');
fprintf(fid,'5,0,0,0,0,0,1,1,0,0,0,1,1,0,                                            *cont.6 \n');
fprintf(fid,'200.,0.0,0.0,0.0,0.0,0.0,                                              *cont.7   \n');
fprintf(fid,'endd                            \n');
fprintf(fid,'*                               \n');
fprintf(fid,'*end of data input            \n');
fprintf(fid,'0                               \n');
fclose(fid);
```

```
fid = fopen('DATA.txt', 'wt+'); %Open or create new file
fprintf(fid,' IC=%6.4f    *Inner clad thickness                                    \n',IC);
fprintf(fid,' OC=%6.4f    *Outer clad thickness                                    \n',OC);
fprintf(fid,' IG=%6.4f    *Inner gap thickness                                     \n',IG);
fprintf(fid,' OG=%6.4f    *Outer gap thickness                                     \n',OG);
fprintf(fid,' FT=%6.4f   *Fuel pellet thickness                                    \n',FT);
fprintf(fid,' ID=%6.4f    *Inner diameter                                          \n',ID);
fprintf(fid,' E=%6.4f    *Rod OD                                  \n',E);
fprintf(fid,' M=%6.4f      *Pitch                                                  \n',M);
fprintf(fid,' O=%6.4f       *duct clearance                                        \n',O);
fprintf(fid,' N=%6.4f     *normal gap                                              \n',N);
fprintf(fid,' R=%6.4f      *water rod OD                                           \n',R);
fprintf(fid,' Q=%6.4f    *water rod ID, assume thickness = 2 mm                   \n',Q);
fprintf(fid,' H=%6.4f   *Assembly inner distance                                  \n',H);
fprintf(fid,' *=============================================                      \n');
fprintf(fid,' RX thermal power =%6.1f   (MW)                                     \n',RTP/1.0E6);
fprintf(fid,' RX power density =%6.1f   (kW/L)                                   \n',power_d);
fprintf(fid,' m_FW=%6.4f * Core mass flow rate =2807.0 (kg/s)= 6188.4 (lbm/s) \n',m_FW);
fprintf(fid,' N_R=%6.4f   *# of fuel rods                                        \n',N_R);
fprintf(fid,' HS=%6.4f    *Heat split to water side                              \n',HS);
fprintf(fid,' HCF=%6.4f   *Hot channel factor                                    \n',HCF);
fprintf(fid,' PF=%6.4f    *Power factor                                          \n',PPR);
fprintf(fid,' PPR=%6.4f   * power (kW)/rod                          \n',power);
fprintf(fid,' MF=%6.4f *Mass flow rate factor                                    \n',MPR);
fprintf(fid,' mA=%6.4f *mass flow per   \n',mA);
% fprintf(fid,' * ************************************                           \n');
% fprintf(fid,' * Flow area (FA), Pw and Ph                                      \n');
% fprintf(fid,' * ************************************                           \n');
% fprintf(fid,' FA_C=(O+E/2)^2-E*E*pi/4/4; *Corner                               \n');
% fprintf(fid,' Pw_C=2*(O+E/2)+E*pi*0.25;   *Corner                              \n');
% fprintf(fid,' Ph_C=E*pi*0.25;   *Corner                                        \n');
% fprintf(fid,' FA_E=M*(O+E/2)-E*E*pi/4/2; *Edge                                 \n');
% fprintf(fid,' Pw_E=M+E*pi*0.5;   *Edge                                         \n');
% fprintf(fid,' Ph_E=E*pi*0.5;   *Edge                                           \n');
% fprintf(fid,' FA_F=M*M-E*E*pi/4; *Full                                         \n');
% fprintf(fid,' Pw_F=E*pi;   *Full                                               \n');
% fprintf(fid,' Ph_F=E*pi;   *Full                                               \n');
% fprintf(fid,' FA_W1=M*M-E*E*pi/4*0.75-((R-M)/2)^2; *Water rod 1                \n');
% fprintf(fid,' Pw_W1=E*pi*0.75+(R-M);   *Water rod 1                            \n');
% fprintf(fid,' Ph_W1=E*pi*0.75;   *Water rod 1                                  \n');
% fprintf(fid,' FA_W2=M*M-E*E*pi/4*0.5-(R-M)/2*M; *Water rod 1                   \n');
% fprintf(fid,' Pw_W2=E*pi*0.5+M;   *Water rod 1                                 \n');
% fprintf(fid,' Ph_W2=E*pi*0.5;   *Water rod 1                                   \n');
fclose(fid);
```

Appendix D

Derivation of the Lumped Annular Fuel Dynamics Model

In this work, an annular fuel dynamics model has been developed based on the lumped modeling approach [130] for the ASBWR stability analysis. The SAB code has been modified to incorporate the lumped annular fuel dynamics model to capture the annular fuel features. Figure D-1 illustrates the radii and temperatures of the model.

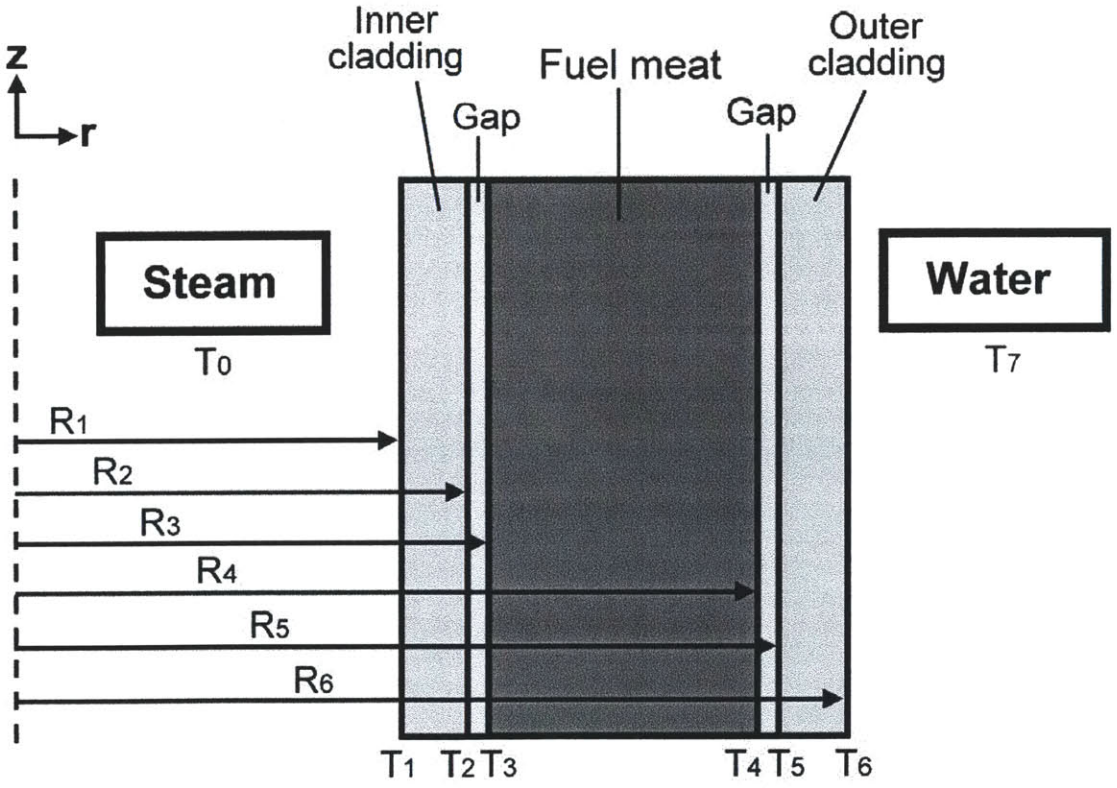

Figure D-1 Illustration of the lumped annular fuel dynamics model

D.1 Derivation of the Lumped Fuel Dynamic Equations

The annular fuel can be considered as a composition of three concentric tubes: the inner cladding, fuel meat and outer cladding. Absorption and storage of heat in the gap are negligible due to the very thin inner and outer gap thicknesses.

Define the area-averaging operator for any function T(r):

$$\overline{T} = \frac{1}{(R_j^2 - R_i^2)} \int_{R_i}^{R_j} T(r) 2rdr \tag{D-1}$$

Therefore, the average temperature of the fuel pin ($\overline{T_{pin}}$) is:

$$\overline{T_{pin}} = \frac{\int_{R_1}^{R_6} T(r) 2rdr}{(R_6^2 - R_1^2)} \approx \frac{(R_2^2 - R_1^2)}{(R_6^2 - R_1^2)} \overline{T_{c,i}} + \frac{(R_4^2 - R_3^2)}{(R_6^2 - R_1^2)} \overline{T_f} + \frac{(R_6^2 - R_5^2)}{(R_6^2 - R_1^2)} \overline{T_{c,o}} \tag{D-2}$$

where $\overline{T_{c,i}}$, $\overline{T_f}$ and $\overline{T_{c,o}}$ are average temperatures of the inner cladding, fuel meat and outer cladding, respectively. For transient response of the average fuel pin temperature:

$$\frac{d\overline{T_{pin}}}{dt} = \frac{(R_2^2 - R_1^2)}{(R_6^2 - R_1^2)} \frac{d\overline{T_{c,i}}}{dt} + \frac{(R_4^2 - R_3^2)}{(R_6^2 - R_1^2)} \frac{d\overline{T_f}}{dt} + \frac{(R_6^2 - R_5^2)}{(R_6^2 - R_1^2)} \frac{d\overline{T_{c,o}}}{dt} \tag{D-3}$$

Fourier's equation, as shown in equation (D-4), is used to describe transient response of temperature in the three tubes.

$$\rho c \frac{\partial T}{\partial t} = \frac{1}{r} \frac{\partial}{\partial r} (rk \frac{\partial T}{\partial r}) + q''' \tag{D-4}$$

where ρ, c, k and q''' refer to density, specific heat capacity, thermal conductivity and volumetric heat generation, respectively.

For average temperature of the fuel meat ($\overline{T_f}$):

A lumped fuel dynamics model with the temperature distribution in the annular fuel pellet developed at Brookhaven National Laboratory (BNL) [130] is applied.

Continuity of convective and conductive heat fluxes requires:

$$-k_f \frac{\partial T_f}{\partial r} = \overline{h_{gap,i}}(T_3 - T_2) \qquad \text{at r} = \text{R}_3 \tag{D-5}$$

$$-k_f \frac{\partial T_f}{\partial r} = \overline{h_{gap,o}}(T_4 - T_5) \qquad \text{at r} = \text{R}_4 \tag{D-6}$$

where $\overline{h_{gap,i}}$ and $\overline{h_{gap,o}}$ are gap conductance for the inner and outer gap, respectively.

Appling the operator defined by equation (D-1) to equation (D-4) and use equations (D-5) and (D-6) to find the single ordinary differential equation:

$$\frac{d\overline{T_f}}{dt} = \frac{q'''}{(\rho c_p)_f} + \frac{\alpha_f}{d^2}\{[(N_{Bi})_i \frac{R_3}{R_m}(T_2 - T_3)] + [(N_{Bi})_o \frac{R_4}{R_m}(T_5 - T_4)]\} \tag{D-7}$$

where $d = R_4 - R_3$, $R_m = \frac{R_3 + R_4}{2}$, $(N_{Bi})_i = \frac{\overline{h_{gap,i}}d}{k_f}$ and $(N_{Bi})_o = \frac{\overline{h_{gap,o}}d}{k_f}$.

To compute the surface temperatures, a polynomial is introduced to approximate the radial temperature distribution in the annular fuel pellet:

$$T_f(r) = \sum_{i=0}^{m} a_i(\tau)\eta^i \text{, where } \eta = \frac{r - R_3}{R_4 - R_3} \text{ is the normalized radius.} \tag{D-8}$$

Equation (D-8) must satisfy equations (D-5) and (D-6), and, because of equation (D-1),

$$\overline{T_f(r)} = \sum_{i=0}^{m} a_i(\tau)\overline{\eta^i} \tag{D-9}$$

These three conditions show that m = 2. Appling these three equations and after some algebra, equation (D-7) can be described in terms of only known quantities:

$$\frac{d\overline{T_f}}{dt} = \frac{q'''}{(\rho c_p)_f} + \frac{(N_{Bi})_i (N_{Bi})_o}{D}\frac{\alpha_f}{d^2}\{\frac{d}{6R_m}(T_2 - T_5) + \frac{R_3}{R_m}[\frac{2+(N_{Bi})_o}{(N_{Bi})_o}](T_2 - \overline{T_f}) + \frac{R_3 + d}{R_m}[\frac{2+(N_{Bi})_i}{(N_{Bi})_i}](T_5 - \overline{T_f})\} \tag{D-10}$$

where $D = 2 + \frac{8R_m + d}{12R_m}(N_{Bi})_i + \frac{8R_m - d}{12R_m}(N_{Bi})_o + \frac{(N_{Bi})_i (N_{Bi})_o}{6}$. (D-11)

Heat fluxes at the inner and outer surfaces are proportional to the temperature differences:

$$T_3 - T_2 = \{[2 + (N_{Bi})_o](\overline{T_f} - T_2) + \frac{4R_m + d}{12R_m}(N_{Bi})_o (T_2 - T_5)\} \Big/ D = (\frac{2R_1}{R_2 + R_3})\frac{q_{,i}''}{h_{gap,i}} \tag{D-12}$$

$$T_4 - T_5 = \{[2 + (N_{Bi})_i](\overline{T_f} - T_5) + \frac{4R_m - d}{12R_m}(N_{Bi})_i (T_5 - T_2)\} \Big/ D = (\frac{2R_6}{R_4 + R_5})\frac{q_{,o}''}{h_{gap,o}} \tag{D-13}$$

Finally, average temperature of the fuel meat can be written in terms of only known quantities:

$$\overline{T_f} = \{D\frac{d^2}{k_f}q''' + (N_{Bi})_i[\frac{2R_3}{R_m} + \frac{6R_3 + d}{6R_m}(N_{Bi})_o]T_2 + (N_{Bi})_o[\frac{2R_4}{R_m} + \frac{6R_4 - d}{6R_m}(N_{Bi})_i]T_5\} / \{\frac{R_3}{R_m}(N_{Bi})_i[2 + (N_{Bi})_o] + \frac{R_4}{R_m}(N_{Bi})_o[2 + (N_{Bi})_i]\} \quad \text{(D-14)}$$

For average temperature of the inner cladding ($\overline{T_{c,i}}$) and outer cladding ($\overline{T_{c,o}}$):

Continuity of convective and conductive heat fluxes requires:

$$-k_c\frac{\partial T_{c,i}}{\partial r} = \overline{h_{,i}}(T_1 - T_0) = q_{,i}'' \quad \text{at r = R}_1 \quad \text{(D-15)}$$

$$-k_c\frac{\partial T_{c,o}}{\partial r} = \overline{h_{,o}}(T_6 - T_7) = q_{,o}'' \quad \text{at r = R}_6 \quad \text{(D-16)}$$

where $\overline{h_{,i}}$ and $\overline{h_{,o}}$ are heat transfer coefficients of the internal and external coolants, respectively.

By applying the operator of the form given in equation (D-1) and using equations (D-4), (D-15) and (D-16), one obtains:

$$\frac{d\overline{T_{c,i}}}{dt} = \frac{2}{(R_2^2 - R_1^2)(\rho c_p)_c}[R_2 k_c \frac{\partial T_{c,i}}{\partial r}\Big|_{r=R_2} - R_1\overline{h_{,i}}(T_1 - T_0)]. \quad \text{(D-17)}$$

for the inner cladding, and

$$\frac{d\overline{T_{c,o}}}{dt} = \frac{2}{(R_6^2 - R_5^2)(\rho c_p)_c}[-R_6\overline{h_{,o}}(T_6 - T_7) - R_5 k_c \frac{\partial T_{c,o}}{\partial r}\Big|_{r=R_5}]. \quad \text{(D-18)}$$

for the outer cladding.

In order to compute the wall temperatures (T_1 and T_6), two power polynomials, (D-19) and (D-20), are introduced to approximate the temperature distribution in the inner and outer cladding, respectively.

$$.T_{c,i}(r) = T_1 + (\frac{r - R_1}{R_2 - R_1})(T_2 - T_1) \qquad \text{(D-19)}$$

$$.T_{c,o}(r) = T_5 - (\frac{r - R_5}{R_6 - R_5})(T_5 - T_6) \qquad \text{(D-20)}$$

Integrating over the region of inner cladding and outer cladding, one obtains

$$.\overline{T_{c,i}} = T_2 - (\frac{2R_2 + R_1}{3R_2 + 3R_1})(T_2 - T_1) \qquad \text{(D-21)}$$

$$\overline{T_{c,o}} = T_5 - (\frac{2R_6 + R_5}{3R_6 + 3R_5})(T_5 - T_6) \qquad \text{(D-22)}$$

For annular fuels, one parameter of great interest is the fraction of heat transferred by the internal coolant and by the external coolant. In this analysis, the heat split ratio (γ), as defined by equation (D-23), is assumed to be constant during the perturbation. Sensitivity study of the heat split ratio will be performed to evaluate its impact on the stability.

$$.\gamma \equiv \frac{q_{,o}"2\pi R_6 dz}{q'''\pi(R_4^2 - R_3^2)dz} = \frac{\text{Amount of heat trasnferred by the external coolant}}{\text{Total amount of heat generated}} \qquad \text{(D-23)}$$

According to energy balance:

$$.q_{,i}"2\pi R_1 dz + q_{,o}"2\pi R_6 dz = q'''\pi(R_4^2 - R_3^2)dz \qquad \text{(D-24)}$$

Thus,

$$q_{,o}" = \frac{\gamma q'''(R_4^{\,2} - R_3^{\,2})}{2R_6} \tag{D-25}$$

$$q_{,i}" = \frac{(1-\gamma)q'''(R_4^{\,2} - R_3^{\,2})}{2R_1} = \frac{(1-\gamma)}{\gamma}\frac{R_6}{R_1}q_{,o}" \tag{D-26}$$

Using equations (D-15), (D-16), (D-25) and (D-26), temperatures on the boundaries of the inner and outer claddings can be written as:

$$T_1 = \frac{(1-\gamma)}{\gamma}\frac{R_6}{R_1}\frac{q_{,o}"}{\overline{\overline{h}}_{,i}} + T_0 \tag{D-27}$$

$$T_2 = [\frac{(R_2 - R_1)}{k_c} + \frac{1}{\overline{\overline{h}}_{,i}}][\frac{(1-\gamma)}{\gamma}\frac{R_6}{R_1}q_{,o}"] + T_0 \tag{D-28}$$

$$T_5 = [\frac{(R_6 - R_5)}{k_c} + \frac{1}{\overline{\overline{h}}_{,o}}][q_{,o}"] + T_7 \tag{D-29}$$

$$T_6 = \frac{q_{,o}"}{\overline{\overline{h}}_{,o}} + T_7 \tag{D-30}$$

Applying equations (D-10) and (D-15) ~ (D-20) to equation (D-3), one obtains

$$\frac{d\overline{T_{pin}}}{dt} = \frac{2(R_2 - R_1)}{(R_6^{\,2} - R_1^{\,2})}\frac{q_{,i}"}{(\rho c_p)_c} + \frac{(R_4^{\,2} - R_3^{\,2})}{(R_6^{\,2} - R_1^{\,2})}\frac{d\overline{T_f}}{dt} + \frac{2(R_5 - R_6)}{(R_6^{\,2} - R_1^{\,2})}\frac{q_{,o}"}{(\rho c_p)_c} \tag{D-31}$$

Rewriting equation (D-31) with substitution of equations (D-25) ~ (D-30), after some rearrangement, one obtains

$$\frac{d\overline{T_{pin}}}{dt} = (C_{gm} - F_{pr})\, q_{,o}" + \frac{(R_4^{\,2} - R_3^{\,2})}{(R_6^{\,2} - R_1^{\,2})} \frac{q'''}{(\rho c_p)_f} \tag{D-32}$$

where

$$C_{gm} = (\frac{2}{R_6^{\,2} - R_1^{\,2}}) \frac{1}{(\rho c_p)_c} [(R_5 - R_6) + (R_2 - R_1)(\frac{R_6}{R_1})(\frac{1-\gamma}{\gamma})] \tag{D-33}$$

$$F_{pr} = [\frac{(N_{Bi})_i \alpha_f}{d^2 \overline{\overline{h_{gap,i}}}} \frac{R_3}{R_m} \frac{2R_1}{(R_2 + R_3)} (\frac{R_6}{R_1})(\frac{1-\gamma}{\gamma}) + \frac{(N_{Bi})_o \alpha_f}{d^2} \frac{R_4}{R_m} \frac{2R_6}{(R_4 + R_5)} \frac{1}{\overline{\overline{h_{gap,o}}}}]. \tag{D-34}$$

Applying equations (D-13), (D-21) and (D-22) to equation (D-3) and using equations (D-25) ~ (D-30), after some rearrangement, one obtains

$$\overline{T_{pin}} = C_1 q_{,o}" + C_2 q_{,i}" + C_3 T_6 + C_4 T_1 \tag{D-35}$$

where

$$C_1 = [\frac{(R_6 - R_5)^2}{(R_6^{\,2} - R_1^{\,2})} \frac{(R_6 + 2R_5)}{3k_c} + \frac{(R_4^{\,2} - R_3^{\,2})}{(R_6^{\,2} - R_1^{\,2})} \frac{R_6}{R_5} \frac{D}{\overline{\overline{h_{gap,o}}}(2 + (N_{Bi})_i)} + \frac{(R_4^{\,2} - R_3^{\,2})}{(R_6^{\,2} - R_1^{\,2})} \frac{(N_{Bi})_i}{(2 + (N_{Bi})_i)} \frac{(4R_m - d)}{12R_m} \frac{(R_6 - R_5)}{k_c}] \tag{D-36}$$

$$C_2 = [\frac{(R_2 - R_1)^2}{(R_6^{\,2} - R_1^{\,2})} \frac{(R_2 + 2R_1)}{3k_c} + \frac{(R_4^{\,2} - R_3^{\,2})}{(R_6^{\,2} - R_1^{\,2})} \frac{(N_{Bi})_i}{(2 + (N_{Bi})_i)} \frac{(4R_m - d)}{12R_m} \frac{(R_2 - R_1)}{k_c}] \tag{D-37}$$

$$C_3 = [\frac{(R_6^{\,2} - R_5^{\,2})}{(R_6^{\,2} - R_1^{\,2})} - \frac{(R_4^{\,2} - R_3^{\,2})}{(R_6^{\,2} - R_1^{\,2})} \frac{(N_{Bi})_i}{(2 + (N_{Bi})_i)} \frac{(4R_m - d)}{12R_m}] \tag{D-38}$$

$$C_4 = [\frac{(R_2^{\,2} - R_1^{\,2})}{(R_6^{\,2} - R_1^{\,2})} + \frac{(R_4^{\,2} - R_3^{\,2})}{(R_6^{\,2} - R_1^{\,2})} \frac{(N_{Bi})_i}{(2 + (N_{Bi})_i)} \frac{(4R_m - d)}{12R_m}] \tag{D-39}$$

D.2 Coupling of Fuel Dynamics to Coolant Thermal-hydraulics Model

The fuel dynamics model is coupled to the coolant thermal hydraulics model through the dynamics of the fluctuation of the fuel rods surface heat flux.

Perturbation, linearization and Laplace transformation of equation (D-32), one obtains:

$$s\overline{\delta T_{pin}} = (C_{gm} - F_{pr})\,\delta q_{,o}" + \frac{(R_4^{\,2} - R_3^{\,2})}{(R_6^{\,2} - R_1^{\,2})}\frac{\delta q'''}{(\rho c_p)_f} \tag{D-40}$$

Perturbation, linearization and Laplace transformation of Equation (D-35), one obtains:

$$\overline{\delta T_{pin}} = [C_1 + (\frac{R_6}{R_1})(\frac{1-\gamma}{\gamma})(C_2 + \frac{C_4}{h_{,i}}) + \frac{C_3}{h_{,o}}]\delta q_{,o}" - \frac{q_{,o}"}{h_{,o}}\frac{\overline{\delta h_{,o}}}{h_{,o}} + C_3\delta T_7 + C_4\delta T_0 \tag{D-41}$$

Combining the above equations (D-40) and (D-41), after some rearrangement, one obtains:

$$\begin{aligned}[C_1 + (\frac{R_6}{R_1})(\frac{1-\gamma}{\gamma})(C_2 + \frac{C_4}{h_{,i}}) + \frac{C_3}{h_{,o}} - \frac{(C_{gm} - F_{pr})}{s}]\delta q_{,o}" = \\ \frac{q_{,o}"}{h_{,o}}\frac{\overline{\delta h_{,o}}}{h_{,o}} - C_3\delta T_7 - C_4\delta T_0 + \frac{(R_4^{\,2} - R_3^{\,2})}{s(R_6^{\,2} - R_1^{\,2})}\frac{\delta q'''}{(\rho c_p)_f}\end{aligned} \tag{D-42}$$

Plugging equation (D-42) into the coolant thermal-hydraulic dynamics model, the characteristic equation of the coupled fuel dynamics model could be derived.

Appendix E

Input Files

E.1 VIPRE-01 Input for the ASBWR Assembly Analysis

```
*   A-SBWR Assembly with one square water rod
*
*   Yu-Chih Ko 12/20/09
*
*************************************************************************
*A-SBWR Assembly with one square water rod
1,0,0,                                                          *vipre.1
A-SBWR Assembly                                                   *vipre.2
*
geom,80,80,60,0,0,0,     *80 channels, 60 axial nodes
*
118.11,0.0,0.5,          *geom.2     3 m = 118.11 inches
*
* START of geom 4
*
1,0.1783,1.6927,0.6061,2,2,0.1575,0.8608,10,0.1575,0.8608,
2,0.2581,2.1176,1.2121,2,3,0.1575,0.9055,11,0.1339,0.8608,
3,0.2581,2.1176,1.2121,2,4,0.1575,0.9055,12,0.1339,0.8608,
4,0.2581,2.1176,1.2121,2,5,0.1575,0.9055,13,0.1339,0.8608,
5,0.2581,2.1176,1.2121,2,6,0.1575,0.9055,14,0.1339,0.8608,
6,0.2581,2.1176,1.2121,2,7,0.1575,0.9055,15,0.1339,0.8608,
7,0.2581,2.1176,1.2121,2,8,0.1575,0.9055,16,0.1339,0.8608,
8,0.2581,2.1176,1.2121,2,9,0.1575,0.8608,17,0.1339,0.8608,
9,0.1783,1.6927,0.6061,1,18,0.1575,0.8608,
*
10,0.2581,2.1176,1.2121,2,11,0.1339,0.8608,19,0.1575,0.9055,
11,0.3523,2.4242,2.4242,2,12,0.1339,0.9055,20,0.1339,0.9055,
12,0.3523,2.4242,2.4242,2,13,0.1339,0.9055,21,0.1339,0.9055,
13,0.3523,2.4242,2.4242,2,14,0.1339,0.9055,22,0.1339,0.9055,
14,0.3523,2.4242,2.4242,2,15,0.1339,0.9055,23,0.1339,0.9055,
15,0.3523,2.4242,2.4242,2,16,0.1339,0.9055,24,0.1339,0.9055,
16,0.3523,2.4242,2.4242,2,17,0.1339,0.9055,25,0.1339,0.9055,
17,0.3523,2.4242,2.4242,2,18,0.1339,0.8608,26,0.1339,0.9055,
18,0.2581,2.1176,1.2121,1,27,0.1575,0.9055,
*
19,0.2581,2.1176,1.2121,2,20,0.1339,0.8608,28,0.1575,0.9055,
20,0.3523,2.4242,2.4242,2,21,0.1339,0.9055,29,0.1339,0.9055,
21,0.3523,2.4242,2.4242,2,22,0.1339,0.9055,30,0.1339,0.9055,
22,0.3523,2.4242,2.4242,2,23,0.1339,0.9055,31,0.1339,0.8549,
23,0.3523,2.4242,2.4242,2,24,0.1339,0.9055,32,0.1339,0.7185,
24,0.3523,2.4242,2.4242,2,25,0.1339,0.9055,33,0.1339,0.8549,
25,0.3523,2.4242,2.4242,2,26,0.1339,0.9055,34,0.1339,0.9055,
26,0.3523,2.4242,2.4242,2,27,0.1339,0.8608,35,0.1339,0.9055,
27,0.2581,2.1176,1.2121,1,36,0.1575,0.9055,
*
28,0.2581,2.1176,1.2121,2,29,0.1339,0.8608,37,0.1575,0.9055,
29,0.3523,2.4242,2.4242,2,30,0.1339,0.9055,38,0.1339,0.9055,
```

30,0.3523,2.4242,2.4242,2,31,0.1339,0.8549,39,0.1339,0.9055,
31,0.3293,2.5662,1.8182,2,32,0.1457,0.9561,40,0.1457,0.9561,
32,0.2474,2.1176,1.2121,1,33,0.1457,0.9561,
33,0.3293,2.5662,1.8182,2,34,0.1339,0.8549,41,0.1457,0.9561,
34,0.3523,2.4242,2.4242,2,35,0.1339,0.9055,42,0.1339,0.9055,
35,0.3523,2.4242,2.4242,2,36,0.1339,0.8608,43,0.1339,0.9055,
36,0.2581,2.1176,1.2121,1,44,0.1575,0.9055,
*
37,0.2581,2.1176,1.2121,2,38,0.1339,0.8608,45,0.1575,0.9055,
38,0.3523,2.4242,2.4242,2,39,0.1339,0.9055,46,0.1339,0.9055,
39,0.3523,2.4242,2.4242,2,40,0.1339,0.7185,47,0.1339,0.9055,
40,0.2474,2.1176,1.2121,1,48,0.1457,0.9561,
41,0.2474,2.1176,1.2121,2,42,0.1339,0.7185,50,0.1457,0.9561
42,0.3523,2.4242,2.4242,2,43,0.1339,0.9055,51,0.1339,0.9055,
43,0.3523,2.4242,2.4242,2,44,0.1339,0.8608,52,0.1339,0.9055,
44,0.2581,2.1176,1.2121,1,53,0.1575,0.9055,
*
45,0.2581,2.1176,1.2121,2,46,0.1339,0.8608,54,0.1575,0.9055,
46,0.3523,2.4242,2.4242,2,47,0.1339,0.9055,55,0.1339,0.9055,
47,0.3523,2.4242,2.4242,2,48,0.1339,0.8549,56,0.1339,0.9055,
48,0.3293,2.5662,1.8182,2,49,0.1457,0.9561,57,0.1339,0.8549,
49,0.2474,2.1176,1.2121,2,50,0.1457,0.9561,58,0.1339,0.7185,
50,0.3293,2.5662,1.8182,2,51,0.1339,0.8549,59,0.1339,0.8549,
51,0.3523,2.4242,2.4242,2,52,0.1339,0.9055,60,0.1339,0.9055,
52,0.3523,2.4242,2.4242,2,53,0.1339,0.8608,61,0.1339,0.9055,
53,0.2581,2.1176,1.2121,1,62,0.1575,0.9055,
*
54,0.2581,2.1176,1.2121,2,55,0.1339,0.8608,63,0.1575,0.9055,
55,0.3523,2.4242,2.4242,2,56,0.1339,0.9055,64,0.1339,0.9055,
56,0.3523,2.4242,2.4242,2,57,0.1339,0.9055,65,0.1339,0.9055,
57,0.3523,2.4242,2.4242,2,58,0.1339,0.9055,66,0.1339,0.9055,
58,0.3523,2.4242,2.4242,2,59,0.1339,0.9055,67,0.1339,0.9055,
59,0.3523,2.4242,2.4242,2,60,0.1339,0.9055,68,0.1339,0.9055,
60,0.3523,2.4242,2.4242,2,61,0.1339,0.9055,69,0.1339,0.9055,
61,0.3523,2.4242,2.4242,2,62,0.1339,0.8608,70,0.1339,0.9055,
62,0.2581,2.1176,1.2121,1,71,0.1575,0.9055,
*
63,0.2581,2.1176,1.2121,2,64,0.1339,0.8608,72,0.1575,0.8608,
64,0.3523,2.4242,2.4242,2,65,0.1339,0.9055,73,0.1339,0.8608,
65,0.3523,2.4242,2.4242,2,66,0.1339,0.9055,74,0.1339,0.8608,
66,0.3523,2.4242,2.4242,2,67,0.1339,0.9055,75,0.1339,0.8608,
67,0.3523,2.4242,2.4242,2,68,0.1339,0.9055,76,0.1339,0.8608,
68,0.3523,2.4242,2.4242,2,69,0.1339,0.9055,77,0.1339,0.8608,
69,0.3523,2.4242,2.4242,2,70,0.1339,0.9055,78,0.1339,0.8608,
70,0.3523,2.4242,2.4242,2,71,0.1339,0.8608,79,0.1339,0.8608,
71,0.2581,2.1176,1.2121,1,80,0.1575,0.8608,
*
72,0.1783,1.6927,0.6061,1,73,0.1575,0.8608,
73,0.2581,2.1176,1.2121,1,74,0.1575,0.9055,
74,0.2581,2.1176,1.2121,1,75,0.1575,0.9055,
75,0.2581,2.1176,1.2121,1,76,0.1575,0.9055,
76,0.2581,2.1176,1.2121,1,77,0.1575,0.9055,
77,0.2581,2.1176,1.2121,1,78,0.1575,0.9055,
78,0.2581,2.1176,1.2121,1,79,0.1575,0.9055,
79,0.2581,2.1176,1.2121,1,80,0.1575,0.8608,
80,0.1783,1.6927,0.6061,

```
*
* END of geom.4
*
prop,0,1,2,1      *internal EPRI functions *prop.1
*
rods,1,65,1,3,2,0,0,0,0,0,0    *3types of rod,two types of mat. *rods.1
118.11,0.0,0,0                                                    *rods.2
*
*
26                                                  *rods3
*One axial profile only    (rods.4)
0.00,0.00,?
2.46,0.38,?
7.38,0.69,?
12.30,0.93,
17.22,1.10,?
22.14,1.21,?
27.06,1.30,?
31.97,1.47,
36.89,1.51,?
41.81,1.49,?
46.73,1.44,?
51.65,1.36,
56.57,1.28,?
61.49,1.16,?
66.41,1.06,?
71.33,1.01,
76.25,0.97,?
81.17,0.94,?
86.09,0.97,?
91.01,0.96,
95.92,0.91,?
100.84,0.77,?
105.76,0.59,?
110.68,0.38,
115.6,0.12,?
118.11,0.00,
*
*
*
******rods geometry input                                  *rods.9
* Radial peaking is based on CASMO Results
*091112 Control Rod and Gd, A12.out, zero burnup
*
1,1,1.183,1,1,0.25,2,0.25,10,0.25,11,0.25,
2,1,1.290,1,2,0.25,3,0.25,11,0.25,12,0.25,
3,1,1.184,1,3,0.25,4,0.25,12,0.25,13,0.25,
4,1,1.150,1,4,0.25,5,0.25,13,0.25,14,0.25,
5,1,1.150,1,5,0.25,6,0.25,14,0.25,15,0.25,
6,1,1.184,1,6,0.25,7,0.25,15,0.25,16,0.25,
7,1,1.290,1,7,0.25,8,0.25,16,0.25,17,0.25,
8,1,1.183,1,8,0.25,9,0.25,17,0.25,18,0.25,
*
9,1,1.244,1,10,0.25,11,0.25,19,0.25,20,0.25,
10,1,0.926,1,11,0.25,12,0.25,20,0.25,21,0.25,
11,1,0.511,1,12,0.25,13,0.25,21,0.25,22,0.25,
```

12,1,0.888,1,13,0.25,14,0.25,22,0.25,23,0.25,
13,1,0.888,1,14,0.25,15,0.25,23,0.25,24,0.25,
14,1,0.511,1,15,0.25,16,0.25,24,0.25,25,0.25,
15,1,0.926,1,16,0.25,17,0.25,25,0.25,26,0.25,
16,1,1.244,1,17,0.25,18,0.25,26,0.25,27,0.25,
*
17,1,1.182,1,19,0.25,20,0.25,28,0.25,29,0.25,
18,1,0.511,1,20,0.25,21,0.25,29,0.25,30,0.25,
19,1,0.855,1,21,0.25,22,0.25,30,0.25,31,0.25,
20,1,1.043,1,22,0.25,23,0.25,31,0.25,32,0.25,
21,1,1.043,1,23,0.25,24,0.25,32,0.25,33,0.25,
22,1,0.855,1,24,0.25,25,0.25,33,0.25,34,0.25,
23,1,0.511,1,25,0.25,26,0.25,34,0.25,35,0.25,
24,1,1.182,1,26,0.25,27,0.25,35,0.25,36,0.25,
*
25,1,1.148,1,28,0.25,29,0.25,37,0.25,38,0.25,
26,1,0.888,1,29,0.25,30,0.25,38,0.25,39,0.25,
27,1,1.042,1,30,0.25,31,0.25,39,0.25,40,0.25,
28,1,1.042,1,33,0.25,34,0.25,41,0.25,42,0.25,
29,1,0.888,1,34,0.25,35,0.25,42,0.25,43,0.25,
30,1,1.148,1,35,0.25,36,0.25,43,0.25,44,0.25,
*
31,1,1.148,1,37,0.25,38,0.25,45,0.25,46,0.25,
32,1,0.888,1,38,0.25,39,0.25,46,0.25,47,0.25,
33,1,1.042,1,39,0.25,40,0.25,47,0.25,48,0.25,
34,1,1.042,1,41,0.25,42,0.25,50,0.25,51,0.25,
35,1,0.888,1,42,0.25,43,0.25,51,0.25,52,0.25,
36,1,1.148,1,43,0.25,44,0.25,52,0.25,53,0.25,
*
37,1,1.182,1,45,0.25,46,0.25,54,0.25,55,0.25,
38,1,0.511,1,46,0.25,47,0.25,55,0.25,56,0.25,
39,1,0.855,1,47,0.25,48,0.25,56,0.25,57,0.25,
40,1,1.043,1,48,0.25,49,0.25,57,0.25,58,0.25,
41,1,1.043,1,49,0.25,50,0.25,58,0.25,59,0.25,
42,1,0.855,1,50,0.25,51,0.25,59,0.25,60,0.25,
43,1,0.511,1,51,0.25,52,0.25,60,0.25,61,0.25,
44,1,1.182,1,52,0.25,53,0.25,61,0.25,62,0.25,
*
45,1,1.244,1,54,0.25,55,0.25,63,0.25,64,0.25,
46,1,0.926,1,55,0.25,56,0.25,64,0.25,65,0.25,
47,1,0.511,1,56,0.25,57,0.25,65,0.25,66,0.25,
48,1,0.888,1,57,0.25,58,0.25,66,0.25,67,0.25,
49,1,0.888,1,58,0.25,59,0.25,67,0.25,68,0.25,
50,1,0.511,1,59,0.25,60,0.25,68,0.25,69,0.25,
51,1,0.926,1,60,0.25,61,0.25,69,0.25,70,0.25,
52,1,1.244,1,61,0.25,62,0.25,70,0.25,71,0.25,
*
53,1,1.183,1,63,0.25,64,0.25,72,0.25,73,0.25,
54,1,1.290,1,64,0.25,65,0.25,73,0.25,74,0.25,
55,1,1.184,1,65,0.25,66,0.25,74,0.25,75,0.25,
56,1,1.150,1,66,0.25,67,0.25,75,0.25,76,0.25,
57,1,1.150,1,67,0.25,68,0.25,76,0.25,77,0.25,
58,1,1.184,1,68,0.25,69,0.25,77,0.25,78,0.25,
59,1,1.290,1,69,0.25,70,0.25,78,0.25,79,0.25,
60,1,1.183,1,70,0.25,71,0.25,79,0.25,80,0.25,
*

```
*
*   *Water rod (ext)
*
61,2,0.0,1,31,0.1131,33,0.1131,48,0.1131,50,0.1131,?
32,0.1369,40,0.1369,41,0.1369,49,0.1369,
*
*   *Channel (Inner surface)
*
-62,3,0.0,1,1,0.07317,2,0.12195,3,0.12195,4,0.12195,?
5,0.12195,6,0.12195,7,0.12195,8,0.12195,9,0.07317,
*
-63,3,0.0,1,1,0.07317,10,0.12195,19,0.12195,28,0.12195,?
37,0.12195,45,0.12195,54,0.12195,63,0.12195,72,0.07317,
*
-64,3,0.0,1,9,0.07317,18,0.12195,27,0.12195,36,0.12195,?
44,0.12195,53,0.12195,62,0.12195,71,0.12195,80,0.07317,
*
-65,3,0.0,1,72,0.07317,73,0.12195,74,0.12195,75,0.12195,?
76,0.12195,77,0.12195,78,0.12195,79,0.12195,80,0.07317,
*
*
*
0               *End of rods.9
*
*
*fuel geometry
1,nucl,0.7717,0.7008,12,0.4646,0.0315   *rods.62
0,0,2,0,0,1056.66,0.955,0.0,        *rods 63 T91 or Inconel cladding in RODs 70 =2
*constant radial power in the pellet, no power in the clad
*
*water tube
2,tube,1.8658,1.7770,1    *rods.68
3,1,0.04442,1.0,       *rods.69
*wall
3,wall,7.4252,0.0,1      *rods.68
3,1,0.1,1.0,    *rods.69    Assume wall thickness = 0.1"
*
*
1,1,409.7,clad,              *rods 70    Zir2
662,0.076,10.05,             *rods 71
*T91 density=7.79 g/cm^3; specific heat = 560J/kg-K at 300 C; Thermal conductivity=29 W/mK
2,1,486.582,TT91,             *rods 70    T91
662,0.1338,16.77,             *rods 71
*Inconel 718 density=8.19 g/cm^3; specific heat = 435 J/kg-K; Thermal conductivity=15.5 W/mK
*2,1,511.57,I718,             *rods 70    Inconel 718
*662,0.1039,8.956,             *rods 71
**********************************
*P,T
oper,1,1,0,1,0,1,0,0,0,                          *oper.1    /flow is specified
-1.0,0.0,2.0,0.005,                               *oper.2
0                                                      *oper.3
1035.0,536.36,37.613,113.71,0.0       *oper.5
*
*Rod power got from total power divided total number of rods
0,                          *no forcing functions     *oper.12
**********************************
```

```
*correlations
corr,1,2,0,                                                              *corr.1
epri,epri,epri,none,                                                     *corr.2
0.2,                                                                        *corr.3
ditb,chen,chen,epri,cond,g5.7,       *correlation for boiling curve     *corr.6
epri,                                 *corr.9,DNB Analysis
1,0,0.0,                             *corr.16,for epri
**********************
mixx,0,0,0,
0.8,0.0048,0.0,
**********************************************************
grid,0,7,                                        *grid.1 => seven local grid loss IDs
9.4609,1.203,0.3751,21.089,182.049,312.0,729.0 *grid2 value of the seven local grid loss IDs
80,10,                                                *grid.4 ; 80 rods, 10 axial locations
1,2,3,4,5,6,7,8,9,10,11,12,13,14,15,16,                          *grid.5
17,18,19,20,21,22,23,24,25,26,27,28,29,30,31,32,
33,34,35,36,37,38,39,40,41,42,43,44,45,46,47,48,
49,50,51,52,53,54,55,56,57,58,59,60,61,62,63,64,
65,66,67,68,69,70,71,72,73,74,75,76,77,78,79,80,
*grid.5
*
0.000,4,5.9063,1,15.7771,2,31.554,2,47.3314,2,63.1085,2,78.8856,2,94.6628,2     *grid6
110.4399,2,115.6989,3                                                                              *grid6
0,                                                       *End of Grid input
**********************************************************
cont,                                                                      *cont.1
0.0,0,500,100,3,0,     *iterative solution                          *cont.2
0.10,0.00001,0.001,0.05,0.01,0.9,1.5,1.0,                          *cont.3
5,0,0,0,0,0,1,1,0,0,0,1,1,0,                                        *cont.6
200.,0.0,0.0,0.0,0.0,0.0,                                           *cont.7
endd
*
*end of data input
0
```

E.2 MCNP Input for the Benchmark Study

```
Superheat BWR pin model
c   z = 30 cm
c   See 090514 TH-input
c
c      cell specification
c
c   #     mt   density          geometry
     c section     1
    11     5    -2.3840E-02      -1          101 -102        imp:n=1
    12     3    -7.7943E+00       1      -2   101 -102        imp:n=1
    13     2    -4.7584E-03       2      -3   101 -102        imp:n=1
    14     1    -1.0400E+01       3      -4   101 -102        imp:n=1
    15     2    -5.4273E-03       4      -5   101 -102        imp:n=1
    16     3    -7.7943E+00       5      -6   101 -102        imp:n=1
    17     4    -7.5300E-01       6   101 -102   -11 12   -13   14          imp:n=1 $same as CASMO
  1000   0                        #(101 -102 -11 12 -13 14) imp:n=0 $ outside of the model
c      end of cell specification
c LEAVE A SPACE

c
c      surface specification
c
c      trn card    constants for equations
    1     cz     0.5                  $ inner clad inner radius
    2     cz     0.58                 $ inner clad outer radius
    3     cz     0.59                 $ fuel inner radius
    4     cz     0.89                 $ fuel outer radius
    5     cz     0.90                 $ inner clad inner radius
    6     cz     0.98                 $ outer clad outer radius
    *101   pz     -2                 $Reflective BSc
    *102   pz      2
    *11    px      1.2144              $ front boundary
    *12    px     -1.2144              $ back boundary
    *13    py      1.2144              $ right boundary
    *14    py     -1.2144              $ left boundary
c      end of surface specification
c LEAVE A SPACE

c        data specification
c
c Tally cards
c
fc14          Flux Tally in 4 sections and total
f14:n         14
c
c
c      material specification
c
c       Fuel (UO2) 1200k 4.5% enr
m1     92234.36c 8.44037E-06     $ consistent with CASMO
       92235.36c 1.05505E-03
       92238.36c 2.21442E-02
       8016.36c 4.64154E-02
c
```

```
c       He (gap) 800K
m2        2004.36c    3.76497E-05
c
c       T91    (7.79426g/cc) 700 K
c       Detailed version
c m3          24052.35c -0.0826
c             28059.35c -0.0013
c             25055.35c -0.0038
c             23000.35c -0.0020
c             41093.35c -0.0008
c             42096.35c -0.0095
c             13027.35c -0.0002
c             29065.35c -0.0008
c             33075.35c -0.0002
c             50119.35c -0.0001
c              6000.35c -0.0011
c              7014.35c -0.0006
c             15031.35c -0.0001
c             14028.35c -0.0043
c             26056.35c -0.8927
c - Simplfied version - same as CASMO
m3          24052.35c -0.0921
            28059.35c -0.0013
            25055.35c -0.0038
            14028.35c -0.0043
            26056.35c -0.8975
c
c       H2O (7.0MPa at 552.2K)    (0.753g/cc)
m4          8016.34c 2.35652e-2
            1001.34c 4.71033e-2
mt4         lwtr07.31t
c       Steam (7.0MPa at 696.0K)    (0.0238g/cc)
m5          8016.35c 2.35652e-2
            1001.35c 4.71033e-2
mt5         lwtr07.31t
c
c       shield (B4C) approximate
c m5          5010.35c     -1.0
c
c      end of material specification
c
c      1. phys energy physics cutoff cards
c             emax    emcnf
phys:n       20      0.0
c
c       3. tmp free-gas thermal temperature card
c      t1n t2n...n=index of time,t1n=temp for cell 1 at time n
   #             tmp1                          $                      kb=        8.61734E-05     ev/K
11          5.9974E-08
12          6.1638E-08
13          6.3490E-08
14          6.5390E-08
15          5.5174E-08
16          4.8779E-08
17          4.7583E-08
1000          6.032135E-08                  $ MeV          T= 700   K
```

```
c       data specification
c
c
kcode     10000      1.0   20      220
ksrc 0 0 0
        0 0 -2.5
        0 0 2.5
prdmp     220 220 220
print
```

E.3 CASMO Input for the Benchmark Study

```
TTL * ASBWR Single Pin Model Benchmark with MNCP
*******Z=30 cm => see 090514 TH-input
***** STATE POINT PARAMETERS *****
TFU=758.82 TMO=552.18 VOI=0.0

***** OPERATING PARAMETERS *****
PRE 70.0 * RX PRESSURE, bars
PDE 45 'KWL' * POWER DENSITY,

***** MATERIAL COMPOSITIONS - 4.54% enrichment*****
FUE 1 /1.05505E+21 92234=8.44037E+18 92238=2.21442E+22 8000=4.64154E+22
MI1 0.0238,0,695.97/1001=11.19 8000=88.81 *Steam coolant, Z=30 (cm)
MI2 7.7943,12.E-6,860.74/24000=8.0 28000=0.10
25000=0.30 14000=0.50 6000=0.12 26000=90.98 *T91 inner
CAN 7.7943,12.E-6,860.74/24000=8.0 28000=0.10
25000=0.30 14000=0.50 6000=0.12 26000=90.98 *T91 inner
***** GEOMETRY SPECIFICATION *****
PIN 1 0.5 0.58 0.59 0.89 0.90 0.98/
        'MI1'  'MI2'  'AIR'    'I'    'AIR'  'CAN'
PWR 2 2.4288     *Single pin model, Use PWR card to eliminate Box and water gap
DEP 0 0.1 0.5 1 5 10 20 30 40 50 60 70 80 90 100
STA
END
```

E.4 CASMO Input for the ASBWR Assembly Analysis

```
TIT * ASBWR Assembly Model refer to SP model SP02;
***** STATE POINT PARAMETERS *****
TFU=800 TMO=560 VOI=45.0
MOD 0.7566 *Mod density
***** OPERATING PARAMETERS *****
PDE 50.5 'KWL'
***** MATERIAL COMPOSITIONS *****
FUE 1 10.1/4.8 64016=5.0 * dummy fuel
FUE 2 10.1/7.5 64016=3.0
FUE 3 10.4/3.5
FUE 4 10.4/5.5
FUE 5 10.4/6.4
FUE 6 10.4/7.0
MI1 0.0213,0,757.35/1001=11.19 8000=88.81 *Steam coolant
MI2 7.7943,12.E-6,860.74/24000=8.0 28000=0.10
25000=0.30 14000=0.50 6000=0.12 26000=90.98 *T91 inner
CAN 7.7943,12.E-6,860.74/24000=8.0 28000=0.10
25000=0.30 14000=0.50 6000=0.12 26000=90.98 *T91 inner
***** GEOMETRY SPECIFICATION *****
BWR 8 2.3 18.86 0.254 0.75 0.75
PIN 1 2.0 2.1/'MOD' 'BOX'//-4.0 * Square Water rod
PIN 2 0.5 0.58 0.59 0.89 0.90 0.98/
      'MI1'  'MI2'  'AIR'   '2'  'AIR'  'CAN'
PIN 3 0.5 0.58 0.59 0.89 0.90 0.98/
      'MI1'  'MI2'  'AIR'   '3'  'AIR'  'CAN'
PIN 4 0.5 0.58 0.59 0.89 0.90 0.98/
      'MI1'  'MI2'  'AIR'   '4'  'AIR'  'CAN'
PIN 5 0.5 0.58 0.59 0.89 0.90 0.98/
      'MI1'  'MI2'  'AIR'   '5'  'AIR'  'CAN'
PIN 6 0.5 0.58 0.59 0.89 0.90 0.98/
      'MI1'  'MI2'  'AIR'   '6'  'AIR'  'CAN'
LPI
3
4 5
5 2 6
5 6 5 1
5 6 5 1 1
5 2 6 5 5 6
4 5 2 6 6 2 5
3 4 5 5 5 5 4 3
***** BASE DEPLETIONS (UNRODDED, HVOI=40) *****
DEP -60
STA
END
```

E.5 Single Channel Stability Analysis Input

```
%Matlab script for calculating the Decay Ratios of the typical BWR single channel stability.
%HEM model was used for two phase flow
%DB correlation was used for the heat transfer in single phase
%Chen's correlation was used for the heat transfer in two phase
%Written by Jiyun Zhao, Feb. 7, 2004
%Rewrite by Yu-chih Ko 04/12/10

%%%%%%%%% Beginning of the input file

%water properties at the saturation state
P=7.136*1.0e6;%Pa, system pressure
vf=0.00135629; %kg/m^3, liquid specific volume
vg=0.0267941; %kg/m^3, vapor sepcific volume
hf=1274.63;%KJ/kg, liquid specific enthalpy
hg=2770.84;%KJ/kg, vapor specific enthalpy
Cpf=5.42992;%kJ/kg, liquid specific heat
kf=569.741e-3;%J/kg, liquid heat conductivity
Prf=0.864884;% liquid Prandtl number
dviscf=0.0000907488; % liquid dynamic viscocity
dviscg=0.00001902;% vapor dynamic viscocity
xigmaf=0.0173297;%N/m surface tension
Tf=560.2;%K, saturation temperature

%assembly and fuel variables
d_pin=0.0196;%m, pin diameter
d_pellet=17.8e-3;%m, pellet diameter
N_pin=60;% number of the pins per assembly
L=3.0;%m, active length of the core
L_tot=3.8;%m, total length of the core   *ASSUMED for now
d_assm=0.1886;%m, assembly inner side
hgap=5.661;%kW/m^2-K, gap gas conductance
denfuel=10421;%kg/m^3, fuel density,95% of the theoretical density

%power and flow   %refer to VIPRE input
%(listed here is for power factor = 1.3 but in the folder the VIPRE input
%has a power factor = 1.2 => convert by a factor of 1.3/1.2
%power factor = 1.3 corresponds to a power density of ~50kW/L
%refer to A10812 DATA.txt
xx=1.0; %sensitivity on power density
%massem=18.747;%kg/s, mass flow rate per assembly => 38.1157*1.3/1.2*0.454
massem=17.06*xx;%kg/s, mass flow rate per assembly => 34.2*1.3/1.2*0.454
%Qassem=4.6215e3;%kW, average assembly power => 103.095 (kW/rod) *60 (rods)*1.3/1.2/1.45
Qassem=4.7e3*xx;%kW, average assembly power => 106.82 (kW/rod) *60 (rods)*1.3/1.2/1.45
Fpower=1.45;%radial power factor, a uniform power distribution was assumed

%inlet conditions
hin=1227.55;%kJ/kg, inlet enthalpy
Tin=278.3+273.15;%K, inlet temperature

%the inlet orifice coefficient
kin=21.089;

%the spacer coefficient
%dL_spacer=L/9; % distance between two spacer
```

```
n_spacer=7;
% L_spacer=[0.2484 0.7551 1.26354 1.78295 2.29135 2.79976 3.30646]; %spacer location
L_spacer=[0.4006 0.8014 1.2022 1.6030 2.0038 2.8052 2.9388]; %spacer location, YKO 02/04/10 acording
to VIPRE input
klp=9.4609; % lower tieplate coefficient
kup=0.3751; % upper tieplate coefficient
ksp0=1.203; % spacer coefficient


%input the initial guess of the dominate root
root_re=-0.5;
root_im=4.0;

%%%%%%%%%%%%%%%%end of the input file
```

E.6 In-Phase Channel Stability Analysis Input

```
%Matlab script for calculating the Decay Ratios of the BWR in-phase stability
%
%HEM model was used for two phase flow
%
%input file
%
%Written by Rui Hu, June, 2008

%%%%%%%%% Beginning of the input file

%water properties at the saturation state
P=7.136*1.0e6;%Pa, system pressure
vf=0.00135629; %kg/m^3, liquid specific volume
vg=0.0267941; %kg/m^3, vapor sepcific volume
hf=1274.63;%KJ/kg, liquid specific enthalpy
hg=2770.84;%KJ/kg, vapor specific enthalpy
Cpf=5.42992;%kJ/kg, liquid specific heat
kf=569.741e-3;%J/kg, liquid heat conductivity
Prf=0.864884;% liquid Prandtl number
dviscf=0.0000907488; % liquid dynamic viscocity
dviscg=0.00001902;% vapor dynamic viscocity
xigmaf=0.0173297;%N/m surface tension
Tf=560.2;%K, saturation temperature

%assembly and fuel variables
d_pin=0.0196;%m, pin diameter
d_pellet=17.8e-3;%m, pellet diameter
N_pin=60;% number of the pins per assembly
N_assm=195;%total assembly number
L=3.0;%m, active length of the core
L_tot=3.8;%m, total length of the core    *ASSUMED for now
d_assm=0.1886;%m, assembly inner side
hgap=5.661;%kW/m^2-K, gap gas conductance
denfuel=10421;%kg/m^3, fuel density,95% of the theoretical density

%core power and flow
Qcore=1003.0e3;%kW
mcore=4250.;%kg/s, core flow rate (coolant + bypass)
%feedwater
%mfw=1855.504;%feedwater flow rate
mfw=600.504;%feedwater flow rate    assumed for now
hfw=975.6;% feed water enthalpy
%
%1. Core channel groups parameters
%high power channel group parameters
kin_h=21.089;%high power channel group inlet orifice
%assem_h=148;%high power channel group assembly number
assem_h=38;%high power channel group assembly number, assumed for now
mhigh=18.635; %kg/s, high power channel group flow rate per assembly
Fpr_h=1.3;%high power channel factor relative to the core average power

%middle power channel parameters
kin_m=21.089;
assem_m=127;
```

```
m_m=19.827;
Fpr_m=1.004;%middle power channel factor relative to the core average power

%low power channel parameters
kin_l=182.049;
assem_l=30;
mlow=10.50;
Fpr_l=0.60;%low power channel factor relative to the core average power
%%%%%%End of Channel groups parameters

%the spacer coefficient
%dL_spacer=L/9; % distance between two spacer
n_spacer=7;
% L_spacer=[0.2484 0.7551 1.26354 1.78295 2.29135 2.79976 3.30646]; %spacer location
L_spacer=[0.4006 0.8014 1.2022 1.6030 2.0038 2.8052 2.9388]; %spacer location, YKO 02/04/10 acording
to VIPRE input
klp=9.4609; % lower tieplate coefficient
kup=0.3751; % upper tieplate coefficient
ksp0=1.203; % spacer coefficient

%2.upper plenum
Aup_ex=3.9328;%upper plenum exit area equals riser area
Aup=17.709;%upper plenum area
Lup=1.524;%length

%3.riser
De_rs=0.15405;%m, riser equivalent diameter
A_rs=3.9328;%riser area equals the exit of upper plenum
L_rs=2.718;

%4. steam separator
De_sep=0.2267;%m, equivalent diameter of the steam separator
L_sep=2.266;
A_sep=8.5164;%m^2, flow area
Ksep=5.3232;%equivalent loss coefficient of the steam separator for a typical BWR

%5. downcomer parameters
%RPV parameters
Drpv=6.375;%m, inside diameter of RPV
Trpv=0.16;%m, RPV wall thickness
denv=7.8e3;%kg/m^3, density of the RPV wall
Cpv=0.58;%kJ/kg, Specific heat of the RPV wall

%first part Downcomer parameters
Ldc1=2.1980;
Adc1=22.176;
De_dc1=0.6433;

%Second part Downcomer parameters
Ldc2=1.5943;
Adc2=8.551;
De_dc2=0.8508;

%jet pump part Downcomer parameters
Mra=1.96;%M ratio of the recirculation loop
Njet=20;%number of the jet pump
```

```
Asuction_jet=0.04;%suction flow area per jet pump
Ksuction=0.35;%suction loss coefficient
Athroat_jet=0.0354;%m^2, throat area per jet pump
Lthroat=2.5766;%m, throat length
De_throat=0.21224;%equivalent diameter of throat
Dediff1_in=0.21224;%upper part diffuser inlet diameter
Dediff1_out=0.2535;%upper part diffuser outlet diameter
Ldiff1=0.3053;%upper part diffuser length
Dediff2_in=0.2535;%low part diffuser inlet diameter
Dediff2_out=0.4826;
Ldiff2=1.8865;
Adis_jet=0.183;%m^2, discharge part area per jet pump
Ldis=0.2432;%discharge part length
De_dis=0.4826;%equivalent diameter of discharge part
Kdis=1.0;%form loss coefficient of discharge part


%%%%%%%%%%neutronic parameters
Ctem=-1.7e-5;%temperature coefficient
% Cvoid1=-0.15; %coefficient in quadratic void coefficient calculation
% Cvoid2=0.12005;
% Cvoid3=-0.1755;
 Cvoid1=-0.144; %coefficient in quadratic void coefficient calculation
 Cvoid2=-0.144;
 Cvoid3=-0.144;

T_neu=2.8e-5;%time constant

betaf=0.0067;% six groups delayed neutron fraction
betaf1=betaf*0.033;
betaf2=betaf*0.219;
betaf3=betaf*0.196;
betaf4=betaf*0.395;
betaf5=betaf*0.115;
betaf6=betaf*0.042;
lamdaf1=0.0124;% six groups decay constant
lamdaf2=0.0305;
lamdaf3=0.111;
lamdaf4=0.301;
lamdaf5=1.14;
lamdaf6=3.01;
%%%%%%%%end of neutronics variables value assignment

%inlet conditions
hin=1227.55;%kJ/kg, inlet enthalpy
Tin=278.3+273.15;%K, inlet temperature

%input the initial guess of the dominate root
root_re=-0.5;
root_im=3.0;
%%%%%%%%%%%%%%%%end of the input file
```